

**SYNTHESIS AND CATALYTIC PERFORMANCE OF  
IMMOBILIZED VANADIUM AND MOLYBDENUM  
COMPLEXES**

**Ph.D. THESIS**

by

**NAVEEN KUMAR**



**DEPARTMENT OF CHEMISTRY  
INDIAN INSTITUTE OF TECHNOLOGY ROORKEE  
ROORKEE-247 667 (INDIA)  
May, 2015**

**SYNTHESIS AND CATALYTIC PERFORMANCE OF  
IMMOBILIZED VANADIUM AND MOLYBDENUM  
COMPLEXES**

**A THESIS**

*Submitted in partial fulfilment of the  
requirements for the award of the degree*

*of*

**DOCTOR OF PHILOSOPHY**

*in*

**CHEMISTRY**

*by*

**NAVEEN KUMAR**



**DEPARTMENT OF CHEMISTRY  
INDIAN INSTITUTE OF TECHNOLOGY ROORKEE  
ROORKEE-247 667 (INDIA)  
May, 2015**

**©INDIAN INSTITUTE OF TECHNOLOGY ROORKEE, ROORKEE-2015  
ALL RIGHTS RESERVED**



# INDIAN INSTITUTE OF TECHNOLOGY ROORKEE ROORKEE

## CANDIDATE'S DECLARATION

I hereby certify that the work which is being presented in the thesis entitled **“SYNTHESIS AND CATALYTIC PERFORMANCE OF IMMOBILIZED VANADIUM AND MOLYBDENUM COMPLEXES”** in partial fulfilment of the requirements for the award of the Degree of Doctor of Philosophy and submitted in the Department of Chemistry of the Indian Institute of Technology Roorkee, Roorkee is an authentic record of my own work carried out during a period from July, 2011 to May, 2015 under the supervision of Dr. Mannar R. Maurya, Professor; Department of Chemistry, Indian Institute of Technology Roorkee, Roorkee.

The matter presented in this thesis has not been submitted by me for the award of any other degree of this or any other Institute.

**(NAVEEN KUMAR)**

This is to certify that the above statement made by the candidate is correct to the best of my knowledge.

Date:

(Mannar R. Maurya)  
Supervisor

*Dedicated To*  
*My Parents*  
*And*  
*My Guruji,*  
*Mr. Rajveer Singh*

## ACKNOWLEDGEMENTS

I am on the brink of giving a final shape to my dream. It is very cheerful and pulsating moment of my life to acknowledge the persons who are directly or indirectly associated with this thrashing task.

First and foremost thanks to God for his all Divine blessing showered on me for my success. It gives me immense pleasure in expressing deep sense of gratitude and admire to my mentor **Prof. Mannar R. Maurya** for his valuable and scrupulous guidance, enthusiastic interest throughout my research work with affectionate treatment. I am highly indebted for his gentle and benign behavior, patient correcting my mistakes during my research work. I am highly grateful to him for articulating this path and being a constant source of inspiration. My thanks also go to Mrs. Usha Maurya, for caring, kindness and generosity. I seek her pious blessing ever in my life.

I would like to gratefully acknowledge Prof. & Head Anil Kumar, Department of Chemistry, Indian Institute of Technology Roorkee, for providing me essential infrastructural facilities to carry out this research work.

My special thanks to the Head, Institute Instrumentation Centre of our institute for providing me necessary instrumentation facilities. My sincere thank to Mr. Madan Pal and other technical and non-technical staff members, who helped me from time to time during my research work. I am also grateful to all the members of Chemistry Department for their cooperation in many ways.

I am grateful to Prof. Dr. Joao Costa-Pessoa, Dr. Pedro Adão and Dr. Amit Kumar, Instituto Superior Tecnico, Portugal for carrying out the EPR studies and  $^{51}\text{V}$  NMR spectra of some of my samples. I would also like to thank Prof. Fernando

Avecilla, Departamento de Química Fundamental, Facultad de Ciencias, Universidade da Coruña, Spain for carrying out Single crystal data of some of my samples.

I want to express my sincere gratitude to my seniors and laboratory colleagues Dr. Priyanka Saini, Dr. Chancel Haldar, Dr. Nikita Chaudhary, Mrs. Sarita Dhaka, Ms. Ruchi Singh and juniors Mr. Neeraj Saini, Ms. Bhawna Uprety, Ms. Bithika Sarkar and Ms. Lata Rana for their lively company and motivation for the completion of my work. My convivial and humungous thank to my seniors and friends Dr. Sudhir Kumar Gupta, Mr. Himanshu Gupta, Mr. Anuj Kumar and Harshit Mahandra for their affectionate company, cooperation and moral support. I will always remain very grateful to them to be with me in all the circumstances.

I was extraordinarily fortunate in having Mr. Rajveer Singh as my Guruji. I could never have embarked and started all of this without his prior teachings which opened up unknown areas to me. I would like to thank Dr. K. P. Singh, D.A.V. College, Muzafarnagar (U.P) for moral support and cooperation.

I thank my friends in my home town Pramod, Sauraj, Praveen, Mohit, Monu, Rajdeep, Sajid and Sayeed for their lovely company, respect and encouragement. I know they will be always with me in every stage of my life. They are my best friends and their friendship gave me a lot for which I am thankful to them.

I would have not finished this thesis without the support of my family who has always been there for me whenever I need them. The words are not enough to express all my regards, love and thankfulness to my Mother, Mrs. Suman Devi and my Father, Mr. Bhopal Singh for their blessings, love and support at every moment. I

am in dearth of words in expressing my warm feelings to my Brother Satendra and Guddu. . I wish to thank my wife Seema, who is always there with sweet affection, extending helpful hand and cheering me up in her own special way through every thick and thin.

I would like to acknowledge the Council of scientific and Industrial Research (CSIR), New Delhi for the necessary financial support for this research.

Finally, I wish to acknowledge all those whose names have not figured above, but helped me in any form during the entire period of my research work.

**(NAVEEN KUMAR)**



## ABSTRACT

---

---

Catalytic role of transition metal complexes have played a vital role in various organic transformations e.g. oxidation, oxidative halogenation, polymerization etc. Most of the catalytic processes, widely engaged in the manufacture of fine as well as bulk chemicals are homogeneous in nature and produce a large amount of side waste materials that cause a serious environmental problem. The awareness of environmental issues has put a major impact on the development of such catalytic processes that are beneficial from both, industrial and environmental point of view. Environmental issues associated with the disposal of such homogeneous catalysts, coupled with financial concerns due to their increasing costs, have led to considerable research focused towards the development of green and economically viable alternatives such as immobilization or heterogenization of homogeneous transition metal complexes based catalysts. The efficient use of solid support to immobilize such catalysts can go a long way towards achieving these goals. Various thermally stable solid supports such as chemically modified polymer, silica, alumina, mesoporous molecular sieves, multi-wall carbon nanotubes etc. have been invented for the immobilization of homogeneous transition metal complexes.

The catalytic oxidation of organic substrates using transition metal complexes immobilized on polymer as catalyst has been studied well due to commercial and synthetic importance of the resulted functionalized molecules. However, impact of insertion of spacer between polymer support and catalyst has been less explored. Such spacer may allow the better interaction of catalytic center with substrates and oxidant during catalytic reaction which may result in the improved catalytic potential of polymer-supported complexes. It was, therefore, reasonable to undertake systematic study on the synthesis and characterization of new vanadium and molybdenum complexes immobilized on polymer with spacer, and to explore their catalytic potential under optimized reaction conditions.

The thesis entitled “synthesis and catalytic performance of immobilized vanadium and molybdenum complexes”, describes the synthesis of oxidovanadium(IV), oxidomethoxidovanadium(V) and dioxidomolybdenum(VI) complexes with potential coordinating organic ligands immobilized on chloromethylated polymer support and their characterization by various physico-chemical techniques. Different types of catalytic oxidation reactions have been carried out and suitable reaction conditions have been obtained for the maximum oxidation of organic substrates. The reaction products have been analyzed by gas chromatograph (GC) and their identities confirmed by GC-MS. For convenience the work presented in the thesis has been divided in the following chapters.

**First chapter** is the introductory one and describes various types of solid inert support that have been used for the immobilization of homogeneous catalysts. Literature on the catalytic applications of various vanadium and molybdenum complexes has also been reviewed.

**Second chapter** describes the synthesis of ligand H<sub>2</sub>sal-iah (**I**), derived from salicylaldehyde and indole-3-acetic hydrazide, which reacts with [V<sup>IV</sup>O(acac)<sub>2</sub>] in methanol to give oxidovanadium(IV) complex [V<sup>IV</sup>O(sal-iah)(H<sub>2</sub>O)] (**2.1**). In the presence of KOH, aerial oxidation of **2.1** in methanol yields dioxidovanadium(V) complex K[V<sup>V</sup>O<sub>2</sub>(sal-iah)]·H<sub>2</sub>O (**2.2**). Complex **2.1** has been grafted via covalent bonding through imino nitrogen of the indole group to chloromethylated polystyrene cross-linked with 5% divinylbenzene {now abbreviated as PS-[V<sup>IV</sup>O(sal-iah)(H<sub>2</sub>O)] (**2.3**)}. Its oxidomethoxidovanadium(V) analog {PS-[V<sup>V</sup>O(OMe)(sal-iah)] (**2.4**)} has been obtained by aerial oxidation of methanolic suspension of **2.3**. All these complexes have been characterized by various spectroscopic techniques (IR, electronic, <sup>1</sup>H and <sup>51</sup>V NMR, electron paramagnetic resonance (EPR) and thermal as well as field-emission scanning electron micrographs (FE-SEM) studies. The EPR spectrum of **2.3** indicates that the magnetically dilute V<sup>IV</sup>O-centers are well dispersed in the polymer matrix while EPR spectrum of **2.1** shows slightly different binding mode around vanadium center. <sup>1</sup>H and <sup>51</sup>V NMR spectra of **2.2** are compatible with the existence of expected dioxide species as the major product and oxidomethoxido species as a minor component in solution.

Independent of the species presents in methanol, complexes **2.1** and **2.2** upon treatment with  $\text{H}_2\text{O}_2$  both change to same oxidoperoxido species. The polymer-grafted complex **2.4** catalyzes the oxidation, by  $\text{H}_2\text{O}_2$ , of styrene and cyclohexene. Under optimized reaction conditions, the oxidation of styrene gave 95 % conversion where styrene oxide, benzaldehyde, benzoic acid, 1-phenylethane-1,2-diol and phenylacetaldehyde are products. Oxidation of cyclohexene gave 96 % conversion with cyclohexene oxide, 2-cyclohexene-1-ol, cyclohexane-1,2-diol and 2-cyclohexene-1-one as the major products. Neat complex  $\text{K}[\text{V}^{\text{V}}\text{O}_2(\text{sal-iah})]\cdot\text{H}_2\text{O}$  (**2.2**) is equally active but the recyclability and heterogeneity tests of polymer-grafted complex makes it better over neat analog.

**Third chapter** presents reaction between  $[\text{V}^{\text{IV}}\text{O}(\text{acac})_2]$  and ONO donor tridentate ligand  $\text{H}_2\text{hap-iah}$  (**II**) [ $\text{H}_2\text{hap-iah}$  = Schiff base obtained by the condensation of equimolar amounts of *o*-hydroxyacetophenone (hap) and indole-3-acetic hydrazide (iah)] in equimolar ratio under oxygen atmosphere in refluxing methanol which gives  $[\text{V}^{\text{V}}\text{O}(\text{OMe})(\text{hap-iah})]$  (**3.1**). Treatment of **3.1** in methanol with  $\text{H}_2\text{O}_2$  in presence of KOH results in the formation of  $\text{K}[\text{V}^{\text{V}}\text{O}(\text{O}_2)(\text{hap-iah})]$  (**3.2**). Complex **3.1** has been grafted in chloromethylated polystyrene cross-linked with 5% divinylbenzene {now abbreviated as PS- $[\text{V}^{\text{V}}\text{O}(\text{OMe})(\text{hap-iah})]$  (**3.3**)} via covalent bonding through imino nitrogen of the indole group. First two complexes were characterized by various spectroscopic techniques (IR, electronic,  $^1\text{H}$  and  $^{13}\text{C}$  NMR, ESI-MS), analytical and thermal studies. Complex **3.3** was also analyzed by field-emission scanning electron micrographs (FE-SEM) as well as Energy dispersive X-ray (EDAX) studies.  $^{51}\text{V}$  NMR spectrum of **3.1** is compatible with the existence of complex in three conformations. The polymer-grafted compound **3.3** was used as catalyst for the peroxidase-like oxidation of pyrogallol to purpurogallin at pH 7 buffer solution. Its high peroxidase mimicking ability, stability in a wide pH range, the easy separation from the reaction medium, and the reusability without considerable decrease in activity, suggest the practical utility of the catalyst.

**Fourth Chapter** presents reaction of  $[\text{Mo}^{\text{VI}}\text{O}_2(\text{acac})_2]$  with  $\text{H}_2\text{sal-iah}$  (**I**) in methanol which gives dioxidomolybdenum(VI) complex  $[\text{Mo}^{\text{VI}}\text{O}_2(\text{sal-iah})(\text{MeOH})]$  (**4.1**). Drop wise addition of 30% aqueous  $\text{H}_2\text{O}_2$  to the methanolic solution of **4.1** yields complex

[Mo<sup>VI</sup>O(O<sub>2</sub>)(sal-iah)(MeOH)] (**4.2**). Complex **4.1** has been grafted via covalent bonding through imino nitrogen of the indole to chloromethylated polystyrene cross-linked with 5% divinylbenzene {now abbreviated as PS-[Mo<sup>VI</sup>O<sub>2</sub>(sal-iah)(MeOH)] (**4.3**)}. All these complexes have been characterized by various spectroscopic techniques (IR, electronic, <sup>1</sup>H and <sup>13</sup>C NMR) and thermal as well as field-emission scanning electron micrographs (FE-SEM) studies. The crystal structure of **4.1** has been determined, confirming the *ONO* binding mode of **I**. The polymer-grafted complex **4.3** catalyzes the oxidative bromination, by H<sub>2</sub>O<sub>2</sub>, of styrene and *trans*-stilbene. Under the optimized reaction conditions, the oxidative bromination of styrene gave 98 % conversion in 2 h time where 2-bromo-1-phenylethane-1-ol and 1,2-dibromo-1-phenylethane are the main products and 1-phenylethane-1,2-diol is the product obtained by the attack of nucleophile water on the α-carbon of 2-bromo-1-phenylethane-1-ol. Oxidative bromination of *trans*-stilbene gave 96% conversion with 2,3-diphenyloxirane (*trans*-stilbene oxide), 1,2-dibromo-1,2-diphenylethane and 2-bromo-1,2-diphenylethanol as the products. Suitable reaction mechanisms for both reactions have been suggested. Neat complex [Mo<sup>VI</sup>O<sub>2</sub>(sal-iah)(MeOH)] (**4.1**) is equally active but the recyclability and heterogeneity tests of polymer-grafted complex makes it better over neat analog.

Reaction of [Mo<sup>VI</sup>O<sub>2</sub>(acac)<sub>2</sub>] with H<sub>2</sub>hap-iah (**II**) in 1:1 ratio in refluxing methanol gives [Mo<sup>VI</sup>O<sub>2</sub>(hap-iah)(MeOH)] (**5.1**). Complex **5.1** has been grafted in chloromethylated polystyrene cross-linked with 5% divinylbenzene {now abbreviated as PS-[Mo<sup>VI</sup>O<sub>2</sub>(hap-iah)(MeOH)] (**5.2**)} via covalent bonding through imino nitrogen of the indole group. Both complexes are characterized by various spectroscopic techniques (IR, electronic, <sup>1</sup>H and <sup>13</sup>C NMR), analytical and thermal studies. Complex **5.2** is also analyzed by atomic force microscopy (AFM), field-emission scanning electron micrographs (FE-SEM) as well as Energy dispersive X-ray (EDAX) studies. This study has been presented in **Fifth Chapter**. The polymer-grafted compound **5.2** has used for the catalytic oxidation of styrene and cyclohexene in the presence of NaHCO<sub>3</sub> using aqueous H<sub>2</sub>O<sub>2</sub> as oxidant. The intermediate peroxido species, expected to be involved during catalytic action, has also been generated from solution of **5.1** and studied by UV-

Vis. Various reaction conditions were considered to optimize reactions conditions for the maximum oxidation of substrates. Styrene under optimized reaction conditions gave mainly styrene oxide as a major product. Oxidation of cyclohexene gave cyclohexene oxide. The polymer-grafted complex shows higher conversions than its neat counterpart. The polymer-grafted complex provides additional advantage over its homogeneous counterpart in terms of increased catalyst lifetime and easier separation from the reaction mixture and allows for recyclable catalytic system.

Finally, summary and over all conclusions based on the achievements are presented.

## LIST OF PAPERS

### PUBLISHED/AcCEPTED/COMMUNICATED

1. M.R. Maurya and **Naveen Kumar**, “Chloromethylated polystyrene cross-linked with divinylbenzene and grafted with vanadium(IV) and vanadium(V) complexes having ONO donor ligand for the catalytic activity”, *J. Mol. Catal. A: Chem.*, **383–384** (2014) 172– 181.
2. M.R. Maurya, **Naveen Kumar** and F. Avecilla, “Polymer and non-polymer-grafted dioxidomolybdenum(VI) complexes having ONO donor ligand and their catalytic activities for the oxidative bromination of organic substrates”, *J. Mol. Catal. A: Chem.*, **392** (2014) 50–60.
3. M.R. Maurya, **Naveen Kumar** and N. Chaudhary, “Polymer grafted oxidomethoxido vanadium(V) complex of ONO donor ligand mimicking peroxidase activity”, *Polyhedron*, Accepted for publication.
4. M.R. Maurya and **Naveen Kumar**, “Sodium bicarbonate assisted oxidation, by H<sub>2</sub>O<sub>2</sub>, of styrene and cyclohexene using polymer grafted dioxidomolybdenum(VI) complex as a catalyst”, Submitted for publication.

\*\*\*\*\*

## LIST OF PAPERS

### PRESENTED IN CONFERENCES/WORKSHOPS

1. Mannar R. Maurya, **Naveen Kumar**, “Polymer –grafted and neat oxidovanadium(IV), dioxidovanadium(V) and dioxidomolybdenum(VI) complexes having ONO donor ligand and their catalytic activities”, 50<sup>th</sup> annual convention of chemists 2013 held at the Department of Chemistry & Centre for advanced studies in chemistry, Punjab University, Chandigarh, December 04 – 07, 2013, IAC(AP) – 04.
2. Mannar R. Maurya, **Naveen Kumar**, “Synthesis, characterization and crystal structure of dinitrosylmolybdenum(0) complexes of monobasic bidentate ligands”,

National conference on global challenges, New Frontiers in chemical sciences, (GC: NFCS-2012), Kurukshetra University, Kurukshetra, September 22 – 23, 2012, Poster presentation.

3. Attended a Workshop entitled “Nano Drug Delivery Systems (Industry-Academia Interaction)”, organized Centre of Excellence: Nanotechnology, IIT Roorkee on January 10, 2015.

\*\*\*\*\*

# **CONTENTS**

	Page No.
CANDIDATE'S DECLARATION	–
ACKNOWLEDGEMENTS	(i)
ABSTRACT	(iv)
LIST OF PUBLICATIONS	(ix)
CONTENTS	(xi)

## **CHAPTER 1**

*General introduction: Design of immobilized metal complexes, polymer-anchored vanadium and molybdenum complexes and their catalytic properties*

1.1 Introduction	1
1.2 Supports used for the immobilization of metal complexes	1
1.3 Polymers as support for the immobilization of metal complexes	11
1.4 Polymer-supported vanadium complexes and their catalytic applications: A literature survey	16
1.5 Polymer-supported molybdenum complexes	32
1.6 Objective of the present investigation	41

## **CHAPTER 2**

*Chloromethylated polystyrene cross-linked with divinylbenzene and grafted with vanadium(IV) and vanadium(V) complexes having ONO donor ligand for the catalytic activity*

2.1 Introduction	42
------------------	----



2.2	Experimental	43
2.2.1	Materials	43
2.2.2	Physical methods and analysis	43
2.2.3	Synthesis	44
2.2.4	Catalytic activity	46
2.3	Results and discussion	47
2.3.1	Synthesis and Characterization	47
2.3.2	Field Emission-scanning Electron Micrograph (FE-SEM) and Energy Dispersive X-Ray Analysis (EDAX) studies	49
2.3.3	Thermogravimetric (TGA) studies	50
2.3.4	IR spectral studies	51
2.3.5	UV-visible spectral studies	52
2.3.6	EPR study	55
2.3.7	$^1\text{H}$ and $^{51}\text{V}$ NMR studies	56
2.3.8	Catalytic activity studies	58
2.3.9	Reactivity of $\text{K}[\text{V}^{\text{V}}\text{O}_2(\text{sal-iah})]\cdot\text{H}_2\text{O}$ with $\text{H}_2\text{O}_2$ and possible reaction pathway	73
2.4	Conclusions	75

## CHAPTER 3

### *Polymer grafted oxidomethoxidovanadium(V) complex of ONO donor ligand mimicking peroxidase activity*

3.1	Introduction	76
3.2	Experimental	77
3.2.1.	Materials	77
3.2.2.	Physical methods and analysis	77
3.2.3.	Synthesis	77

3.2.4. Peroxidase mimetic activity: catalytic oxidation of pyrogallol	79
3.3. Results and Discussion	80
3.3.1. Synthesis and characterization	80
3.3.2. Thermogravimetric Analysis (TGA) studies	81
3.3.3. Field emission-scanning electron microscope (FE-SEM) and energy dispersive X-ray analysis (EDAX) studies	83
3.3.4. IR spectral studies	84
3.3.5. UV-visible spectral studies	87
3.3.6. $^1\text{H}$ , $^{13}\text{C}$ and $^{51}\text{V}$ NMR studies	89
3.3.7. Electrospray ionization mass spectrometric study	95
3.3.8. Peroxidase mimetic activity of polymer grafted complex	96
3.3.9. Reactivity of $[\text{V}^{\text{V}}\text{O}(\text{OMe})(\text{hap-iah})]$ and $\text{K}[\text{V}^{\text{V}}\text{O}(\text{O}_2)(\text{hap-iah})]$ with $\text{H}_2\text{O}_2$ and possible reaction pathway	107
3.4. Conclusions	108

## CHAPTER 4

### *Polymer and non-polymer-grafted dioxidomolybdenum(VI) complexes having ONO donor ligand and their catalytic activities for the oxidative bromination of organic substrates*

4.1. Introduction	110
4.2. Experimental	111
4.2.1. Materials	111
4.2.2. Physical methods and analysis	111
4.2.3. Synthesis	111
4.2.4. X-Ray crystal structure determination	112

4.2.5. Catalytic activity	114
4.3. Results and Discussion	115
4.3.1. Synthesis and Characterization	115
4.3.2. Structure description	116
4.3.3. Field emission-scanning electron micrograph (FE-SEM) and energy dispersive X-ray analysis (EDAX) studies	120
4.3.4. Thermogravimetric Analysis (TGA) studies	121
4.3.5. IR spectral studies	122
4.3.6. UV-visible spectral study	123
4.3.7. $^1\text{H}$ and $^{13}\text{C}$ NMR studies	126
4.3.8. Catalytic activity studies	130
4.3.9. Reactivity of $[\text{Mo}^{\text{VI}}\text{O}_2(\text{sal-iah})(\text{MeOH})]$ (4.1) with $\text{H}_2\text{O}_2$ and possible reaction pathway	139
4.4. Conclusions	143

## CHAPTER 5

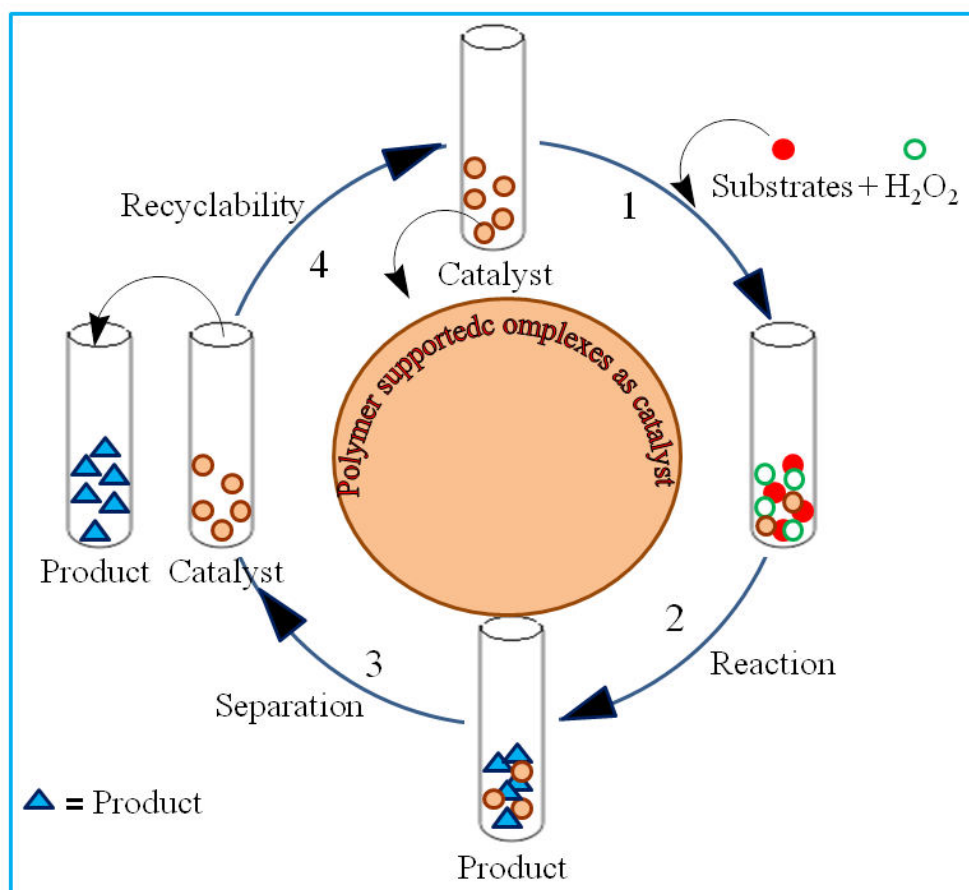
### *Sodium bicarbonate assisted oxidation, by $\text{H}_2\text{O}_2$ , of styrene and cyclohexene using polymer grafted dioxidomolybdenum(VI) complex as a catalyst*

5.1. Introduction	145
5.2. Experimental	146
5.2.1. Materials	146
5.2.2. Physical methods and analysis	146
5.2.3. Synthesis	146
5.2.4. Catalytic activity	147
5.3. Results and Discussion	148
5.3.1. Synthesis and characterization	148
5.3.2. Field emission-scanning electron micrograph (FE-SEM)	

and energy dispersive X-ray analysis (EDAX) studies	149
5.3.3. Atomic force microscopic (AFM) study	151
5.3.4. Thermogravimetric study	152
5.3.5. IR spectral studies	153
5.3.6. UV-visible spectral studies	154
5.3.7. $^1\text{H}$ and $^{13}\text{C}$ NMR studies	156
5.3.8. Catalytic activity studies	160
5.3.9. Reactivity of $[\text{Mo}^{\text{VI}}\text{O}_2(\text{hap-iah})(\text{MeOH})]$ (5.1) with $\text{H}_2\text{O}_2$ and $\text{NaHCO}_3$ and possible reaction pathway	170
5.4. Conclusions	175
<b>REFERENCES</b>	176
<b>SUMMARY AND CONCLUSIONS</b>	192

# CHAPTER 1

**General introduction: Design of immobilized metal complexes, polymer-anchored vanadium and molybdenum complexes and their catalytic properties**



## 1.1. INTRODUCTION

Catalytic role of transition metal complexes have played a vital role in various organic transformations e.g. oxidation, hydrogenation, polymerization etc. Most of the catalytic processes, widely engaged in the manufacture of fine as well as bulk chemicals are homogeneous in nature and produce a large amount of side waste materials that cause a serious environmental problem. The awareness of environmental issues has put a major impact on the development of such catalytic processes that are beneficial from both, industrial and environmental point of view. Environmental issues associated with the disposal of such homogeneous catalysts, coupled with financial concerns due to their increasing costs, have led to considerable research focused towards the development of green and economically viable alternatives such as immobilization or heterogenization of homogeneous transition metal complexes based catalysts. The efficient use of solid support to immobilize such catalysts can go a long way towards achieving these goals [1]. Various solid supports have been invented for the immobilization of homogeneous transition metal complexes.

## 1.2. Supports used for the immobilization of metal complexes

The thermally stable materials (organic or inorganic) can be used as support for the immobilization of metal complexes if they either have suitable functional group(s) or can be functionalized easily. One important condition for such materials is their chemical inertness after immobilization of catalysts. Amongst various supports, alumina and silica are readily available inorganic compounds and can be modified to immobilize various catalysts by direct reaction of surface hydroxyl groups with reactive species.

Silica has been used as support to immobilize metal complexes after certain modifications. Hybrid silica material containing the di(2-pyridyl)methylamine-palladium dichloride complex from the silylated monomer has been prepared by sol-gel co-gelification method. The monosilylatedpalladium(II) complex of di(2-pyridyl)methylamine-palladium dichloride and the hybrid silica catalytic materials derived thereof were prepared as summarized in Fig. 1.1 [2].

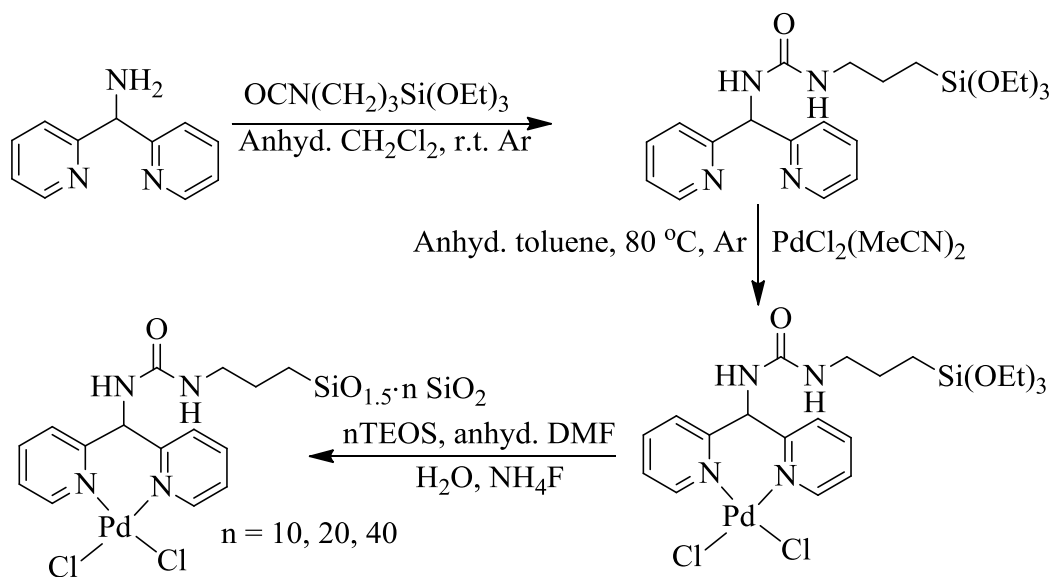


**Figure 1.1.** Synthetic route to prepare silica supported palladium(II) complex. TEOS = tetraethyl orthosilicate

In one report poly(4-vinylpyridine-co-styrene) (P-4-VP-co-St) was grafted on silica gel particles to give P-4-VP-co-St@SiO<sub>2</sub> which was then used as support to immobilize cobalt tetraphenylporphyrin (CoTPP) via the axial coordination reaction between CoTPP and the pyridine groups of the grafted P-4-VP-co-St, resulting in the heterogenized catalyst CoTPP-P-4-VP-co-St@SiO<sub>2</sub> [3] as shown in Fig. 1.2.

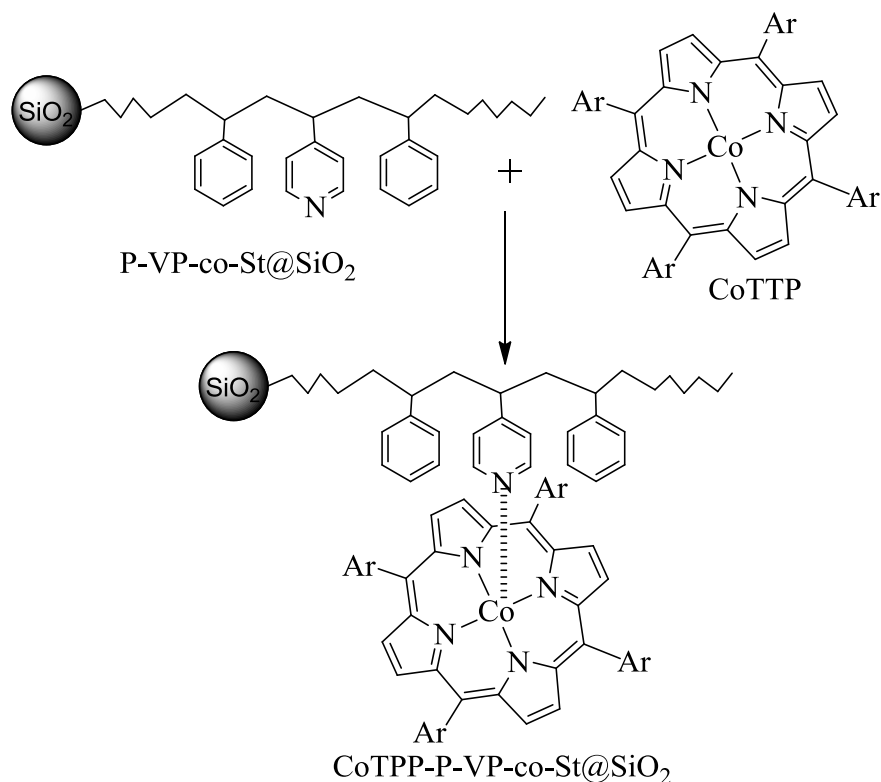


**Figure 1.2.** Modification of SiO<sub>2</sub> by functionalized polymer, poly(4-vinylpyridine-co-styrene) to immobilize Co-porphyrin complex.

Alumina and silica have been modified to attach suitable ligands for binding of metal ions as shown in Fig. 1.3 [4, 5].

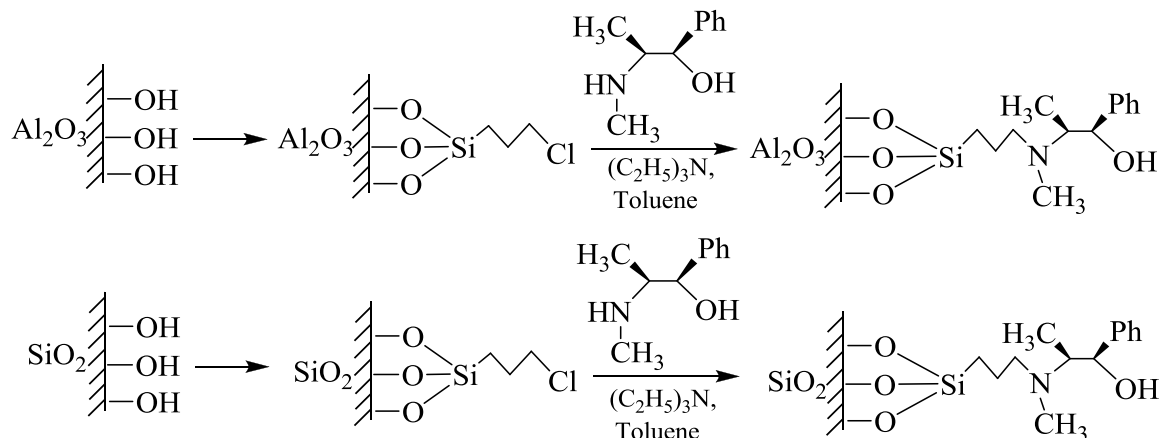


**Figure 1.3.** Synthetic schemes for the binding of ligands on modified alumina or silica.



Similar to silica and alumina, mesoporous molecular sieves such as Si-MCM-41 and Si-SBA-15 also have hydroxyl groups present on the surface and can be used as support for the immobilization of catalysts after modification(s). Thus, covalent grafting of MCM-41 with 3-chloropropyl trimethoxysilane and subsequent reaction with ligand N, N'-bis(2-pyrrolmethylideneaminopropyl)amine (pypr) followed by  $[\text{MoO}_2(\text{acac})_2]$  afforded MCM-41- $[\text{MoO}_2(\text{pypr})]$ . The X-ray diffraction and nitrogen sorption analyses confirmed the preservation of the textural properties of the support as well as accessibility of the channel system despite sequential reduction in surface area, pore volume and pore size [6].

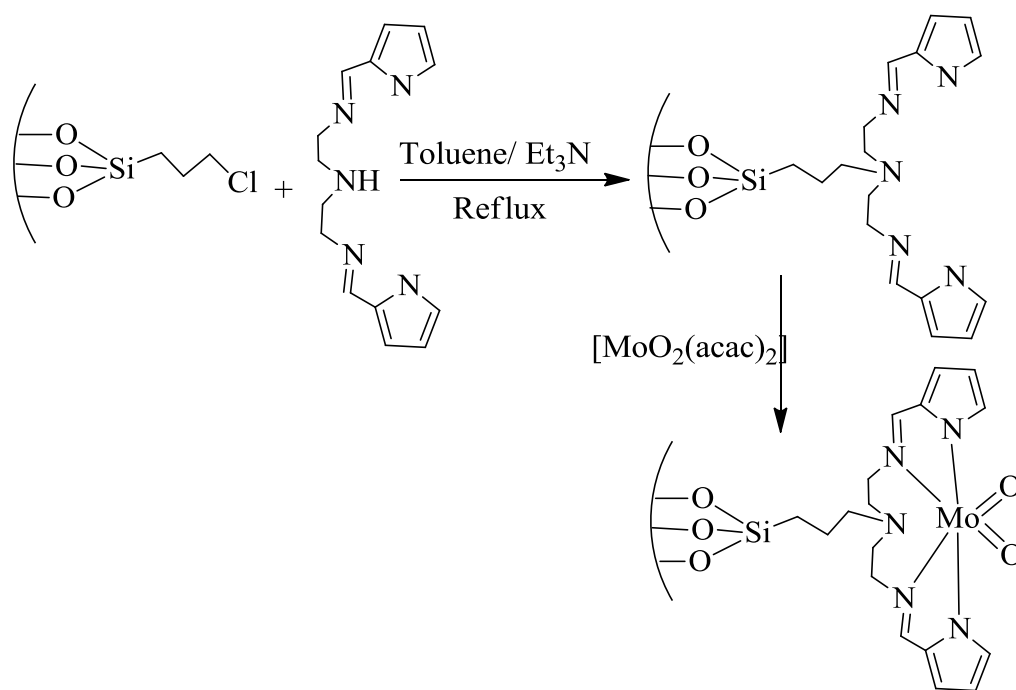


**Figure 1.4.** Scheme for the immobilization of Mo complex on MCM-41.

Same way  $[\text{H}_3\text{Ru}_4(\text{CO})_{12}]$  has been immobilized onto MCM-41; Fig.1.5 [7].



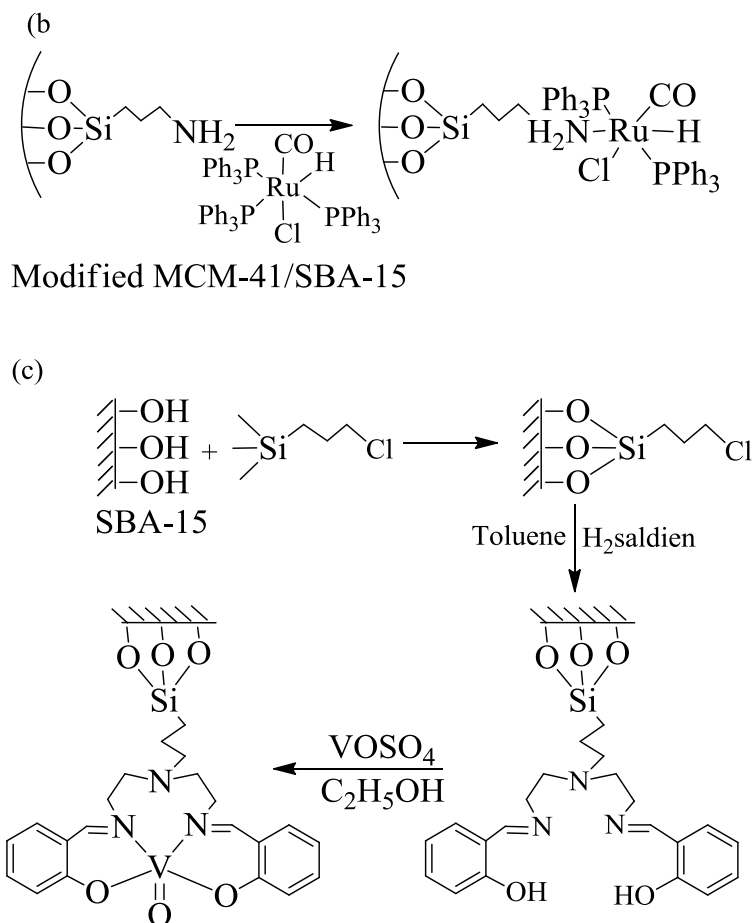


**Figure 1.6.** Schemes for the immobilization of catalysts on modified MCM-41/ SBA-15.

The manganese complex,  $[\text{Mn}(4\text{-OHsalophen})\text{Cl}]$  has been directly attach to MCM-41, using a 1,4-diisocyanatobutane (DIC-4) as a binder in single step. Catalyst was prepared by refluxing the unmodified MCM-41 and DIC-4, in dry toluene, for 3 h. After cooling down,  $[\text{Mn}(4\text{-OHsalophen})\text{Cl}]$  was added and the mixture was again refluxed for another 6 h [11].

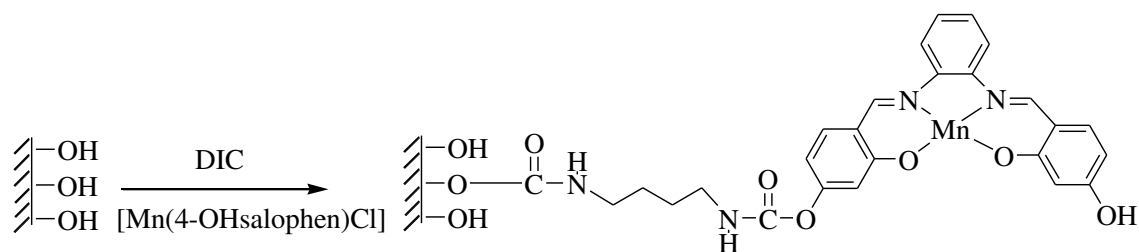


**Figure 1.7.** Synthetic route to prepare MCM-41-[Mn(4-OHsalophen)DIC].

Using similar method, binol-derived monodentatephosphorothioite (PS) ligand was synthesized from binol and thiopropyltriethoxysilane, and its iridium complex was covalently anchored to mesoporous silica supports like SBA-15, MCM-41, and MCM-48 [12].

Chiral Ti–binol complex was immobilized onto ionic liquid modified SBA-15 according to following schemes; Fig. 1.8 [13]. The catalyst showed excellent enantioselectivity in the heterogeneous asymmetric oxidation of prochiral sulfides to sulfoxides and subsequent oxidative kinetic resolution of the sulfoxides using aqueous *tert*-butylhydroperoxide as the oxidant. The catalyst was highly stable and could be readily recycled and reused for over one month with no apparent loss of activity and enantioselectivity (up to >99.9%).

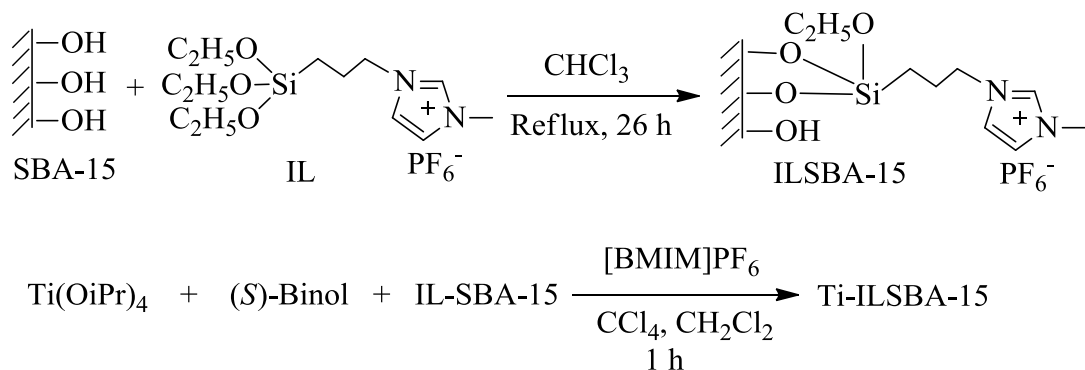


**Figure 1.8.** Synthetic route for the immobilization of Ti(S)-binol on to ionic liquid modified SBA-15.

Similarly, metal ion-containing ionic liquids on silica surfaces (ImmM IL) have been prepared and characterized, Fig. 1.9 [14].

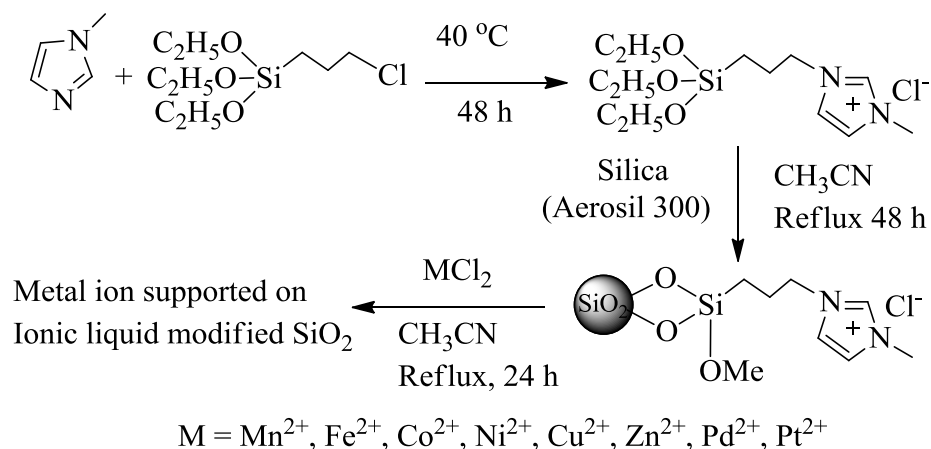


**Figure 1.9.** Metal ion-containing ionic liquids supported on silica surface.

Hydroxyapatite  $[\text{Ca}_{10}(\text{PO}_4)_6(\text{OH})_2]$  (HAP) is an important class of biomaterial, which is chemically similar to the mineral component of mammalian bones. HAP was prepared and used as support for  $\text{Rh}(\text{CO})_2(\text{acac})$  (acac = acetylacetonate) [15].

Complex  $[\text{Al}(\text{salen})\text{Cl}]$  (salen = N,N'-bis(salicylidene)ethylenediamine dianion) has been supported onto macrocyclic oligomeric cyclooctene through linkers of varying length and flexibility to demonstrate the importance of support architecture on catalyst activity; Fig. 1.10. For the bimetallic cyanide addition to  $\alpha, \beta$ -unsaturated imides, the flexibility and ability of the cyclooctene support to enhance interaction between neighboring  $[\text{Al}(\text{salen})\text{Cl}]$  units makes the catalysts superior to their unsupported analogues [16].

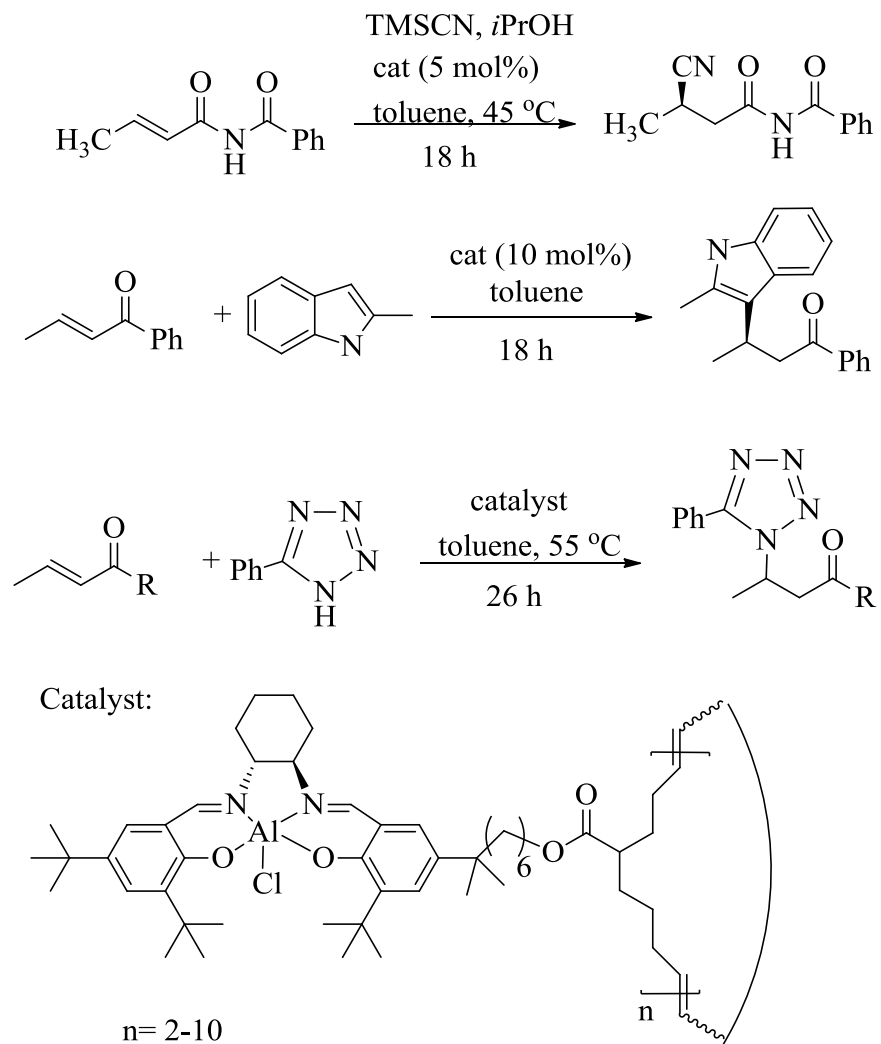


**Figure 1.10.** Various catalytic reactions and catalysts used.

Amines modified multi-wall carbon nanotube (MWCNTs) supported molybdenum catalysts (Fig. 1.11), prepared by refluxing UV irradiated  $\text{Mo}(\text{CO})_6$  with modified carbon nanotube in THF have been used as catalyst for the epoxidation of various alkenes. They give ca. 95% conversion and show good recyclability [17]. Two other MWCNTs supported molybdenum catalyst has also been prepared similarly and used for the epoxidation of alkene; Fig. 1.12 [18]

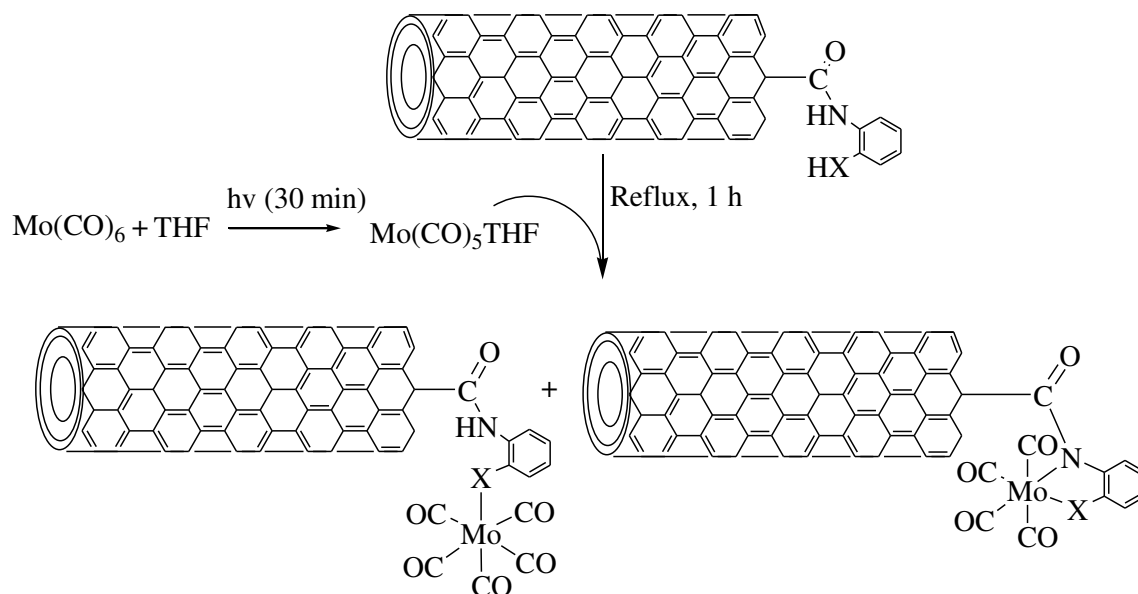


**Figure 1.11.** Amines modified multi-wall carbon nanotube (MWCNTs) supported molybdenum catalysts.

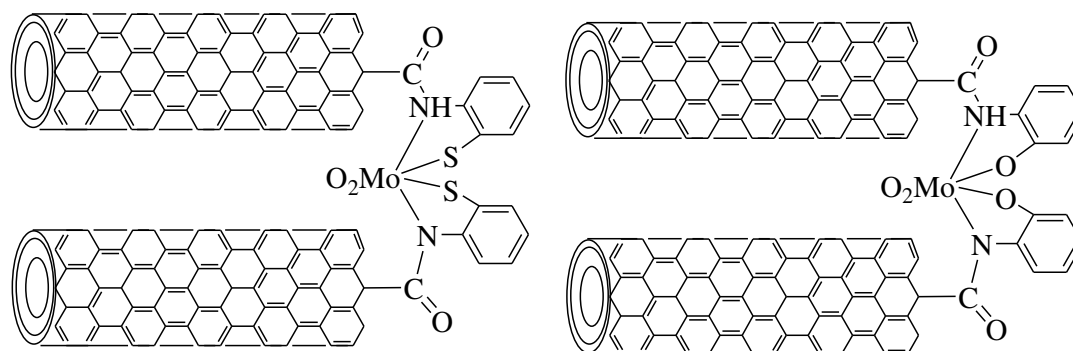


**Figure 1.12.** MWCNTs supported molybdenum catalyst.

The reaction of  $[\text{Mo(CO)}_3(\text{CH}_3\text{CN})_3]$  with poly(4-vinylpyridine) (P(4-VP)) in acetonitrile results in the formation of pyridyl group coordinated polymer immobilized complex P- $[\text{Mo(CO)}_3(4\text{-VP})_3]$ . Here, the pyridyl groups of the organic polymer are covalently bonded to the Mo centers [19].

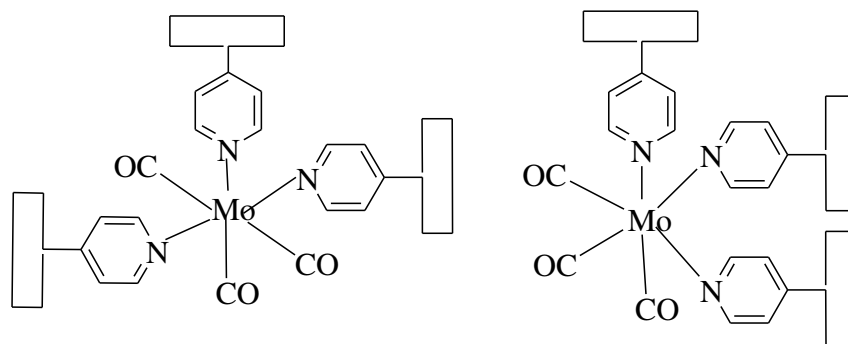


**Figure 1.13.** Proposed structures of supported Mo(0) complexes.

### 1.3. Polymers as support for the immobilization of metal complexes

Polymers are considered generally non-reactive and thermally stable materials. However, some of them can be used as support to immobilize metal complexes after modifying them with suitable functional groups [20-23] while some others can be reacted directly with metal salts/ other suitable metal precursors to preparing metal complexes [24] if they have binding capability.

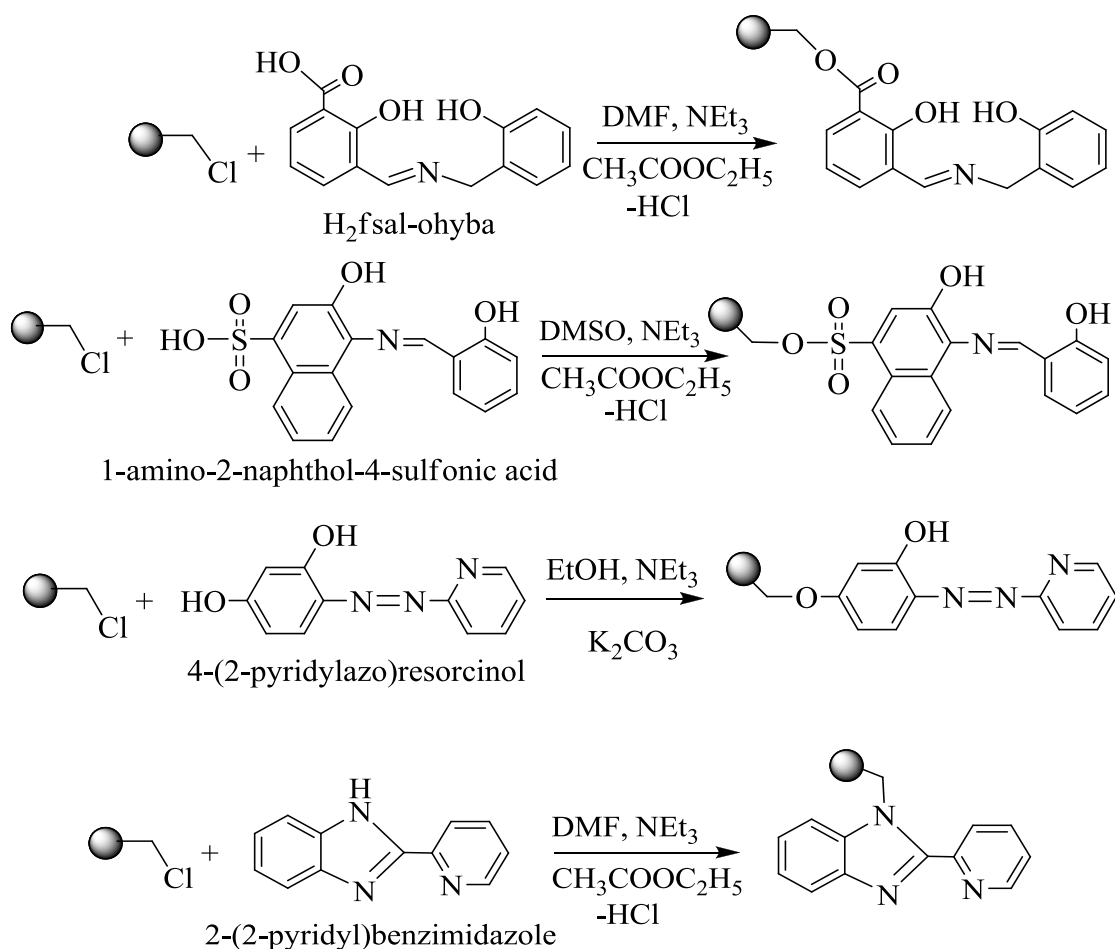
The metal complexes supported onto polymer are called polymer supported, polymer grafted or polymer-anchored complexes. The functionalized polymers (cross-linked as well as non-cross-linked) have widely been used as support to immobilize metal complexes through covalent bonding. Polymer-supported transition metal complexes have widely been used as catalyst [23,24-26] for many organic transformations due to their additional advantages over simple transition metal complexes like operational flexibility due to their insolubility, recycle ability, better product selectivity and activity due to active site isolation and high surface area.

There are several methods to immobilize metal complexes onto polymer support. The most useful method is the covalent bonding of organic molecule having suitable coordinating site(s) (e.g. ligand) with functionalized polymer followed by its coordination with metal ion. Other methods include direct covalent bonding of functionalized polymer to the ligand of the pre-synthesized metal complex and covalent bonding of the central



metal ion of the complex through suitable coordinating atom appended on the polymer [23-26].

Chloromethylated polystyrene cross-linked with divinylbenzene (PS-Cl) has been used extensively for immobilization of metal complexes. Ligands having functional groups like carboxylic acids, sulfonic acids, hydroxyl, imine group etc. can be attached to the chloromethylated polystyrene in the presence of triethylamine as shown in Fig. 1.14 [27-31].



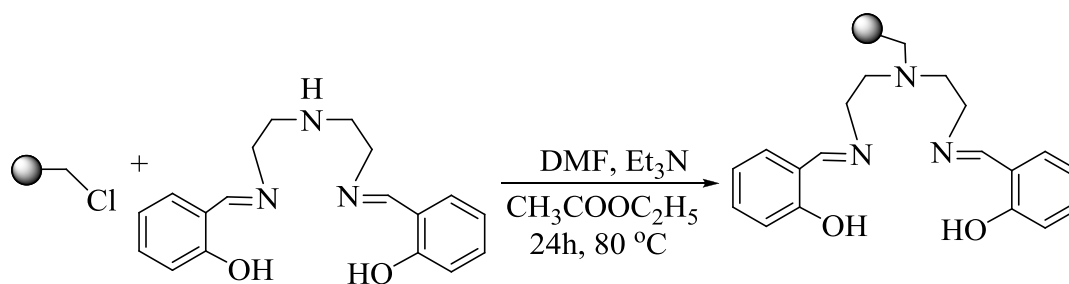
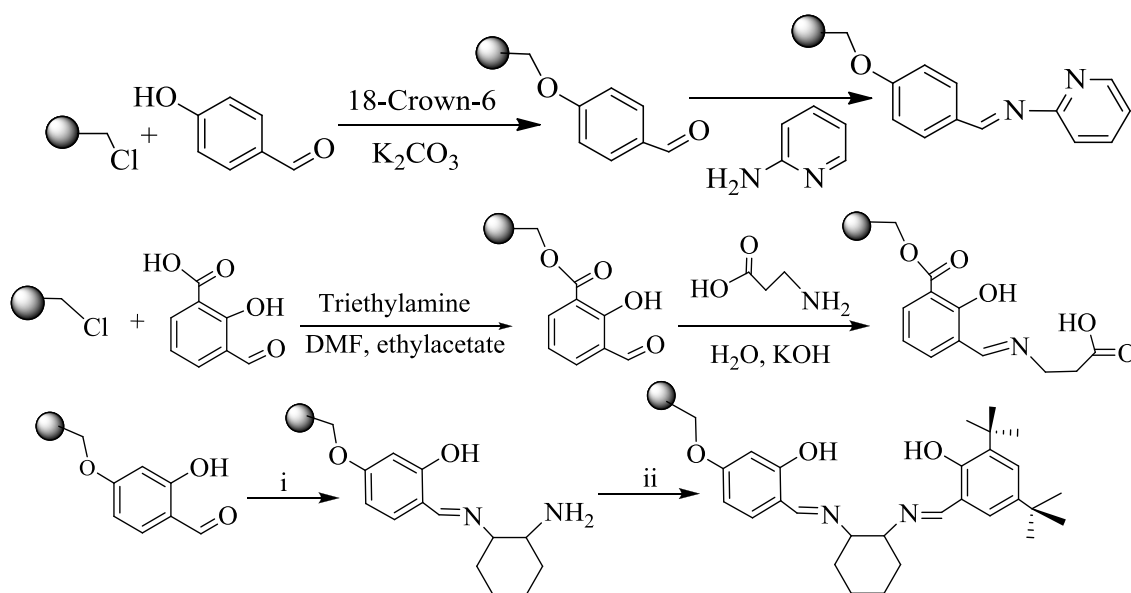


**Figure 1.14.** Schemes for the immobilization of catalysts on modified chloromethylated polystyrene.

Starting from suitable aldehyde polymer-anchored bidentate, tridentate and tetradentate ligands have been prepared in two steps as shown in Fig. 1.15 [32-35].



(i) (S, S)-1, 2-diaminocyclohexane, dioxane, 18-Crown-6,  $K_2CO_3$ ,  $85^\circ C$ , 3 days.

(ii) Salicylaldehyde derivatives, 18-Crown-6,  $K_2CO_3$ ,  $85^\circ C$ , 3 days.

**Figure 1.15.** Reaction schemes for the synthesis of polymer-supported ligands starting from aldehyde or its derivative.

Phenolic hydroxyl group easily reacts with chloromethylated polystyrene in the presence of alkali carbonate along with triethylamine in solvent [36]. This method is also applicable to immobilize porphyrins such as 5,10,15-tris(4-R-phenyl)-20-(4-hydroxyphenyl)porphyrins (Fig. 1.16) bearing peripheral hydroxyl group onto chloromethylated polystyrene in DMF [37].

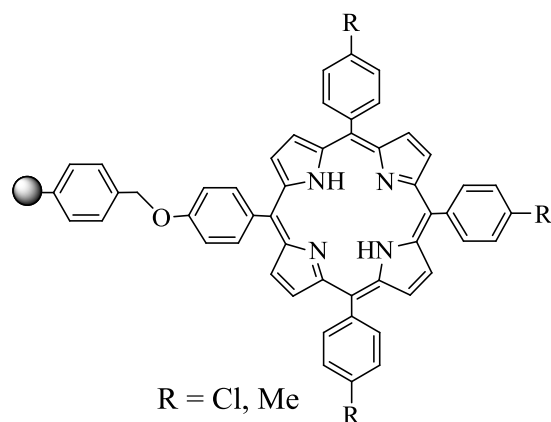


**Figure 1.16.** Example of polymer-anchored porphyrin.

Poly(ethyleneglycol) (PEG) has been used as support to immobilize iron(II) porphyrin using a copper-catalyzed azide-alkyne [3+2] cycloaddition as shown in Fig. 1.17 [38].

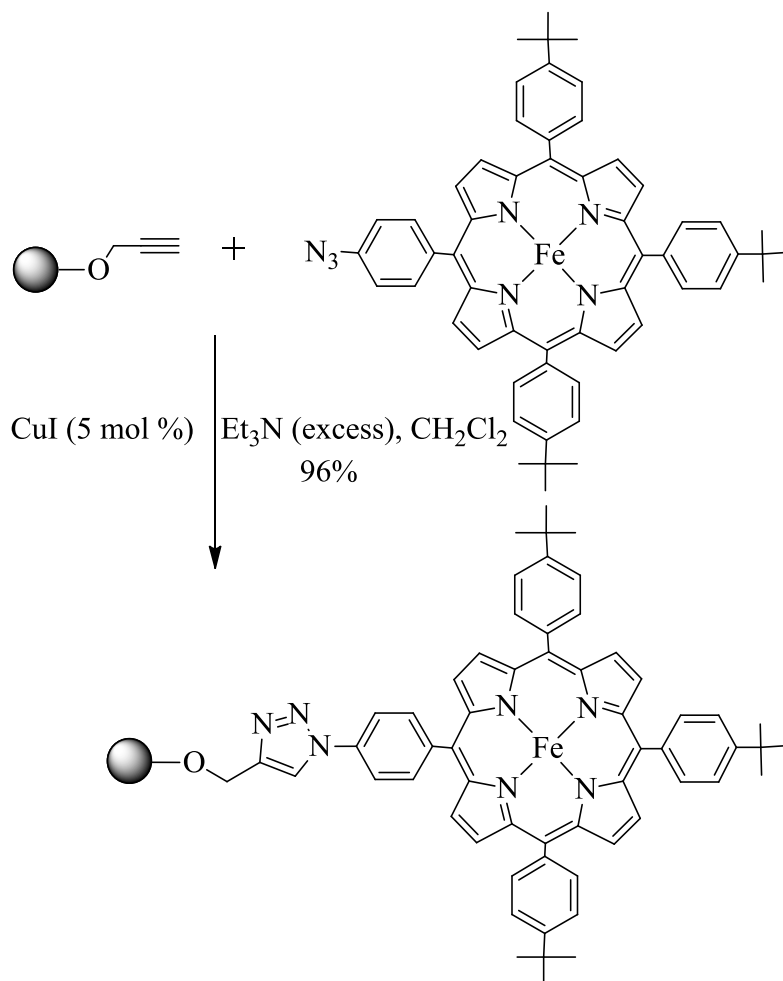


**Figure 1.17.** Synthetic route to prepare poly(ethyleneglycol) (PEG) immobilized ironporphyrin.

Alkene group present on the ligand is also suitable in the formation of polymer-anchored metal complexes where metal complexes directly react with in-situ generated polymer; Fig. 1.18 [39].

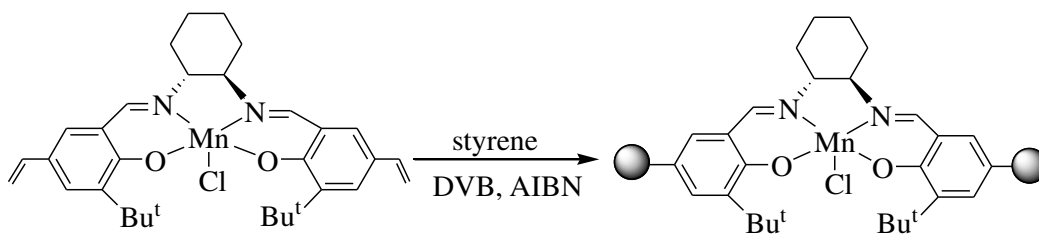


**Figure 1.18.** Route to prepare polymer-supported complex. DVB = divinyl benzene, AIBN = azobisisobutyronitrile.

Covalent bonding of functionalized group to polymer followed by coordination of appended functional group directly to the metal complexes has also been reported in the literature; Fig. 1.19 [40].

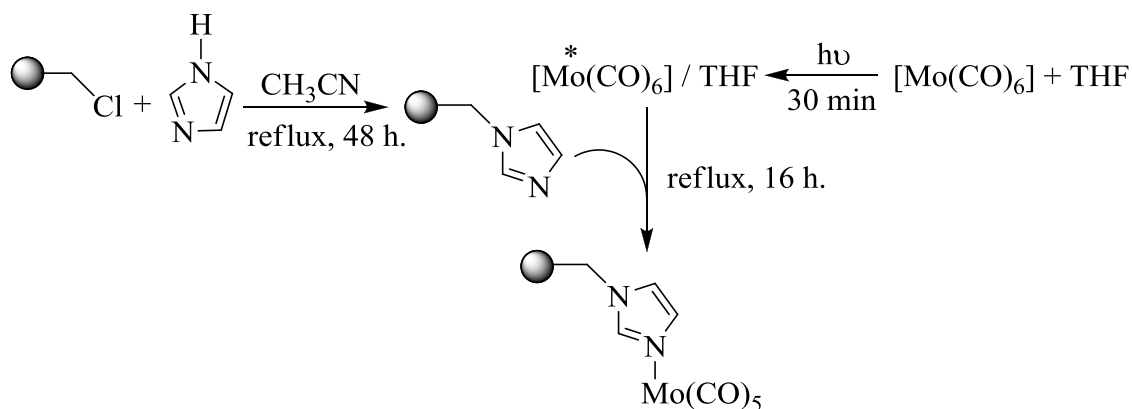


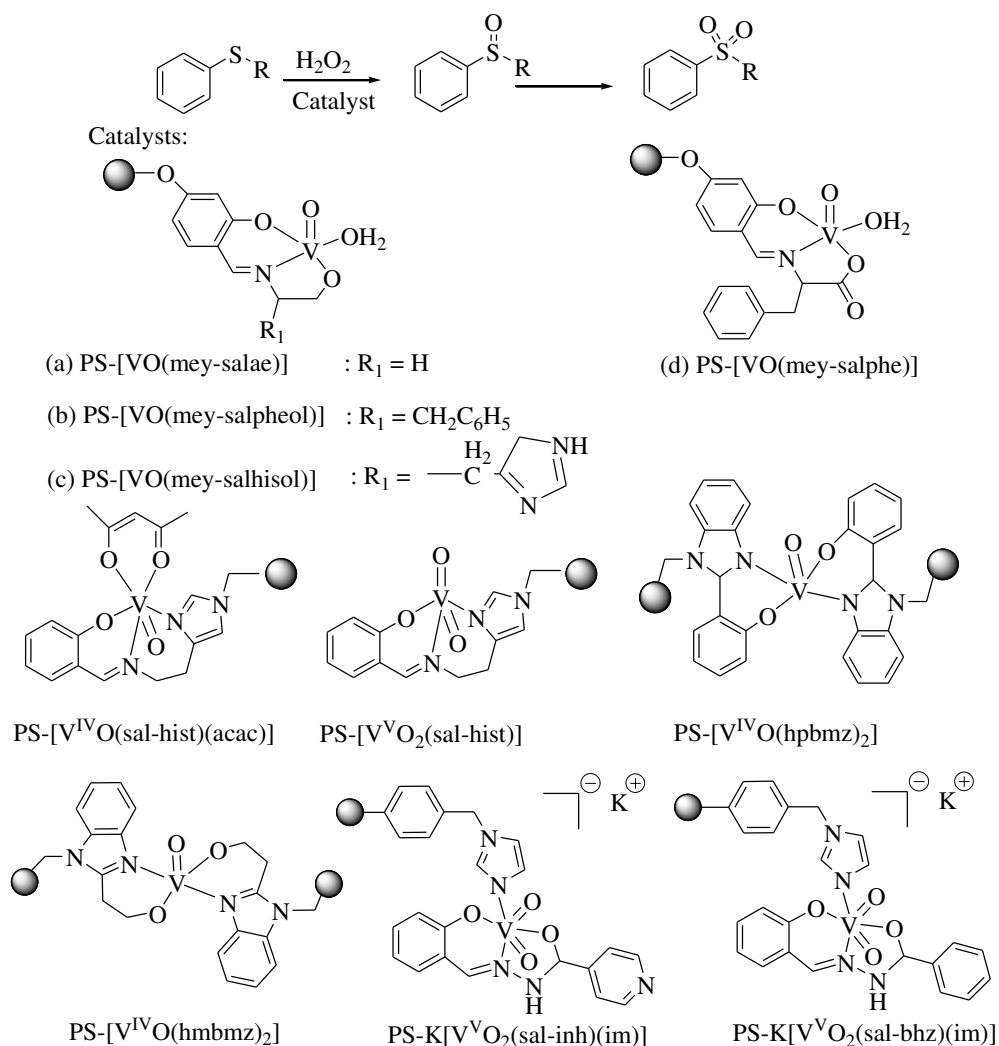
**Figure 1.19.** Reaction scheme for the synthesis of polymer-supported complex.

#### 1.4. Polymer-supported vanadium complexes and their catalytic applications: A literature survey

Advances in polymer-supported vanadium complexes have recently been reviewed by Maurya *et al.* [25, 26]. Similar to model vanadium complexes, polymer-supported complexes also model the catalytic activity shown by vanadium-dependent haloperoxidases. These polymer-supported complexes have also shown excellent results in other vanadium mediated oxygen transfer reactions. A brief advances in catalytic applications of polymer-supported vanadium complexes are summarized below:

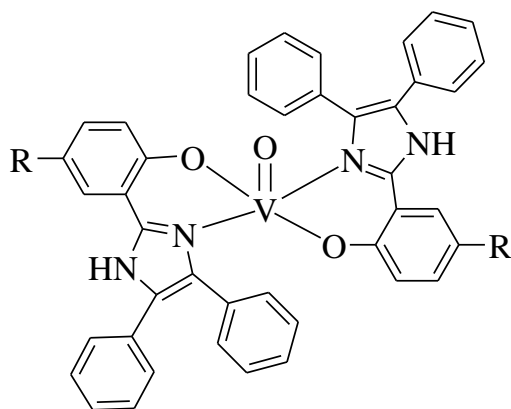
Polymer-supported complexes, PS- $[\text{mer-V}^{\text{IV}}\text{O}(\text{salae})]$ , PS- $[\text{mer-V}^{\text{IV}}\text{O}(\text{salpheol})]$ , PS- $[\text{mer-V}^{\text{IV}}\text{O}(\text{salhisol})]$  and PS- $[\text{mer-V}^{\text{IV}}\text{O}(\text{salphe})]$  have been used as catalysts for the oxidation of methyl phenyl sulfide (mps) in the presence of TBHP and give 81 – 91 % conversion of methyl phenyl sulfide to sulfoxide in 1.5 h. Enantiomeric excess of mps

was as high as 40 % with PS-[*mer*-VO(salhisol)] [36]. Complexes also catalyze the oxidation of methyl phenyl sulfide (mps) in the presence of H<sub>2</sub>O<sub>2</sub> as oxidant with 97 – 100 % selectivity towards sulfoxide along with high turn-over frequency (TOF) in 2 h of reaction time. Complexes PS-[V<sup>IV</sup>O(sal-hist)(acac)], PS-[V<sup>V</sup>O<sub>2</sub>(sal-hist)] [41] PS-[V<sup>IV</sup>O(hpbmz)<sub>2</sub>] [42], PS-K[V<sup>V</sup>O<sub>2</sub>(sal-inh)(im)] and PS-K[V<sup>V</sup>O<sub>2</sub>(sal-bhz)(im)] [43] (Fig. 1.20) are also excellent catalysts for the oxidation of sulfides (methyl phenyl sulfide and diphenyl sulfide) and show high turn over frequency. The reusable oxidovanadium(IV) complexes of Schiff bases derived from substituted salicylaldehyde and optically active amino alcohols supported on polyacrylate and polystyrene also catalyze the oxidation of methyl phenyl sulfide in presence of H<sub>2</sub>O<sub>2</sub> and *tert*-butyl hydroperoxide [44].



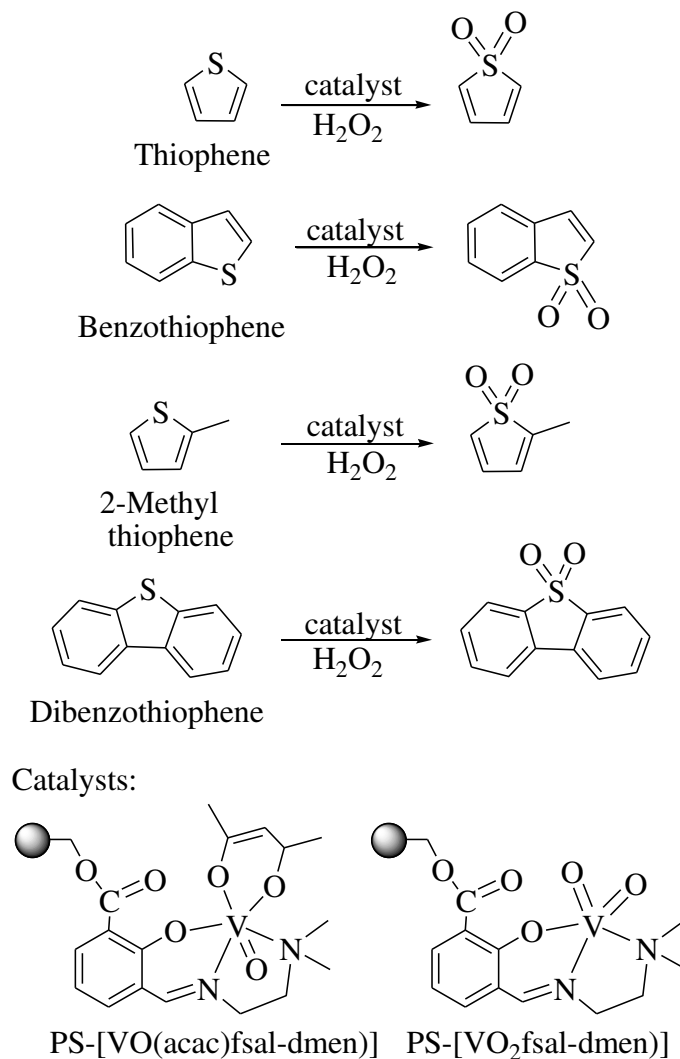
**Figure 1.20.** Catalysts used for the oxidation of sulfides. R = CH<sub>3</sub> : methyl phenyl sulfide (mps), R = C<sub>6</sub>H<sub>5</sub>: diphenyl sulfide (dps).

Fiber-based oxidovanadium(IV) catalysts (Fig. 1.21) for the oxidation of methyl phenyl sulfide using a continuous flow set up by incorporating complexes into polystyrene and electrospinning to produce nano-fiber mats has also been developed [45]. It has been found that substituent on ligands (R = NO, Br, H, MeO) affects the oxidation of methyl phenyl sulfide by hydrogen peroxide in acetonitrile at 25 °C. The catalytic efficiency of the complexes follows the order: NO<sub>2</sub>>Br>H>MeO.



**Figure 1.21.** Structure of complex incorporated into polystyrene and electrospun to produce nano-fiber mats. R = NO, Br, H, MeO.

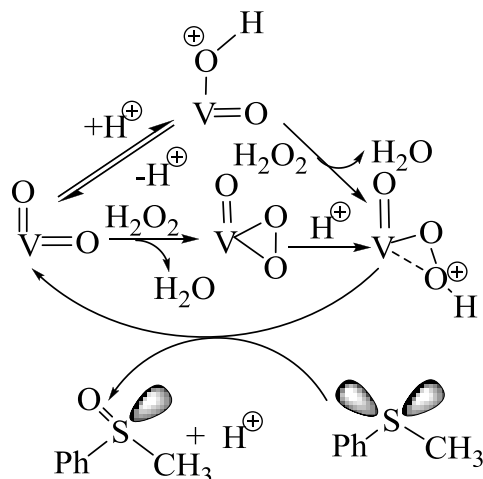
Oxidation of model diesel fuel having different model organic sulfides has also been reported using catalysts PS-[V<sup>IV</sup>O(sal-dmen)(acac)] and PS-[V<sup>V</sup>O<sub>2</sub>(sal-dmen)] and neat dioxidovanadium(V) complex [V<sup>V</sup>O<sub>2</sub>(sal-dmen)]. The 500 ppm concentration of model organosulfur compounds such as thiophene, benzothiophene, dibenzothiophene and 2-methylthiophene was prepared in heptane [46] and 87 - 99% oxidation has been carried out using 30 % H<sub>2</sub>O<sub>2</sub> to substrate molar ratio of 3 : 1 at 60 °C.



**Figure 1.22.** Polymer supported vanadium complexes used to catalyze oxidation of organosulfur compounds.

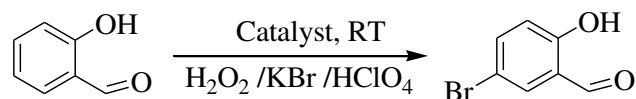
A reaction mechanism proposed for the catalytic oxidation of sulfide is presented in Fig. 1.23. Generally, oxidovanadium(IV) and dioxidovanadium(V) complexes generate oxidoperoxido species on treatment with  $\text{H}_2\text{O}_2$ , followed by a hydroperoxidovanadium(V) complex in the presence of  $\text{H}^+$ . This species enhances the electrophilicity of the peroxido intermediate [47, 48], which is subjected to a nucleophilic attack by the sulfide to give final product. Thus, the sulfur atom of the sulfide is electron rich and undergoes electrophilic oxidation giving sulfoxide.





**Figure 1.23.** Proposed reaction mechanism for oxidation of organic sulfides.

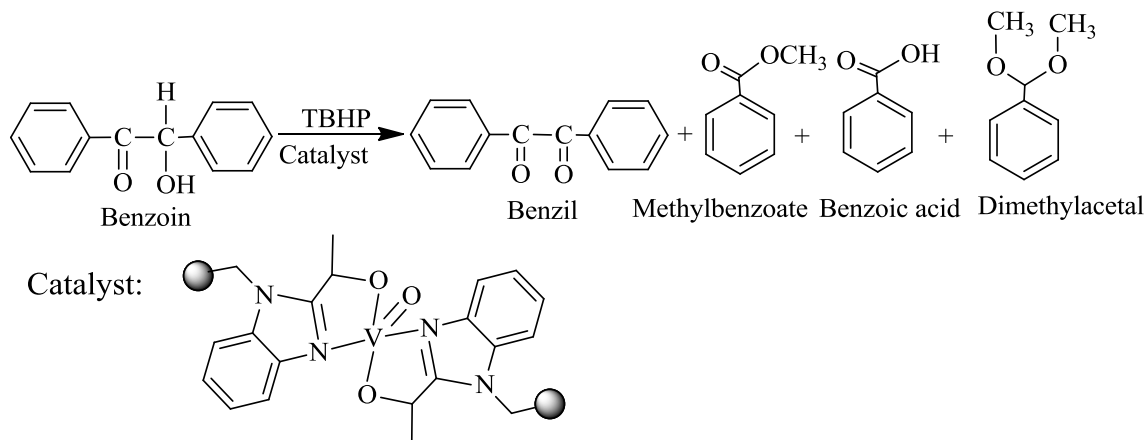
Complexes, PS-K[V<sup>V</sup>O<sub>2</sub>(sal-inh)(im)] and PS-K[V<sup>V</sup>O<sub>2</sub>(sal-bhz)(im)] and PS-[VO(hmbmz)<sub>2</sub>] also catalyze the oxidative bromination of salicylaldehyde using H<sub>2</sub>O<sub>2</sub>/KBr and HClO<sub>4</sub> in water [42, 43]. Under the optimized reaction conditions, a maximum of ca. 85 % conversion of salicylaldehyde by K[V<sup>V</sup>O<sub>2</sub>(sal-inh)(im)] and 82 % by PS-K[V<sup>V</sup>O<sub>2</sub>(sal-bhz)(im)] with ca. 90 % selectivity of 5-bromosalicylaldehyde (Fig. 1.24) was obtained. Complex PS-[VO(hmbmz)<sub>2</sub>] gives 5-bromosalicylaldehyde selectively in quantitative yield. Addition of HClO<sub>4</sub> in four equal portions was suggested to avoid decomposition of catalysts [42]. Several potential polymeric phosphate containing structural haloperoxidase model vanadium complexes have been reported by McLauchlan et al. but no catalytic activity has been tried [49-51].



**Figure. 1.24.** Oxidative bromination of salicylaldehyde.

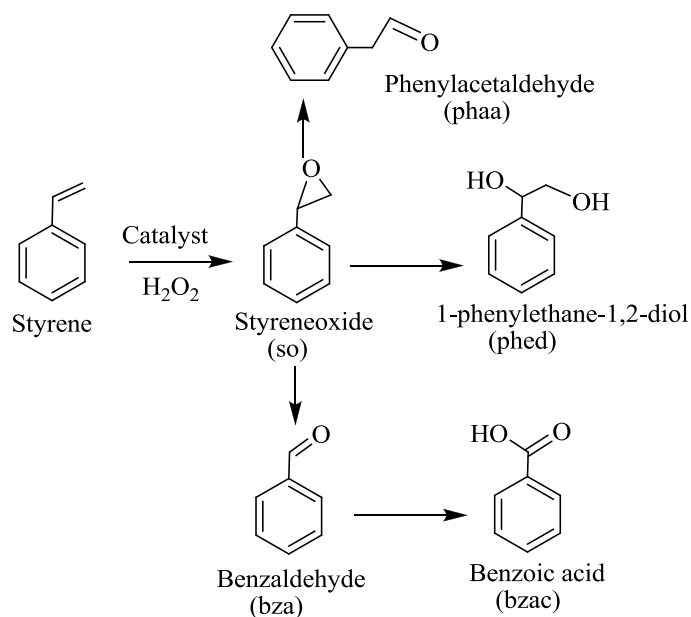
Complexes PS-[VO(hebzmz)<sub>2</sub>] [Hhebzmz = 2-( $\alpha$ -hydroxyethyl)benzimidazole], PS-[V<sup>IV</sup>O(sal-hist)(acac)] and PS-[V<sup>V</sup>O<sub>2</sub>(sal-hist)] have been used as catalyst for the

oxidation of benzoin using *tert*-butylhydroperoxide as an oxidant.; Fig. 1.25. Under the optimized reaction conditions, a maximum of ca. 90 % conversion of the benzoin in 6 h was achieved where selectivity of the obtained reaction products varied in the order: methylbenzoate >benzil >dimethylacetal > benzoic acid [41, 52].

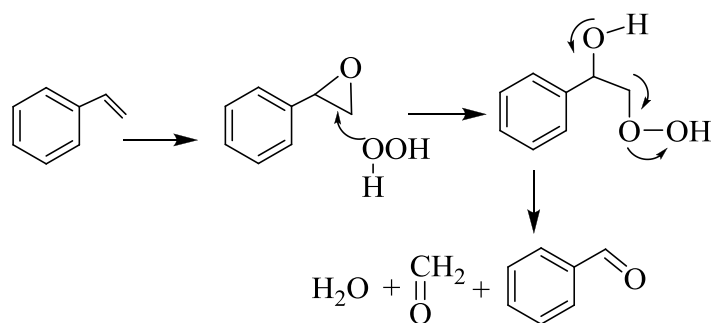


**Figure 1.25.** Oxidation products of benzoin and catalysts used for this reaction.

Oxidation of styrene catalyzed by PS-[V<sup>IV</sup>O(fsal-β-Ala)(DMF)] [33], PS-[VO(hmbmz)<sub>2</sub>] [42], PS-[V<sup>IV</sup>O(fsal-ea)(DMF)], PS-[V<sup>IV</sup>O(fsal-pa)(DMF)] and PS-[V<sup>IV</sup>O(fsal-amp)(DMF)] [53] show mild to good catalytic activity towards the oxidation of styrene in the presence of *tert*-butyl hydroperoxide/ H<sub>2</sub>O<sub>2</sub> and give three to five major products, styrene oxide, benzaldehyde, 1-phenylethane-1,2-diol, phenylacetaldehyde and benzoic acid; Fig. 1.26. The formation of benzaldehyde is highest amongst all these products. Polymer-supported oxidoperoxovanadium(V) complexes of 2-(2-pyridimyl)benzimidazole (2-pybmz) and 2-(3-pyridimyl)benzimidazole (3-pybmz) have also been used as catalyst for the oxidation of styrene using H<sub>2</sub>O<sub>2</sub> as an oxidant [54]. Again the formation of benzaldehyde is highest for these catalyst and is justified by direct oxidative cleavage of the styrene side chain double bond via radical mechanism; Fig.1.27 [55].

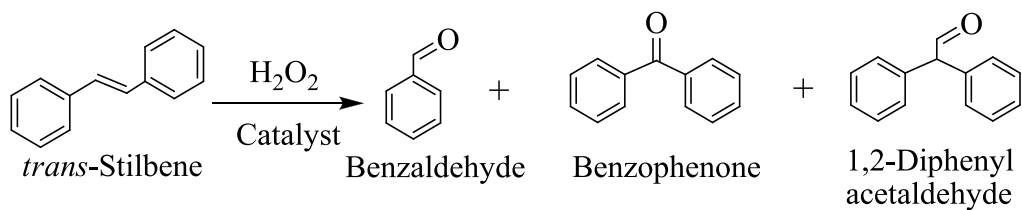


**Figure 1.26.** Various oxidation products of styrene.



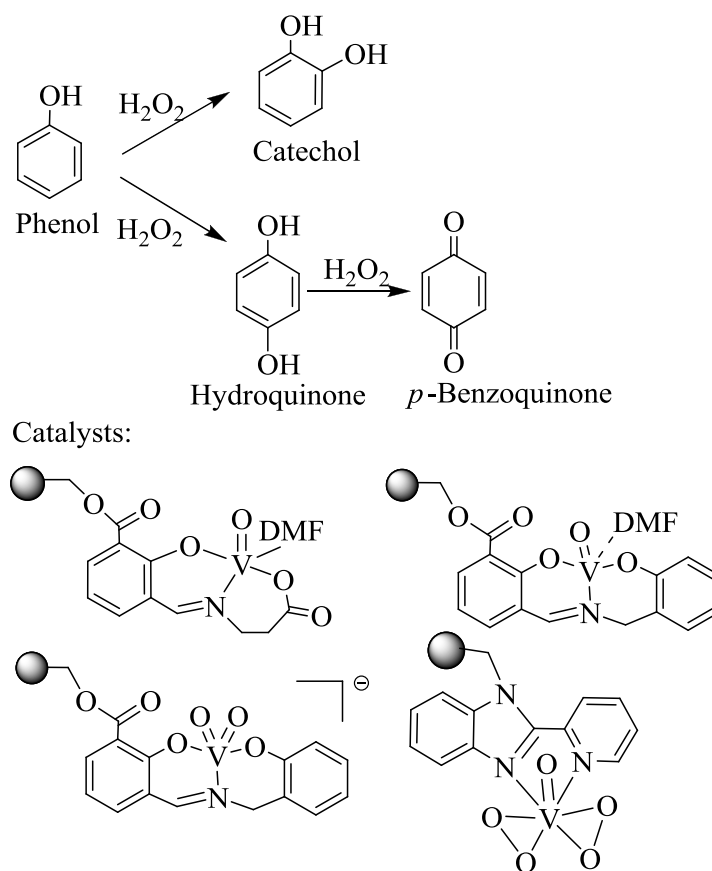
**Figure 1.27.** Proposed reaction mechanism adopted from ref. [55].

The formation of benzaldehyde (97%) along with two more products 1,2-diphenyl acetaldehyde (*ca.* 2 %), and benzophenone (*ca.* 1 %) has also been obtained by the oxidation of *trans*-stilbene using PS-[ $\text{V}^{\text{IV}}\text{O}(\text{fsal}-\beta\text{-Ala})(\text{DMF})$ ] as catalyst in the presence of  $\text{H}_2\text{O}_2$ ; Fig. 1.28. However, over all conversion of *trans*-stilbene was found to be only *ca.* 16 % after 6 h. Under the optimized reaction conditions, no epoxide was detected amongst the reaction products obtained possibly due to its further oxidation to other products [33].



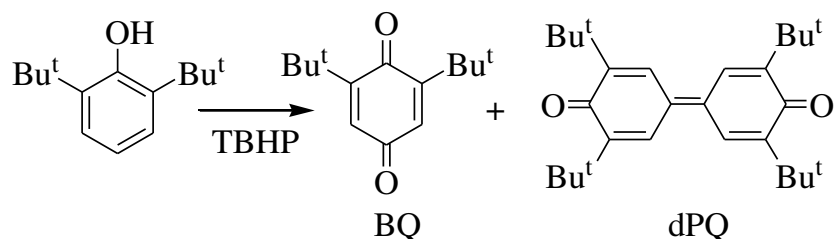
**Figure 1.28.** Reaction products of oxidation of *trans*-stilbene.

Oxidation of phenol and hydroquinone (Fig. 1.29) using polymer-supported complexes PS-[V<sup>IV</sup>O(saldien)] [31], PS-[VO(fsalsalicylate)·DMF], PS-K[VO<sub>2</sub>(fsalsalicylate)] [56], PS-[VO(O<sub>2</sub>)<sub>2</sub>(2-pybmz)] and PS-[VO(O<sub>2</sub>)<sub>2</sub>(3-pybmz)] [54] as catalyst have been carried out. About 35 % of phenol conversion with ~60 % selectivity towards catechol and ~40 % towards *p*-hydroquinone has also been reported. It was observed that solvent plays an important role in altering the selectivity of reaction products. It gives catechol and hydroquinone upon the oxidation of phenol in acetonitrile while in water it is more selective towards catechol and *p*-benzoquinone. At lower temperature (*ca.* 70 °C) *p*-benzoquinone is stable in solution for longer period of time while at higher temperature (*ca.* 80 °C), it polymerizes slowly with the elapse of time. Oxidation of hydroquinone was also found to be pH dependent. Porous methacrylate resin supported vanadium complex of dithiocarbamate catalyzes the oxidation of 2-methylphenol and 2,6-dimethylphenol to the corresponding quinones in presence of *tert*-butyl hydroperoxide [57].



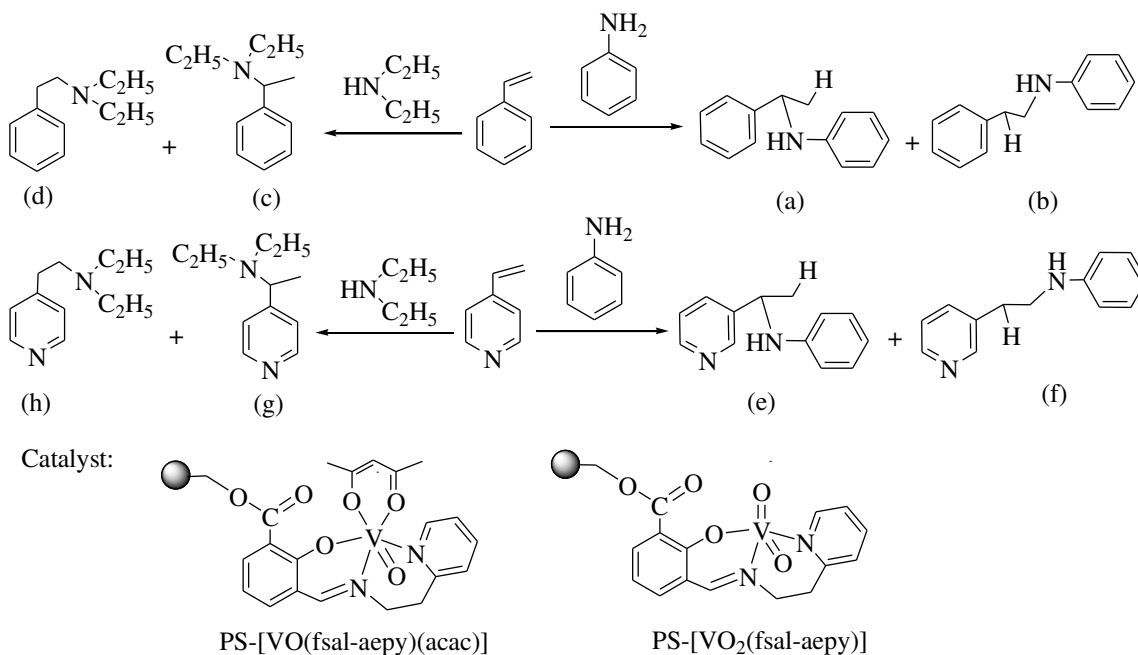
**Figure 1.29.** Oxidation products of phenol and further oxidation of hydroquinone to *p*-benzoquinone.

The oxidation of 2,6-di-*tert*-butylphenol to 2,6-di-*tert*-butylbenzoquinone (BQ) and 3,3',5,5'-tetra-*tert*-butyldiphenoquinone (dPQ) in the presence of *tert*-butylhydroperoxide (Fig. 1.30) [58] has also been carried out using polymer-anchored vanadium(IV) complexes of salicylaldoxime, *N,N'*-bis(salicylidene)-propane-1,3-diamine and *N,N'*-bis(salicylidene)phenyl-1,2-diamine.



**Figure 1.30.** Oxidation of 2,6-di-*tert*-butylphenol.

Maurya et al. have used recyclable PS-[VO(fsal-aepy)(acac)] and PS-[VO<sub>2</sub>(fsal-aepy)] as catalyst for the hydroamination of styrene and vinyl pyridine with amines such as aniline and diethylamine. Two hydroamination products form (Fig. 1.31 as two possible intermediate amino-styrene complexes react in different ways; Fig. 1.32. Amongst the mixture of two hydroaminated products formed under the optimized reaction conditions, the regioselectivity favors the anti-Markownikoff product over the Markownikoff product [59] as this would result in least steric hindrance for the intermediate amino-styrene addition product.

**Figure 1.31.** Products of hydroamination of styrene and vinyl pyridine.

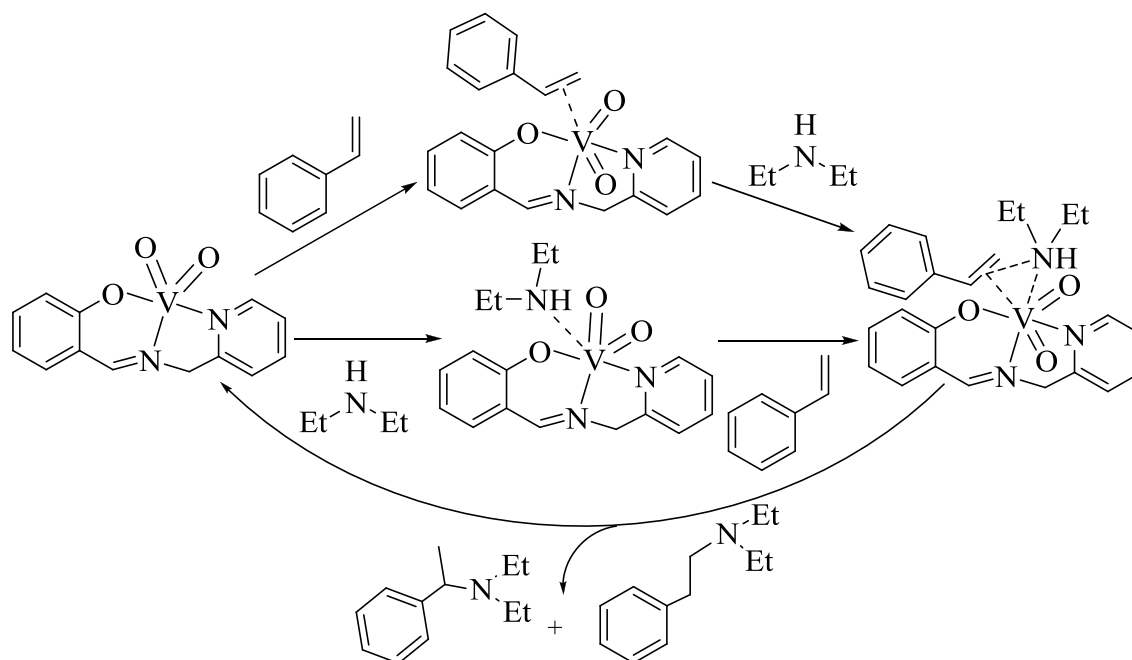


**Figure 1.32.** Possible reaction mechanism for the hydroamination process catalysed by  $[V^V O_2(sal-aepy)]$  considering hydroamination of styrene with diethylamine. Adopted from ref. [59].

Oxidative amination of styrene with diethylamine, imidazole, and benzimidazole in the presence of oxygen and triethylamine has also been reported using catalyst precursor  $PS-[V^{IV}O(sal-cys)(DMF)]$  ( $H_2sal-cys =$  Schiff base derived from salicylaldehyde and cysteine). Fig. 1.33 presents the reaction products obtained [60]. Again, under the optimized reaction conditions, the anti-Markownikoff product was favoured over the Markownikoff one due to the presence of steric hindrance.

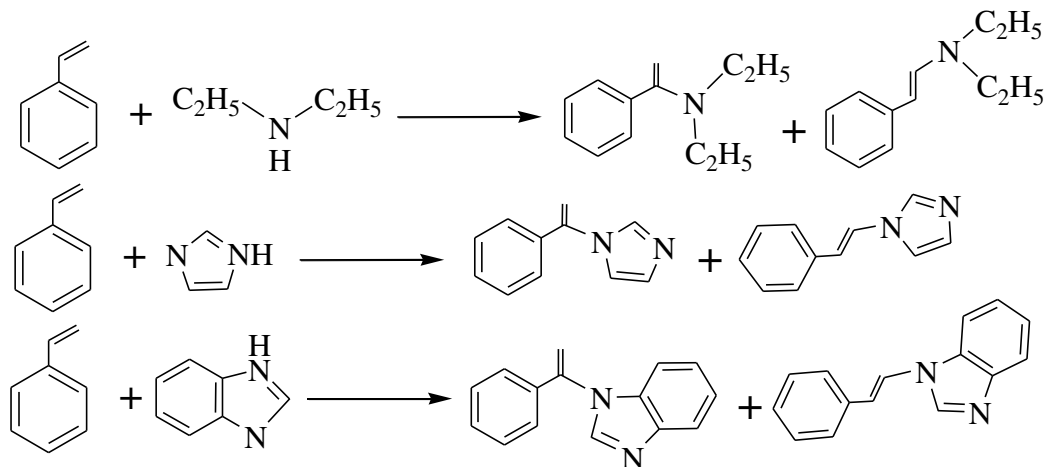


**Figure 1.33.** Oxidative amination of styrene with diethylamine, imidazole, and benzimidazole using catalyst precursor PS-[V<sup>IV</sup>O(sal-cys)(DMF)].

Catalytic activity of PS-[V<sup>IV</sup>O(fsal-DL-ala)(H<sub>2</sub>O)], PS-[V<sup>IV</sup>O(fsal-L-ile)(H<sub>2</sub>O)] [34] and PS-[V<sup>IV</sup>O(fsal-β-ala)(DMF)] [33] towards the oxidation of cyclohexene in presence of H<sub>2</sub>O<sub>2</sub>/ tert-butylhydroperoxide have been studied. The oxidation of cyclohexene gave at least four oxidized products, cyclohexeneoxide, 2-cyclohexene-1-ol, 2-cyclohexene-1-one and cyclohexene-1,2-diol; Fig. 1.34. Catalyst PS-[V<sup>IV</sup>O(ligand)<sub>n</sub>] (ligand = 2-thiomethylbenzimidazole) also catalyzes the oxidation of cyclohexene efficiently and gives 86% conversion with all these products mentioned above [61].

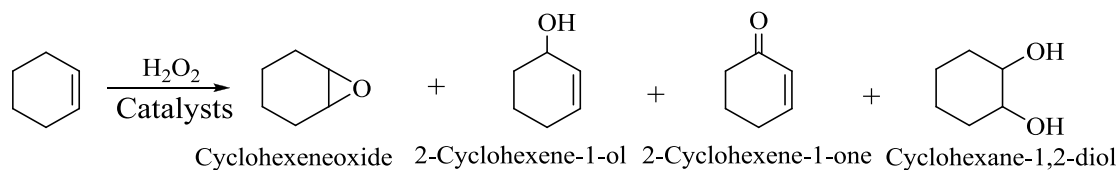


**Figure 1.34.** Various oxidation products of cyclohexene.

Dioxidovanadium(V) complexes K[V<sup>V</sup>O<sub>2</sub>(sal-inh)(H<sub>2</sub>O)] and K[V<sup>V</sup>O<sub>2</sub>(sal-bhz)(H<sub>2</sub>O)] react with imidazolomethylpolystyrene (PS-im) in DMF to give the imidazolomethylpolystyrene bound complexes PS-K[V<sup>V</sup>O<sub>2</sub>(sal-inh)(im)] and PS-



$K[V^V O_2(\text{sal-bhz})(\text{im})]$ , respectively; Fig. 1.35 [43]. These complexes have been used for the oxidative bromination of salicylaldehyde.

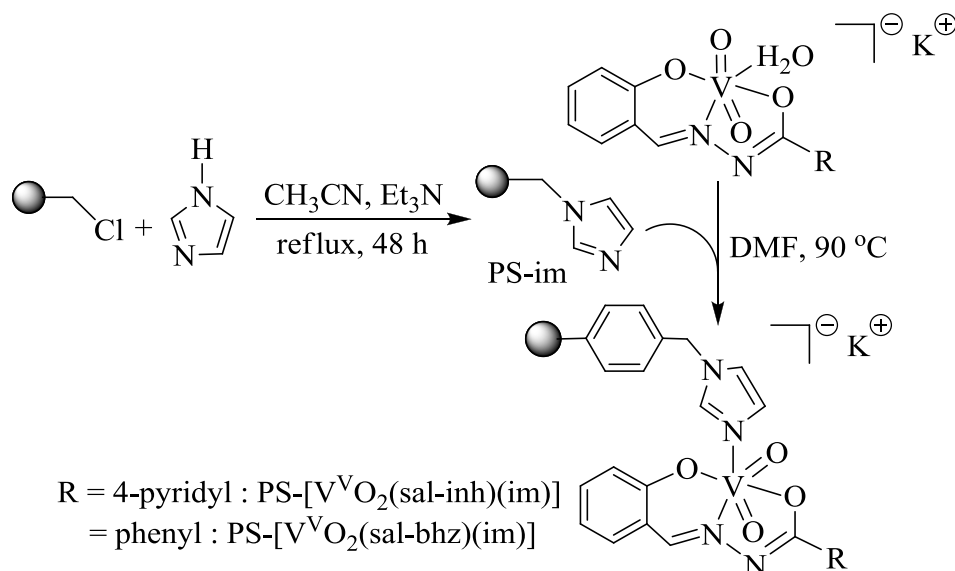
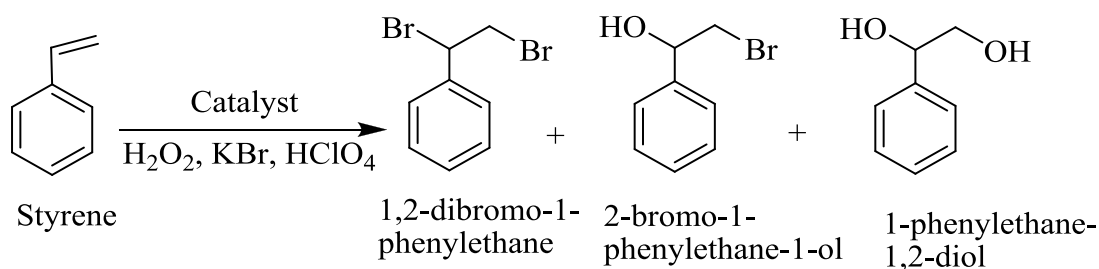
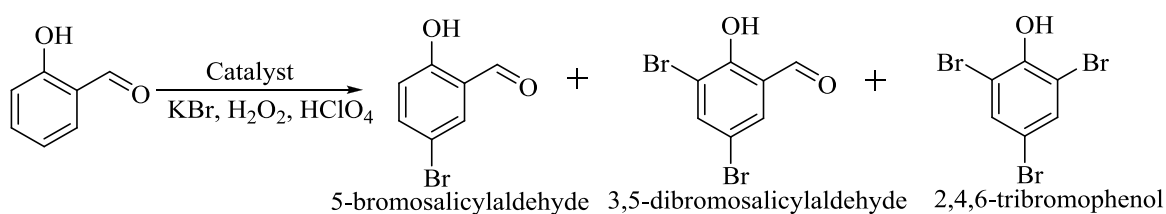


**Figure 1.35.** Formation of  $\text{PS-K}[V^V O_2(\text{sal-inh})(\text{im})]$  and  $\text{PS-K}[V^V O_2(\text{sal-bhz})(\text{im})]$ .

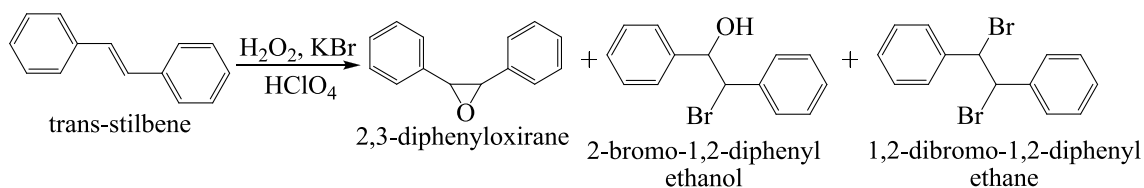
Similarly prepared polymer-grafted dioxidovanadium(V) complexes,  $\text{PS-im}[V^V O_2(\text{pan})]$  (4),  $\text{PS-im}[V^V O_2(\text{acpy-bhz})]$ ,  $\text{PS-im}[V^V O_2(\text{acpy-inh})]$  and  $\text{PS-im}[V^V O_2(\text{acpy-nah})]$  (Fig. 1.36) have been used for the oxidative bromination of styrene, salicylaldehyde and *trans*-stilbene [62, 63]. Various parameters, such as amounts of catalyst, oxidant (aqueous 30 %  $\text{H}_2\text{O}_2$ ),  $\text{KBr}$  and aqueous 70%  $\text{HClO}_4$  have been optimized to obtain the maximum oxidative bromination of substrates. Styrene, under the optimized reaction conditions, gave a maximum of 99 % conversion after 2 h of reaction and the reactions products follow the following selectivity order: 1-phenylethane-1,2-diol (75%) > 2-bromo-1-phenylethane-1-ol (20%) > 1,2-dibromo-1-phenylethane (1.2%). With almost similar conversion in similar reaction time, oxidative bromination of salicylaldehyde gave three products with the selectivity order: 5-bromosalicylaldehyde > 2,4,6-tribromophenol > 3,5-dibromosalicylaldehyde. About 91 % conversion of *trans*-stilbene has been obtained in 3 h of reaction time where selectivity of the products follows the order: 2,3-diphenyloxirane (*trans*-stilbene oxide) > 1,2-dibromo-1,2-diphenylethane > 2-bromo-1,2-diphenylethanol.



(a) Oxidative brominated products of styrene.



(b) Oxidative brominated products of salicylaldehyde.



(c) Oxidative brominated products of *trans*-stilbene.

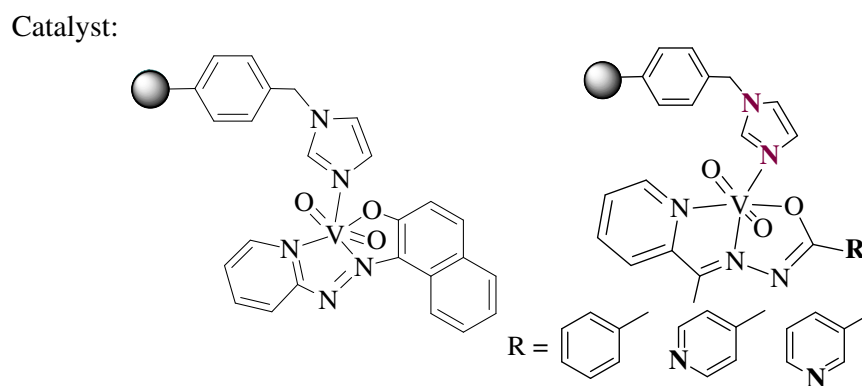


**Figure 1.36.** Catalytic reactions and catalysts used.

Polymer-supported catalysts, PS-im[V<sup>V</sup>O<sub>2</sub>(bzpy-tch)(MeOH)] and PS-im[V<sup>V</sup>O<sub>2</sub>(bzpy-inh)(MeOH)] have been used for the catalytic oxidation of isoeugenol using aqueous H<sub>2</sub>O<sub>2</sub> as oxidant; Fig. 1.37. The intermediate peroxido species, expected to be involved during catalytic action, were also generated from the corresponding neat complexes and studied by UV-Vis and <sup>51</sup>V NMR. Under the optimized reaction conditions, the consumption of isoeugenol and formation of various products using PS-im[V<sup>V</sup>O<sub>2</sub>(bzpy-inh)] as catalyst follow the patterns as shown in Fig. 1.38 [64].

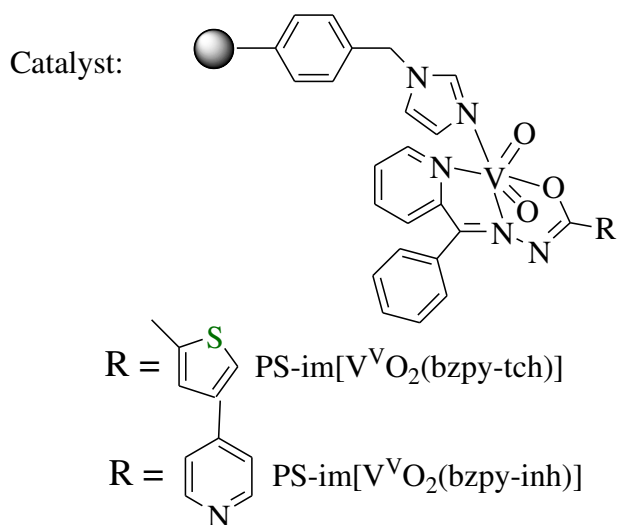
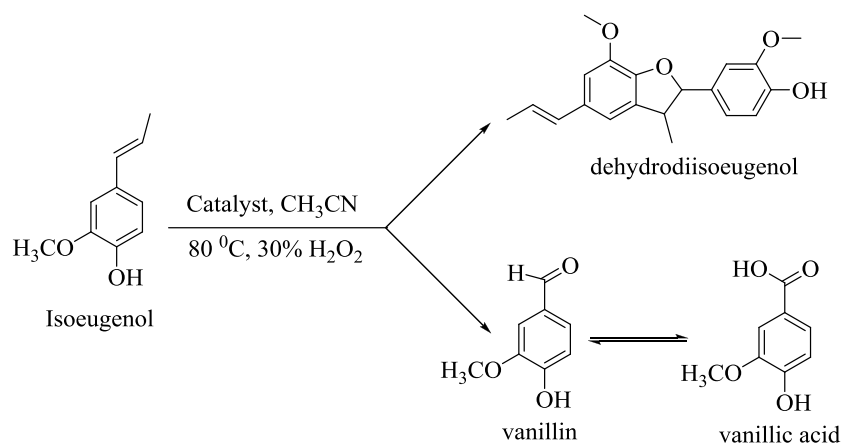


**Figure 1.37.** Oxidation products of isoeugenol using PS-im[V<sup>V</sup>O<sub>2</sub>(bzpy-inh)(MeOH)] and PS-im[V<sup>V</sup>O<sub>2</sub>(bzpy-tch)(MeOH)] as catalyst.

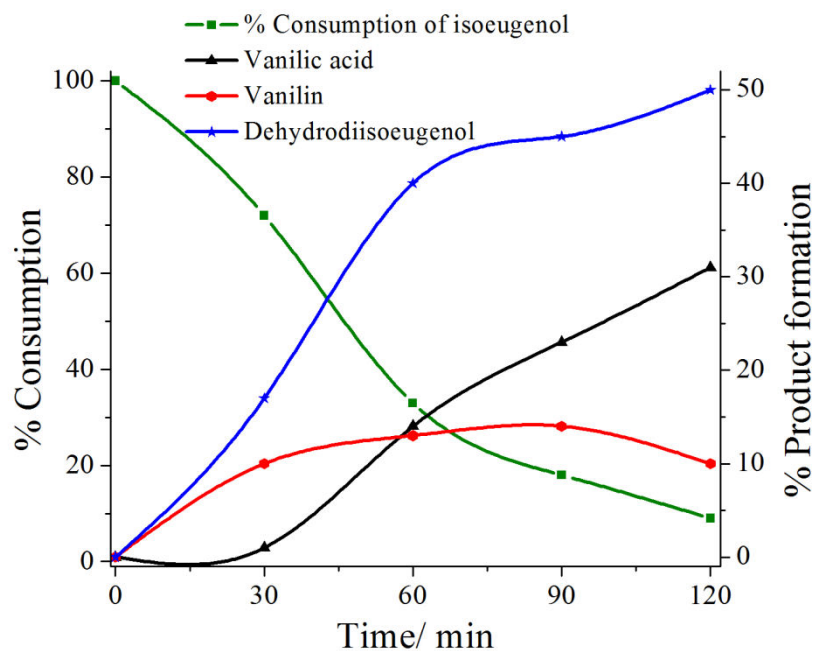


**Figure.1.38.** Percentage consumption of isoeugenol and formation of products with time using PS-im[V<sup>V</sup>O<sub>2</sub>(bzpy-inh)] as catalyst precursor under the optimized conditions. Adopted from ref. [64].

The polymer-supported oxidovanadium(IV) complex PS-[V<sup>IV</sup>O(sal-dahp)] (H<sub>3</sub>sal-dahp = dibasic pentadentate ligand derived from salicylaldehyde and 1,3-diamino-2-hydroxypropane) has been used for the oxidation of pyrogallol to purpurogallin at pH 7 buffered solution; Fig. 1.39 [65]. Based on various unique characteristics such as high peroxidase mimicking ability of the catalyst its stability in a wide pH range, the easy separation from the reaction media, and the reusability without considerable decrease in activity, this heterogeneous catalyst has been recommended for industrial application.

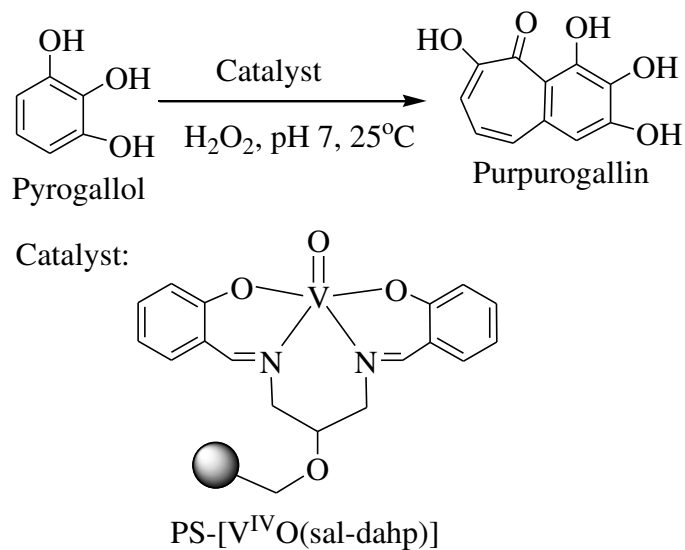


**Figure 1.39.** Oxidation of pyrogallol to purpurogallin catalyzed by PS-[V<sup>IV</sup>O(sal-dahp)].

### 1.5. Polymer-supported molybdenum complexes

Polymer-supported molybdenum complexes have also been prepared and used as catalysts for various reactions [24]. Oxidation of styrene catalyzed by polymer-anchored complex PS-[Mo<sup>VI</sup>O<sub>2</sub>(fsal-ohyba)·DMF] gives five oxidation products but the overall conversion is only 17.5 %; Fig. 1.40. The selectivity of the reaction products under optimized reaction conditions is in the order: benzaldehyde (64.0 %) > 1-phenylethane-1,2-diol (16.4 %) > benzoic acid (8.7 %) > phenylacetaldehyde (4.8 %) > styrene oxide (4.2 %) [32]. The poor catalytic action of the catalyst has been explained as difficulty in transferring oxygen from the intermediate peroxido complex to the substrate [56]. The polymer-anchored complex [PS-[Mo<sup>VI</sup>O<sub>2</sub>(hpbmz)<sub>2</sub>] shows little better activity (23.4%) and gives all these products in almost similar selectivity [42].

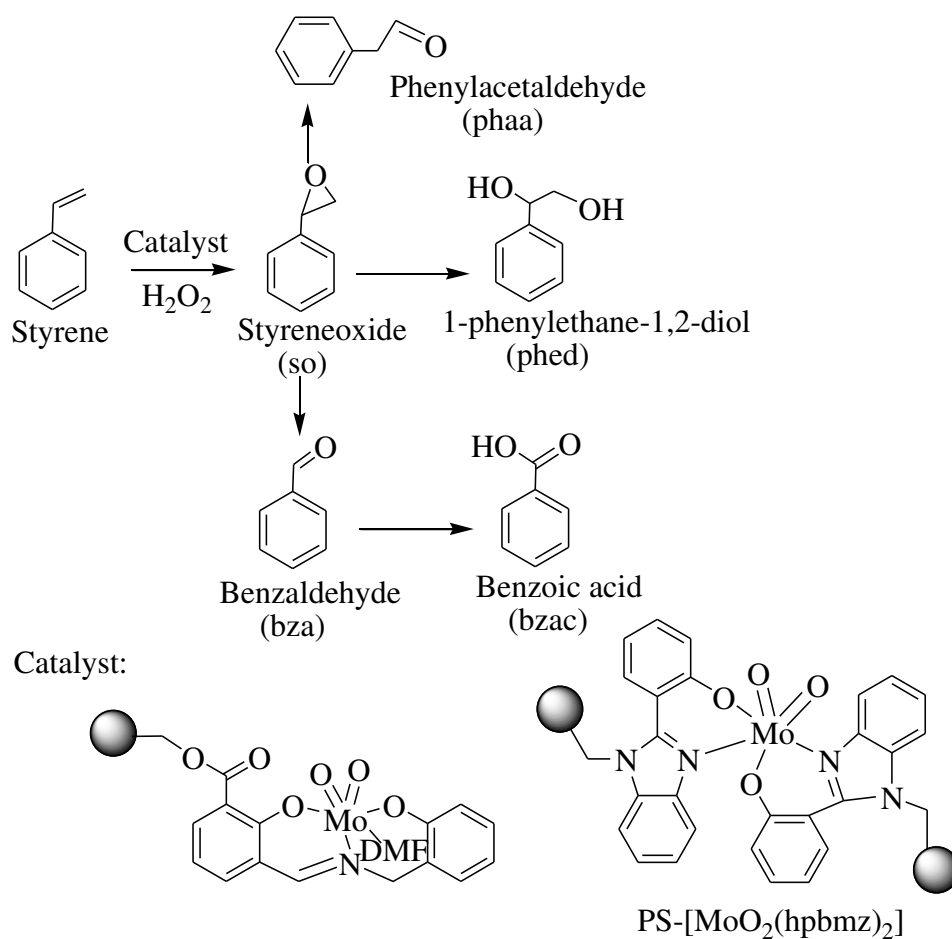


**Figure 1.40.** Oxidation products of styrene.

The oxidation of phenol in  $\text{CH}_3\text{CN}$  catalyzed by PS-[Mo<sup>VI</sup>O<sub>2</sub>(fsal-ohyba)·DMF] using  $\text{H}_2\text{O}_2$  as an oxidant gave two major products, catechol and *p*-hydroquinone. The overall conversion of phenol is very low (ca. 10%) at 80 °C with 59 % selectivity towards catechol and 39 % towards *p*-hydroquinone [56].

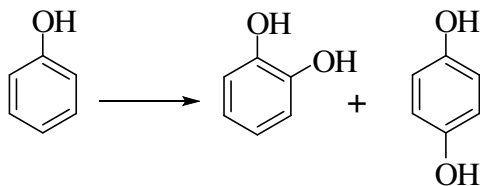


**Figure 1.41.** Oxidation products of phenol.

Catalyst PS-[Mo<sup>VI</sup>O<sub>2</sub>(fsal-ohyba)·DMF] also catalyzes the oxidative bromination where 92 % conversion of salicylaldehyde with 83 % selectivity towards 5-bromosalicylaldehyde and 17% towards 3,5-dibromosalicylaldehyde using H<sub>2</sub>O<sub>2</sub> / KBr in the presence of H<sub>2</sub>SO<sub>4</sub> in aqueous solution with the turn over frequency of 213 h<sup>-1</sup> has been achieved [56].

Catalysts PS-[Mo<sup>VI</sup>O(O<sub>2</sub>)<sub>2</sub>(2-pybmz)] and PS-[Mo<sup>VI</sup>O(O<sub>2</sub>)<sub>2</sub>(3-pybmz)] , lose one of the peroxy groups at elevated temperature ( ca. 80 °C) but catalyze the oxidation of styrene in only 3.8 – 6.6 % conversion in the presence of TBHP. This conversion could slightly be improved (13.5 to 16.5 %) with aqueous 30 % H<sub>2</sub>O<sub>2</sub> but the obtained high selectivity of styrene oxide with TBHP (42.7 – 51.2 %) reduced considerably (7.5 – 13.2 %) [54].

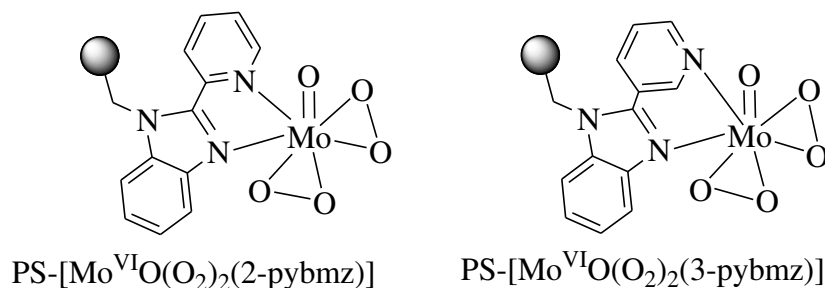


**Figure 1.42.** Structure of PS-[Mo<sup>VI</sup>O(O<sub>2</sub>)<sub>2</sub>(2-pybmz)] and PS-[Mo<sup>VI</sup>O(O<sub>2</sub>)<sub>2</sub>(3-pybmz)].

Dioxidomolybdenum(VI) complexes of 2-aminomethylpyridine functionalized poly(styrene-divinylbenzene) with 53 % amination (abbreviated as PS.AMP.Mo1) and with 90 % amination (abbreviated as PS.AMP.Mo2), and polybenzimidazole (abbreviated as PBI.Mo) have used as catalyst in the epoxidation reactions e.g. the epoxidation of cyclohexene, 1-octene, limonene and  $\alpha$ -pinene using dry TBHP as oxidant; Fig. 1.43. Small amount of leaching of Mo in case of PS.AMP.Mo1 was observed during catalytic cycle while others are highly active and selective in 10 consecutive reactions [66, 67, 68].

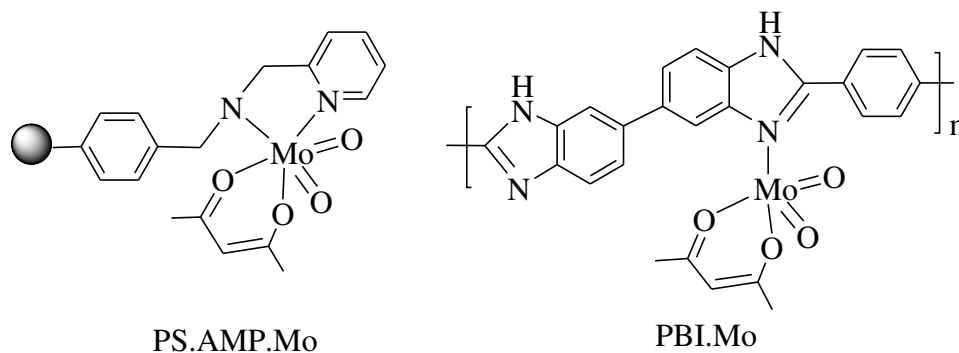


**Figure 1.43.** Proposed structures of polystyrene and polybenzimidazole bound  $\text{Mo}^{\text{VI}}$  complexes. Only idealized structural units are shown.

The oxidation of alkenes e.g. 1-octene, cyclooctene, (*Z*)-cyclododecene, (*E*)-cyclododecene, (*Z*)-2-hexen-1-ol, (*E*)-2-hexen-1-ol, (*Z*)-stilbene and (*E*)-stilbene using polymer supported dioxidomolybdenum(VI) catalysts, PS- $\text{MoO}_2(\text{acac})$  and PS- $\text{MoO}_2(\text{MT})$  and oxidant TBHP have also been reported and they give corresponding epoxide selectively in high yield in toluene [69]. The *E* and *Z* configurations are retained in the corresponding epoxides of olefins.

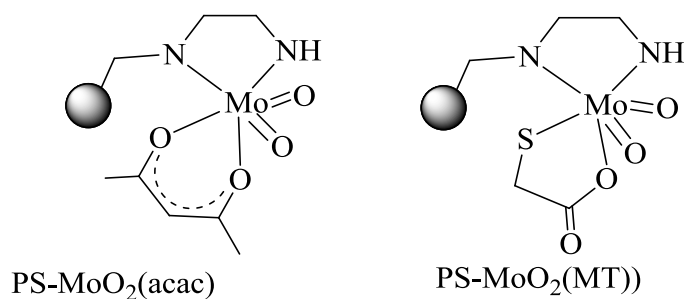


**Figure 1.44.** Idealized structures of catalyst PS- $\text{MoO}_2(\text{acac})$  and PS- $\text{MoO}_2(\text{MT})$  ref. [69].



Molybdenum pentacarbonyl derived polymer supported catalysts (PS-[(im)Mo<sup>0</sup>(CO)<sub>5</sub>], PS-[(dpm)Mo<sup>0</sup>(CO)<sub>5</sub>] (dpm = methylenediphosphine), PS-[(dpe)Mo<sup>0</sup>(CO)<sub>5</sub>] (dpe = ethylene diphosphene) [40, 70], PS-[(pipz)Mo<sup>0</sup>(CO)<sub>5</sub>] (pipz = piperazine) and other related catalysts, PS-[(en)Mo<sup>0</sup>(CO)<sub>4</sub>] (en = ethane-1,2-diamine), PS-[(detn)Mo<sup>0</sup>(CO)<sub>3</sub>] (detn = N<sup>1</sup>-(2-aminoethyl)ethane-1,2-diamine) covalently bonded to polystyrene have also been prepared similarly and characterized [71, 72, 73]. These catalysts are excellent in the epoxidation of various terminal alkenes. The polymer-supported bis(2-hydroxylanyl)acetylacetonate dioxidomolybdenum(VI) prepared as shown in Fig. 1.46 is also highly active and selective in the epoxidation of various alkenes in the presence of tert-butyl hydroperoxide (TBHP) in CCl<sub>4</sub> [74].

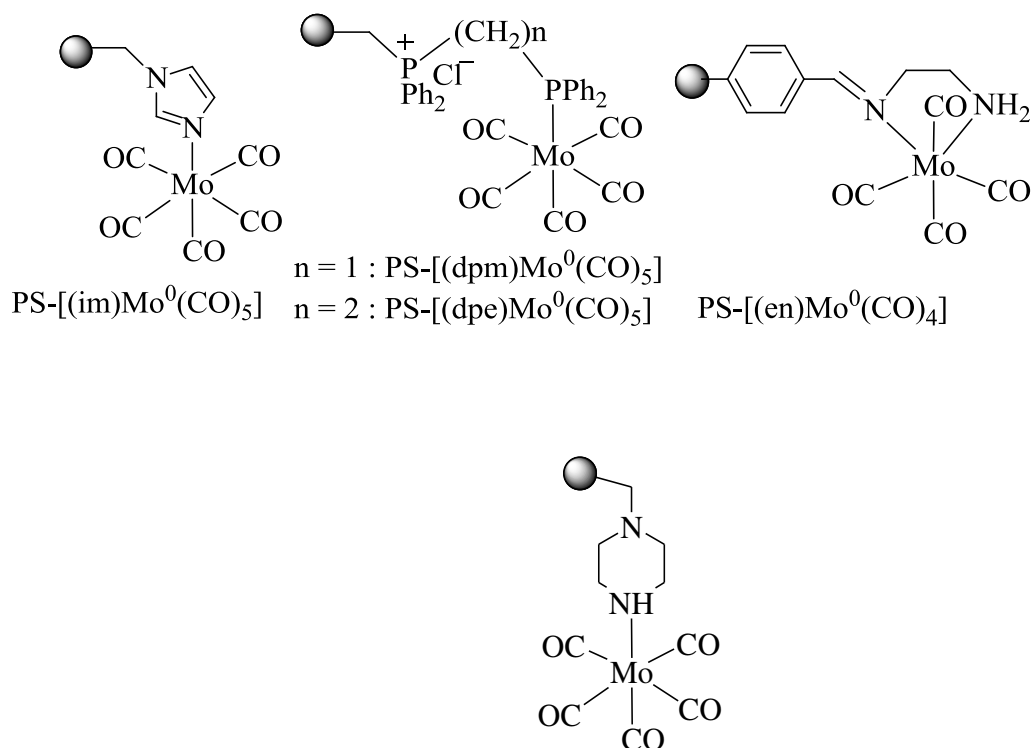


**Figure 1.45.** Various polymer supported molybdenum carbonyl based catalysts.

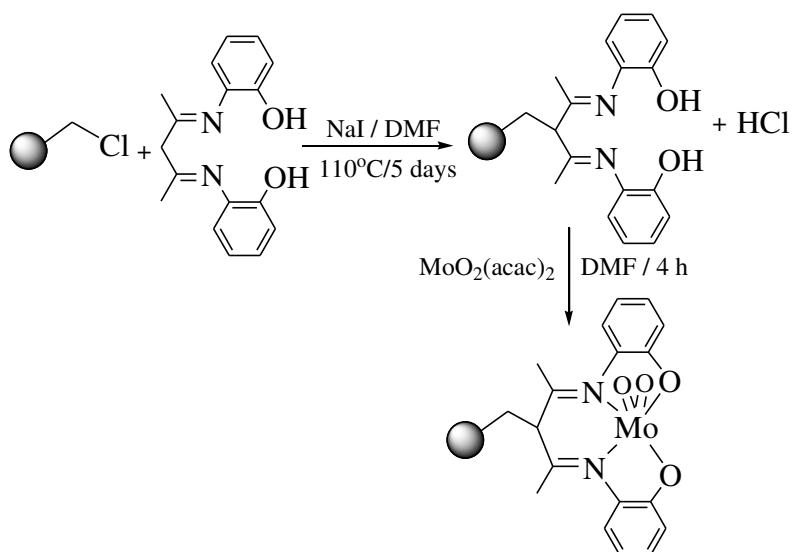


**Figure 1.46.** Preparation of polymer-supported bis(2-hydroxyphenyl)acetylacetonone dioxidomolybdenum(VI) catalyst.

The polymer supported catalysts,  $\text{PS}[\text{MoO}_2(\text{O}_2)(\text{L})_2]^{2-}$  ( $\text{L} = \text{valine}$  or  $\text{alanine}$ ) and ( $\text{PS} = \text{Merrifield resin}$ ) has been used for the oxidation of various sulphides. With the isolated yield of more than 95% in most cases, the obtained products are respective sulfoxide and sulfone [75].

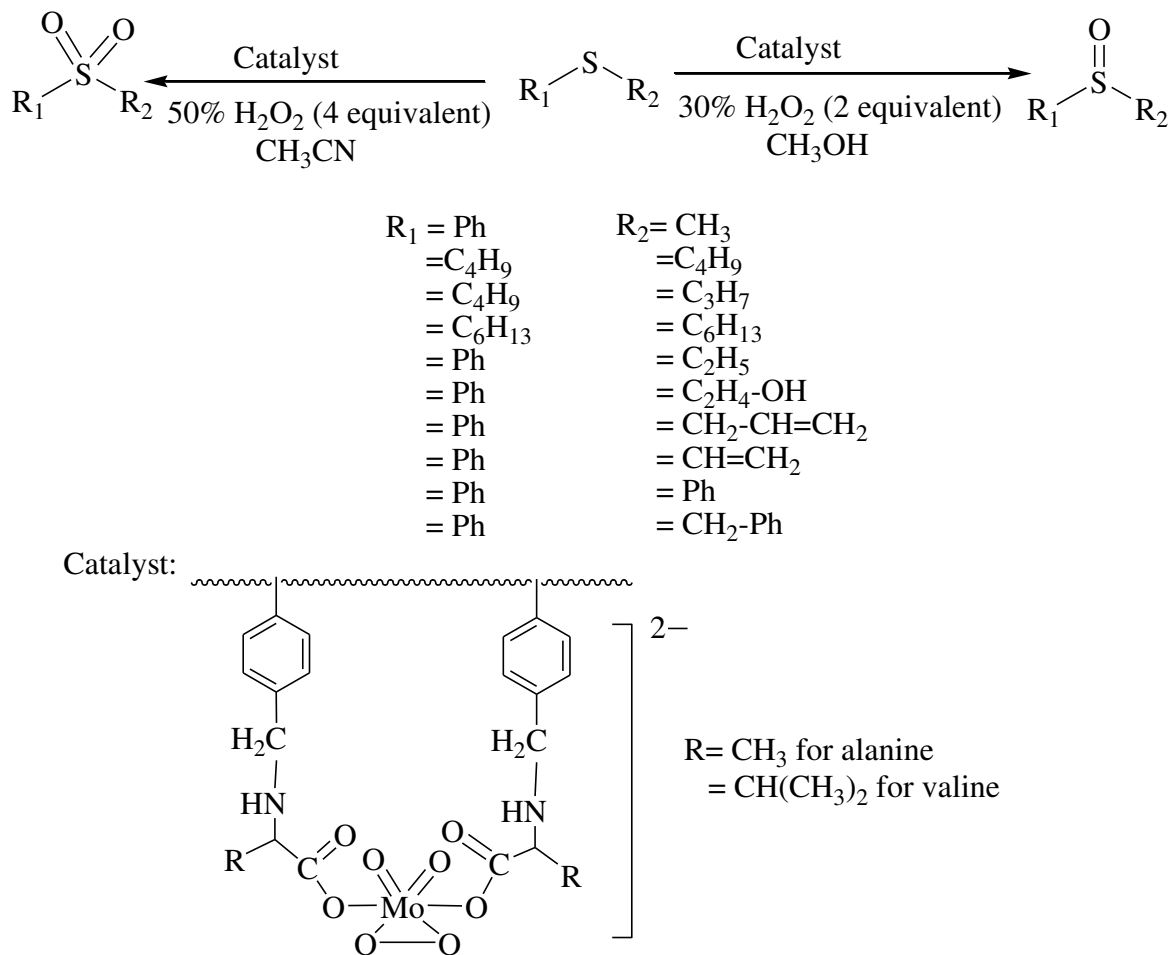


**Figure 1.47.** Merrifield resin supported molybdenum complexes (“*wavy*” represents polymer chain) for the oxidation of organic sulfides.

Catalytic epoxidation of geraniol has also been carried out by chiral Mo<sup>VI</sup> – complexes (Fig. 1.48) immobilized on chloromethylated polystyrene [76]. The yields as well as ee are poor and the polymer catalysts are unstable.

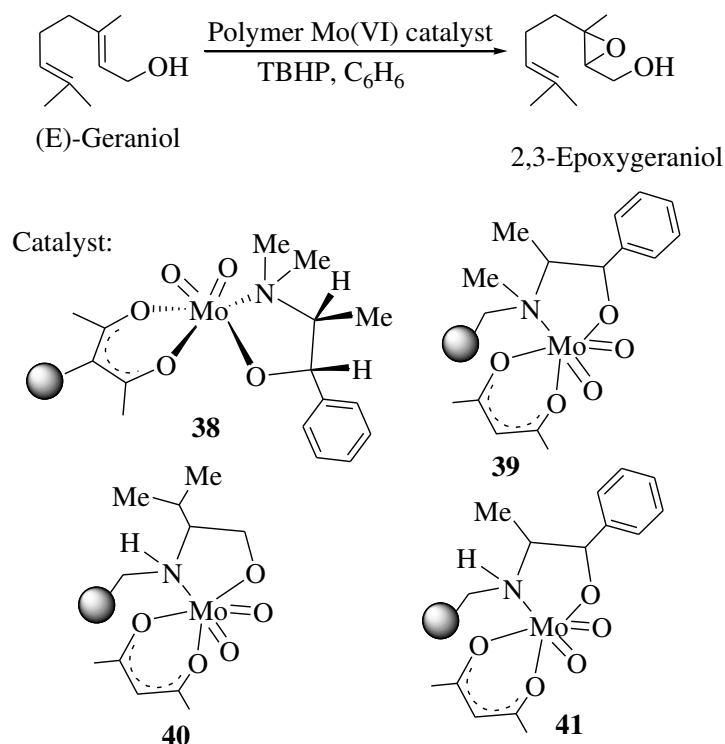


**Figure 1.48.** Chiral dioxidomolybdenum(VI) complexes used for the oxidation of geraniol ref. [76].

Polymeric resin (XAD-4) and alumina (A) supported molybdenum complexes XAD-[Mo<sup>VI</sup>O<sub>2</sub>(salphen)], XAD-[Mo<sup>VI</sup>O<sub>2</sub>(saloxim)<sub>2</sub>], A-[Mo<sup>VI</sup>O<sub>2</sub>(salphen)] and XAD-[Mo<sup>VI</sup>O<sub>2</sub>(saloxim)<sub>2</sub>] are selective for benzil formation by the oxidation of benzoin in the presence of TBHP [77]. Using catalyst XAD-[Mo<sup>VI</sup>O<sub>2</sub>(saloxim)<sub>2</sub>], the selectivity of benzil is as high as 42.8 %. Other products are methylbenzoate (with 9.7 % selectivity) and benzoic acid (with 25.7 % selectivity) with 78.0 % conversion of benzoin. The catalytic activity of alumina supported complexes are poor than XAD supported.

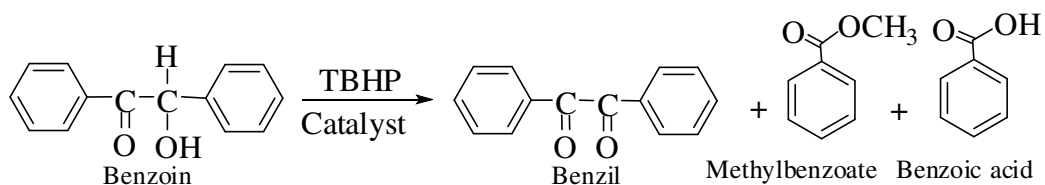


**Figure 1.49.** Oxidation products of benzoin using XAD supported molybdenum complexes.

A poly(acrylonitrile) (PAN) based supported peroxidomolybdate(VI) compound, PAN- [MoO<sub>2</sub>(O<sub>2</sub>)] was obtained by reacting polymer with H<sub>2</sub>MoO<sub>4</sub> in the presence of 30% H<sub>2</sub>O<sub>2</sub> at nearly neutral pH. Its catalytic activity in the oxidative bromination of organic substrates (aniline, p-aminophenol, m-aminophenol, o-aminophenol, p-nitroaniline, m-nitroaniline, o-nitroaniline, quinol, pyrogallol, resorcinol, acetanilide, salicylaldehyde, o-methoxytoluene and catechol) has been carried out [78] Fig. 1.50. The yield of the brominated products is extremely high in all cases and catalyst is recyclable. [Mo<sub>2</sub>O<sub>2</sub>(O<sub>2</sub>)<sub>4</sub>(carboxylate)]-PA [PA = poly-(sodium acrylate)], [MoO(O<sub>2</sub>)<sub>2</sub>(carboxylate)]-PMA [PMA = poly(sodium methacrylate)] and [MoO(O<sub>2</sub>)<sub>2</sub>(amide)]-PAm [PAm = poly(acrylamide)] have also been isolated and characterized but their catalytic properties have not been explored [79].

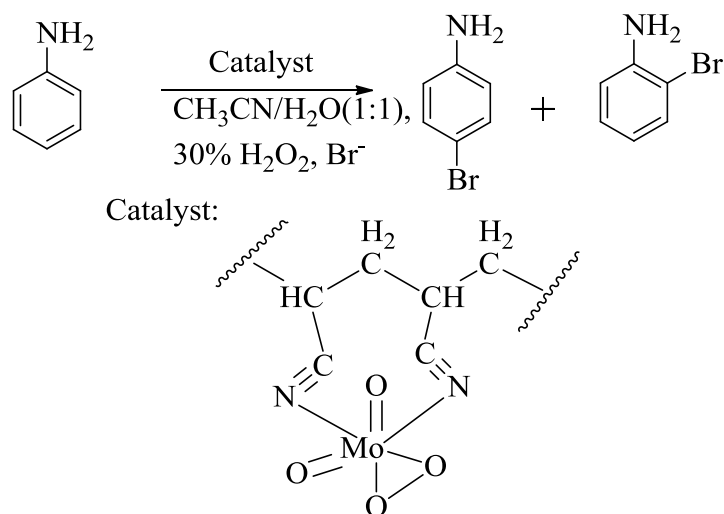


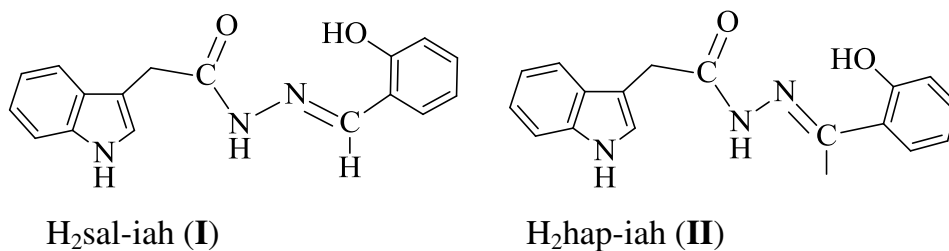
**Figure 1.50.** Example of oxidative bromination of organic substrate.

Immobilized complex P-[Mo(CO)<sub>3</sub>(4-VP)<sub>3</sub>] is an effective catalyst for the hydrogenation of styrene to ethylbenzene by H<sub>2</sub> in 2-ethoxyethanol in the presence of PPh<sub>3</sub>. The addition of PPh<sub>3</sub> is to generate the mixed carbonyl/phosphine Mo immobilized species which is, in fact, the catalytically active species. The catalyst is highly resistant to decomposition without significant loss of metal ion from the system over several runs [19].

## 1.6. OBJECTIVE OF THE PRESENT INVESTIGATION

It is clear from the review of the literature that polymer supported vanadium and molybdenum complexes have provided opportunities to explore effective catalysts for oxidation, sulfoxidation, oxidative halogenation etc. for various substrates. However, impact of insertion of spacer between polymer support and catalyst has been less explored. Such spacer may allow the better interaction of catalytic center with substrates and oxidant during catalytic reaction which may results in improved catalytic potential. Further, in most catalytic reactions optimization of the reaction conditions for highest performance of catalysts have not been considered. It was, therefore, reasonable to undertake systematic study on the synthesis and characterization of new polymer-supported vanadium and molybdenum complexes with spacer, and to explore their catalytic potential under optimized reaction conditions.

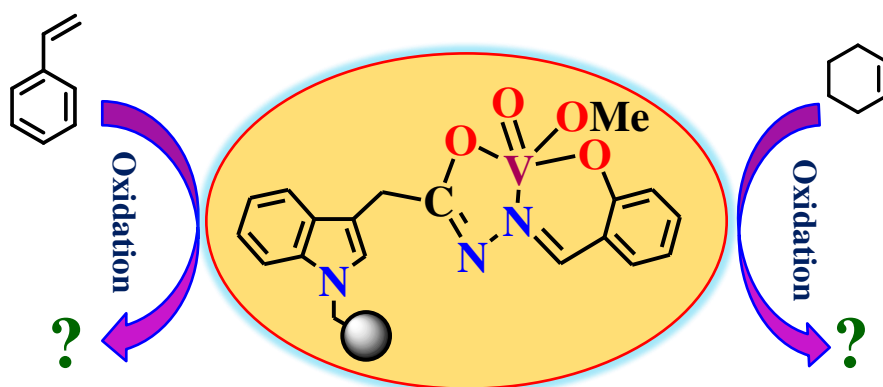
Present study is aimed to describe the synthesis of oxidovanadium(IV), oxidomethoxidovanadium(V) and dioxidomolybdenum(VI) complexes of the following ligands covalently bonded to the chloromethylated polystyrene:



Synthesized complexes have been characterized by chemical, spectral (IR, electronic, EPR and NMR) and thermal studies, scanning electron micrographs and atomic force microscopic imaging. Catalytic potential of these complexes have been explored for various organic transformations. Where ever possible corresponding neat complexes have also been prepared and their catalytic potentials have been compared with the supported ones.

# CHAPTER 2

Chloromethylated polystyrene cross-linked with divinylbenzene and grafted with vanadium(IV) and vanadium(V) complexes having ONO donor ligand for the catalytic activity



PS-[VO(OMe)(sal-iah)] as catalyst

## 2.1. Introduction

The immobilization of catalysts on solid support has attracted attention of researchers because this allows the design of thermally more stable catalysts and environment-friendly synthetic routes to fine chemicals. This way expensive homogeneous catalyst also become separable from the reaction mixture by simple filtration and meets the industrial demand of recyclability which in turn improves the efficiency of the catalyst [80-83]. Several strategies have been put forward on immobilization of homogeneous catalysts. Even review articles highlight some of these methods and explore the catalytic activities of such immobilized metal complexes [84,23-26]. Our effort using chloromethylated polystyrene cross-linked with divinyl benzene (PS-CH<sub>2</sub>Cl) as a solid support to immobilize vanadium complexes and explore their catalytic potential for organic transformations offer some real prospects for the development of more environmentally benign synthetic routes to fine chemicals leading to technological applications [25,26]. Here in, we report polymer-grafted oxidovanadium(IV) and oxidomethoxido vanadium(V) complexes of the indole-derived ONO donor ligand PS-H<sub>2</sub>sal-iah (**I**, Scheme 2.1) for the oxidation of styrene and cyclohexene. Additional methylene group attached to hydrazone moiety in combination with covalent bonding through ring nitrogen of indole will act as spacer and hence would enhance the availability of grafted complexes on the surface of the polymer which may allow better interaction of substrates and oxidant with metal center during catalytic reaction. The corresponding non polymer-grafted vanadium complexes have also been prepared for comparison of their catalytic performance.



## 2.2. Experimental

### 2.2.1. Materials

Chloromethylated polystyrene [18.9 % Cl (5.35 mmol Cl per gram of resin)] cross-linked with 5 % divinylbenzene was obtained from Thermax Limited, Pune, India. Analytical reagent grade  $V_2O_5$ , salicylaldehyde, cyclohexene (Sisco, India), indole-3-acetic hydrazide, styrene (Aldrich, USA) and 30 % aqueous  $H_2O_2$ , (Rankem, India) were used as obtained.  $[V^{IV}O(acac)_2]$  was prepared according to method reported in the literature [85]. Other chemicals and solvents of analytical reagent grades were used without purifications.

### 2.2.2. Physical methods and analysis

Elemental analyses of the complexes were obtained with an Elementar model Vario-EL-III. Vanadium content in polymer-grafted complexes was obtained by Inductively Coupled Plasma spectrometry (ICP; Labtam 8440 plasma lab). Thermogravimetric analyses of the complexes were carried out using Perkin Elmer (Pyris Diamond) having weight sensitivity of 0.2  $\mu g$  under oxygen atmosphere. IR spectra were recorded (16 scans) as KBr pellets on a Nicolet NEXUS Aligent 1100 FT-IR spectrometer having a resolution of 4  $cm^{-1}$ . UV-visible spectra of the polymer-grafted complexes were recorded with a medium scan speed in Nujol on a Shimadzu 1601 UV-Vis spectrophotometer having 0.1 nm wavelength accuracy by layering a mull of the sample on the inside of one of the cuvettes while keeping the other one layered with Nujol as reference. Using  $BaSO_4$  as a background, electronic spectra of the polymer-grafted complexes were also recorded after diluting sample with  $BaSO_4$ . Spectra of non-polymer-grafted ligands and complexes were recorded in methanol.  $^1H$  NMR spectra (using Bruker Avance III 500 MHz spectrometer) and  $^{51}V$  NMR spectra (using Bruker Avance III 400 MHz spectrometer) with the common parameter settings were recorded with samples dissolved in  $DMSO-d_6$ , and the  $\delta$  ( $^{51}V$ ) values are referenced relative to neat

$V^{VOCl_3}$  as external standard. EPR spectra were recorded with a Bruker ESP 300E X-band spectrometer and the spin Hamiltonian parameters were obtained by simulation of the spectra with the computer program of Rockenbauer and Korecz [86]. The energy dispersive X-ray analyses (EDAX) of anchored complexes were recorded on a FEI Quanta 200 FEG. The samples were coated with a thin film of gold to prevent surface charging, to protect the surface material from thermal damage by the electron beam and to make the sample conductive. A Shimadzu 2010 plus gas-chromatograph fitted with a Rtx-1 capillary column ( $30\text{ m} \times 0.25\text{ mm} \times 0.25\text{ }\mu\text{m}$ ) and a FID detector was used to analyze the reaction products and their quantifications were made on the basis of the relative peak area of the respective product. The identity of the products was confirmed using a GC-MS Perkin-Elmer, model Clarus 500 and comparing the fragments of each product with the library available. For more than one cycle of catalytic experiment, the experiment was a bit difficult as catalyst amount taken in original experiment was too less and samples recovered from two such experiments were taken together for first recycle study.

### 2.2.3. Synthesis

#### 2.2.3.1. $H_2sal\text{-}iah$ (I)

A mixture of indole-3-acetic hydrazide (1.89 g, 10 mmol ) and salicylaldehyde (1.22 g, 10 mmol) in 100 mL of methanol was stirred for 2 h. A white solid precipitated during this period was filtered off, washed with methanol and dried. Recrystallization from methanol yielded pure **I** as a white solid. Yield 2.5 g. (85%). *Anal.* Calc. for  $C_{17}H_{15}N_3O_2$  (293.33): C, 69.61; H, 5.15; N, 14.33. Found: C, 69.7; H, 5.2; N, 13.9%.

### 2.2.3.2. $[V^{IV}O(sal-iah)(H_2O)]$ (2.1)

A hot solution of  $H_2sal-iah$  (2.93 g, 10 mmol) in methanol (150 mL) was treated with  $[V^{IV}O(acac)_2]$  (2.65 g, 10 mmol) in one portion and the resulting mixture was heated under reflux for 6 h. After reducing the solvent volume to *ca.* 20 mL and standing the solution under sealed flask for 24 h, the dark brown solid precipitated. This was filtered, washed with methanol and dried *in vacuo*. Yield 2.1 g (55.8%) *Anal.* Calc. for  $C_{17}H_{15}N_3O_4V$  (376.27): C, 54.27; H, 4.02; N, 11.17. Found: C, 54.4; H, 4.1; N, 11.3%.

### 2.2.3.3. $K[V^VO_2(sal-iah)] \cdot H_2O$ (2.2)

Complex **2.1** (0.376 g, 1 mmol) was dissolved in methanol (40 mL) having KOH (0.056 g, 1 mmol) and air was slowly passed through the solution with occasional shaking while maintaining the solvent volume to 40 mL. After 2 days the dark brown solution gradually changed to light brown. After reducing the solvent to *ca.* 20 mL the flask was kept at ambient temperature for overnight where light brown solid precipitated. This was filtered off, washed with methanol and dried. Yield 0.23 g, (55.7%) *Anal.* Calc. for  $C_{17}H_{15}N_3O_5KV$  (431.36): C, 47.34; H, 3.50; N, 9.74. Found: C, 48.9; H, 3.8; N, 9.4 %.

### 2.2.3.4. PS- $[V^{IV}O(sal-iah)(H_2O)]$ (2.3)

Chloromethylated polystyrene (3.0 g) was allowed to swell in DMF (20 mL) for 2 h. A solution of  $[V^{IV}O(sal-iah)(H_2O)]$  (3.0 g, 7.98 mmol) in DMF (20 mL) was added to the above suspension followed by triethylamine (4.0 g) in ethylacetate (20 mL), and the obtained reaction mixture was heated at 80 °C for 24 h with continuous but slow stirring. After cooling to room temperature, the polymer-grafted complex was separated by filtration, washed with hot DMF, followed by hot methanol and dried in an oven in air at 110 °C.

### 2.2.3.5. PS-[V<sup>V</sup>O(OMe)(sal-iah)] (2.4)

Air was slowly passed through the methanolic (100 mL) suspension of PS-[V<sup>IV</sup>O(sal-iah)(H<sub>2</sub>O)] (2.3) in the presence of KOH (0.3 g, 5.35 mmol) for ca. 4 days. The light brown beads were filtered off, washed with hot methanol and dried in an oven in air at 110 °C.

### 2.2.4. Catalytic activity

The catalytic oxidation of styrene and cyclohexene was carried out in a 50 mL flask fitted with a water circulated condenser. Polymer-grafted catalysts were kept in CH<sub>3</sub>CN for 1 h before use.

#### 2.2.4.1. Oxidation of styrene

In a typical reaction, an aqueous solution of 30% H<sub>2</sub>O<sub>2</sub> (3.40 g, 30 mmol) and styrene (1.04 g, 10 mmol) were mixed in 5 mL of CH<sub>3</sub>CN and the reaction mixture was heated at 80 °C with continuous stirring in an oil bath. The reaction was considered to begin after addition of 0.020 g (polymer-grafted) or 1.898×10<sup>-3</sup> g of (non-polymer-grafted) catalyst. During the reaction, the reaction products were analyzed using a gas chromatograph by withdrawing small aliquots after specific interval of time and confirming their identity by GC-MS.

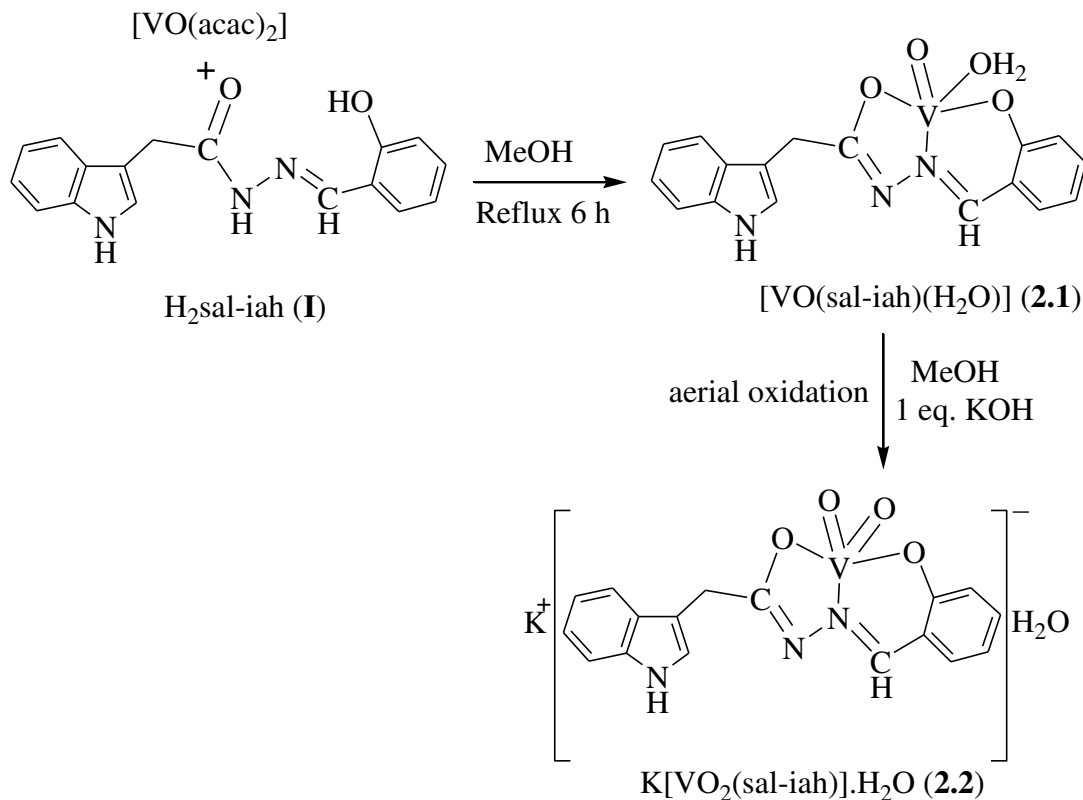
#### 2.2.4.2. Oxidation of cyclohexene

An aqueous solution of 30% H<sub>2</sub>O<sub>2</sub> (1.135 g, 10 mmol), cyclohexene (0.82 g, 10 mmol) and 0.010 g (polymer-grafted) or 0.949×10<sup>-3</sup> g of (non-polymer-grafted) catalyst were mixed in 5 mL of CH<sub>3</sub>CN and the reaction mixture was heated at 80 °C for 3 h while stirring in an oil bath. After removing the catalyst by filtration, the reaction products were analyzed as mentioned above.

## 2.3. Results and discussion

### 2.3.1. Synthesis and characterization

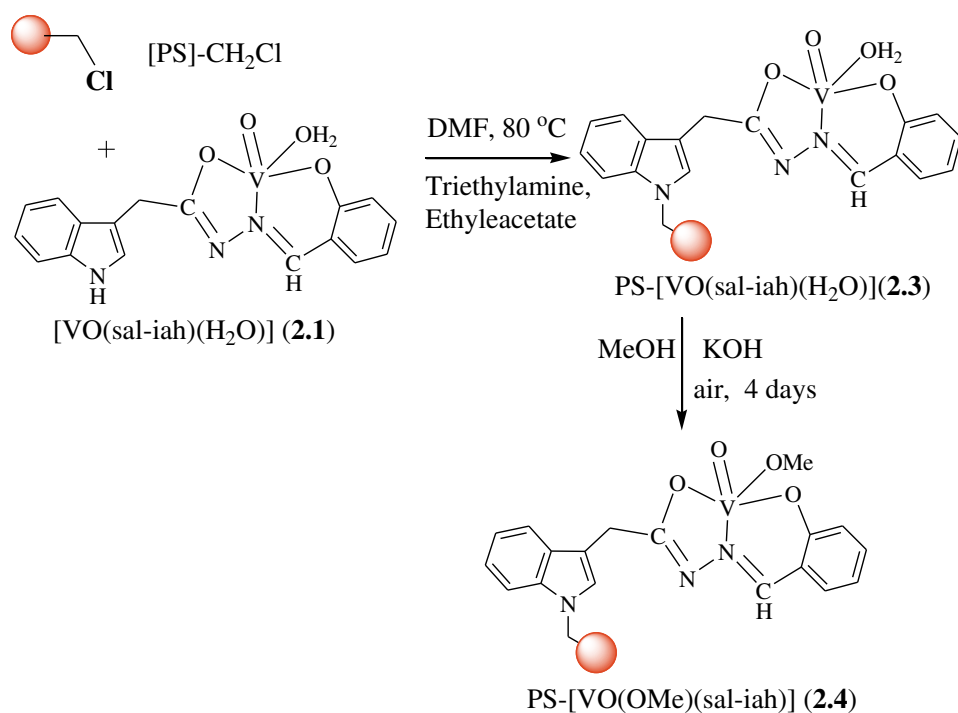
Reaction between equimolar amounts of indole-3-acetic hydrazide and salicylaldehyde in refluxing methanol gave ligand  $H_2sal-iah$  (**I**). The ligand **I** reacts with  $[V^{IV}O(acac)_2]$  in MeOH to give  $[V^{IV}O(sal-iah)(H_2O)]$  (**2.1**). Complex  $K[V^V O_2(sal-iah)] \cdot H_2O$  (**2.2**) can be isolated by aerial oxidation of **2.1** in the presence of one equivalent of KOH in methanol; Scheme 2.1. Elemental analyses and spectroscopic (IR, UV-vis, EPR,  $^1H$  and  $^{51}V$  NMR) studies of ligand and complexes are in agreement with the proposed structures.



**Scheme 2.1.** Synthetic routes to prepare complexes **2.1** and **2.2**

The reaction of chloromethylated polystyrene (cross linked with 5% divinylbenzene) with oxidovanadium(IV) complex **2.1** in DMF at 80 °C in the presence of triethylamine leads to the formation of polymer-anchored complex PS-[V<sup>IV</sup>O(sal-iah)(H<sub>2</sub>O)] (**2.3**). During this process, the labile proton of NH group of indole reacts with CH<sub>2</sub>Cl group of polymer. Complex **2.3** on aerial oxidation in methanol in the presence of KOH, gave the oxidomethoxido vanadium(V) complex, PS-[V<sup>V</sup>O(OMe)(sal-iah)] (**2.4**). Upon contact of **2.4** with dimethyl sulfoxide (DMSO) for 15 h, the GC-MS detected the presence of MeOH in solution confirming the presence of MeO<sup>-</sup> in the complex.

The whole synthetic procedures are presented in Scheme 2.2. The ICP-MS analysis of vanadium in the polymer-grafted complexes suggest vanadium loading of 0.36 and 0.23 mmol g<sup>-1</sup> of polymer resin in **2.3** and **2.4**, respectively.



**Scheme 2.2.** Synthetic routes to prepare PS-[V<sup>IV</sup>O(sal-iah)(H<sub>2</sub>O)] (**2.3**) and PS-[V<sup>V</sup>O(OMe)(sal-iah)] (**2.4**); PS (or ball) represents the backbone of the chloromethylated polystyrene.

### 2.3.2. Field Emission-scanning Electron Micrograph (FE-SEM) and Energy Dispersive X-Ray Analysis (EDAX) studies

Single beads of pure chloromethylated polystyrene and polymer-grafted complex PS-[V<sup>V</sup>O(OMe)(sal-iah)] (**2.4**) were selected to record field emission-scanning electron micrographs (Fe-SEM) in order to understand the morphological changes. Representative image of each one is reproduced in Fig. 2.1. The pure chloromethylated polystyrene bead has smooth and flat surface while anchored complex shows slight roughening of the top layer. Accurate information on the morphological changes in terms of exact orientation of ligand coordinated to the metal ion has not been possible due to poor loading of the metal complex. However, energy dispersive X-ray analysis (EDAX) of PS-[V<sup>V</sup>O(OMe)(sal-iah)] (**2.4**) estimates ca. 2.4 weight percentage of vanadium content. This observation confirms the grafting of metal complex onto polystyrene beads and part of the covalently bonded complexes is present on the surface while remaining at various sites.

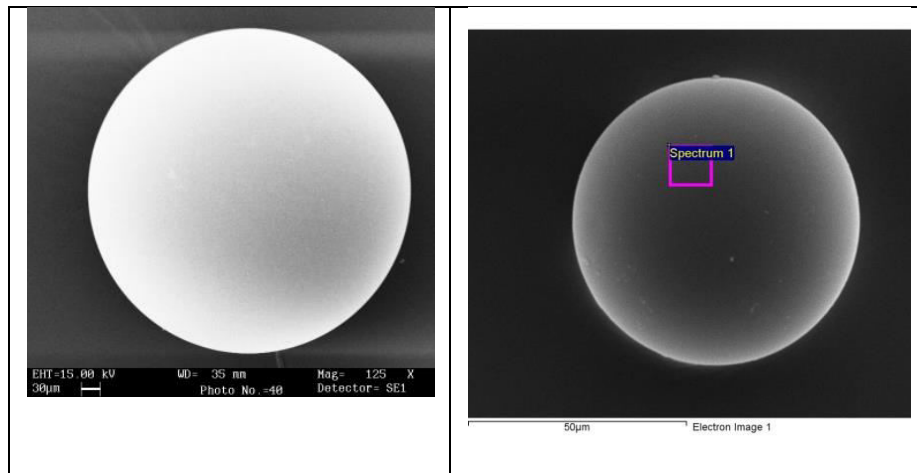


**Figure 2.1.** Scanning electron micrographs (SEM) of chloromethylated polystyrene (left) and PS-[V<sup>V</sup>O(OMe)(sal-iah)] (**2.4**) (right).

### 2.3.3. Thermogravimetric (TGA) studies

Thermogravimetric analysis of polymer-grafted complexes carried out under an oxygen atmosphere shows their good stability up to *ca.*180 °C except small weight loss between 100 – 190 °C possibly due to loss of residual/ coordinated water. Thereafter, they decompose in three major fragments with exothermic weight loss at higher temperature. Quantitative measurement of weight loss and distinction between decomposition pattern of complex and polymer matrix at various stages were not possible due to overlapping nature of the decompositions. However, the final residues of 6.3 % (equivalent to 0.35 mmol g<sup>-1</sup> of resin in **2.3**) and 5.0 % (equivalent to 0.28 mmol g<sup>-1</sup> of resin in **2.4**) at *ca.* 515 °C suggest the formation of V<sub>2</sub>O<sub>5</sub> and metal complexes are grafted into polymer support. A representative plot is shown in Fig. 2.2.

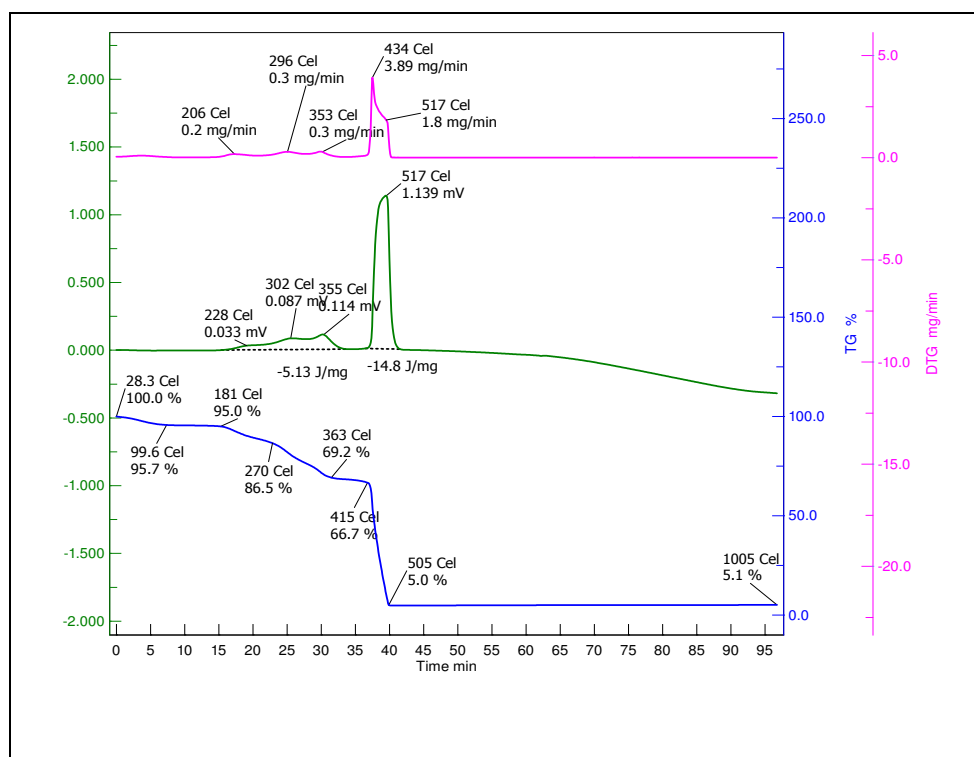


**Figure 2.2.** TGA, DTA and DTG plots of PS-[VO(OMe)(sal-iah)].



### 2.3.4. IR spectral studies

A partial list of IR spectral data of the ligand and the complexes is presented in Table 2.1. A band appearing at  $1618\text{ cm}^{-1}$  in  $\text{H}_2\text{sal-iah}$  (**I**) corresponds to azomethine group, and this band moves towards lower wave number by  $26\text{ cm}^{-1}$  (in **2.1**) and  $08\text{ cm}^{-1}$  (in **2.2**) indicating the coordination of azomethine nitrogen to the vanadium [87,88]. In the polymer-bound complexes this band appears at  $1608\text{ cm}^{-1}$  (in **2.3**) and  $1610\text{ cm}^{-1}$  (in **2.4**). The IR spectrum of the ligand exhibits  $\nu(\text{NH})$  and  $\nu(\text{C}=\text{O})$  at  $3186$  and  $1670\text{ cm}^{-1}$ , respectively while DFT calculation on similar system suggests the assignment of later band due to entire  $\text{N}(\text{H})\text{C}(\text{=O})$  amide group [89]. These are indicative of its ketonic nature in the solid state. The absence of later band in the spectra of all complexes is consistent with the enolisation of the amide functionality and subsequent coordination of enolic oxygen to the metal ion after proton replacement. A new band appearing in the region  $1280\text{ cm}^{-1}$  is assigned to the  $\nu(\text{C}-\text{O})(\text{enolic})$  stretching of the coordinated hydrazone fragment. The band at  $3400\text{ cm}^{-1}$  corresponds to the free  $-\text{OH}$  group present in  $\text{H}_2\text{sal-iah}$  ligand. However, the presence of this band in complexes **2.1–2.3** may possibly be due the presence of coordinated/ residual water. The chloromethylated polystyrene shows strong peaks at  $1264$  and  $673\text{ cm}^{-1}$  due to  $\text{C}-\text{H}$  wagging ( $-\text{CH}_2\text{Cl}$ ) and  $\text{C}-\text{Cl}$  stretch, respectively [90] and the absence of these peaks in  $\text{PS}-[\text{V}^{\text{VO}}(\text{OMe})(\text{sal-iah})]$  (**2.4**) suggests the covalent bonding of chloromethylated polystyrene with  $\text{K}[\text{V}^{\text{VO}}\text{O}_2(\text{sal-iah})]\cdot\text{H}_2\text{O}$  (cf. Scheme 2.2) through nitrogen of the benzimidazole ring. This is further supported by the absence of  $\nu(\text{NH})$  band appearing at  $3054\text{ cm}^{-1}$  in  $\text{K}[\text{V}^{\text{VO}}\text{O}_2(\text{sal-iah})]\cdot\text{H}_2\text{O}$ . The presence of multiple bands of medium intensity covering the  $2800\text{--}2900\text{ cm}^{-1}$  regions suggests the existence of  $-\text{CH}_2$  group.

The non polymer-grafted complex **2.1** exhibits a sharp band at  $933\text{ cm}^{-1}$  due to  $\nu(\text{V}=\text{O})$  while **2.2** exhibits two such bands at  $885$  and  $963\text{ cm}^{-1}$  corresponding to  $\nu_{\text{sym}}(\text{O}=\text{V}=\text{O})$  and  $\nu_{\text{asym}}(\text{O}=\text{V}=\text{O})$  modes, respectively. The corresponding polymer-bound

vanadium complexes display these bands at  $900\text{ cm}^{-1}$  (in **2.3**) and  $906\text{ cm}^{-1}$  (in **2.4**) [87,88].

**Table 2.1.** IR spectral data ( $\text{cm}^{-1}$ ) of compounds.

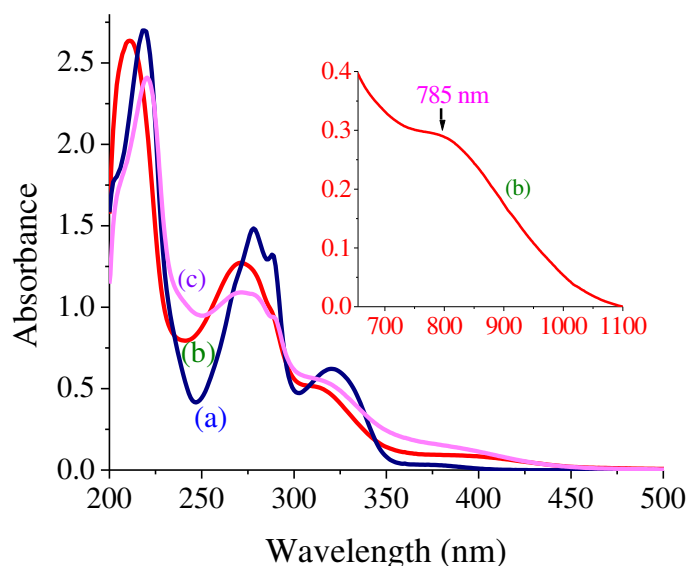
Compound	$\nu(\text{OH})$	$\nu(\text{C}=\text{O})$	$\nu(\text{NH})$	$\nu(\text{C}=\text{N})$	$\nu(\text{V}=\text{O})$
$\text{H}_2\text{sal-iah}$ ( <b>I</b> )	3400	1670	3186	1618	-
$[\text{V}^{\text{IV}}\text{O}(\text{sal-iah})(\text{H}_2\text{O})]$ ( <b>2.1</b> )	3350		3182	1592	933(s)
$\text{K}[\text{V}^{\text{V}}\text{O}_2(\text{sal-iah})]\cdot\text{H}_2\text{O}$ ( <b>2.2</b> )	3330		3054	1610	963, 885(s) <sup>a</sup>
$\text{PS}-[\text{V}^{\text{IV}}\text{O}(\text{sal-iah})(\text{H}_2\text{O})]$ ( <b>2.3</b> )	3420			1608	900(s)
$\text{PS}-[\text{V}^{\text{V}}\text{O}(\text{OMe})(\text{sal-iah})]$ ( <b>2.4</b> )				1610	906

<sup>a</sup> Bands correspond to asymmetric and symmetric ( $\text{O}=\text{V}=\text{O}$ ) modes, respectively

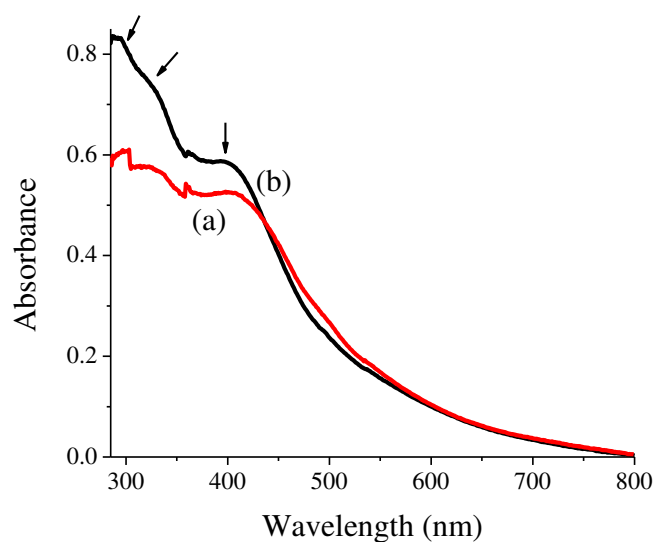
### 2.3.5. UV-visible spectral studies

Table 2.2 includes UV-visible spectral data of the ligand and complexes; Fig. 2.3 and Fig. 2.4 presents spectra. Ligand  $\text{H}_2\text{sal-iah}$  (**I**) exhibits three spectral bands in the UV region corresponding to  $\sigma\rightarrow\sigma^*$  (220 nm),  $\pi\rightarrow\pi^*$  (279 nm) and  $n\rightarrow\pi^*$  (321 nm) transitions. The additional band at 289 nm is possibly due to splitting of  $\pi\rightarrow\pi^*$  transition. All these bands also appear in the spectra of complexes **2.1** and **2.2** with slight variations. They also exhibit a ligand to metal charge transfer (LMCT) transition at ca. 400 nm from the phenolate oxygen atom to an empty d-orbital of the vanadium atom [91,92]. In addition, a new band at 785 nm in **2.1** is assigned due to d – d transition [93]. As  $\text{V}^{\text{V}}$ -complex **2.2** has  $3d^0$  configuration, d – d band is not expected. Complexes **2.3** and **2.4** have very similar electronic spectral patterns (Fig. 2.4) in the UV/visible region in Nujol.

In addition to  $\pi \rightarrow \pi^*$  (at ca. 300 nm) and  $n \rightarrow \pi^*$  (at ca. 325 nm) transitions, a ligand to metal charge transfer (LMCT) transition at ca. 400 nm [87,89,91] has also been observed in these complexes. The expected d – d transition in **2.3** could not be observed in Nujol possibly due to poor loading of complex in polymer matrix; however, diffuse reflectance spectrum of PS-[V<sup>IV</sup>O(sal-iah)(H<sub>2</sub>O)] in BaSO<sub>4</sub> exhibits a weak broad band at ca. 630 nm; Fig. 2.5.



**Figure 2.3.** : UV-visible spectra of (a) H<sub>2</sub>sal-iah, (b) [V<sup>IV</sup>O(sal-iah)(H<sub>2</sub>O)] (**2.1**) and (c) K[V<sup>V</sup>O<sub>2</sub>(sal-iah)]·H<sub>2</sub>O (**2.2**) recorded in methanol. (B): UV-visible spectra of (a) PS-[V<sup>IV</sup>O(sal-iah)(H<sub>2</sub>O)] (**2.3**) and (b) PS-[V<sup>V</sup>O(OMe)(sal-iah)] (**2.4**) recorded after dispersing them in Nujol.



**Figure 2.4.** : UV-visible spectra of (a) PS-[V<sup>IV</sup>O(sal-iah)(H<sub>2</sub>O)] (**2.3**) and (b) PS-[V<sup>V</sup>O(OMe)(sal-iah)] (**2.4**) recorded after dispersing them in Nujol.

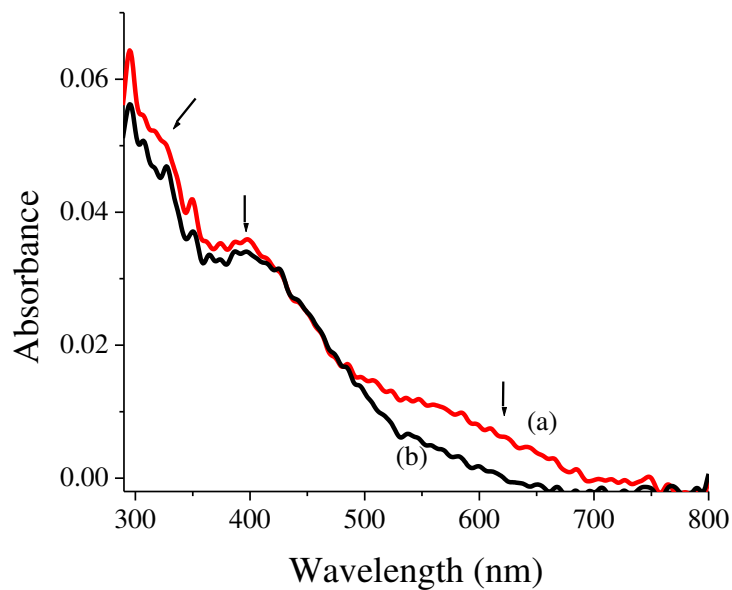


**Figure 2.5.** Diffuse reflectance spectra in solid phase (in BaSO<sub>4</sub>). (a) PS-[V<sup>IV</sup>O(sal-iah)(H<sub>2</sub>O)] (b) PS-[V<sup>V</sup>O(OMe)(sal-iah)].

**Table 2.2.** UV-visible spectral data of ligand and complexes.

Compound	Solvent	$\lambda_{\max}$ / nm
H <sub>2</sub> sal-iah ( <b>1</b> )	MeOH	220, 279, 289, 321
[V <sup>IV</sup> O(sal-iah)(H <sub>2</sub> O)] ( <b>2.1</b> )	MeOH	211, 271, 286, 312, 398, 785
K[V <sup>V</sup> O <sub>2</sub> (sal-iah)]·H <sub>2</sub> O ( <b>2.2</b> )	MeOH	220, 270, 289, 312, 400
PS-[V <sup>IV</sup> O(sal-iah)(H <sub>2</sub> O)] ( <b>2.3</b> )	Nujol	300, 325, 405
PS-[V <sup>V</sup> O(OMe)(sal-iah)] ( <b>2.4</b> )	Nujol	292, 322, 402

### 2.3.6. EPR study

The EPR spectra of neat complex [V<sup>IV</sup>O(sal-iah)(H<sub>2</sub>O)] (**2.1**) in “frozen” (77 K) DMSO solution and polymer-grafted complex PS-[V<sup>IV</sup>O(sal-iah)(H<sub>2</sub>O)] (**2.3**) in DMSO at room temperature are depicted in Fig. 2.6. The spectra were simulated and the spin Hamiltonian parameters obtained by simulation of the spectra are included in Table 2.3. The value of  $A_{\parallel}$  can be calculated using the additivity relationship [ $A_z^{\text{est}} = \sum A_{z,i}$  (i = 1 to 4)] proposed by Wüthrich [94] and Chasteen [95], with estimated accuracy of  $\pm 3 \times 10^{-4} \text{ cm}^{-1}$ . Assuming the binding modes involving ( $O_{\text{water}}$ ,  $O_{\text{phenolate}}$ ,  $O_{\text{enolate}}$ ,  $N_{\text{imine}}$ )<sub>equatorial</sub>, ( $O_{\text{oxido}}$ )<sub>axial</sub>, the  $A_z^{\text{est}}$  values have been calculated for **2.1** and **2.3** from the partial contributions of the equatorial donor groups relevant in the present case {H<sub>2</sub>O ( $45.7 \times 10^{-4} \text{ cm}^{-1}$ ),  $O_{\text{phenolate}}$  ( $38.9 \times 10^{-4} \text{ cm}^{-1}$ ),  $N_{\text{imine}}$ , ( $38.1$  to  $43.7 \times 10^{-4} \text{ cm}^{-1}$ ),  $O_{\text{enolate}}^{(-)}$  ( $37.6 \times 10^{-4} \text{ cm}^{-1}$ )}. The calculated value of  $160.3 \times 10^{-4} \text{ cm}^{-1}$  for PS-[V<sup>IV</sup>O(sal-iah)(H<sub>2</sub>O)] (**2.3**) is in good agreement with experimental value ( $160.82 \times 10^{-4} \text{ cm}^{-1}$ ) while the calculated value of  $165.9 \times 10^{-4} \text{ cm}^{-1}$  for [V<sup>IV</sup>O(sal-iah)(H<sub>2</sub>O)] (**2.1**) slightly differs with the experimental value of  $174.11 \times 10^{-4} \text{ cm}^{-1}$ , suggesting the involvement of some other binding atom as well.

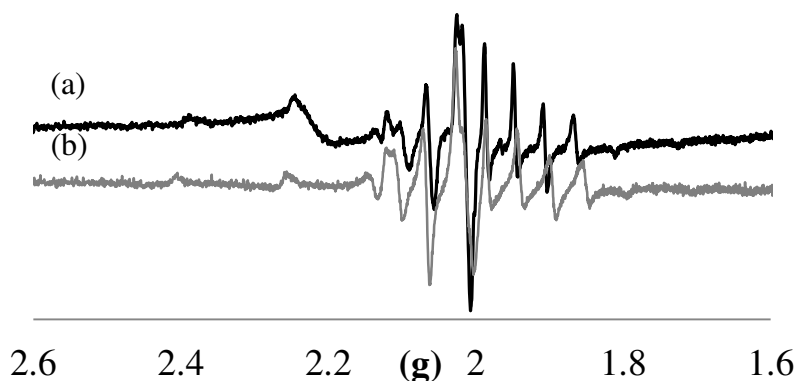


**Figure 2.6.** 1<sup>st</sup> derivative EPR spectra of (a) PS-[V<sup>IV</sup>O(sal-iah)(H<sub>2</sub>O)] (**2.3**) at room temperature and (b) [V<sup>IV</sup>O(sal-iah)(H<sub>2</sub>O)] (**2.1**) at frozen (77 K) solutions (ca. 4 mM) in DMSO.

**Table 2.3.** Spin Hamiltonian parameters obtained by simulation of the experimental 1<sup>st</sup> derivative EPR spectra.

Complexes	$g_{\parallel}$	$A_{\parallel} (\times 10^{-4} \text{ cm}^{-1})$	$g_{\perp}$	$A_{\perp} (\times 10^{-4} \text{ cm}^{-1})$
[V <sup>IV</sup> O(sal-iah)(H <sub>2</sub> O)]	1.942	174.11	1.979	63.96
PS-[V <sup>IV</sup> O(sal-iah)(H <sub>2</sub> O)]	1.949	160.82	1.983	57.79

### 2.3.7. <sup>1</sup>H and <sup>51</sup>V NMR studies

The <sup>1</sup>H NMR spectrum of the ligand exhibits two sets of singlet with about 1:2 ratio each for azomethine (-CH=N-), methylene (-CH<sub>2</sub>-) and NH (of -C(O)-NH- group) protons and one signal each for phenolic (-OH, singlet) and NH (doublet) protons of indole, indicating its existence in the two isomeric forms. In the complex K[V<sup>V</sup>O<sub>2</sub>(sal-iah)]·H<sub>2</sub>O (**2.2**), absence of 11.17 ppm signal due to the phenolic proton and shift of the azomethine signals from 8.38 and 8.41 ppm to 8.77 and 8.81 ppm indicates the coordination of the phenolic oxygen after proton replacement and the azomethine nitrogen. The signals at 3.66 and 4.02 ppm due to methyl protons collapse into one and

appear at 3.84 ppm while doublet at ca. 10.9 remains almost constant. Aromatic protons of ligand and complex **2.2** resonate at nearly same positions; however, complexity of signals in aromatic region does not allow separating their positions. Thus,  $^1\text{H}$  NMR data suggests the formation of complex but the presence of two azomethine signals of about 2:3 ratio hints towards the existence of two different vanadium(V) species (vide infra) in solution.

The  $^{51}\text{V}$  NMR spectrum of  $\text{K}[\text{V}^{\text{V}}\text{O}_2(\text{sal-iah})]\cdot\text{H}_2\text{O}$  (**2.2**) shows three resonances at  $\delta = -534.3$  ppm (72 %),  $-567.3$  ppm (22 %) and  $-467$  ppm (6.1 %); Fig. 2.7. The resonance at  $\delta = -534.3$  ppm (72 %) corresponds to proposed dioxido species and is in the range reported for several dioxidovanadium(V) complexes containing a mixed O/N donor set [87,88,96]. Other band at  $-567$  ppm (21.9%) is probably due to methoxido complex  $[\text{V}^{\text{V}}\text{O}(\text{OMe})(\text{MeOH})(\text{sal-iah})]$ . Such methoxido complexes are known to form upon keeping corresponding dioxidovanadium(V) species in methanol for prolonged period of time [87,89]. These observations supplement the data obtained from  $^1\text{H}$  NMR study. Interpretation of minor species showing signal at  $\delta = -467$  ppm (6 %) remains elusive.

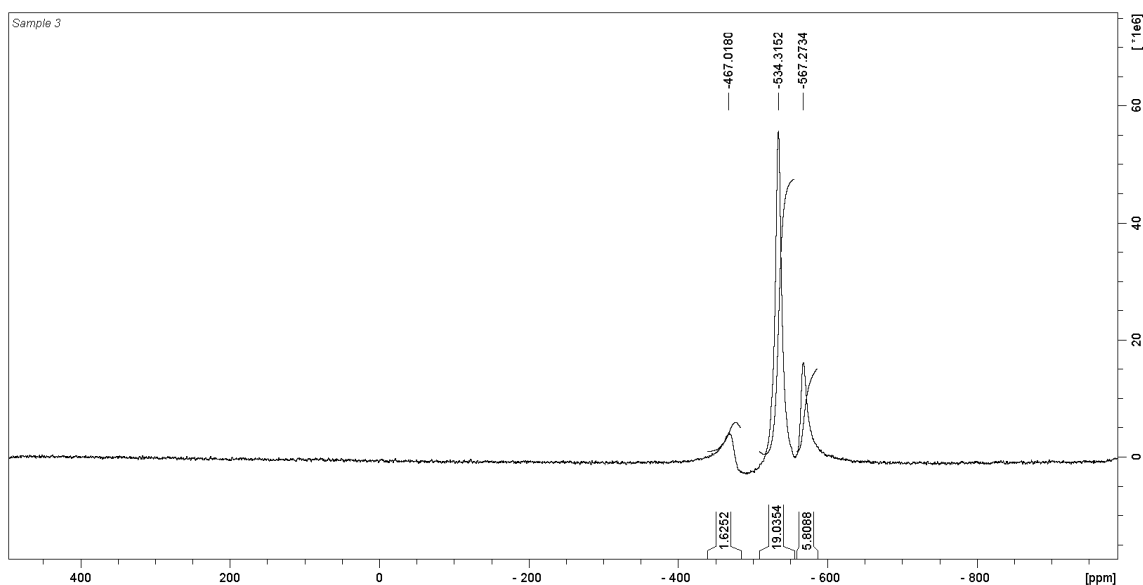
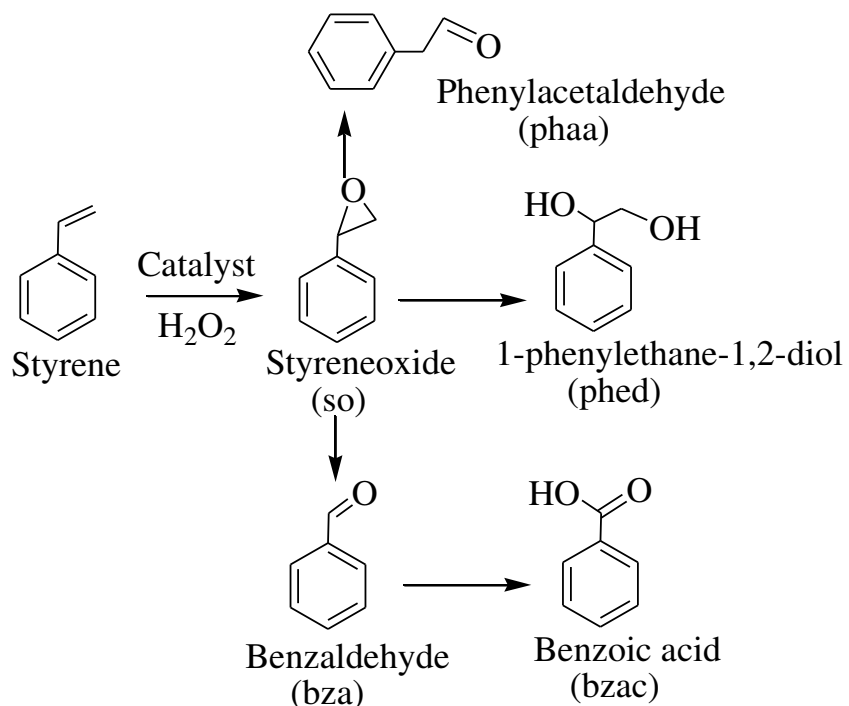


**Figure 2.7.**  $^{51}\text{V}$  NMR spectrum of  $\text{K}[\text{VO}_2(\text{sal-iah})]\cdot\text{H}_2\text{O}$ .

## 2.3.8. Catalytic activity studies

### 2.3.8.1. Oxidation of styrene

Oxidation of styrene has been reported using homogeneous as well as heterogeneous catalysts [42,53,55,56,97-99]. Amongst the various oxidation products of styrene, styrene oxide, is an important intermediate in organic synthesis and in the manufacture of the perfumery chemical, phenyl ethyl alcohol. Using 30 % aqueous  $\text{H}_2\text{O}_2$  as an oxidant, the oxidation of styrene was carried out taking  $\text{PS}[\text{V}^{\text{V}}\text{O}(\text{OMe})(\text{sal-iah})]$  (**2.4**) as catalyst and five oxidation products namely styreneoxide, benzaldehyde, 1-phenylethane-1,2-diol, benzoic acid and phenyl acetaldehyde were obtained along with small amount of unidentified product; Scheme 2.3.



**Scheme 2.3.** Oxidation products of styrene using  $\text{PS}[\text{V}^{\text{V}}\text{O}(\text{OMe})(\text{sal-iah})]$  (**2.4**) as catalyst.

With the objective to achieve suitable reaction conditions for the maximum oxidation of styrene different parameters, namely, the amount of oxidant (mol of  $\text{H}_2\text{O}_2$



per mol of styrene), catalyst (amount of catalyst per mole of styrene), solvent and temperature of the reaction mixture were tested.

For three different amounts (i.e. 0.015, 0.020 and 0.025 g) of catalyst, the fixed amount of styrene (1.04 g, 10 mmol) and H<sub>2</sub>O<sub>2</sub> (3.40 g, 30 mmol) were taken in 5 mL of CH<sub>3</sub>CN and the reaction was carried out at 80 °C. The formation of products was regularly analyzed at definite time intervals. As illustrated in Fig. 2.8, the conversion increases on increasing the amount of catalyst from 0.015 g to 0.020 g and a maximum of 95% conversion was achieved with 0.020 g of catalyst. The oxidation improved only marginally upon further increasing the amount of catalyst to 0.025 g. Therefore, an amount of 0.020 g catalyst may be considered as optimum to obtain the maximum conversion of styrene.

To study the effect of oxidant, three different styrene : aqueous 30 % H<sub>2</sub>O<sub>2</sub> molar ratios viz. 1:1, 1:2, and 1:3 were considered while taking the amount of styrene (1.04 g, 10 mmol) and catalyst (0.020 g) in 5 mL of CH<sub>3</sub>CN and the reaction was carried out at 80 °C. As illustrated in Fig. 2.9, increasing the styrene to oxidant ratio from 1:1 to 1:2 improved the conversion from 69 to 89%. A maximum of 95% conversion of styrene was obtained on increasing this ratio to 1 : 3. However, further increasing the ratio, no predominant conversion took place. The reason for this may be due to the dilution of the reaction mixture by the presence of larger amount of water molecules in H<sub>2</sub>O<sub>2</sub> solution. Therefore, styrene to H<sub>2</sub>O<sub>2</sub> molar ratio of 1:3 was taken for further optimization of other parameters.

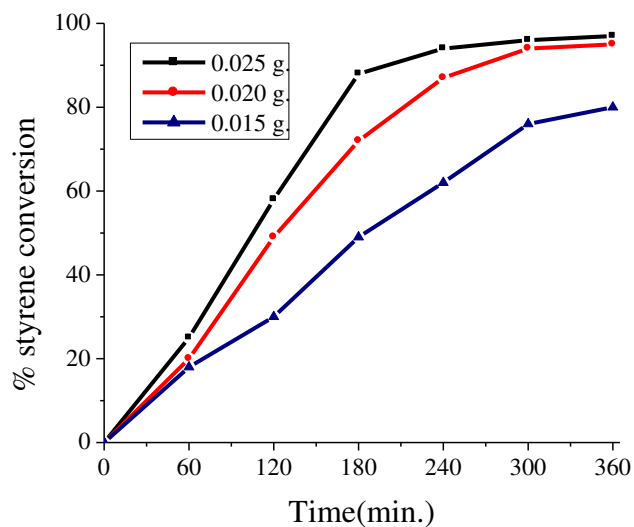


**Figure 2.8.** Effect of the amount of catalyst PS-[V<sup>V</sup>O(OMe)(sal-iah)] (2.4) on the oxidation of styrene. Reaction conditions: styrene (1.04 g, 10 mmol), 30% H<sub>2</sub>O<sub>2</sub> (3.40 g, 30 mmol), CH<sub>3</sub>CN (5 mL) and reaction temp. (80 °C).

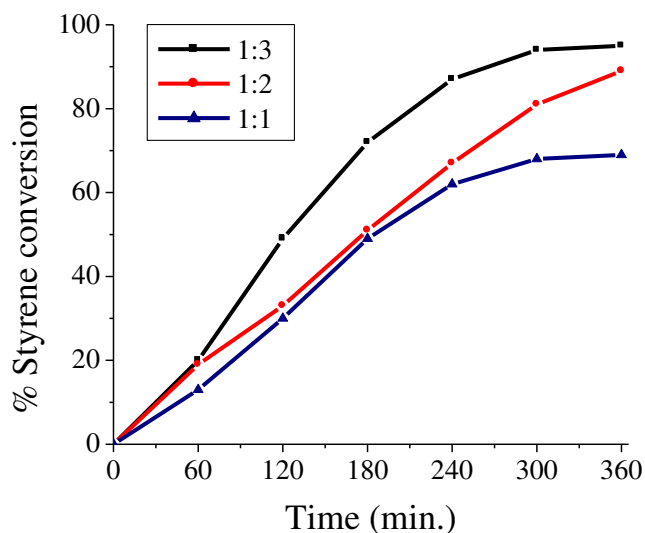


**Figure 2.9.** Effect of volume of H<sub>2</sub>O<sub>2</sub> amount (H<sub>2</sub>O<sub>2</sub>/ styrene molar ratio) on the oxidation of styrene. Reaction conditions: styrene (1.04 g, 10 mmol), catalyst (0.020 g), CH<sub>3</sub>CN (5 mL) and reaction temp. (80 °C).

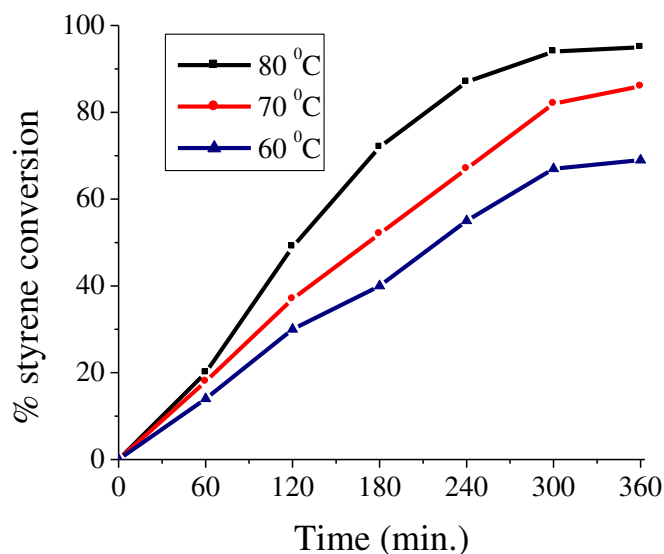


**Figure 2.10.** Effect of temperature on the oxidation of styrene. Reaction conditions: styrene (1.04 g, 10 mmol), catalyst (0.020 g), 30% H<sub>2</sub>O<sub>2</sub> (3.40 g, 30 mmol) and CH<sub>3</sub>CN (5 mL).

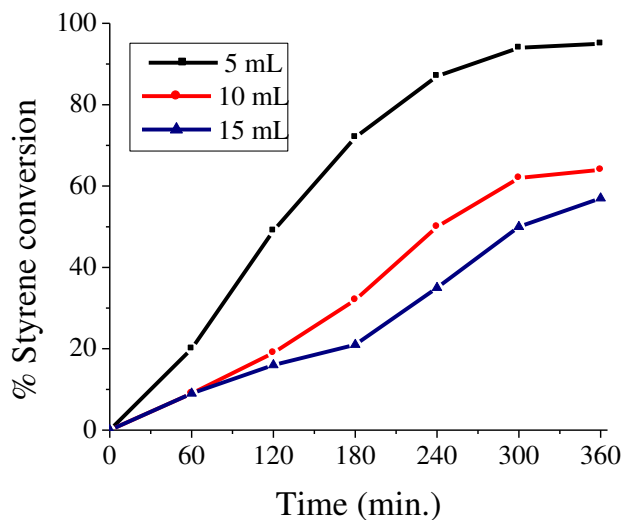


**Figure 2.11.** Effect of solvent (acetonitrile) volume on the oxidation of styrene. Reaction conditions: styrene (1.04 g, 10 mmol), catalyst (0.020 g), 30% H<sub>2</sub>O<sub>2</sub> (3.40 g, 30 mmol) and reaction temp. (80 °C).

Under above optimized reaction conditions, temperature of the reaction mixture was also optimized and found that 80 °C [Fig. 2.10] is the most suitable one to obtain highest conversion. Similarly, 5 mL of acetonitrile was found to be the most suitable one to obtain a maximum of 95% conversion of styrene in 6 h of reaction time (Fig. 2.11). Table 2.4 provides conversion of styrene under different reaction conditions and selectivity of different reaction products under particular condition after 6 h of reaction time. From the data presented in table, it is clear that the best suited reaction conditions (entry no. 2, Table 2.4) for the maximum oxidation of 10 mmol of styrene are: PS-[V<sup>V</sup>O(OMe)(sal-iah)] (**2.4**) (0.020 g), aqueous 30% H<sub>2</sub>O<sub>2</sub> (3.40 g, 30 mmol), CH<sub>3</sub>CN (5 mL) and reaction temperature (80 °C).

**Table 2.4.** Percent conversion for 10 mmol of styrene under different reaction conditions using PS-[V<sup>V</sup>O(OMe)(sal-iah)] (**2.4**) as catalyst and products selectivity of products after 6 h of reaction time.

Entry No.	Catalyst (g)	Temp. (°C)	H <sub>2</sub> O <sub>2</sub> (g, mmol)	CH <sub>3</sub> CN (mL)	% Conv.	TOF
1.	0.015	80	3.40, 30	5	80	387
2	0.020	80	3.40, 30	5	95	344
3	0.025	80	3.40, 30	5	97	282
4	0.020	60	3.40, 30	5	69	250
5	0.020	70	3.40, 30	5	86	312
6	0.020	80	1.135, 10	5	69	250
7	0.020	80	2.27, 20	5	89	327
8	0.020	80	3.40, 30	10	64	232
9	0.020	80	3.40, 30	15	46	167

Entry No.	% Selectivity <sup>a</sup>					
	so	bza	phed	bzac	phaa	Others
1.	3.5	63.6	11.6	9.0	2.9	9.4
2	3.3	66.9	4.5	16.6	5.2	3.5
3	4.2	73.4	4.1	11.1	5.5	1.7
4	4.1	87.8	0.0	4.1	4.0	0.00
5	4.6	75.0	3.4	7.3	5.9	3.8
6	5.0	50.4	20.9	8.8	6.0	8.9
7	3.0	56.7	16.5	8.5	3.8	11.5
8	2.2	67.7	4.5	10.1	3.8	11.7
9	1.8	55.1	22.3	5.9	3.7	11.2

<sup>a</sup> so: styrene oxide; bza: benzaldehyde; phed: 1-phenylethane-1,2-diol;  
bzac: benzoic acid; phaa: phenyl acetaldehyde.

The conversion of styrene and the selectivity of different reaction products using PS-[V<sup>VO</sup>(OMe)(sal-iah)] (**2.4**) as catalyst under the optimized reaction conditions have been analyzed as a function of time and are presented in Fig. 2.12. It is clear from the plot that the selectivity of the formation of benzaldehyde is good in the beginning but decreases slowly with time and reaches 66.9% at the end of 6 h. The selectivity of the formation of all other products is much low and falls between 3 to 17 %. Thus, with the maximum styrene oxidation of 95 % at the end of 6 h under optimized reaction conditions, the selectivity of different products follows the order: benzaldehyde (66.9%) > benzoic acid (16.6%) > phenyl acetaldehyde (5.2%) > 1-phenylethane-1,2-diol (4.5%) > styrene oxide (3.3%).

The formation of benzaldehyde is generally considered to proceed by the direct oxidative cleavage of the styrene side chain double bond by a radical mechanism [55,99]. A nucleophilic attack of H<sub>2</sub>O<sub>2</sub> on styrene oxide followed by cleavage of the intermediate

hydroperoxystyrene also provides benzaldehyde [100]. The oxidation of benzaldehyde provides benzoic acid while the formation of other products such as phenylacetaldehyde is possible through isomerisation of styrene oxide.

The recycled catalyst showed slightly less conversion (93 %) compared to fresh one. Under the above reaction conditions catalytic activity of non-polymer-grafted complex  $K[V^V O_2(\text{sal-iah})] \cdot H_2O$  gave 90% conversion with essentially same order of the selectivity of reaction products (Fig. 2.13). Thus, polymer-grafted complex is better catalyst over neat complex. Further, the recyclability of the polymer-grafted catalyst makes it better over the non polymer-grafted one. The literature contains very limited reports on the polymer-grafted vanadium based catalysts for the oxidation of styrene [30,42,53,56,99-101]. However, the catalytic activity of polymer-grafted catalyst reported here compares well with the catalytic activity reported in the literature. For example, PS- $K[V^V O_2(\text{sal-ohyba})]$  ( $H_2\text{sal-ohyba}$  = Schiff base derived from 3-formylsalicylic acid and *o*-hydroxybenzylamine) exhibited as high as 73 % conversion [56] while PS- $[V^{IV} O(\text{hmbmz})_2]$  gave only 48% conversion [30]. Other polymer-grafted oxidovanadium(IV) complexes PS- $[V^{IV} O(\text{fsal-ea}) \cdot \text{DMF}]$ , PS- $[V^{IV} O(\text{fsal-pa}) \cdot \text{DMF}]$  and PS- $[V^{IV} O(\text{fsal-amp}) \cdot \text{DMF}]$  (where  $H_2\text{fsal-ea/ pa / amp}$  = Schiff bases derived from 3-formylsalicylic acid and 2-aminoethanol/ 3-aminopropanol / 2-amino-2-methylpropanol) showed 82-95% conversion [53]. In the absence of catalyst, the reaction mixture gave only 15% conversion of styrene under above optimized reaction conditions.

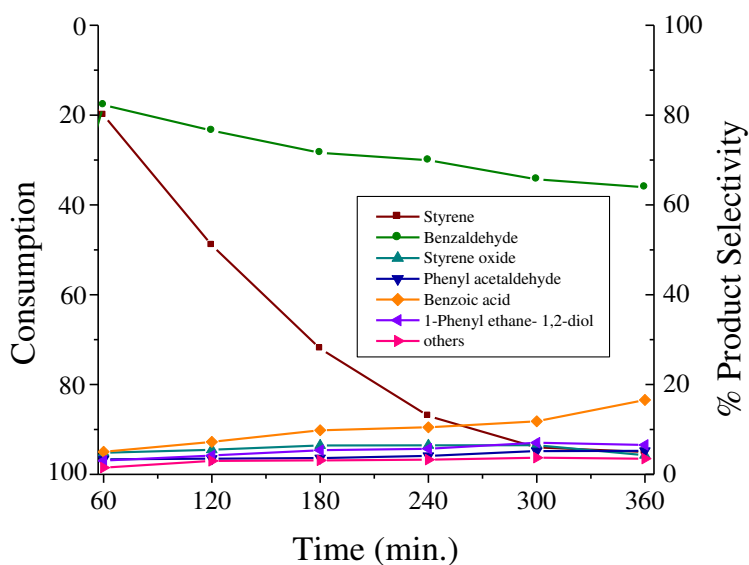


**Figure 2.12.** Consumption of styrene and variation in the selectivity of different reaction products as a function of time. Reaction conditions: styrene (1.04 g, 10 mmol), catalyst (0.020 g), 30%  $\text{H}_2\text{O}_2$  (3.40 g, 30 mmol),  $\text{CH}_3\text{CN}$  (5 mL) and reaction temp. ( $80^\circ\text{C}$ ).

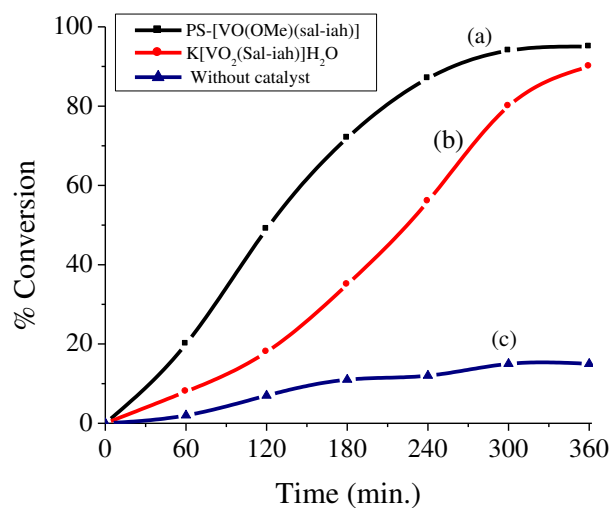
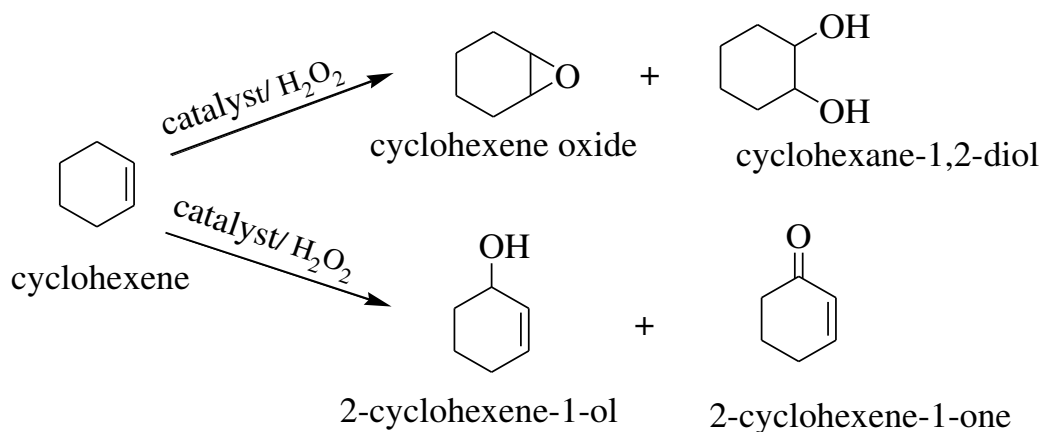


**Figure 2.13.** Conversion of styrene with time: (a)  $\text{PS}-[\text{V}^{\text{VO}}(\text{OMe})(\text{sal-iah})]$  (**2.4**), (b)  $\text{K}[\text{V}^{\text{VO}}\text{O}_2(\text{sal-iah})]\cdot\text{H}_2\text{O}$  (**2.2**) and (c) without catalyst.

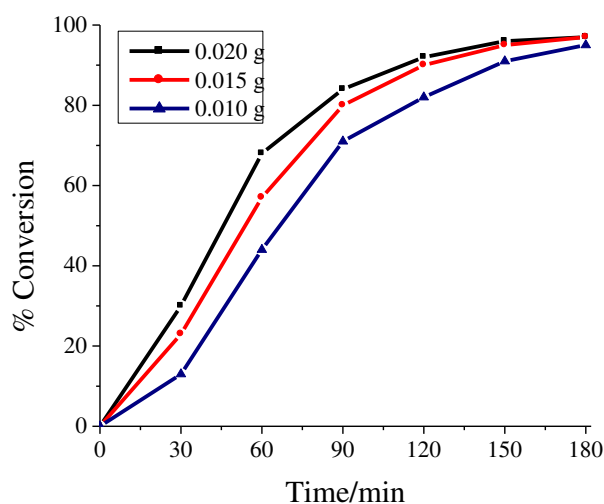
### 2.3.8.2. Oxidation of cyclohexene

Cyclohexene epoxide, an oxidation product of cyclohexene, is a highly reactive and selective organic intermediate widely used in the synthesis of enantioselective drugs, epoxy paints and rubber promoters. Oxidation of cyclohexene catalyzed by PS-[V<sup>V</sup>O(OMe)(sal-iah)] (**2.4**) gave cyclohexene epoxide, 2-cyclohexene-1-ol, cyclohexane-1,2-diol and 2-cyclohexene-1-one as presented in Scheme 2.4. For this catalytic reaction, conditions were also optimized using 10 mmol (0.82 g) of cyclohexene, varying the amount of catalyst (0.010, 0.015 and 0.020 g), 30 % aqueous H<sub>2</sub>O<sub>2</sub> (10, 20 and 30 mmol), temperature of the reaction mixture (60, 70 and 80 °C) and volume of acetonitrile (5, 10 and 15 mL). About 3 h was required to attain the equilibrium. Figs. 2.14-2.17 provide plots for the conversion of cyclohexene at various reaction conditions as a function of time and Table 2.5 summarizes all conditions and conversion obtained under particular condition. From the data in the table and plots shown, the best suited reaction conditions concluded for the catalytic activity of PS-[V<sup>V</sup>O(OMe)(sal-iah)] (**2.4**) for the maximum oxidation (96 %) of 10 mmol (0.82 g) of cyclohexene are: catalyst (0.010 g), 30% aqueous H<sub>2</sub>O<sub>2</sub> (1.135 g, 10 mmol), CH<sub>3</sub>CN (5 mL) and reaction temperature (80 °C). Under these conditions (entry no. 6, Table 2.5) the selectivity of different reaction products are: cyclohexene epoxide (39.3%) > 2-cyclohexene-1-ol (23.9%) > cyclohexane-1,2-diol (22.9%) > 2-cyclohexene-1-one (7.9%). The preferential attack of the activated C–H bond over the C = C bond favors the formation of allylic oxidation products 2-cyclohexene-1-one and 2-cyclohexene-1-ol while epoxidation occurs via the direct reaction of the olefin with the coordinated peroxido group to vanadium [102]. The species responsible for the cyclohexene oxidation is the product formed from the cleavage of the O–O bond [103].

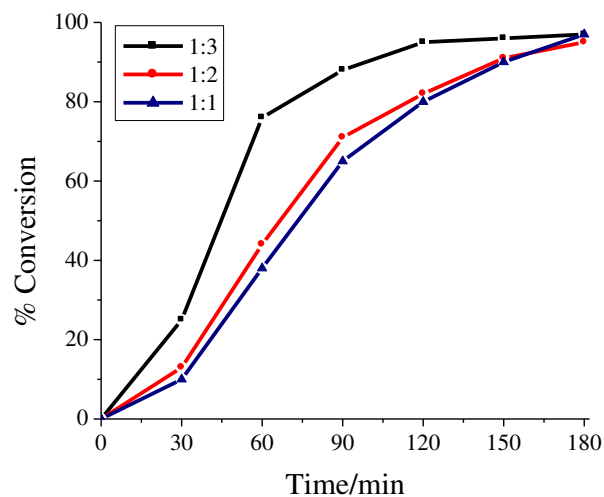




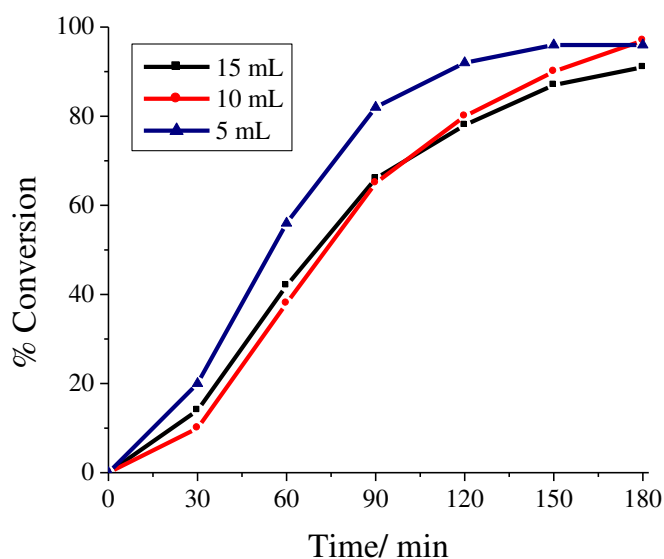
**Scheme 2.4.** Various oxidation products of cyclohexene.



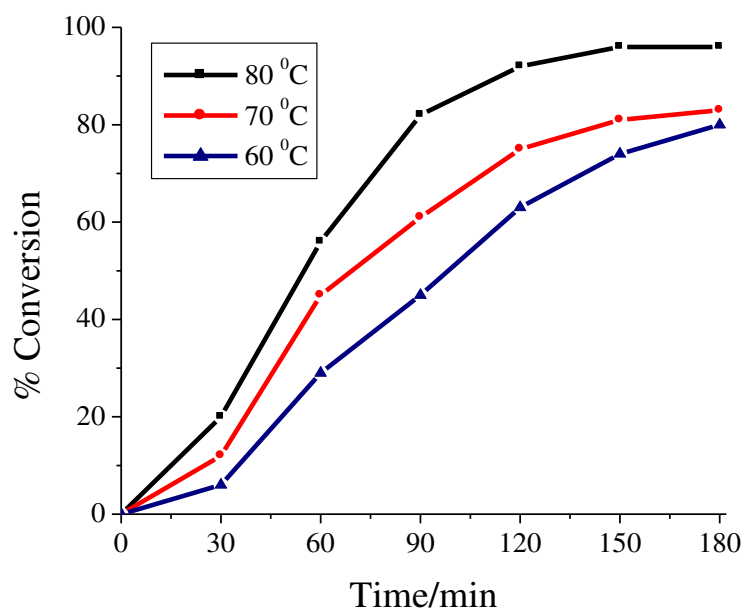
**Figure 2.14.** Effect of the amount of catalyst {PS-[V<sup>V</sup>O(OMe)(sal-iah)] (2.4)} on the oxidation of cyclohexene. Reaction conditions: cyclohexene (0.82 g, 10 mmol), 30% H<sub>2</sub>O<sub>2</sub> (1.135 g, 10 mmol), CH<sub>3</sub>CN (10 mL) and reaction temp. (80 °C).



**Figure 2.15.** Effect of amount of  $\text{H}_2\text{O}_2$  ( $\text{H}_2\text{O}_2$ / styrene molar ratio) on oxidation of cyclohexene. Reaction conditions: cyclohexene (0.82 g, 10 mmol), catalyst (0.010 g),  $\text{CH}_3\text{CN}$  (10 mL) and reaction temp. ( $80^\circ\text{C}$ ).



**Figure 2.16.** Effect of volume of solvent (acetonitrile) on the oxidation of cyclohexene. Reaction conditions: cyclohexene (0.82 g, 10 mmol), catalyst (0.010 g), 30% aqueous  $\text{H}_2\text{O}_2$  (1.135 g, 10 mmol) and reaction temp. ( $80^\circ\text{C}$ ).

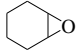
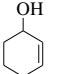
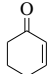
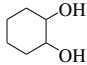


**Figure 2.17.** Effect of temperature on the oxidation of cyclohexene. Reaction conditions: cyclohexene (0.82 g, 10 mmol), catalyst (0.010 g), 30% aqueous H<sub>2</sub>O<sub>2</sub> (1.135 g, 10 mmol) and CH<sub>3</sub>CN (5 mL).

**Table 2.5.** Percent conversion of 10 mmol (0.82 g) of cyclohexene using PS-[V<sup>V</sup>O(OMe)(sal-iah)] (**2.4**) as catalyst after 3 h of reaction time and selectivity of products.

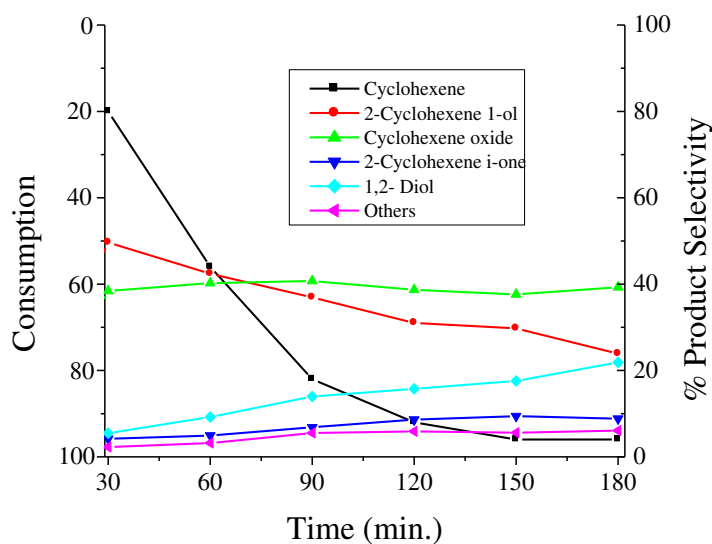
Entry No.	Catalyst (g)	Temp (°C)	H <sub>2</sub> O <sub>2</sub> (g, mmol)	CH <sub>3</sub> CN (mL)	% Conv.	TOF
1.	0.010	80	2.27, 20	10	95	1379
2	0.015	80	2.27, 20	10	97	939
3	0.020	80	2.27, 20	10	98	711
4	0.010	80	1.135, 10	10	97	1408
5	0.010	80	3.40, 30	10	97	1408
6	0.010	80	1.135, 10	5	96	1393
7	0.010	80	1.135, 10	15	91	1321
8	0.010	60	1.135, 10	5	82	1190
9	0.010	70	1.135, 10	5	83	1205

Entry No.	% Selectivity				
					Other
1.	32.6	37.5	5.6	18.5	5.8
2	36.5	23.9	10.7	17.3	11.6
3	39.7	29.2	7.2	15.8	8.1
4	39.1	30.1	5.8	20.4	4.6
5	26.6	44.1	5.6	16.7	7.0
6	39.3	23.9	7.9	22.9	6.0
7	33.8	32.4	6.5	21.4	5.9
8	39.2	30.8	8.4	15.6	6.0
9	35.6	41.7	5.1	15.5	2.1

The consumption of cyclohexene and the selectivity of different products under the optimized reaction conditions have also been analyzed as a function of time and are presented in Fig. 2.18. The selectivity of cyclohexene oxide and 2-cyclohexene-1-ol remains nearly constant with time during reaction while that of 2-cyclohexene-1-ol decreases from 45 % at 1/2 h to 23.9 % after 3 h and cyclohexane-1,2-diol increases from 5 % to 22.9 %. The catalytic activity of recycled catalyst shows slightly less (92 %) conversion. Under the above reaction conditions the catalytic activity of non-polymer-grafted complex  $K[V^V O_2(\text{sal-iah})] \cdot H_2O$  gave 90% conversion with essentially similar selectivity of reaction products. Control experiment without catalyst under above reaction conditions gave only 20 % conversion (Fig. 2.19).

Polymer-grafted vanadium complex reported here shows better conversion than polymer-grafted vanadium complexes reported in the literature [26]. Amino acids based polymer-grafted oxidovanadium(IV) complexes show as high as 79 % conversion of cyclohexene with ca. 39 % selectivity of cyclohexene oxide and ca. 50 % of 2-cyclohexene-1-ol [34, 33]. A maximum of 86 % conversion of cyclohexene with major product of cyclohexane-1,2-diol (81 % selectivity) and only minor product of cyclohexene oxide (3 % selectivity) was noted by thiomethylbenzimidazole based oxidovanadium(IV) complex immobilized on chloromethylated polystyrene [61].



**Figure 2.18.** Consumption of cyclohexene and variation in the selectivity of different reaction products as a function of time. Reaction conditions: cyclohexene (0.82 g, 10 mmol), catalyst (0.010 g), 30%  $\text{H}_2\text{O}_2$  (1.135 g, 10 mmol),  $\text{CH}_3\text{CN}$  (5 mL) and reaction temp. ( $80^\circ\text{C}$ ).

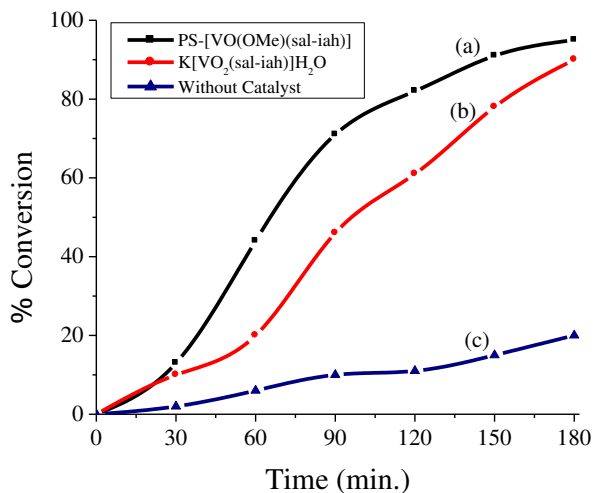


**Figure 2.19.** % Conversion of cyclohexene with time (a) PS-[V<sup>V</sup>O(OMe)(sal-iah)] (2.4), (b) K[VO<sub>2</sub>(sal-iah)]H<sub>2</sub>O, and (c) without catalyst.

**2.3.9. Reactivity of  $K[V^V O_2(\text{sal-iah})] \cdot H_2O$  with  $H_2O_2$  and possible reaction pathway**

The oxidoperoxidovanadium(V) complex  $[V^V O(O_2)(\text{sal-iah})]$ , one of the important intermediate form during catalytic reaction, could not be isolated in the solid state by the reaction of  $K[V^V O_2(\text{sal-iah})] \cdot H_2O$  (**2.2**) and  $H_2O_2$  due to its instability at ambient temperature. However, its formation has been established in solution by electronic absorption spectroscopy. The observed spectral changes are depicted in Fig. 2.20 and Fig. 2.21. Thus, the titration of a methanolic solution of  $K[V^V O_2(\text{sal-iah})] \cdot H_2O$  ( $4.0 \times 10^{-5}$  M) with 30 %  $H_2O_2$  (two drops) dissolved in 5 mL of MeOH results in the shift of 400 nm band to 390 nm along with slight increase in intensity; Fig 2.20. The band at 312 nm remains nearly unchanged with partial reduction in intensity. Such changes in the UV/Vis spectra have been interpreted as involving the progressive conversion of dioxido complex into oxidoperoxido species [87, 88]. The d-d band appearing at 785 nm recorded with a concentrated solution ( $2.4 \times 10^{-2}$  M) of  $[V^{IV} O(\text{sal-iah})(H_2O)]$  (**2.1**) in DMSO slowly decreases the intensity and finally becomes indistinguishable; Fig. 2.21. Effect of  $H_2O_2$  on the spectral changes in the remaining region (300 – 500 nm) is nearly same as observed for **2.2** when dilute solution of **2.1** was employed. This shows the progressive oxidation of  $V^{IV} O$  species and the formation of a oxidoperoxidovanadium(V) complex possibly via dioxidovanadium(V) species. The oxidoperoxido species then transfer oxygen to the substrates to give oxidized species.

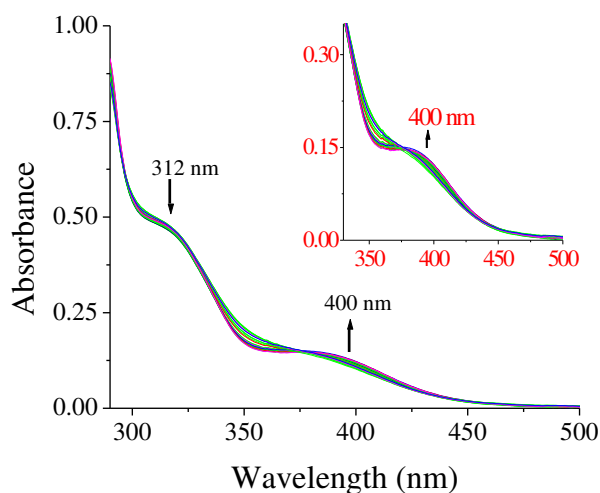


**Figure 2.20.** UV-Vis spectral changes observed during titration of  $K[V^V O_2(\text{sal-iah})] \cdot H_2O$  (**2.2**) with  $H_2O_2$ . The spectra recorded after successive addition of one drop portions of dilute  $H_2O_2$  (2 drops of 30%  $H_2O_2$  in 5 mL MeOH) to 50 mL of  $4.0 \times 10^{-5}$  M solution of (**2.2**).

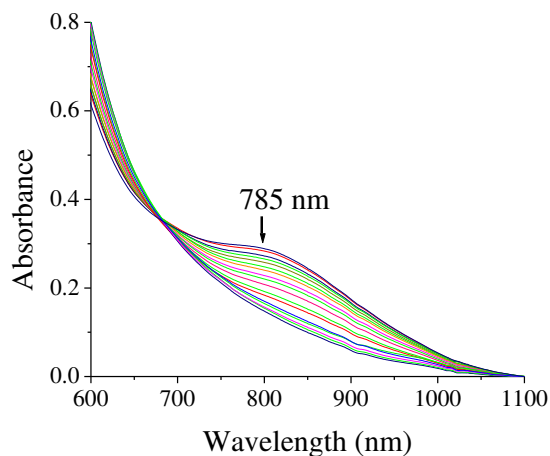


**Figure 2.21.** UV-Vis spectral changes observed during titration of  $K[V^V O_2(\text{sal-iah})] \cdot H_2O$  (**2.2**) with  $H_2O_2$ . The spectra recorded after successive addition of one drop portions of dilute  $H_2O_2$  (3 drops of 30%  $H_2O_2$  in 10 mL DMSO) to 50 mL of  $2.4 \times 10^{-2}$  M DMSO solution of  $[V^{IV}O(\text{sal-iah})(H_2O)]$  (**2.1**).



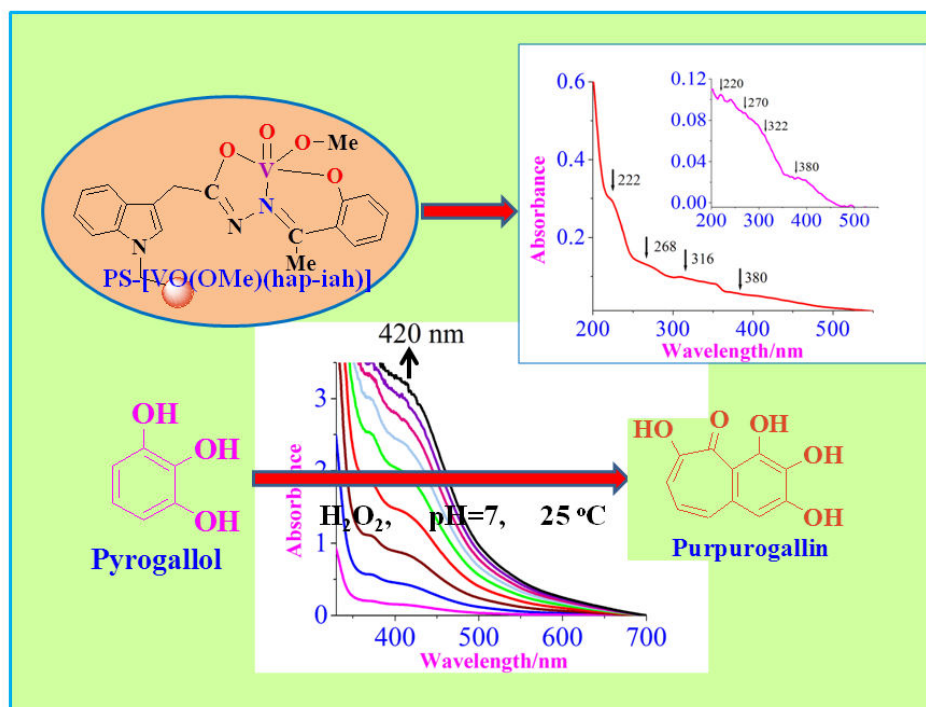
## 2.4. Conclusions

Dibasic tridentate ONO donor ligand H<sub>2</sub>sal-iah derived from salicylaldehyde and indole-3-acetic hydrazide has been used to prepare oxidovanadium(IV) and dioxidovanadium(V) complexes, [V<sup>IV</sup>O(sal-iah)(H<sub>2</sub>O)] (**2.1**) and K[V<sup>V</sup>O<sub>2</sub>(sal-iah)]·H<sub>2</sub>O. These complexes upon treatment with H<sub>2</sub>O<sub>2</sub> in methanol gave same oxidoperoxido species in solution. These complexes have also been grafted successfully through covalent bonding of the nitrogen of the indole group to chloromethylated polystyrene cross-linked with 5% divinylbenzene where **2.1** retains the same structure in PS-[V<sup>IV</sup>O(sal-iah)(H<sub>2</sub>O)] (**2.3**) while **2.2** changes to PS-[V<sup>V</sup>O(OMe)(sal-iah)] (**2.4**).

The polymer-grafted complex **2.4** catalyzes the oxidation of styrene and cyclohexene efficiently in the presence of H<sub>2</sub>O<sub>2</sub>. As high as 95 % conversion of the styrene with styrene oxide, benzaldehyde, benzoic acid, 1-phenylethane-1,2-diol and phenylacetaldehyde as major products were obtained under the optimized reaction conditions. Oxidation of cyclohexene gave 96 % conversion with cyclohexene oxide, 2-cyclohexen-1-ol, cyclohexane-1,2-diol and 2-cyclohexen-1-one as the major products. The presence of some of the metal centers on the surface of the polymer, supported by EDAX study, due to insertion of spacer between polymer support and catalyst possibly allowed their better interaction with substrates and oxidant during catalytic reaction resulting in better performance of the catalyst. Neat complex K[V<sup>V</sup>O<sub>2</sub>(sal-iah)]·H<sub>2</sub>O (**2.2**) has shown equally active catalytic potential towards styrene and cyclohexene but the recyclability and heterogeneity tests of polymer-grafted complex make it better over neat analog.

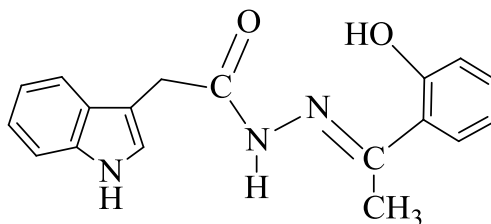
# CHAPTER 3

**Polymer grafted oxidomethoxido vanadium(V) complex of ONO donor ligand mimicking peroxidase activity**



### 3.1. Introduction

Vanadium complexes are known for various catalytic oxidation reactions in the presence of oxidants like  $\text{H}_2\text{O}_2$  and *tert*-butylhydroperoxide (TBHP) as they easily form intermediate species containing an electron rich peroxido group which are able to transfer oxygen to the organic substrate [104-106]. Grafting these complexes into polymer matrices and using them as catalyst precursors [25,26,56,61] has additional advantage in the direction of their technological usages because of their thermal stability, recyclability and high turnover rates resulting in environmentally benign synthetic routes to fine chemicals. Recently we observed that inserting spacer (an extra  $\text{CH}_2$  group) between polymer support and catalyst enhanced the catalytic performance of such grafted catalysts possibly due to the presence of more catalytic centers on the surface of polymer support which allow the better interaction of catalytic center with substrate and oxidant during catalytic reaction [see chapter 2, 107,108]. Peroxidase-like activity e.g. the oxidation of 2,2'-azino-bis(3-ethylbenzthiazoline-6-sulfonic acid (ABTS), a classical chromogenic heme peroxidase substrate, catalyzed by vanadium haloperoxidases has been reported [109]. However, the catalytic applications of model vanadium complexes have rarely been looked for peroxidase-like activity [65]. Recently, peroxidase-like activity e.g. the oxidation of pyrogallol to purpurogallin has successfully been achieved under mild reaction conditions at pH 7 buffered solutions in aqueous medium using homogeneous as well as heterogeneous model oxidovanadium(IV) complexes as catalyst [65]. These results encouraged us to design oxidovanadium(V) complex with ONO donor ligand  $\text{H}_2\text{hap-iah}$  (**II**, derived from *o*-hydroxyacetophenone and indole-3-acetic hydrazide; Scheme 3.1). It's grafting into chloromethylated polystyrene (PS), characterization and catalytic potential towards the oxidation of pyrogallol to purpurogallin (a peroxidase mimicking activity) are reported here. The corresponding non polymer-grafted oxidovanadium(V) complex has also been prepared for comparing its catalytic performance.



**Scheme 3.1.** Structure of ligand used in this study.

## 3.2. Experimental

### 3.2.1. Materials

Phosphate buffers of ionic strength (1.0 M) and appropriate pH were prepared according to the method of Christian and Purdy [110] by mixing the solutions of  $\text{H}_3\text{PO}_4$ ,  $\text{Na}_2\text{HPO}_4$  and  $\text{NaH}_2\text{PO}_4$ . *o*-hydroxyacetophenone, pyrogallol (Loba Chemie, India) were used as such. Other reagents and solvents were used as analytical reagent grades.

### 3.2.2. Physical methods and analysis

High resolution mass spectrum (HRMS) in positive ion electro spray ionization mass spectrum mode was obtained on a Bruker micrOTOF-Q II mass spectrometer in  $\text{CH}_3\text{CN}$ . Other instrumentation details are presented in Chapter 2.

### 3.2.3. Synthesis

#### 3.2.3.1. $\text{H}_2\text{hap-iah}$ (II)

A mixture of indole-3-acetic hydrazide (3.78 g, 20 mmol) and *o*-hydroxyacetophenone (2.72 g, 20 mmol) in 100 mL of methanol was refluxed for 4 h. After reducing the solvent volume to ca. 15 mL and standing the solution in air for 24 h, an off white solid precipitated which was filtered off, washed with methanol and dried *in vacuo*. Recrystallization from methanol yielded pure ligand. Yield: 5.5 g (89%). *Anal.* Calc. for  $\text{C}_{18}\text{H}_{17}\text{N}_3\text{O}_2$  (307): C, 70.34; H, 5.58; N, 13.67. Found: C, 69.94; H, 5.53; N, 13.81%.

### 3.2.3.2. [V<sup>V</sup>O(OMe)(hap-iah)] (3.1)

A methanolic (absolute) solution of [V<sup>IV</sup>O(acac)<sub>2</sub>] (0.265 g, 1 mmol in 10 mL) was added to a solution of H<sub>2</sub>hap-iah (**II**) (0.307 g, 1mmol) dissolved in dry methanol (30 mL) and the obtained reaction mixture was heated at reflux for 6 h to give dark brown solution. Slow evaporation of the solvent at room temperature under air gave a dark brown solid, which was filtered, washed with methanol and dried *in vacuo*. Yield: 0.285 g (70.7%). *Anal. Calc.* for C<sub>19</sub>H<sub>18</sub>N<sub>3</sub>O<sub>4</sub>V (403.31): C, 56.58; H, 4.50; N, 10.42. Found: C, 56.81; H, 4.48; N, 10.60%. <sup>51</sup>V NMR (DMSO-d<sub>6</sub>, δ/ ppm): -520.8 (62%), -540.0 (9%) and -549.5 (29%) ppm.

### 3.2.3.3. K[V<sup>V</sup>O(O<sub>2</sub>)(hap-iah)] (3.2)

Complex **3.1** (0.201 g, 0.5 mmol) was dissolved in methanol (20 mL) and to this aqueous 30% H<sub>2</sub>O<sub>2</sub> (1 mL) diluted in 2 mL MeOH and KOH (0.023 g, 0.5 mmol) dissolved in 2 mL MeOH were added with stirring. After 5 h of stirring a light pale yellow solid was filtered off, washed with methanol and dried in air. Yield: 0.130 g (59%). *Anal. Calc.* for C<sub>18</sub>H<sub>15</sub>N<sub>3</sub>O<sub>5</sub>KV (443.37): C, 48.76; H, 3.41; N, 9.48. Found: C, 48.51; H, 3.32; N, 9.26%. <sup>51</sup>V NMR (DMSO-d<sub>6</sub>, δ/ ppm): -540.0 (55%) and -551.0 (45%) ppm.

### 3.2.3.4. PS-[V<sup>V</sup>O(OMe)(hap-iah)] (3.3)

Chloromethylated polystyrene (2.0 g) was suspended in DMF (15 mL) for 2 h. A solution of [V<sup>V</sup>O(OMe)(hap-iah)] (2.0 g, 4.96mmol) in DMF (15 mL) was added to the above suspension followed by triethylamine (2.66 g) in ethylacetate (15 mL), and the obtained reaction mixture was heated at 90 °C for 24 h with continuous but slow stirring. After cooling to room temperature, the polymer-grafted complex was separated by filtration, washed with hot DMF, followed by hot methanol. It was then further refluxed in methanol for ca. 12 h and dried in an oven in air at 110 °C. Recovery yield: 2.1 g.

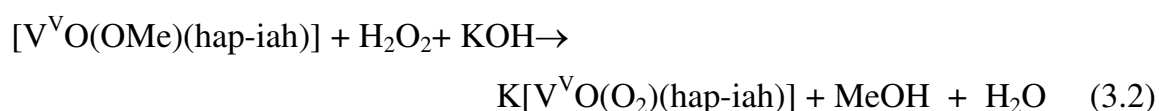
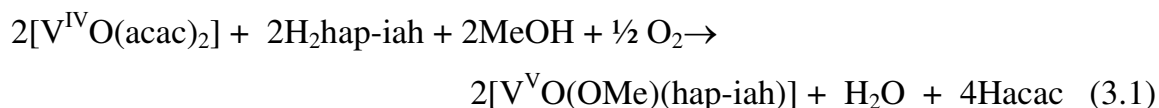
### 3.2.4. Peroxidase mimetic activity: catalytic oxidation of pyrogallol

Catalyst PS-[V<sup>V</sup>O(OMe)(hap-iah)] (3.3) was suspended in acetonitrile for 2 h before starting the reaction. The peroxidase mimetic activity was determined using UV-Vis spectrophotometer by monitoring the absorbance increment at 420 nm (due to the formation of purpurogallin) up to 1.5 h [111]. Initially, 1 mL of  $2.5 \times 10^{-2}$  M solution of 30% H<sub>2</sub>O<sub>2</sub>, 1 mL of  $2.5 \times 10^{-2}$  M pyrogallol solution and 0.015 g of catalyst PS-[V<sup>V</sup>O(OMe)(hap-iah)] were taken in 3 mL of phosphate buffer (1 M, pH 7) and the maximum measurable absorbance was recorded. In second step, various parameters such as different amounts of oxidant and catalyst and pH of the reaction medium were optimized to evaluate the best reaction conditions for the maximum oxidation of pyrogallol. The steady state kinetics was performed by varying the concentration of pyrogallol (0.2–2.2 mM) for the fixed concentration of H<sub>2</sub>O<sub>2</sub> ( $2.5 \times 10^{-4}$  M/ 0.25 mM) in the presence of catalyst PS-[V<sup>V</sup>O(OMe)(hap-iah)] (0.010 g). The reaction was carried out in 2 mL of phosphate buffer (1 M, pH 7) and monitored spectrophotometrically by measuring the formation of purpurogallin from pyrogallol at 420 nm ( $\epsilon = 2640 \text{ M}^{-1} \text{ cm}^{-1}$ ) in time scan mode. The initial reaction rates were calculated and fitted to Michaelis-Menten equation. Lineaweaver-Burk linearizations were performed using Sigma-Plot software (Systat Software Inc.) with enzyme kinetics module to calculate kinetic parameters.

### 3.3. Results and discussion

#### 3.3.1. Synthesis and characterization

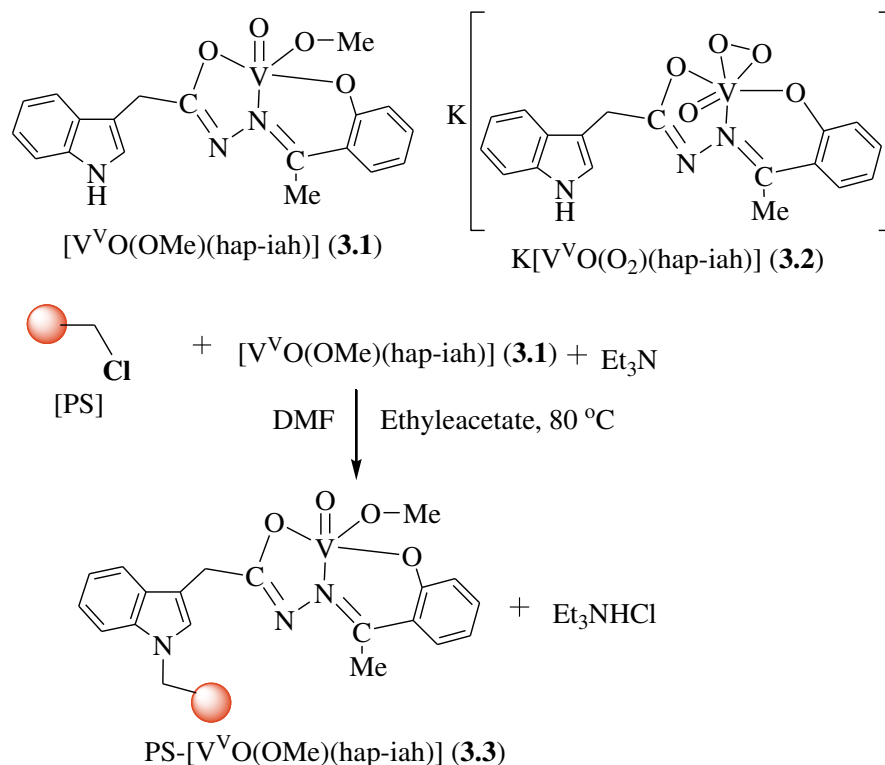
A solution of H<sub>2</sub>hap-iah (**II**) reacted with [V<sup>IV</sup>O(acac)<sub>2</sub>] in MeOH in 1 : 1 molar ratio under aerobic atmosphere at reflux temperature to give a dark brown complex [V<sup>V</sup>O(OMe)(hap-iah)] (**3.1**) [Eq. (3.1)]. Its reaction with 30 % aq. H<sub>2</sub>O<sub>2</sub> in presence of one equivalent KOH in methanol gave complex K[V<sup>V</sup>O(O<sub>2</sub>)(hap-iah)] (**3.2**) [Eq. (3.2)].



Both complexes are soluble in methanol, ethanol, DMF and DMSO. Scheme 3.2 presents the structures proposed for complexes, which are based on the elemental analyses, spectroscopic characterization (IR, electronic, <sup>1</sup>H, <sup>13</sup>C and <sup>51</sup>V NMR) and thermogravimetric pattern. The ligand coordinates through its dianionic (ONO) functionalities.

The reaction of chloromethylated polystyrene (cross linked with 5% divinylbenzene) with complex **3.1** in DMF at 80 °C in the presence of triethylamine followed by extensive reflux in methanol leads to the formation of polymer-grafted complex PS-[V<sup>V</sup>O(OMe)(hap-iah)] (**3.3**) (Scheme 1). During this process, the labile proton of NH group of indole reacts with CH<sub>2</sub>Cl group of polymer. Upon keeping **3.3** in DMSO for 15 h, the GC-MS detected the presence of MeOH in solution confirming the presence of MeO<sup>-</sup> in the complex.

This supported complex was additionally characterized by FE-SEM and EDAX. The ICP-MS analysis of vanadium in the polymer-grafted complex **3.3** suggests vanadium loading of 0.32 mmol g<sup>-1</sup> of polymer resin.



**Scheme 3.2.** Proposed structures of complexes **3.1** and **3.2**, and synthetic route to prepare **3.3**; PS (or ball) represents the backbone of the chloromethylated polystyrene.

### 3.3.2. Thermogravimetric Analysis (TGA) studies

Thermogravimetric analysis under an oxygen atmosphere shows the good stability of polymer-grafted complex  $PS-[V^V O(OMe)(hap-iah)]$  (**3.3**) up to *ca.*  $200\text{ }^\circ\text{C}$  except small weight loss (*ca.* 4%) between  $50$  and  $190\text{ }^\circ\text{C}$  possibly due to loss of residual/coordinated solvent. Thereafter, it decomposes with exothermic weight loss at higher temperature; Fig. 3.1. The final residues of 5.5 % (equivalent to  $0.302\text{ mmol g}^{-1}$  of V) at *ca.*  $465\text{ }^\circ\text{C}$  suggests the formation of  $V_2O_5$  and metal complex is grafted into polymer support. Corresponding non grafted complex  $[V^V O(OMe)(hap-iah)]$  (**3.1**) is stable up to *ca.*  $150\text{ }^\circ\text{C}$  and then loses 7.3 % (*Anal Cal.* 7.6%) weight between  $150$  and  $180\text{ }^\circ\text{C}$  equivalent to one coordinated methoxido group. On further increasing the temperature the complex decomposes in three major fragments with exothermic weight loss which



completes at ca. 700 °C; Fig. 3.2. The obtained residue at this temperature is 21.1%. A slight deviation from calculated value of 22.4% for  $V_2O_5$  is possibly due to the presence of traces of ligand's impurity in sample.

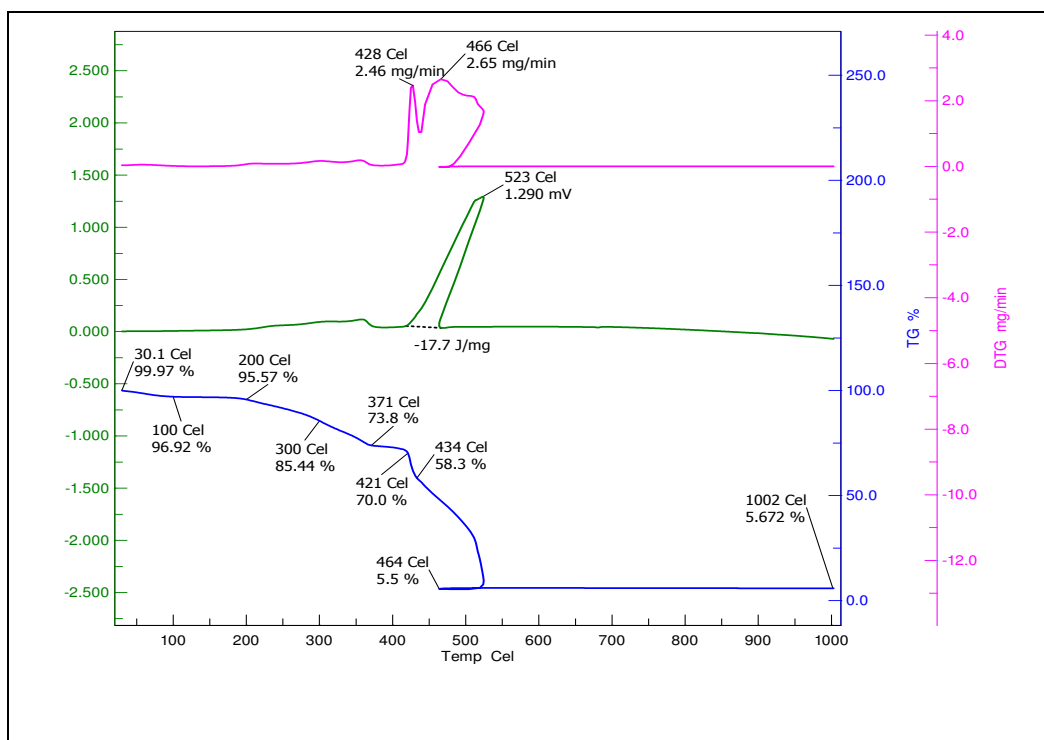


**Figure 3.1.** Thermogravimetric analysis (TGA) plot of PS-[V<sup>V</sup>O(OMe)(hap-iah)] (3.3).

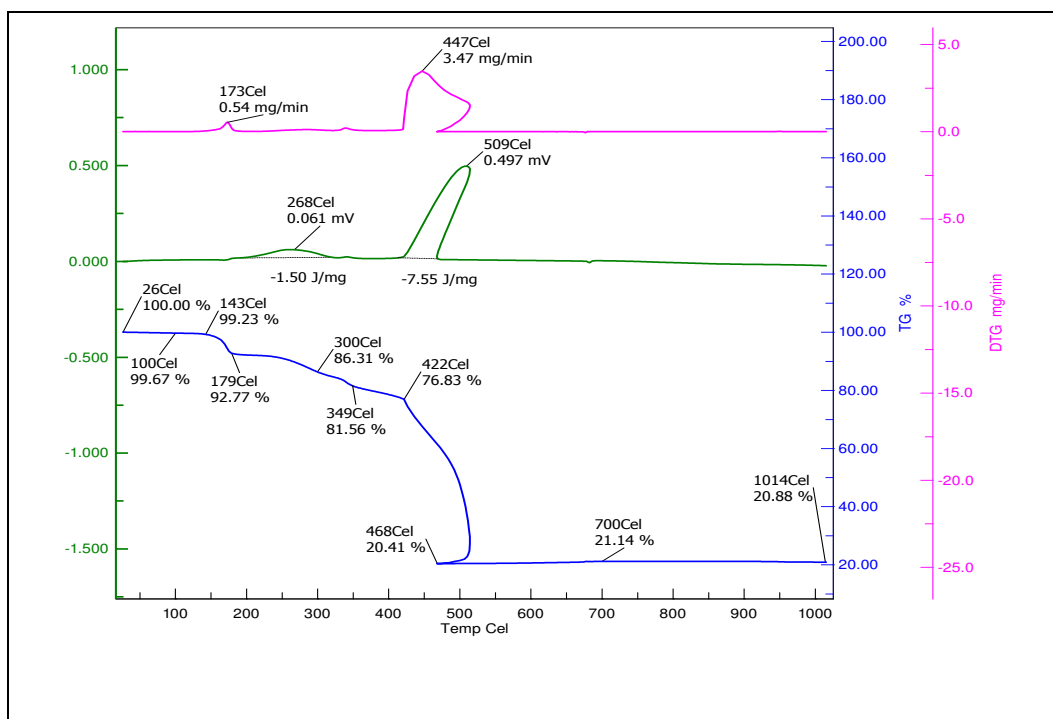


**Figure 3.2.** Thermogravimetric analysis (TGA) plot of  $[V^V O(OMe)(hap-iah)](3.1)$

### 3.3.3. Field Emission-scanning Electron Micrograph (FE-SEM) and Energy Dispersive X-Ray Analysis (EDAX) studies

Fig. 3.3 shows the images of chloromethylated polystyrene (cross-linked with 5% divinylbenzene) and polymer-grafted vanadium complex PS- $[V^V O(OMe)(hap-iah)]$  (3.3). Comparison of images clearly indicates that the smooth and flat surface of the fresh polystyrene bead [Fig. 3.3 (a)] has distinctly changed upon grafting the metal complex; Fig. 3.3 (b). The EDAX study (Fig. 3.4) on the spotted area of PS- $[V^V O(OMe)(hap-iah)]$  (3.3) [Fig. 3.4 (b)] estimates ca. 3.4 weight percentage of vanadium content and 75, 10 and 10 weight percentage of C N and O, respectively. This observation confirms the grafting of metal complex into polystyrene beads and part of the covalently bonded complexes is present on the surface while remaining at various sites.

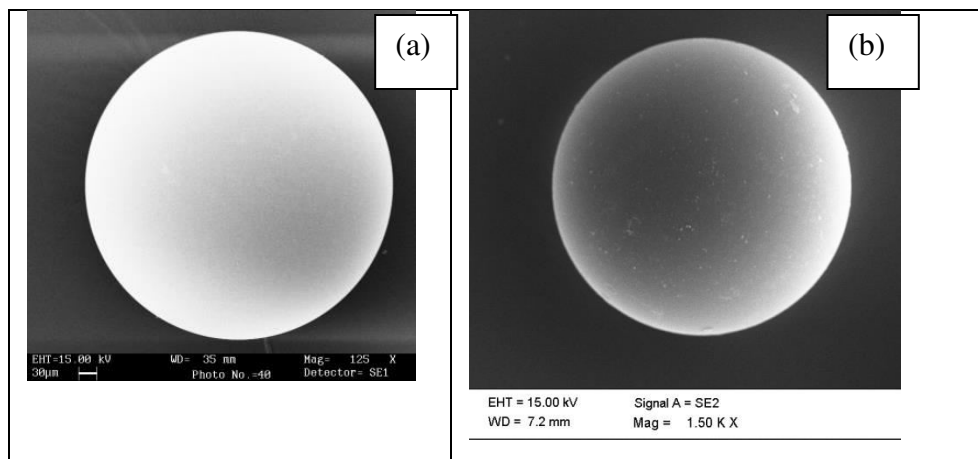


**Figure 3.3.** Scanning electron micrographs of (a) PS-Cl and (b) PS-[V<sup>V</sup>O(OMe)(hap-iah)].

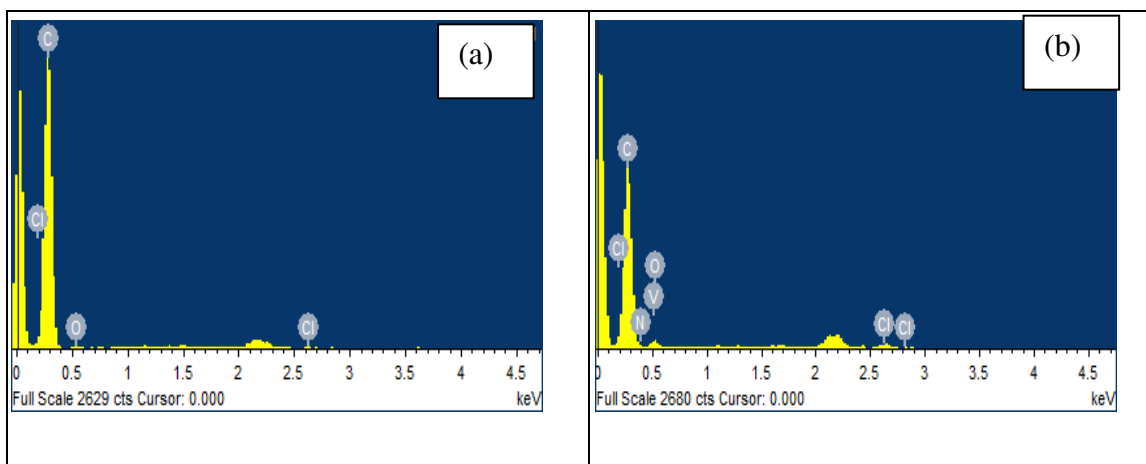


**Figure 3.4.** EDAX profiles of (a) PS-Cl and (b) PS-[V<sup>V</sup>O(OMe)(hap-iah)].

### 3.3.4. IR spectral studies

The IR spectrum of H<sub>2</sub>hap-iah (**II**) shows absorptions at 1624 cm<sup>-1</sup> due to  $\nu(\text{C}=\text{N}_{\text{azomethine}})$ , 1302 cm<sup>-1</sup> due to  $\nu(\text{C}-\text{O}_{\text{phenolic}})$ , 1671 cm<sup>-1</sup> due to  $\nu(\text{C}=\text{O}_{\text{ketonic}})$ , and 3192 cm<sup>-1</sup> due to  $\nu(\text{NH}_{\text{hydrazide}})$ ; Fig. 3.5. The absence of bands due to  $\nu(\text{C}=\text{O}_{\text{ketonic}})$ , and  $\nu(\text{NH}_{\text{hydrazide}})$  in the spectra of complexes suggests the enolisation of the amide functionality and subsequent coordination of enolic oxygen to the metal ion after proton

replacement. This is further supplemented by the appearance of a band at ca. 1240 (in **3.1**), 1246 (in **3.2**) and 1247  $\text{cm}^{-1}$  (in **3.3**) assignable to the  $\nu(\text{C}-\text{O}_{\text{enolic}})$  mode of the coordinated hydrazido fragment. A shift of the  $\nu(\text{C}=\text{N}_{\text{azomethine}})$  band to the lower frequency side by 37  $\text{cm}^{-1}$  (in **3.1**) and 26  $\text{cm}^{-1}$  (in **3.2**) suggests the coordination of the azomethine nitrogen to the vanadium. A sharp band at 3348  $\text{cm}^{-1}$  corresponding to the free  $-\text{NH}$  group present in **II** slightly shifts to higher wave numbers. Absence of this sharp band in **3.3** indicates the interaction of  $-\text{NH}$  group with polymer through chloromethylated group while the presence of only weak and broad band at 3400  $\text{cm}^{-1}$  in this may possibly be due the presence of coordinated/ residual water.

In addition, the neat complex **3.1** displays one sharp band at 983  $\text{cm}^{-1}$  due to  $\nu(\text{V}=\text{O})$  mode. The peroxido complex **3.2** shows three IR active vibrational modes associated with the  $\{\text{V}(\text{O}_2)\}$  moiety, namely the symmetric  $\text{V}(\text{O}_2)$  stretch at 579  $\text{cm}^{-1}$ , the antisymmetric  $\text{V}(\text{O}_2)$  stretch at 770  $\text{cm}^{-1}$ , and the  $\text{O}-\text{O}$  stretch at 928  $\text{cm}^{-1}$ , in addition to the  $\nu(\text{V}=\text{O})$  stretch at 976  $\text{cm}^{-1}$ . The corresponding polymer-bound complex **3.3** shows the  $\nu(\text{V}=\text{O})$  stretching frequency at ca. 960  $\text{cm}^{-1}$ . The presence of multiple bands of medium intensity covering the 2800–2900  $\text{cm}^{-1}$  regions suggests the existence of  $-\text{CH}_2$  group. The comparison of IR spectrum of the pure chloromethylated polystyrene beads with that of the complex grafted polymer beads confirms the loading of  $[\text{V}^{\text{V}}\text{O}(\text{OMe})(\text{hap-iah})]$  (**3.1**). The chloromethylated polystyrene shows strong peaks at 1264 and 673  $\text{cm}^{-1}$  due to  $\text{C}-\text{H}$  wagging ( $-\text{CH}_2\text{Cl}$ ) and  $\text{C}-\text{Cl}$  stretch, respectively [90], and these peaks are absent in  $\text{PS}-[\text{V}^{\text{V}}\text{O}(\text{OMe})(\text{hap-iah})]$  (**3.3**), suggesting the covalent bonding of chloromethylated polystyrene with **3.1** (cf. Scheme 3.2) through nitrogen of the indole ring.

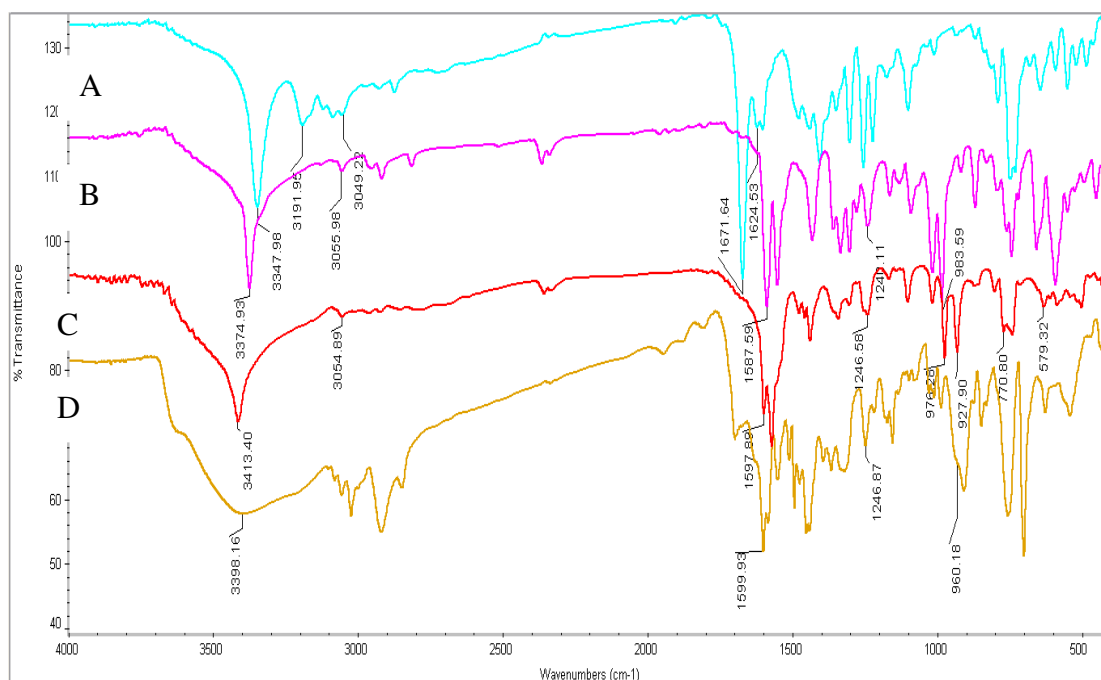
**Table 3.1.** IR spectral data ( $\text{cm}^{-1}$ ) of compounds.

Compound	$\nu(\text{OH})$	$\nu(\text{C}=\text{O})$	$\nu(\text{NH})_{\text{amide}}$
$\text{H}_2\text{hap-iah}$	3348	1671	3190
$[\text{V}^{\text{V}}\text{O}(\text{OMe})(\text{hap-iah})]$	3375	-	-
$\text{K}[\text{V}^{\text{V}}\text{O}(\text{O}_2)(\text{hap-iah})]^{\text{a}}$	3413	-	-
$\text{PS}-[\text{V}^{\text{V}}\text{O}(\text{OMe})(\text{hap-iah})]$	3398	-	-

Compound	$\nu(\text{NH})_{\text{indole}}$	$\nu(\text{C}=\text{N})$	$\nu(\text{V}=\text{O})$
$\text{H}_2\text{hap-iah}$	3049	1624	-
$[\text{V}^{\text{V}}\text{O}(\text{OMe})(\text{hap-iah})]$	3055	1587	983
$\text{K}[\text{V}^{\text{V}}\text{O}(\text{O}_2)(\text{hap-iah})]^{\text{a}}$	3054	1598	975
$\text{PS}-[\text{V}^{\text{V}}\text{O}(\text{OMe})(\text{hap-iah})]$	-	1600	960

<sup>a</sup>Bands due to the peroxido group: 927, 770 and 579  $\text{cm}^{-1}$ .



**Figure 3.5.** IR spectra of (A)  $H_2hap-iah$  (**II**), (B)  $[V^VO(OMe)(hap-iah)]$  (**3.1**), (C)  $K[V^VO(O_2)(hap-iah)]$  (**3.2**) and (D)  $PS-[V^VO(OMe)(hap-iah)]$  (**3.3**).

### 3.3.5. UV-visible spectral studies

The UV-visible spectra of the ligand (**II**), non-grafted complexes (recorded in methanol) and of grafted complex (recorded in Nujol as well as reflectance) are presented in Fig. 3.6 (A and B) while Table 3.2 includes spectral data. In the UV region, ligand  $H_2hap-iah$  (**II**) exhibits three spectral bands at 220, 274 and 319 nm corresponding to  $\sigma \rightarrow \sigma^*$ ,  $\pi \rightarrow \pi^*$  and  $n \rightarrow \pi^*$  transitions, respectively [107,108,112]. Upon complex formation, the band due to  $\pi \rightarrow \pi^*$  transition shifts slightly from 274 to 268 nm (in **3.1**) and to 271 nm (in **3.2**). Similarly,  $n \rightarrow \pi^*$  transition slightly shifts from 319 to 316 nm (in **3.1**) and to 322 nm (in **3.2**). The  $\sigma \rightarrow \sigma^*$  transition is observed at 220 nm in ligand as well as in complexes **3.1** and **3.2**. The observed ligand to metal charge transfer (LMCT) transition at ca. 380 nm from the phenolate oxygen atom to an empty d-orbital of the vanadium atom also provides evidence for the coordination of Schiff base to the metal

ion. The electronic spectrum of **3.3** recorded in Nujol shows spectral patterns very similar to **3.1** [Fig. 3.6 (B)] ( $\sigma \rightarrow \sigma^*$  at ca. 222 nm,  $\pi \rightarrow \pi^*$  at ca. 268 nm and  $n \rightarrow \pi^*$  at ca. 316 nm, and LMCT at ca. 380 nm). Further, diffuse reflectance spectrum of PS-[V<sup>V</sup>O(OMe)(hap-iah)] in BaSO<sub>4</sub> also shows all these bands [inset of Fig. 3.6 (B)] confirming the grafting of complex in polymer matrix.

**Table 3.2.** UV-visible spectral data of ligand and complexes.

Compound	Solvent	$\lambda_{\max}/\text{nm}$ ( $\epsilon/M^{-1}\text{cm}^{-1}$ )
H <sub>2</sub> hap-iah	MeOH	220 ( $3.82 \times 10^4$ ), 274 ( $2.05 \times 10^4$ ), 319 ( $8.11 \times 10^3$ )
[V <sup>V</sup> O(OMe)(hap-iah)]	MeOH	220 ( $6.88 \times 10^4$ ), 268 ( $3.29 \times 10^4$ ), 316 ( $1.20 \times 10^4$ ), 380 ( $2.86 \times 10^3$ )
K[V <sup>V</sup> O(O <sub>2</sub> )(hap-iah)]	MeOH	220 ( $4.10 \times 10^4$ ), 271 ( $1.88 \times 10^4$ ), 322 ( $7.55 \times 10^3$ ), 376 ( $2.17 \times 10^3$ )
PS-[V <sup>V</sup> O(OMe)(hap-iah)]	Nujol	222, 268, 316, 380
	Reflectance	220, 270, 322, 380

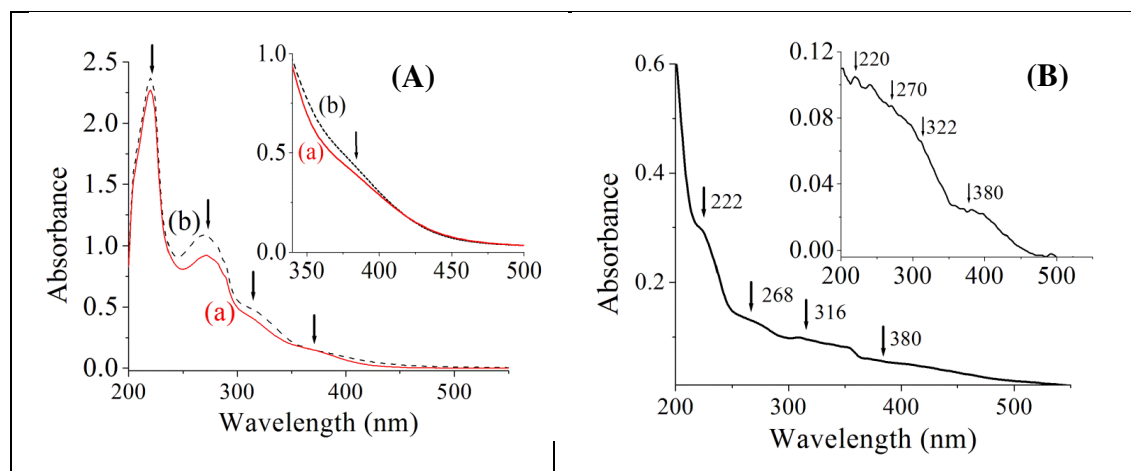


**Figure 3.6.** (A) UV-visible spectra of (a)  $[V^V O(OMe)(hap-iah)]$  (**3.1**) and (b)  $K[V^V O(O_2)(hap-iah)]$  (**3.2**) recorded in methanol. (B) UV-visible spectra of PS- $[V^V O(OMe)(hap-iah)]$  (**3.3**) recorded after dispersing this in Nujol. In inset shows diffuse reflectance spectrum of PS- $[V^V O(OMe)(hap-iah)]$  (**3.3**) recorded in  $BaSO_4$ .

### 3.3.6. $^1H$ , $^{13}C$ and $^{51}V$ NMR studies

The coordination behaviour of  $H_2hap-iah$  (**II**) was also confirmed by comparing its  $^1H$  NMR spectral patterns with complexes. Fig. 3.7 presents the  $^1H$  NMR spectra of **II** and **3.1**, and Fig. 3.8 shows the  $^1H$  NMR spectrum of complex **3.2**. Ligand shows two signals at 11.14 (s, 1H) and 13.21 ppm (s, 1H) due to the  $-NH$  (of  $-C(O)-NH-$  group) and phenolic OH, respectively (Table 3.3). Absence of these signals in the complexes confirms the enolization of  $-C(O)-NH-$  group followed by replacement of H by the metal ion and the coordination of the phenolic oxygen to the vanadium. Protons associated with aromatic, methylene, methyl (of *o*-hydroxyacetophenone) and NH (of indole) groups appear at nearly same positions in ligand as well as in complexes. A singlet due to coordinated methoxido group of complex **3.1** appears at 3.16 ppm [113].



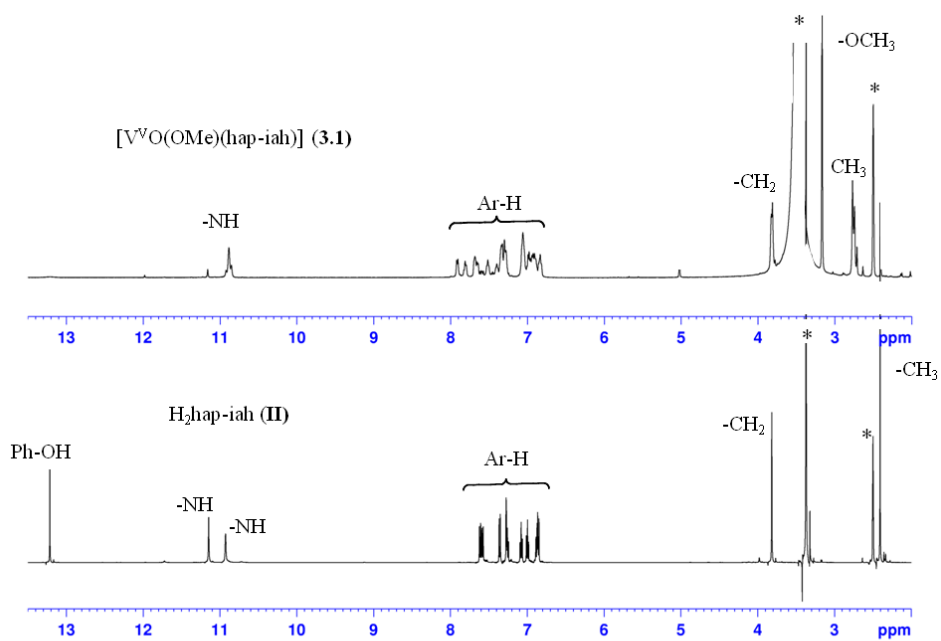


**Figure 3.7.**  $^1\text{H}$  NMR spectra of H<sub>2</sub>hap-iah (II) and  $[\text{V}^{\text{V}}\text{O}(\text{OMe})(\text{hap-iah})]$  (3.1). \* indicate peak due to DMSO-d<sub>6</sub>.

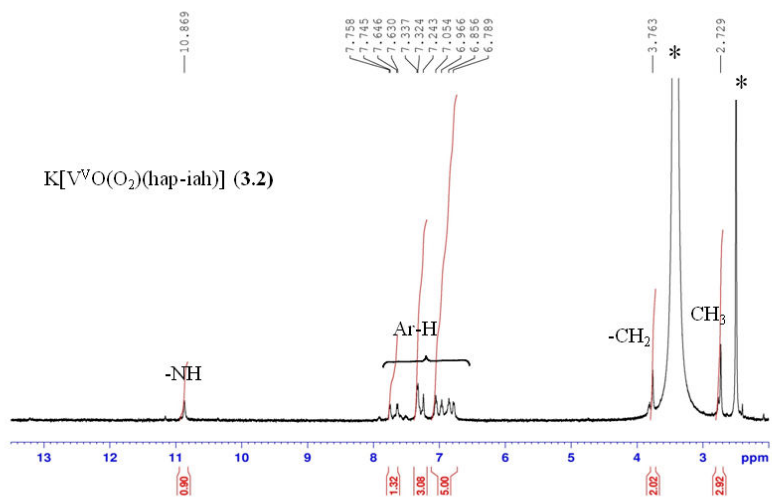


**Figure 3.8.**  $^1\text{H}$  NMR spectrum of  $\text{K}[\text{V}^{\text{V}}\text{O}(\text{O}_2)(\text{hap-iah})]$  (3.2).

**Table 3.3.**  $^1\text{H}$  NMR chemical shifts [ $\delta$  in ppm] of ligand and complexes recorded in DMSO- $d_6$ .

Compound <sup>a</sup>	–OH (phenolic)	–NH– (hydrazide)	–NH– (indole)
<b>II</b>	13.21 (s, 1H)	11.14 (s, 1H)	10.92 (s, 1H)
<b>3.1</b> <sup>b</sup>	-	-	10.88 (s, 1H)
<b>3.2</b>	-	-	10.86 (s, 1H)

Compound <sup>a</sup>	–C(CH <sub>3</sub> )=N–	–CH <sub>2</sub> –	Aromatic
<b>II</b>	2.40 (s, 3H)	3.818 (s, 2H)	6.84-7.62 (m, 9H)
<b>3.1</b> <sup>b</sup>	2.57 (s, 3H)	3.812 (s, 2H)	6.83-7.92 (m, 9H)
<b>3.2</b>	2.73 (s, 3H)	3.763 (s, 2H)	6.78-7.75 (m, 9H)

<sup>a</sup>Letters given in parentheses indicate the signal structure: s = singlet, m = multiplet

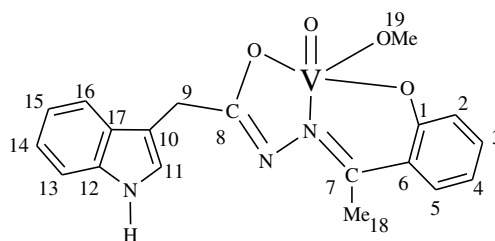
<sup>b</sup>Methyl of methoxy group appears at  $\delta = 3.16$  (s, 3H) ppm.

Table 3.4 provides  $^{13}\text{C}$  NMR spectral data of ligand and complexes and Fig. 3.9 reproduces their spectra. For aromatic carbons less number of signals was observed due to the presence of center of symmetry. However, some signals are thick hinting towards the impurity of other species (also see  $^{51}\text{V}$  NMR). A large coordination-induced shift [ $\Delta\delta = [\delta(\text{complex}) - \delta(\text{free ligand})]$ ] for carbon bearing phenolic oxygen (i.e. C1: 4.3 ppm for **3.1** and 4.6 ppm for **3.2**), carbon bearing azomethine nitrogen (i.e. C7: 5.3 ppm for **3.1** and 5.4 ppm for **3.2**) and carbon bearing enolic oxygen (i.e. C8: 7.0 ppm for **3.1** and 7.1 ppm for **3.2**) demonstrates the coordination of these functionalities to the vanadium. A considerable up field shift of C9 (methylene) carbon and down field shift of C18 (methyl) carbon were also noticed in complexes. The signal of co-ordinated methoxido (OMe) carbon resonates at  $\delta = 49.0$  ppm. Thus,  $^1\text{H}$  and  $^{13}\text{C}$  NMR spectra supplement the conclusion drawn from IR spectra.

The  $^{51}\text{V}$  NMR spectrum of **3.1**, recorded from a solution of **3.1** in a 3:2 mixture of  $\text{CH}_3\text{OH}/\text{CD}_3\text{OD}$ , shows a peak at  $\delta = -527$  ppm. Addition of 1 equivalent of  $\text{H}_2\text{O}_2$  to this

solution does not show any change, however, addition of 4 equivalents of H<sub>2</sub>O<sub>2</sub> shows two additional peaks (Fig. 3.10) centered at  $\delta = -567$  (45%) and  $-645$  ppm (5%), which are possibly due to peroxido complex  $[\text{V}^{\text{V}}\text{O}(\text{O}_2)(\text{hap-iah})]^-$  and free vanadium peroxido species [87,88,96]. The complex **3.2** shows one major peak at  $\delta = -527$  ppm (90%) and a minor peak at  $\delta = -563$  ppm (10%), suggesting that complex **3.2** converts into **3.1** with time in methanol.

The behavior of complexes in DMSO-d<sub>6</sub> is different. The <sup>51</sup>V NMR spectrum of **3.1**, recorded in DMSO-d<sub>6</sub>, shows three resonances at  $\delta = -520.8$  (62%),  $-540.0$  (9%) and  $-549.5$  ppm (29%) [Fig. 3.11(a)] which are tentatively assigned to methoxido complex **1**, DMSO coordinated complex **1** and dioxido complex  $[\text{V}^{\text{V}}\text{O}_2(\text{hap-iah})]^-$ , respectively [87,88,96]. The <sup>51</sup>V NMR spectrum of a solution of **1** in DMSO-d<sub>6</sub> in the presence of small amount of phosphate buffer (pH 7) was also recorded after ca. 5h and it shows only increment of the signal at  $\delta = -540.0$  ppm at the expense of signal at  $\delta = -520.8$  ppm [Fig. 3.11(b)] indicating no formation of any new species in pH 7 buffer.

**Table 3.4.**  $^{13}\text{C}$  NMR spectral data of ligand and complexes

Compound	C <sub>1</sub>	C <sub>2</sub> -C <sub>5</sub>	C <sub>6</sub>	C <sub>7</sub>	C <sub>8</sub>
<b>II</b>	155.2	117.7, 131.5, 121.6, 128.8	118.9	159.0	168.4
<b>3.1</b> ( $\Delta\delta$ ) <sup>a</sup>	159.5 (4.3)	119.4, 133.5, 122.7, 130.3	118.9	164.3 (5.3)	175.4 (7.0)
<b>3.2</b> ( $\Delta\delta$ )	159.8 (4.6)	119.5, 133.5, 121.5, 130.4	118.9	164.4 (5.4)	175.5 (7.1)
Compound	C <sub>9</sub>	C <sub>10</sub> , C <sub>11</sub> , C <sub>12</sub>	C <sub>13</sub> - C <sub>17</sub>	C <sub>18</sub>	C <sub>19</sub>
<b>II</b>	31.2	108.5, 127.7, 136.6	111.9, 124.5, 119.8, 118.9, 127.7	14.1	-
<b>3.1</b> ( $\Delta\delta$ ) <sup>a</sup>	28.1	108.9, 124.3, 136.5	111.7, 121.4, 121.4, 119.4, 127.7	17.7 (3.6)	49.0
<b>3.2</b> ( $\Delta\delta$ )	28.2	109.1, 124.4, 136.6	111.8, 121.5, 121.3, 119.2, 127.5	17.7 (3.6)	-

<sup>a</sup> Coordination-induced shifts [ $\Delta\delta = [\delta(\text{complex}) - \delta(\text{free ligand})]$ ].

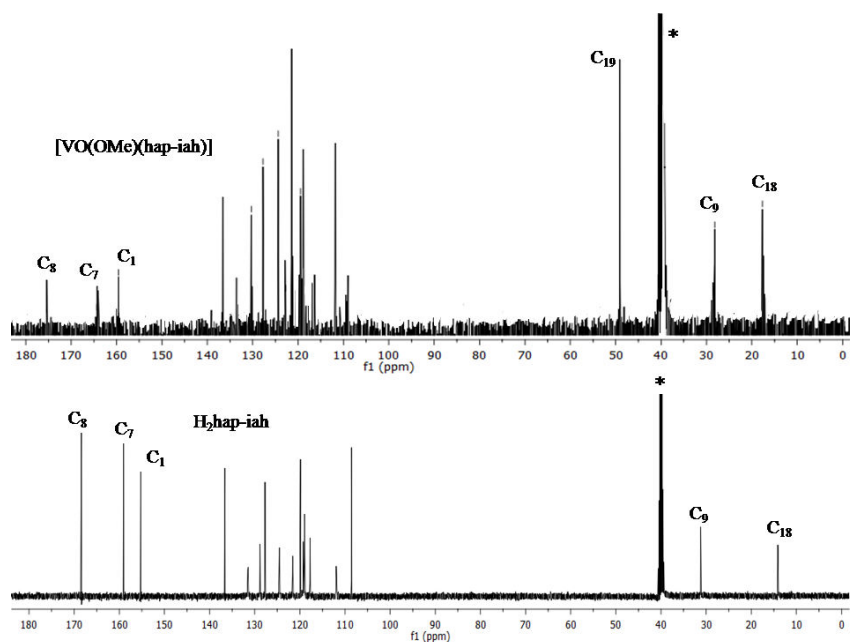


**Figure 3.9.**  $^{13}\text{C}$  NMR spectra of  $\text{H}_2\text{hap-iah}$  (**II**) and  $[\text{V}^{\text{V}}\text{O}(\text{OMe})(\text{hap-iah})]$  (**3.1**).

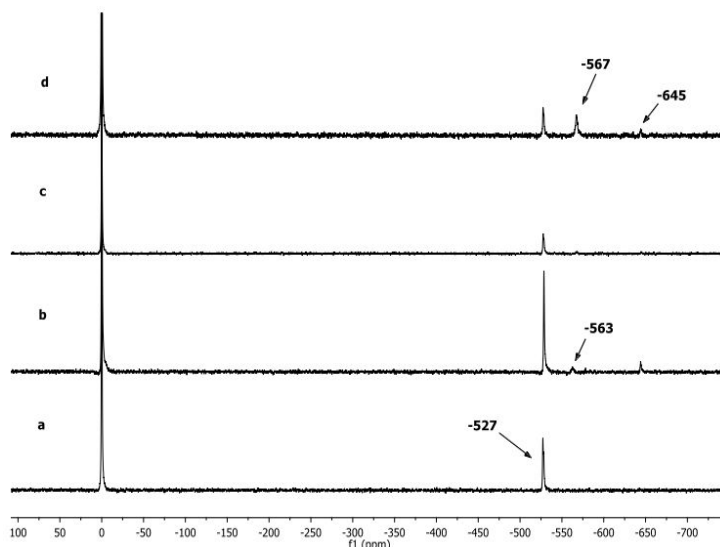


**Figure 3.10.**  $^{51}\text{V}$  spectra of:  $[\text{V}^{\text{V}}\text{O}[(\text{MeO})(\text{hap-iah})]]$  (a);  $[\text{V}^{\text{V}}\text{O}[(\text{O}_2)(\text{hap-iah})]]$  (b); Complex **3.1** with 1 equivalent of aqueous  $\text{H}_2\text{O}_2$  (c) and 4 equivalents of  $\text{H}_2\text{O}_2$  (d). The spectra were measured from solutions in a 3:2 mixture of  $\text{CH}_3\text{OH}/\text{CD}_3\text{OD}$ . The reference is neat  $\text{VOCl}_3$ .

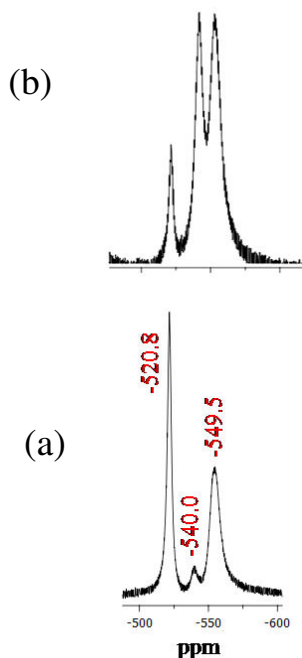


**Figure 3.11.**  $^{51}\text{V}$  NMR spectra [ $\delta$  in ppm] of  $[\text{V}^{\text{V}}\text{O}(\text{OMe})(\text{hap-iah})](\mathbf{3.1})$  recorded in  $\text{DMSO-d}_6$ . (a) Fresh solution of  $\mathbf{3.1}$ . (b) After addition of one drop of 30%  $\text{H}_2\text{O}_2$  to a solution of (a).

### 3.3.7. Electrospray ionization mass spectrometric study

In the high resolution mass spectrometry (ESI positive mode) of complex  $[\text{V}^{\text{V}}\text{O}(\text{OMe})(\text{hap-iah})](\mathbf{3.1})$  in MeCN, peaks obtained at  $m/z = 404.08$ ,  $426.06$  and  $442.03$  (Fig. 3.12) are due to the adduct  $[\text{HV}^{\text{V}}\text{O}(\text{OMe})(\text{hap-iah})]^+$ ,  $[\text{NaV}^{\text{V}}\text{O}(\text{OMe})(\text{hap-iah})]^+$  and  $[\text{KV}^{\text{V}}\text{O}(\text{OMe})(\text{hap-iah})]^+$ , respectively. These peaks confirm that  $\mathbf{3.1}$  is an oxidomethoxido complex. Other two peaks spotted at  $m/z = 330.08$  and  $346.09$  are due to  $[\text{Na}(\text{H}_2 \text{ hap-iah})]^+$  and  $[\text{K}(\text{H}_2 \text{ hap-iah})]^+$  fragmentations, respectively. Keeping this solution for longer time generates another peak at  $m/z = 799.48$  which corresponds to the  $[\text{K}\{\text{VO}(\text{hap-iah})\}_2\mu\text{-O}]^+$ , indicating the slow conversion of  $\mathbf{3.1}$  into  $[(\text{VO})_2\mu\text{-O}]^{2+}$  type complex. Conversion of methoxido- or dioxo- complexes into  $[(\text{VO})_2\mu\text{-O}]^{2+}$  type complex in acetonitrile is well known [89]. A freshly prepared solution of  $\mathbf{3.2}$  in MeCN

gives a prominent peak at  $m/z = 428.32$  corresponding to peroxido species,  $[\text{HNaVO}(\text{O}_2)(\text{hap-iah})]^+$ .

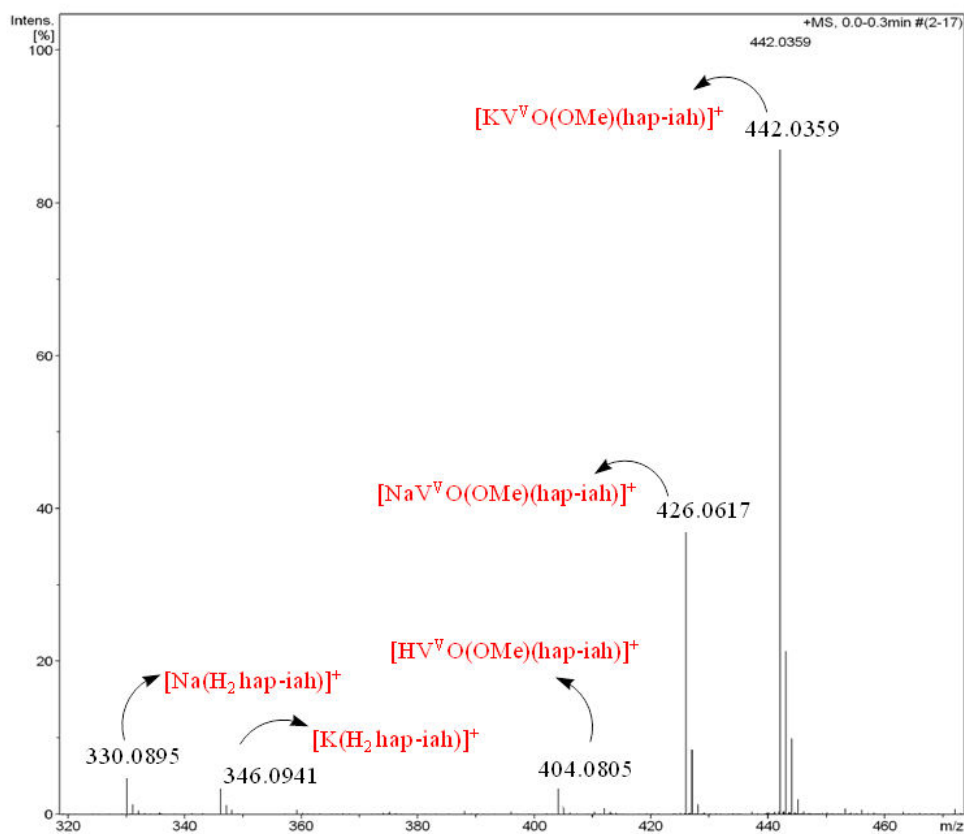
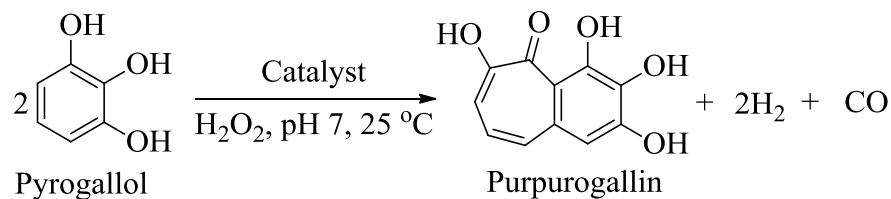


**Figure 3.12.** ESI-MS spectrum of  $[\text{V}^{\text{V}}\text{O}(\text{OMe})(\text{hap-iah})]$  (**3.1**) recorded in MeCN.

### 3.3.8. Peroxidase mimetic activity of polymer grafted complex

The peroxidase mimetic activity of polymer supported complex PS- $[\text{V}^{\text{V}}\text{O}(\text{OMe})(\text{hap-iah})]$  (**3.3**) was investigated by using the typical peroxidase substrate pyrogallol [114] in acetonitrile in the presence of  $\text{H}_2\text{O}_2$ . The peroxidase like oxidation of pyrogallol yields purpurogallin; Scheme 3.3. Its formation can be monitored by UV-visible spectrophotometer.



**Scheme 3.3.** Peroxidase like oxidation of pyrogallol to purpurogallin catalyzed by PS–[V<sup>V</sup>O(OMe)(hap-iah)] (**3.3**).

Preliminary experiments were carried under four different conditions:

- (i) 1 mL of  $2.5 \times 10^{-2}$  M pyrogallol,
- (ii) 1 mL of  $2.5 \times 10^{-2}$  M pyrogallol and 3 mL of 1 M phosphate buffer (pH 7).
- (iii) 1 mL of  $2.5 \times 10^{-2}$  M pyrogallol, 3 mL of 1 M phosphate buffer (pH 7) and 1 mL of  $2.5 \times 10^{-2}$  M solution of 30% H<sub>2</sub>O<sub>2</sub>.
- (iv) 1 mL of  $2.5 \times 10^{-2}$  M pyrogallol, 3 mL of 1 M phosphate buffer (pH 7), 1 mL of  $2.5 \times 10^{-2}$  M solution of 30% H<sub>2</sub>O<sub>2</sub> and 0.015 g of catalyst PS–[V<sup>V</sup>O(OMe)(hap-iah)] (**3.3**) previously swollen in H<sub>2</sub>O.

In all four reactions, the formation of the oxidation product at  $\lambda_{\text{max}} = 420$  nm was followed using UV-visible spectrophotometer after 3 min of their preparations under similar stirring condition. First two sets of solutions do not show any absorption while the transparent pyrogallol solution turns yellow [65] in the presence of H<sub>2</sub>O<sub>2</sub> [set (iii)] showing a very weak absorption at ca. 420 nm. Solutions of set (iv) gradually changed to pink and then to reddish-brown along with the appearance of a band at 420 nm within 3 min after mixing of catalyst, which was not present in the catalyst spectrum, indicating that pyrogallol can be oxidized by H<sub>2</sub>O<sub>2</sub> in the absence as well as in the presence of catalyst. However, the extent of oxidation is different in two cases; Fig. 3.13. The characteristic new band at 420 nm is due to the formation of purpurogallin which is absent in pyrogallol [115,116]. The intensity of this band was monitored with time for the



set (iv). The reaction attained the maximum measurable absorbance in 1.5 h (inset of Fig. 3.13).

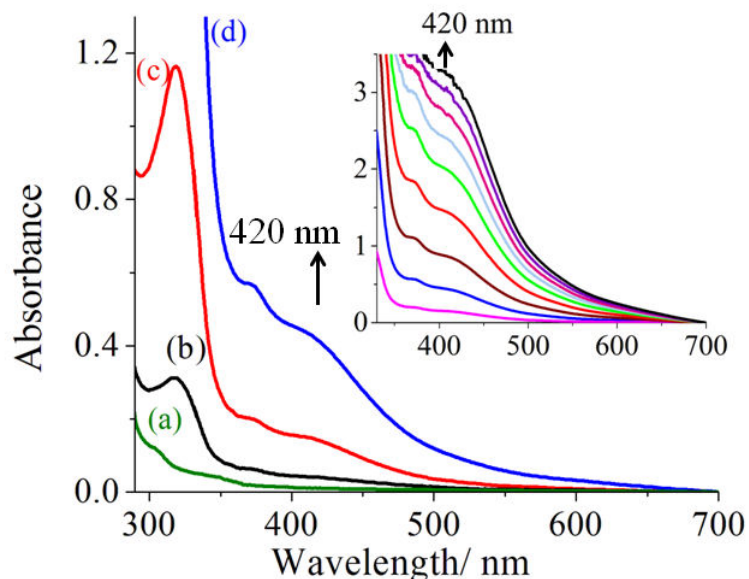


**Figure 3.13.** UV-visible Spectra of (a) pyrogallol solution [set (i)]; (b) pyrogallol in pH 7 buffer solution [set (ii)]; (c) pyrogallol mixed with  $\text{H}_2\text{O}_2$  in pH 7 buffer solution [set (iii)] and (d) Set (iii) in the presence of 0.015 g of catalyst PS-[ $\text{V}^{\text{V}}\text{O}(\text{OMe})(\text{hap-iah})$ ] obtained within 3 min after the preparation of solutions. For experimental details, see text. Inset shows electronic absorption changes observed with time due to the formation of purpurogallin. Reaction conditions: pyrogallol solution 1 mL ( $2.5 \times 10^{-2}$  M) mixed with 1 mL of 30%  $\text{H}_2\text{O}_2$  ( $2.5 \times 10^{-2}$  M), 3 mL phosphate buffer (pH 7, 1 M) and catalyst PS-[ $\text{V}^{\text{V}}\text{O}(\text{OMe})(\text{hap-iah})$ ] (0.015 g) at 25 °C.

Several parameters such as different amount of oxidant and catalyst and pH of the reaction medium were optimized to evaluate the best reaction conditions for maximization of pyrogallol oxidation.

The amount of catalyst was optimized by taking four different amounts (0.005, 0.010, 0.015 and 0.020 g) under the above reaction conditions i.e. 1 mL of  $2.5 \times 10^{-2}$  M pyrogallol, 3 mL of 1 M phosphate buffer (pH 7), 1 mL of  $2.5 \times 10^{-2}$  M solution of 30%  $\text{H}_2\text{O}_2$  and reaction temperature  $25^\circ\text{C}$  (Fig. 3.14). It can be concluded from the plot that the oxidation of pyrogallol increases considerably by using 0.005 g of catalyst (when compared to the reaction without catalyst). Increasing the catalyst amount to 0.010 g slightly improved the activity, while only a small increase was observed upon further increasing the catalyst amount (from 0.010 g to 0.015 g or 0.020 g). However, the overall reaction time to reach a peroxidase activity was considerably reduced with higher amount of catalyst. For example, 0.010 g catalyst showed the activity equivalent to 0.005 g catalyst within 1.5 h and 0.015 g catalyst showed the activity equivalent to 0.005 g catalyst within 1.2 h (data not shown). Therefore, an amount of 0.010 g of catalyst was considered the best one to optimize other reaction conditions.

The dependence of the pyrogallol oxidation at different amounts of oxidant i.e.  $\text{H}_2\text{O}_2$  was also studied. Thus, for a fixed amount of pyrogallol solution (1 mL of  $2.5 \times 10^{-2}$  M), catalyst (0.010 g) and pH 7 phosphate buffer (3 mL, 1 M), 1 mL of four different concentrations of  $\text{H}_2\text{O}_2$  viz.  $2.5 \times 10^{-5}$ ,  $2.5 \times 10^{-4}$ ,  $2.5 \times 10^{-3}$  or  $2.5 \times 10^{-2}$  M were added to each set and the reaction was again monitored at  $25^\circ\text{C}$  for 1.5 h. Fig. 3.15 shows the plots of absorbance at  $\lambda_{\text{max}} = 420$  nm at different concentrations of  $\text{H}_2\text{O}_2$  with time. The catalyst shows good response towards different  $\text{H}_2\text{O}_2$  concentrations. However, a minimum  $\text{H}_2\text{O}_2$  concentration of  $2.5 \times 10^{-4}$  M was considered the best one as higher than this amount of oxidant shows no considerable increase in absorbance.

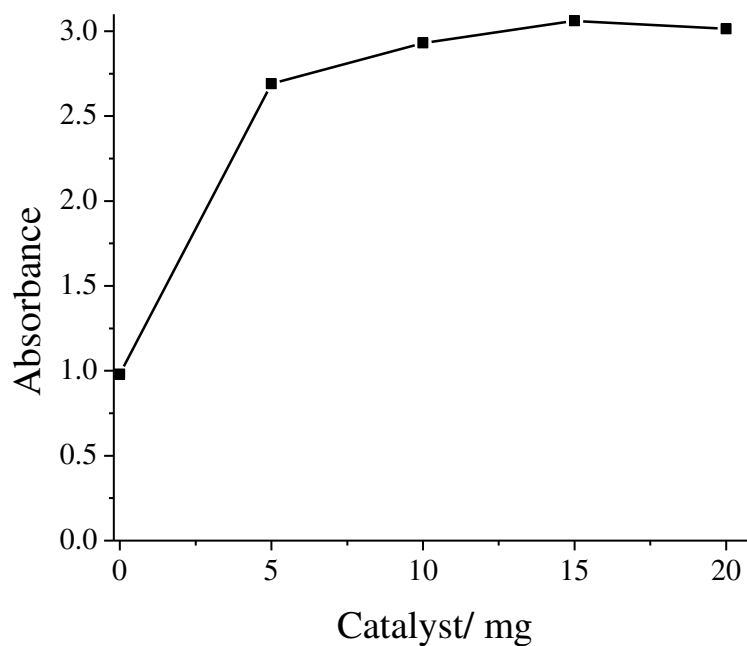


**Figure 3.14.** Plot of maximum absorbance at 420 nm during peroxidase activity with pyrogallol measured using different amounts of catalyst. Other reaction conditions: i.e. 1 mL of  $2.5 \times 10^{-2}$  M pyrogallol, 3 mL of phosphate buffer (pH 7, 1 M), 1 mL of  $2.5 \times 10^{-2}$  M solution of 30%  $H_2O_2$  and reaction temperature  $25^\circ C$  in 1.5 h of reaction time.

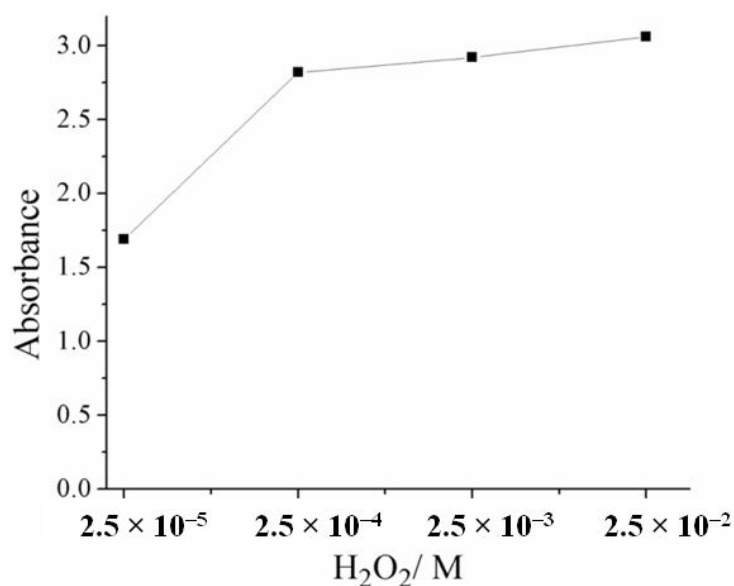


**Figure 3.15.** Plot of maximum absorbance at 420 nm during peroxidase activity with pyrogallol measured using different amounts of oxidant in 1.5 h of reaction time. Other reaction conditions: pyrogallol (1 mL of  $2.5 \times 10^{-2}$  M), pH 7 phosphate buffer (3 mL of 1 M) and catalyst PS-[V<sup>V</sup>O(OMe)(hap-iah)] (0.010 g) at 25 °C.

The peroxidase activity was also evaluated in buffered solutions of five different pH values (5 to 9). The maximum measurable absorbance at  $\lambda_{\max} = 420$  nm, independent of time, is shown in Fig. 3.16. The reaction rate was fastest in pH 9 in which the 420 nm band gained the maximum measurable absorbance within 20 min of reaction time. The peroxidase activity was comparatively slower in pH 8 buffer solutions and it took 40 min to attain the same absorbance as observed for pH 9. A further decrease in activity was noted for pH 7 buffer solution where the 420 nm band gained the maximum measurable absorbance in 1.5 h. Only maximum absorbance of 0.08 and 0.12 could be obtained in buffers of pHs 5 and 6, respectively. In spite of showing maximum activity at pH 9, we have considered pH 7 as optimal pH for our catalyst, since this pH is physiologically relevant and also environmentally similar to natural peroxidases in biological systems.

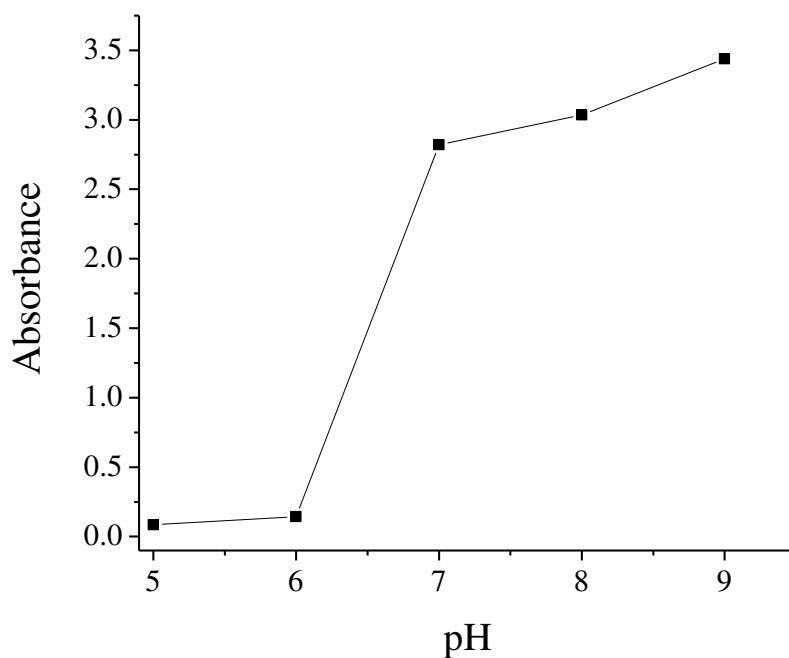


**Figure 3.16.** Plot showing maximum absorbance at  $\lambda_{\max} = 420$  nm by catalyst at different pH values of buffer solutions (3 mL, 1 M). Other reaction conditions: pyrogallol solution (1 mL,  $2.5 \times 10^{-2}$  M), PS-[ $V^V O(OMe)(hap-iah)$ ] (0.010 g), 30%  $H_2O_2$  (1 mL,  $2.5 \times 10^{-4}$  M) and reaction temp. (25 °C).

Catalyst **3.3**, after washing with acetonitrile and drying, was reused up to 4 cycles and exhibited roughly the same activity. To rule out the possibility that the peroxidase like activity is related to free vanadium ion instead of the polymer anchored complex **3.3**, the reaction mixture after catalytic experiments were subjected to ICP-MS. No vanadium content was found in the reaction mixture, demonstrating that the peroxidase like activity is only due to the polymer anchored complex.

Neat complex [ $V^V O(OMe)(hap-iah)$ ] (**3.1**) has also been tested for the oxidation of pyrogallol. Considering  $2.5 \times 10^{-3}$  M of **3.1** in 0.25 mL of acetonitrile (0.0316 mg V content in complex **3.1** vs. 0.1647 mg V content in **3.3** i.e. equivalent to 1/5 of the

complex present in polymer supported one), 1 mL of  $2.5 \times 10^{-2}$  M pyrogallol, 3 mL phosphate buffer (pH 7, 1 M) and 1 mL of  $2.5 \times 10^{-4}$  M solution of 30%  $\text{H}_2\text{O}_2$  and the change in absorbance at 420 nm was measured. The reaction attained the maximum measurable absorbance in 1 h (Fig. 3.17), suggesting that neat complex is more active than the polymer supported analogue. However, other factors noted below makes the supported complex better.

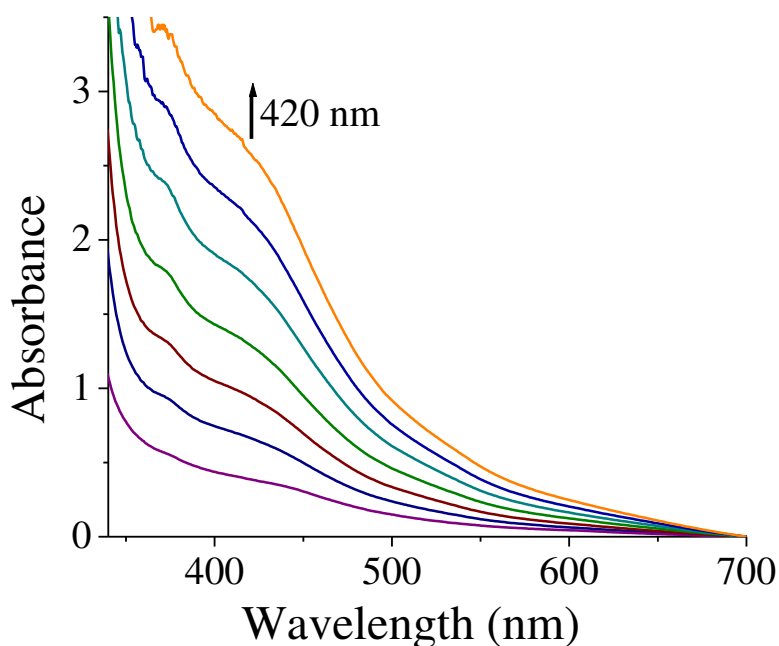


**Figure 3.17.** Plot of maximum absorbance at 420 nm during peroxidase activity with pyrogallol measured using  $2.5 \times 10^{-3}$  M of  $[\text{V}^{\text{V}}\text{O}(\text{OMe})(\text{hap-iah})]$  (**3.1**) in 0.25 mL of acetonitrile. Other reaction conditions: i.e. 1 mL of  $2.5 \times 10^{-2}$  M pyrogallol, 3 mL phosphate buffer (pH 7, 1 M), 1 mL of  $2.5 \times 10^{-4}$  M solution of 30%  $\text{H}_2\text{O}_2$  and reaction temperature  $25^\circ\text{C}$  in 1 h of reaction time.

For better understanding of the peroxidase mimetic activity of **3.3**, the kinetic parameters such as  $V_{\text{max}}$ ,  $K_{\text{M}}$ ,  $K_{\text{cat}}$  were determined. For this purpose, several experiments were conducted in phosphate buffer of pH 7 (1 M) at  $25^\circ\text{C}$  by varying the concentration

of pyrogallol from 0.2 mM to 2.2 mM while keeping concentrations of H<sub>2</sub>O<sub>2</sub> and catalyst constant in all sets of experiment. The reactions were carried out for 10 minutes and initial reaction rates were calculated by measuring the absorbance at 420 nm in kinetic mode. Experiments were run in triplicates and their average was used to calculate initial rates. According to much enzymatic reaction kinetic assay, the reaction rates were fitted to Michaelis-Menten Eq. (3.3):

$$V_i = V_{\max} \times \frac{[S]}{K_M + [S]} \quad (3.3)$$

Where  $V_i$  is the initial reaction rate,  $V_{\max}$  is the maximum rate,  $[S]$  is the concentration of substrate and  $K_M$  is the Michaelis-Menten constant.

We observed that for catalyst **3.3**,  $V_i$  follows saturation kinetics with respect to substrate concentration  $[S]$ . The rate of reaction is first-order for the low substrate concentration  $[S]$  *i.e.* linear plot is obtained for  $V_i$  versus  $[S]$ . At sufficient high  $[S]$ , the catalyst became saturated with the substrate and the rate of reaction is zero-order. Thus, **3.3** follows a Michaelis-Menten behavior towards pyrogallol; Fig. 3.18 (a). The Lineweaver-Burk plot was employed to calculate the kinetic parameters; Fig. 3.18(b). The  $V_{\max}$  obtained was 3.87  $\mu\text{M min}^{-1}$  and the turn over frequency ( $k_{\text{cat}}$ ) was determined 4.79  $\times 10^{-3} \text{ min}^{-1}$  for the catalyst **3.3** for the oxidation of pyrogallol, using the  $V_{\max}$  and the active catalytic site of the catalyst with the help of Eq. (3.4).

$$k_{\text{cat}} = \frac{V_{\max}}{[\text{catalytic site}]} \quad (3.4)$$

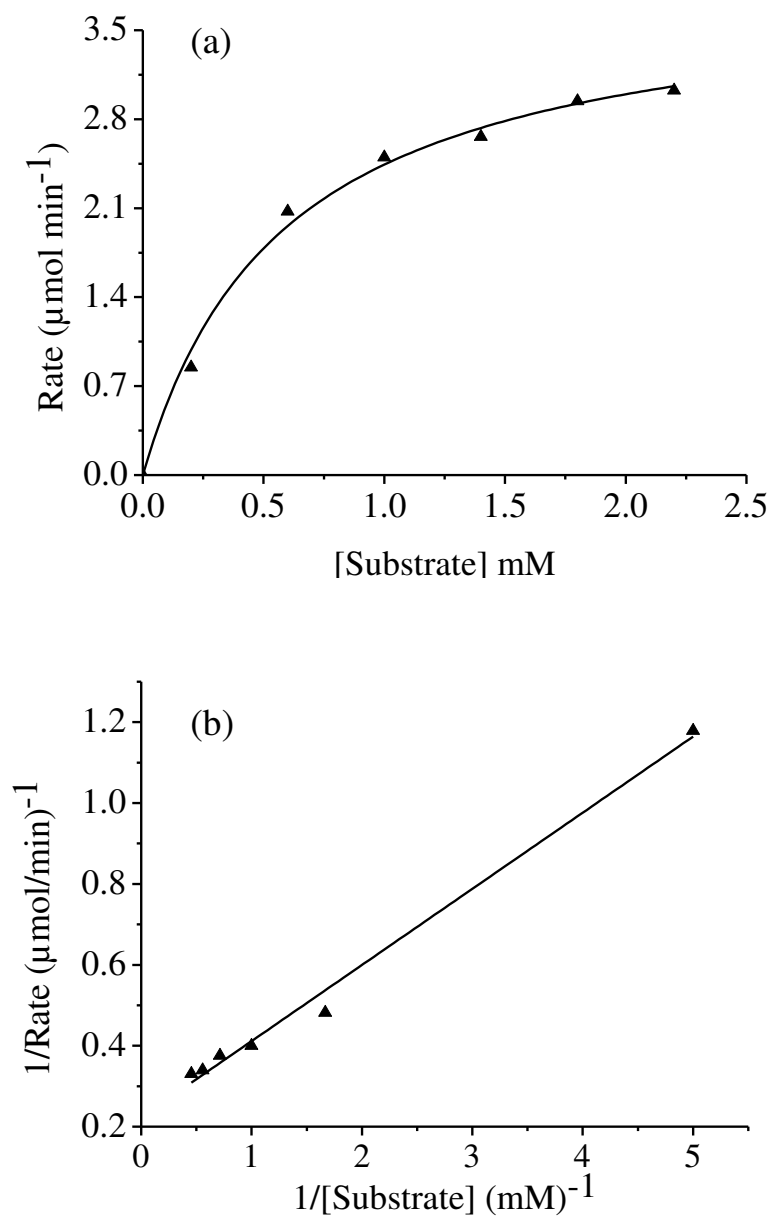


**Figure 3.18.** Michaelis-Menten curve fit (a) for variation of pyrogallol concentration (0.2–2.2 mM) while keeping  $\text{H}_2\text{O}_2$  ( $2.5 \times 10^{-4}$  M) and PS-[ $\text{V}^{\text{V}}\text{O}(\text{OMe})(\text{hap-iah})$ ] (**3.3**) (0.010 g) concentration constant in phosphate buffer (pH7, 1 M) and corresponding Lineweaver-Burk linearization (b).



The stability of the complex PS-[V<sup>V</sup>O(OMe)(hap-iah)] in pH 6, 7 and 8 buffer solutions in acetonitrile was also checked. In each case, after 2 h of stirring, the complex was recovered, dried and IR spectrum was recorded. No significant change was observed by comparing the resulting spectra to that of a fresh complex; Fig. 3.19. Filtrates obtained from these experiments were also checked by ICP-MS and no leaching of metal ions was observed suggesting the possibility of doing reaction under above pHs without any leaching of catalyst.

Thus, it is concluded that PS-[V<sup>V</sup>O(OMe)(hap-iah)] (**3.3**) is a suitable supported catalyst to perform the oxidation of pyrogallol in biological conditions (pH 7 aqueous medium), mimicking peroxidase activity and therefore can be employed to perform environmentally friendly heterogeneous catalytic process.

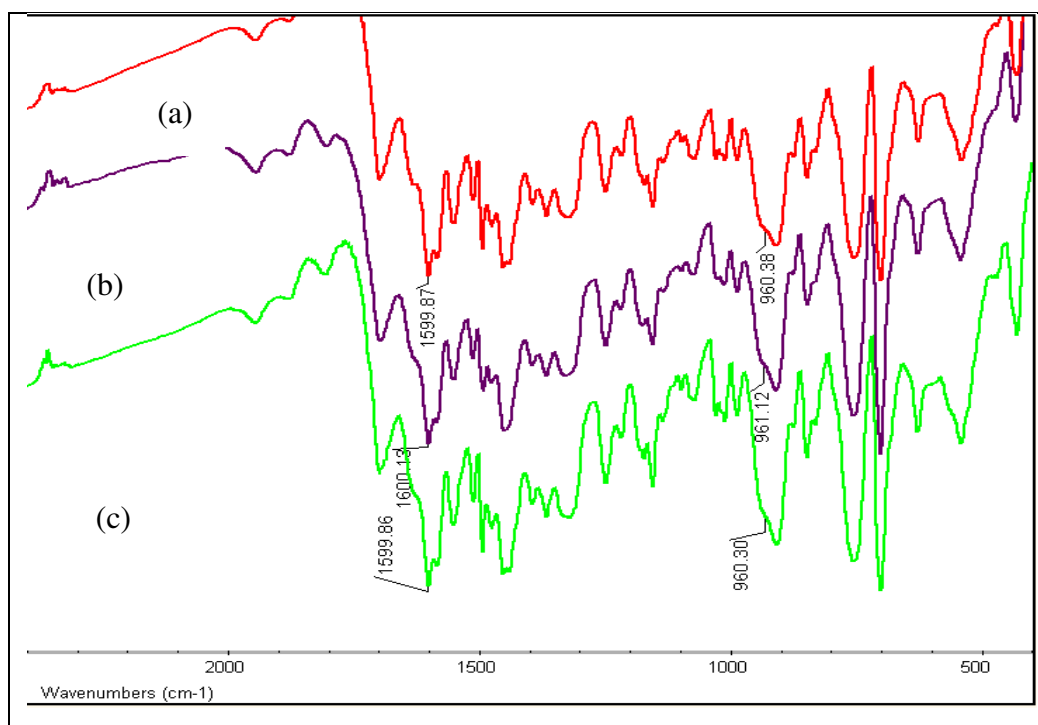


**Figure 3.19.** IR spectra recorded after suspending the complex PS-[V<sup>V</sup>O(OMe)(hap-iah)] in MeCN at different pHs [(a), pH=6; (b), pH=7 and (c), pH=8].

**3.3.9. Reactivity of  $[V^V O(OMe)(hap-iah)]$  and  $K[V^V O(O_2)(hap-iah)]$  with  $H_2O_2$  and possible reaction pathway**

The oxidoperoxidovanadium(V) complex has been proposed as an important intermediate formed during catalytic reaction [65]. We have been able to isolate peroxido complex  $K[V^V O(O_2)(hap-iah)]$  (**3.2**) by the reaction of  $H_2O_2$  and KOH with complex **3.1** and characterize it. Its formation has also been established in solution by Uv-visible spectrophotometer. The titration of a 33 mL of methanolic solution of  $[V^V O(OMe)(hap-iah)]$  ( $1.6 \times 10^{-4}$  M) with 30 %  $H_2O_2$  (one drop, 0.0585 g, 0.52 mmol) dissolved in 10 mL of MeOH results in the shift of 268 nm band to 272 nm along with decrease in intensity. After addition of 6 drops of this diluted  $H_2O_2$  further, no shift was noted in the band's position but intensity decreased regularly. Similarly, other bands i.e. at 220, 316 and 380 nm remain nearly unchanged with only partial reduction in intensity; Fig 3.20. These changes show the generation of oxidoperoxidovanadium(V) complex which was also confirmed by recording  $^{51}V$  NMR and ESI-MS of the resulting solution (vide supra). The peroxidovanadium(V) complex finally transfer oxygen to the substrate through other intermediate(s) as suggested earlier [65].

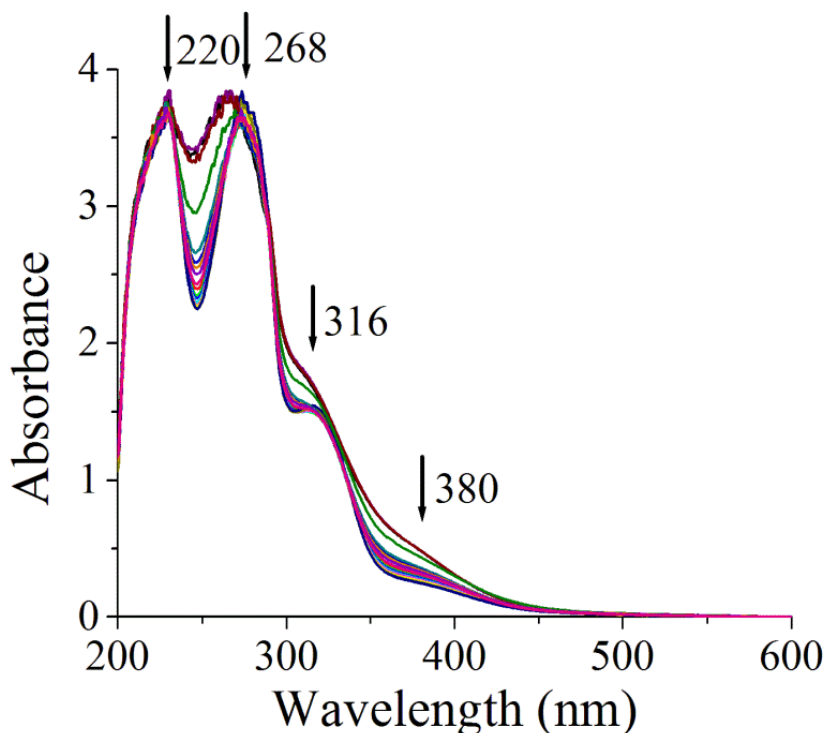


**Figure 3.20.** UV-Vis spectral changes observed during titration of  $[V^V O(OMe)(hap-iah)]$  (**3.1**) with  $H_2O_2$ . The spectra recorded after successive addition of one drop portions of dilute  $H_2O_2$  (1 drop of 30%  $H_2O_2$  in 10 mL MeOH) to 33 mL of  $1.6 \times 10^{-4}$  M solution of **3.1**.

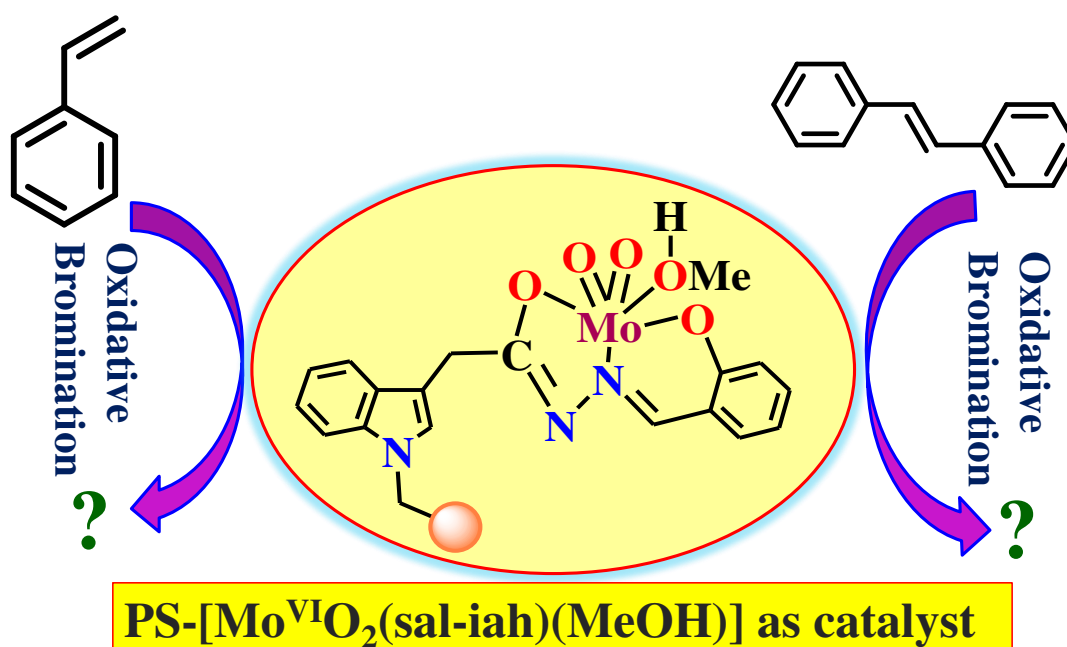
### 3.4. Conclusions

A heterogeneous catalyst  $PS-[V^{VI}O(OMe)(hap-iah)]$  (**3.3**) has been prepared by grafting it in chloromethylated polystyrene cross-linked with 5% divinylbenzene via covalent bonding through imino nitrogen of the indole group of the ligand. Complex  $[V^V O(OMe)(hap-iah)]$  (**3.1**) used for this purpose was prepared by the reaction of  $[V^{IV}O(acac)_2]$  with ONO donor tridentate ligand  $H_2hap-iah$  (**II**). The possible intermediate oxidoperoxo-complex  $K[V^V O(O_2)(hap-iah)]$  (**3.2**) observed during catalytic reaction has also been prepared in the solid state in presence of  $KOH/H_2O_2$  or generated in methanol by the reaction of **3.1** with  $H_2O_2$ . The polymer-grafted complex

**3.3** is able to perform the oxidation of pyrogallol in pH 7 phosphate buffer solution. The catalytic activity of homogeneous catalyst **3.1** is equally good. However, easy separation of **3.3** from the reaction medium of pH 7 buffer and the reusability without considerable decrease in activity, suggest that it can be employed to perform environment friendly peroxidase mimetic activity like oxidation of pyrogallol.

# CHAPTER 4

Polymer and non-polymer-grafted dioxidomolybdenum(VI) complexes having ONO donor ligand and their catalytic activities for the oxidative bromination of organic substrates



## 4.1. Introduction

Catalytic applications of molybdenum complexes in oxidation and oxygen-transfer reactions including oxidation of sulfides [6,56,61,117-135] have extensively been studied. Immobilizations of these homogeneous catalysts on solid support find limited mention in the literature though such catalysts have potential prospect for technological applications [24, 74] because solid supported catalysts meet the industrial demand of recyclability and thermal stability along with high turnover rates and environment-friendly synthetic routes to fine chemicals [1,80-83].

Recently our attention was drawn on the oxidative bromination of organic substrates by vanadium complexes, a reaction normally promoted by vanadium haloperoxidase enzymes [136-138]. These homogeneous as well as heterogeneous vanadium complexes satisfactorily catalyze the oxidative bromination of styrene, *trans*-stilbene and salicylaldehyde [62,63,89,105,139-142]. Such functional similarities have also been demonstrated by some homogeneous molybdenum complexes [78,143,144].

We have recently immobilized dioxidovanadium(V) complex of indole-derived ONO donor ligand H<sub>2</sub>sal-iah (**I**) onto chloromethylated polystyrene cross-linked with divinyl benzene (PS-CH<sub>2</sub>Cl) for the development of more environmentally benign heterogeneous catalyst and have explored their use as possible functional model for haloperoxidase enzymes. Insertion of spacer (extra CH<sub>2</sub> group) between polymer support and catalyst improved the performance of the catalyst by allowing the better interaction of catalytic center with substrates and oxidant during catalytic reaction [107]. We now report the immobilization of dioxidomolybdenum(VI) complex of H<sub>2</sub>sal-iah (**I**) onto chloromethylated polystyrene. Its characterization and catalytic potential toward the oxidative bromination of styrene and *trans*-stilbene are reported here. The corresponding non polymer-grafted molybdenum complex has also been prepared for comparing its catalytic performance.

## 4.2. Experimental

### 4.2.1. Materials

Analytical reagent grade ammonium molybdate, molybdenum trioxide (S. D. Fine, India) and *trans*-stilbene (Lancaster, England) were used as obtained.  $[\text{Mo}^{\text{VI}}\text{O}_2(\text{acac})_2]$  [145] were prepared according to methods reported in the literature. Other chemicals and solvents of analytical reagent grades were used without purifications.

### 4.2.2. Physical methods and analysis

Details of instrumentation and characterization procedures are presented in Chapter 2.

### 4.2.3. Synthesis

#### 4.2.3.1. $[\text{Mo}^{\text{VI}}\text{O}_2(\text{sal-iah})(\text{MeOH})]$ (4.1)

A stirred solution of  $[\text{Mo}^{\text{VI}}\text{O}_2(\text{acac})_2]$  (0.329 g, 1 mmol) dissolved in methanol (15 mL) was added to a solution of  $\text{H}_2\text{sal-iah}$  (0.293 g, 1 mmol) in methanol (25 mL) and the resulting reaction mixture was stirred for ca. 6 h at room temperature. After reducing the solvent volume to ca. 10 mL and standing the solution in air for 24 h, the orange crystalline compound precipitated which was filtered off, washed with methanol and dried *in vacuo*. Yield 0.42 g (93%) *Anal. Cal.* for  $\text{C}_{18}\text{H}_{17}\text{N}_3\text{O}_5\text{Mo}$  (451.29): C, 47.91; H, 3.80; N, 9.31. Found: C, 47.8; H, 4.0; N, 8.9%.

#### 4.2.3.2. $[\text{Mo}^{\text{VI}}\text{O}(\text{O}_2)(\text{sal-iah})(\text{MeOH})]$ (4.2)

Aqueous 30%  $\text{H}_2\text{O}_2$  (ca. 2 mL) was added dropwise to complex **4.1** (0.451 g, 1 mmol) dissolved in methanol (50 mL) with constant stirring at ambient temperature. After ca. 4 h, the solvent was slowly reduced to 10 mL by passing air through the solution and kept at room temperature for slow precipitation of complex. The precipitated solid was filtered, washed with cold methanol (2× 4 mL) and dried in air. Yield 0.23 g

(50%) *Anal.* Cal. for  $C_{18}H_{17}N_3O_6Mo$  (467.29): C, 46.27; H, 3.67; N, 8.99. Found: C, 46.1; H, 3.7; N, 8.8%.

#### 4.2.3.3. PS-[Mo<sup>VI</sup>O<sub>2</sub>(sal-iah)(MeOH)] (4.3)

Chloromethylated polystyrene (1.0 g) was allowed to swell in DMF (8 mL) for 2 h. A solution of [Mo<sup>VI</sup>O<sub>2</sub>(sal-iah)(MeOH)] (1.0 g, 2.2 mmol) in DMF (8 mL) was added to the above suspension followed by triethylamine (1.33 g) in ethylacetate (7 mL), and the obtained reaction mixture was heated at 80 °C for 24 h with continuous but slow stirring. After cooling to room temperature, the polymer-grafted complex was separated by filtration, washed with hot DMF, followed by hot methanol and dried in an oven in air at 110 °C.

#### 4.2.4. X-ray crystal structure determination

Three-dimensional X-ray data for **4.1** were collected on a Bruker SMART Apex CCD diffractometer at room temperature, using a graphite monochromator and Mo- $K_{\alpha}$  radiation ( $\lambda = 0.71073 \text{ \AA}$ ) by the  $\phi$ - $\omega$  scan method. Reflections were measured from a hemisphere of data collected from frames each of them covering 0.3° in  $\omega$ . Of the 33,032 reflections measured, all were corrected for Lorentz and polarization effects and for absorption by multi-scan methods based on symmetry-equivalent and repeated reflections, 4475 independent reflections exceeded the significance level ( $|F|/\sigma|F|$ ) > 4.0. Complex scattering factors were taken from the program package SHELXTL [146]. The structure was solved by direct method and refined by full matrix least-squares on  $F^2$ . Hydrogen atoms were left to refine freely, except to C(4) and C(18) which were included in calculation positions and refined in the riding mode. Refinements were done with allowance for thermal anisotropy of all non-hydrogen atoms. Further details of the crystal structure determination are given in Table 4.1. A final difference Fourier map showed no



residual density outside: 0.432 and  $-0.464 \text{ e.}\text{\AA}^{-3}$ . A weighting scheme  $w = 1/[\sigma^2(F_o^2) + (0.046900P^2) + 0.172800P]$  was used in the latter stages of refinement.

**Table 4.1.** Crystal data and structure refinement for  $[\text{Mo}^{\text{VI}}\text{O}_2(\text{sal-iah})(\text{MeOH})]$  (**4.1**).

Formula	$\text{C}_{18}\text{H}_{17}\text{MoN}_3\text{O}_5$
Formula weight	451.29
T, K	293(2)
Wavelength, $\text{\AA}$	0.71073
Crystal system	Monoclinic
Space group	$\text{P2}_1/\text{c}$
$a/\text{\AA}$	15.3299(4)
$b/\text{\AA}$	15.1955(4)
$c/\text{\AA}$	7.8411(2)
$\beta/^\circ$	103.8140(10)
$V/\text{\AA}^3$	1773.72(8)
Z	4
$F_{000}$	912
$D_{\text{calc}}/\text{g cm}^{-3}$	1.690
$\mu/\text{mm}^{-1}$	0.776
$\theta/^\circ$	1.37-31.89
$R_{\text{int}}$	0.0418
Crystal size/ $\text{mm}^3$	$0.21 \times 0.18 \times 0.16$
Goodness-of-fit on $F^2$	1.093
$R_1[\text{I} > 2\sigma(\text{I})]^a$	0.0311
$wR_2$ (all data) <sup>b</sup>	0.0971
Largest differences peak and hole ( $\text{e}\text{\AA}^{-3}$ )	0.432 and -0.464

$${}^a R_1 = \frac{\sum |F_o| - |F_c|}{\sum |F_o|} \cdot {}^b wR_2 = \left\{ \frac{\sum [w(|F_o|^2 - |F_c|^2)]^2}{\sum [w(F_o^4)]} \right\}^{1/2}$$

#### 4.2.5. Catalytic activity

The catalytic oxidative bromination of styrene and *trans*-stilbene was carried out in a 100 ml flask at ca. 40 °C. Polymer-grafted catalyst was kept in MeOH for 1 h before use.

##### 4.2.5.1. Oxidative bromination of styrene

Catalyst (0.015 g), styrene (1.04 g, 10 mmol), KBr (2.38 g, 20 mmol), aqueous 30 % H<sub>2</sub>O<sub>2</sub> (2.27 g, 20 mmol) and 70 % aqueous HClO<sub>4</sub> (2.86 g, 20 mmol, added in four equal portions at t = 0, 15, 30 and 45 min) were stirred at 40 °C in a biphasic dichloromethane–water (40 mL 50%, v/v mixture) system for 2 h. At every 15 min small aliquot of the reaction mixture present in organic layer was withdrawn and analyzed quantitatively by gas chromatograph.

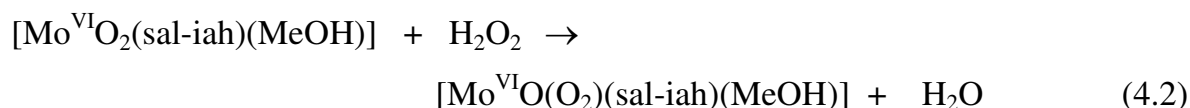
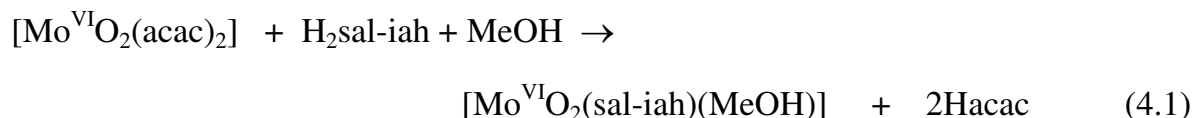
##### 4.2.5.2. Oxidative bromination of *trans*-stilbene

Catalyst (0.015, g) *trans*-stilbene (0.90 g, 5 mmol), KBr (2.38 g, 20 mmol), aqueous 30% H<sub>2</sub>O<sub>2</sub> (2.27 g, 20 mmol) and 70% aqueous HClO<sub>4</sub> (2.86 g, 20 mmol, added in four equal portions at t = 0, 15, 30 and 45 min) were stirred at 40 °C in a biphasic chloroform–water (40 mL 50%, v/v mixture) system for 2 h. After 2 h the reaction mixture was washed with water and the organic layer was separated. Various reaction products were analyzed by gas chromatograph using this organic layer. The separation and identification of the reaction products were done as reported earlier [63].

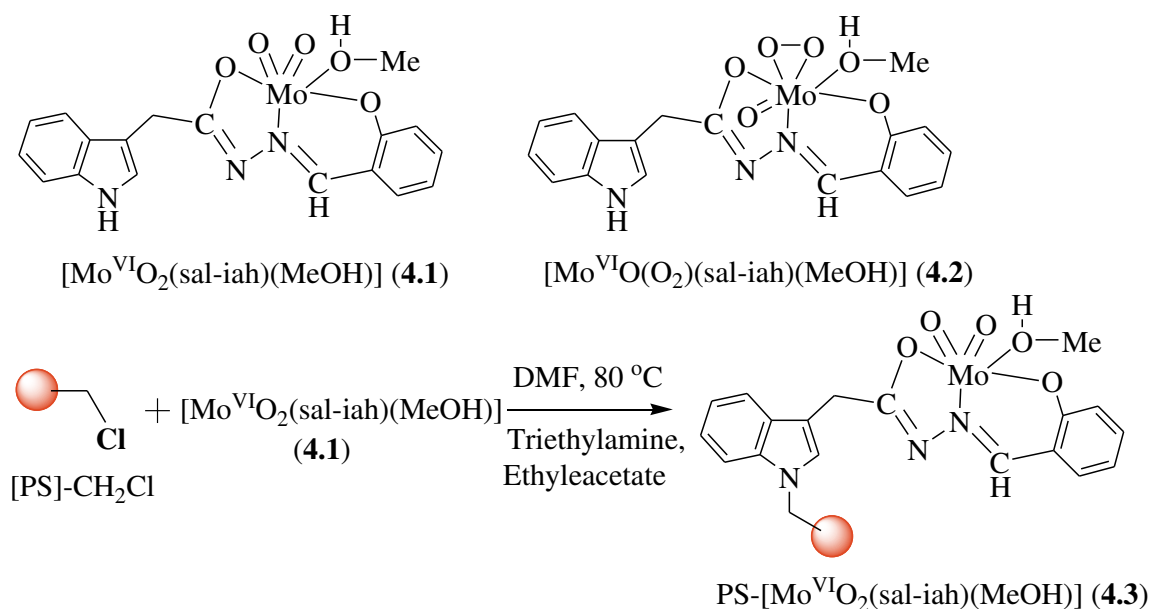
### 4.3. Results and discussion

#### 4.3.1. Synthesis and characterization

Reaction between equimolar amounts of ligand H<sub>2</sub>sal-iah (**I**) and [Mo<sup>VI</sup>O<sub>2</sub>(acac)<sub>2</sub>] in refluxing MeOH gave [Mo<sup>VI</sup>O<sub>2</sub>(sal-iah)(MeOH)] (**4.1**) [Eq. (4.1)]. Its reaction with 30 % *aq.* H<sub>2</sub>O<sub>2</sub> in methanol gave complex [Mo<sup>VI</sup>O(O<sub>2</sub>)(sal-iah)(MeOH)] (**4.2**) [Eq. (4.2)]. Both the complexes are fairly soluble in methanol, DMF and DMSO. Scheme 4.1 presents the structures proposed for these complexes, which are based on the elemental analyses, spectroscopic characterization (IR, electronic, <sup>1</sup>H and <sup>13</sup>C NMR), thermogravimetric patterns and single crystal X-ray analysis of **4.1**. The ligand coordinates through its dianionic (ONO) functionalities.



The reaction of chloromethylated polystyrene (cross linked with 5% divinylbenzene) with dioxidomolybdenum(VI) complex **4.1** in DMF at 80 °C in the presence of triethylamine leads to the formation of polymer-anchored complex PS-[Mo<sup>VI</sup>O<sub>2</sub>(sal-iah)(MeOH)] (**4.3**). During this process, the labile proton of NH group of the indole reacts with CH<sub>2</sub>Cl group of polymer. The whole synthetic procedures are presented in Scheme 4.1. The ICP-MS analysis of molybdenum in the polymer-grafted complexes suggests molybdenum loading of 0.45 mmol g<sup>-1</sup> of polymer in **4.3**.



**Scheme 4.1.** Proposed structures of complexes **4.1**, **4.2** and **4.3**, and synthetic route to prepare **4.3**; PS (or ball) represents the backbone of the chloromethylated polystyrene.

### 4.3.2. Structure description

The ORTEP diagram for the compound  $[\text{Mo}^{\text{VI}}\text{O}_2(\text{sal-iah})(\text{MeOH})]$  (**4.1**) is shown in Fig. 4.1. Fig. 4.2 presents the intermolecular hydrogen bonds and  $\pi$ - $\pi$  interactions. Selected bond distances and angles are given in Table 4.2. The structure of the complex is mononuclear and adopts a six-coordinated distorted octahedral geometry. In this complex phenolic oxygen, alcohol oxygen and azomethine nitrogen atoms of the ligand, which acts as tridentate, and two oxo groups coordinate to molybdenum center. One methanol molecule completes the coordination sphere. The  $\text{O}=\text{Mo}=\text{O}$  angle is  $106.05(9)^\circ$  and  $\text{Mo}=\text{O}$  distances are 1.6851(18) and 1.7024(15) Å. The  $\text{Mo}-\text{O}-\text{C}$  angle and  $\text{Mo}-\text{O}$  distance for  $\text{Mo}-\text{OHCH}_3$  in **4.1** are  $125.13(16)^\circ$  and 2.3794(17) Å, respectively, similar to other examples in literature [147].

The asymmetric unit of complex **4.1** contains only single molecule of  $[\text{Mo}^{\text{VI}}\text{O}_2(\text{sal-iah})(\text{MeOH})]$ . The indole groups of the two complexes interact by  $\pi$ - $\pi$

interactions (see Fig. 4.2). The distances between centroids is:  $d_{c1-c2} = 3.750 \text{ \AA}$  {c1 [N(3O), C(10O), C(11O), C(12O), C(17O)], c2 [C(12A)-C(13A)-C(14A)-C(15A)-C(16A)-C(17A)]}. Intermolecular hydrogen bonds are present in the crystal packing (see Table 4.3).

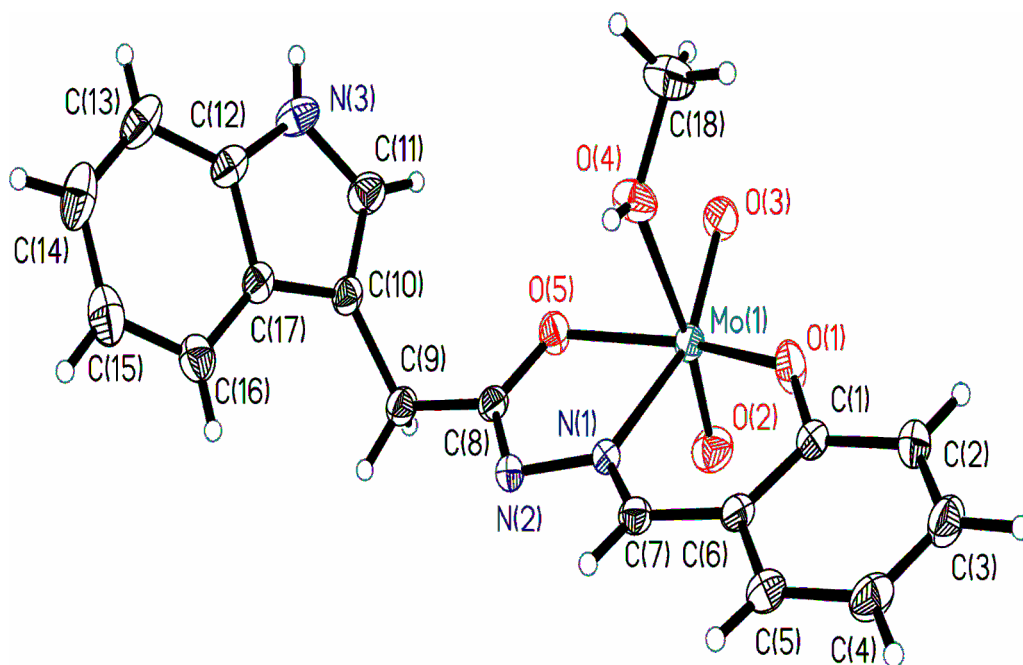


**Figure 4.1.** ORTEP plot of complex  $[\text{Mo}^{\text{VI}}\text{O}_2(\text{sal-iah})(\text{MeOH})]$  (**4.1**). All the non-hydrogen atoms are presented by their 30% probability ellipsoids.

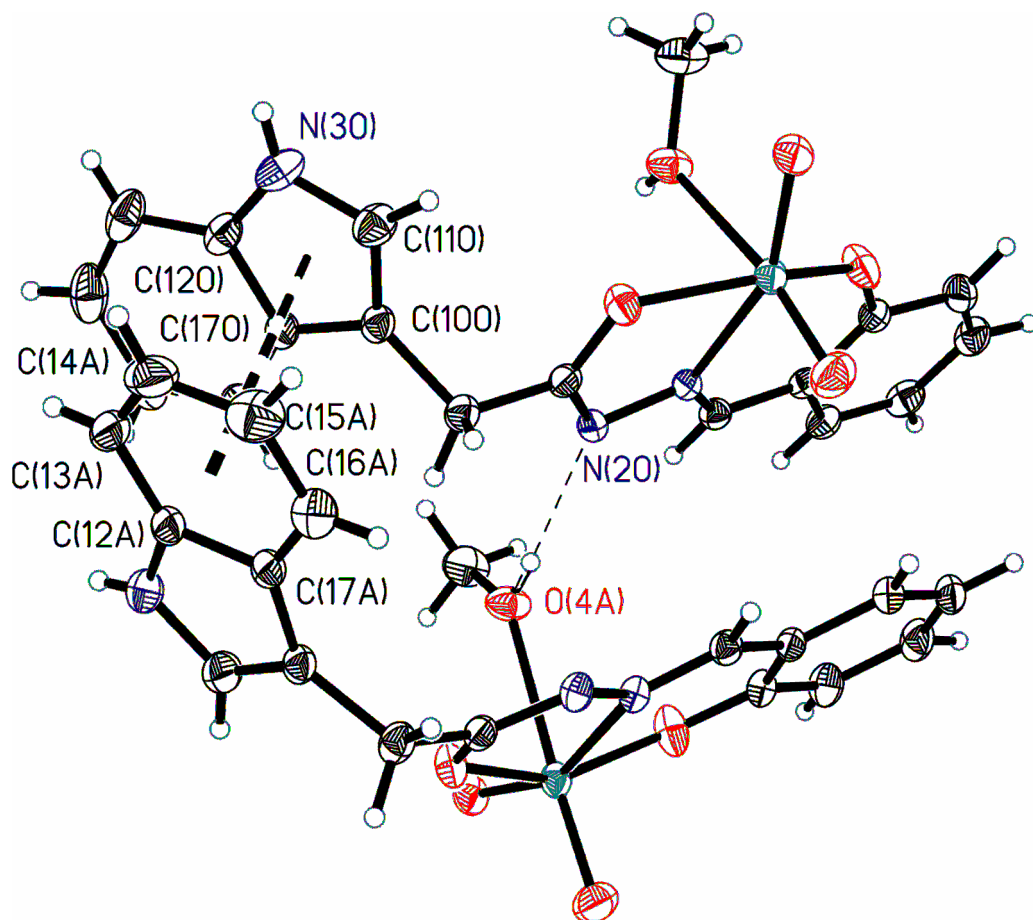


**Figure 4.2.** Fragment of the crystal packing of complex  $[\text{Mo}^{\text{VI}}\text{O}_2(\text{sal-iah})(\text{MeOH})]$  (**4.1**). H-bond between methanol molecule and a nitrogen of the azomethine group is shown with dashed line.  $\pi$ - $\pi$  stacking interaction between indole groups is shown with thick dashed line.

**Table 4.2.** Bond lengths [ $\text{\AA}$ ] and bond angles [ $^\circ$ ] for  $[\text{Mo}^{\text{VI}}\text{O}_2(\text{sal-iah})(\text{MeOH})]$  (**4.1**).

Bond lengths	<b>4.1</b>
Mo(1)-O(1)	1.9157(16)
Mo(1)-O(2)	1.6851(18)
Mo(1)-O(3)	1.7024(15)
Mo(1)-O(4)	2.3794(17)
Mo(1)-O(5)	2.0133(14)
Mo(1)-N(1)	2.2364(18)
Bond angles	<b>4.1</b>
O(2)-Mo(1)-O(3)	106.05(9)
O(2)-Mo(1)-O(1)	100.68(10)
O(3)-Mo(1)-O(1)	103.42(8)
O(2)-Mo(1)-O(5)	95.32(9)
O(3)-Mo(1)-O(5)	96.32(7)
O(1)-Mo(1)-O(5)	149.90(7)
O(2)-Mo(1)-N(1)	96.36(8)
O(3)-Mo(1)-N(1)	155.51(7)
O(1)-Mo(1)-N(1)	81.51(6)
O(5)-Mo(1)-N(1)	71.45(6)
O(2)-Mo(1)-O(4)	171.04(8)
O(3)-Mo(1)-O(4)	81.90(7)
O(1)-Mo(1)-O(4)	81.07(8)
O(5)-Mo(1)-O(4)	79.46(7)
N(1)-Mo(1)-O(4)	75.13(6)

**Table 4.3.** Hydrogen bonds for complex  $[\text{Mo}^{\text{VI}}\text{O}_2(\text{sal-iah})(\text{MeOH})]$  (**4.1**).

D-H...A	d(D-H)	d(H...A)	d(D...A)	<(DHA)
N(3)-H(3N)...O(3)#1	0.75(3)	2.42(3)	3.098(3)	151(3)
O(4)-H(4O)...N(2)#2	0.71(2)	2.05(3)	2.751(2)	170(3)

Symmetry transformations used to generate equivalent atoms: #1  $-x+1, -y, -z+1$   
 #2  $x, -y+1/2, z-1/2$ .

### 4.3.3. Field emission-scanning electron micrograph (FE-SEM) and energy dispersive X-ray analysis (EDAX) studies

The images of field emission-scanning electron micrographs (Fe-SEM) of single beads of pure chloromethylated polystyrene and polymer-grafted complex PS- $[\text{Mo}^{\text{VI}}\text{O}_2(\text{sal-iah})(\text{MeOH})]$  (**4.3**) are presented in Fig. 4.3. The pure chloromethylated polystyrene bead has smooth and flat surface while anchored complex shows slight roughening of the top layer suggesting the incorporation of metal complex into polymer matrices. However, the poor loading of the metal complex does not allow extracting any accurate information on the morphological changes in terms of exact orientation of ligand coordinated to the metal ion. The estimation of ca. 9.2 weight percentage of molybdenum content for PS- $[\text{Mo}^{\text{VI}}\text{O}_2(\text{sal-iah})(\text{MeOH})]$  (**4.3**) by energy dispersive X-ray analysis (EDAX), however, confirms the grafting of metal complex onto polystyrene beads. This observation further suggests that part of the covalently bonded complexes is present on the surface while remaining is at various sites.



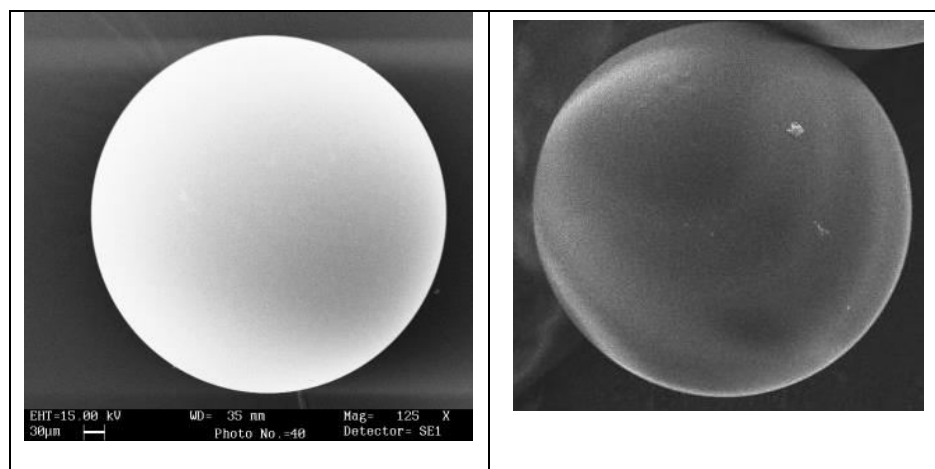


**Figure 4.3.** Scanning electron micrographs (SEM) of chloromethylated polystyrene (left) and PS-[Mo<sup>VI</sup>O<sub>2</sub>(sal-iah)(MeOH)] (**4.3**) (right).

#### 4.3.4. Thermogravimetric Analysis (TGA) studies

Thermogravimetric analysis profile of [Mo<sup>VI</sup>O<sub>2</sub>(sal-iah)(MeOH)] (**4.1**) under an oxygen atmosphere shows that it is stable up to ca. 120 °C and then loses 7 % (*Anal. Cal.* 7.1%) weight between 120 and 180 °C equivalent to one coordinated methanol. On further increasing the temperature, the solvent free complex decomposes in two major fragments with exothermic weight loss which completes at ca. 540 °C. The obtained residue at this temperature is 31% which is close to the theoretical value of 31.9%. The polymer-grafted complex PS-[Mo<sup>VI</sup>O<sub>2</sub>(sal-iah)(MeOH)] (**4.3**) starts losing weight at ca. 80 °C and this step` completes at ca. 170 °C with a total loss of ca. 9% suggesting the presence of coordinated as well as trapped solvent. Thereafter, it decomposes in several fragments with exothermic weight loss at higher temperature. Quantitative measurement of weight loss and distinction between decomposition pattern of complex and polymer matrix at various stages were not possible due to overlapping nature of the decompositions. However, the final residues of 6.7 % (equivalent to 0.47 mmol g<sup>-1</sup> of Mo

in **4.3**) at ca. 520 °C suggest the formation of MoO<sub>3</sub> and metal complex is grafted into polymer support.

#### 4.3.5. IR spectral studies

IR spectral data of the ligand and its neat and anchored complexes are presented in Table 4.4. The neat complex **4.1** exhibits two sharp bands at 911 and 940 cm<sup>-1</sup> due to  $\nu_{\text{sym}}(\text{O}=\text{Mo}=\text{O})$  and  $\nu_{\text{asym}}(\text{O}=\text{Mo}=\text{O})$  modes, respectively [148]. The corresponding polymer-bound molybdenum complex displays these bands at 903 cm<sup>-1</sup> and 957 cm<sup>-1</sup>. Complex [Mo<sup>VI</sup>O(O<sub>2</sub>)(sal-iah)(MeOH)] (**4.2**) exhibits a sharp band at 965 cm<sup>-1</sup> which is assigned due to  $\nu(\text{Mo}=\text{O})$  stretch. In addition, it exhibits three IR active vibrational modes associated with the peroxido moiety [Mo(O<sub>2</sub>)]<sup>2+</sup> at 910, 635 and 556 cm<sup>-1</sup> which are assigned due to the O–O intra stretching, asymmetric Mo(O<sub>2</sub>) stretching and symmetric Mo(O<sub>2</sub>) stretching, respectively [149]. These bands confirmed the  $\eta^2$ -coordination of the peroxido group to the molybdenum.

Ligand H<sub>2</sub>sal-iah (**I**) exhibits four distinct bands at 3400, 3186, 1670 and 1618 cm<sup>-1</sup> due to  $\nu(\text{OH})$ ,  $\nu(\text{NH})$ ,  $\nu(\text{C}=\text{O})$  and  $\nu(\text{C}=\text{N})$  modes, respectively. The presence of sharp bands due to  $\nu(\text{NH})$  and  $\nu(\text{C}=\text{O})$  is indicative of its ketonic nature in the solid state. The absence of these bands in the spectra of all complexes is consistent with the enolisation of the amide functionality and subsequent coordination of enolic oxygen to the metal ion after proton replacement. A new band appearing at ca. 1270 cm<sup>-1</sup> is assigned to the  $\nu(\text{C}=\text{O})(\text{enolic})$  stretching of the coordinated hydrazone fragment. The band due to azomethine group moves toward lower wave number by 11 cm<sup>-1</sup> (in **4.1**), 5 cm<sup>-1</sup> (in **4.2**) and 9 cm<sup>-1</sup> (in **4.3**) indicating the coordination of azomethine nitrogen to the molybdenum. The band corresponding to the free –OH group present in H<sub>2</sub>sal-iah is also present in complexes **4.1** and **4.2** possibly suggesting the presence of coordinated methanol. The presence of multiple bands of medium intensity observed in the region 2800–2900 cm<sup>-1</sup> in all complexes suggests the existence of –CH<sub>2</sub> group.

The chloromethylated polystyrene displays strong peaks at 1264 and 673  $\text{cm}^{-1}$  due to C–H wagging ( $-\text{CH}_2\text{Cl}$ ) and C–Cl stretch, respectively [90]. The absence of these peaks in  $\text{PS}-[\text{Mo}^{\text{VI}}\text{O}_2(\text{sal-iah})(\text{MeOH})]$  (**4.3**) suggests the covalent bonding of chloromethylated polystyrene with  $[\text{Mo}^{\text{VI}}\text{O}_2(\text{sal-iah})(\text{MeOH})]$  (cf. Scheme 4.1) through nitrogen of the indole ring. This is further supported by the absence of  $\nu(\text{NH})$  band that appears at 3250  $\text{cm}^{-1}$  in **4.1**.

**Table 4.4.** IR spectral data ( $\text{cm}^{-1}$ ) of compounds

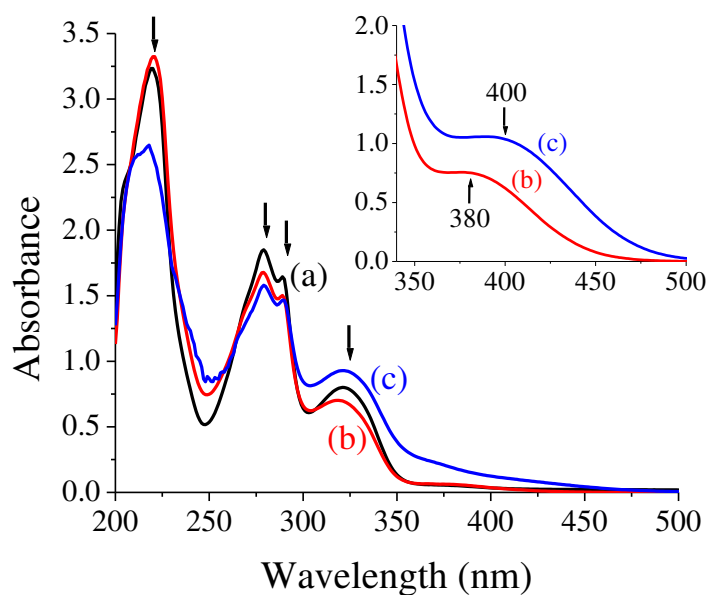
Compound	$\nu(\text{OH})$	$\nu(\text{NH})$	$\nu(\text{C}=\text{O})$	$\nu(\text{C}=\text{N})$	$\nu(\text{Mo}=\text{O})$
$\text{H}_2\text{sal-iah}$	3400	3186	1670	1618	
$[\text{Mo}^{\text{VI}}\text{O}_2(\text{sal-iah})(\text{MeOH})]$	3400	3250	-	1607	911(s), 940(s)
$[\text{Mo}^{\text{VI}}\text{O}(\text{O}_2)(\text{sal-iah})(\text{MeOH})]^a$	3400	3250	-	1613	965
$\text{PS}-[\text{Mo}^{\text{VI}}\text{O}_2(\text{sal-iah})(\text{MeOH})]$	3400	-	-	1609	903(s), 957(s)

<sup>a</sup> Bands due to the peroxido group: 910, 635 and 556  $\text{cm}^{-1}$ .

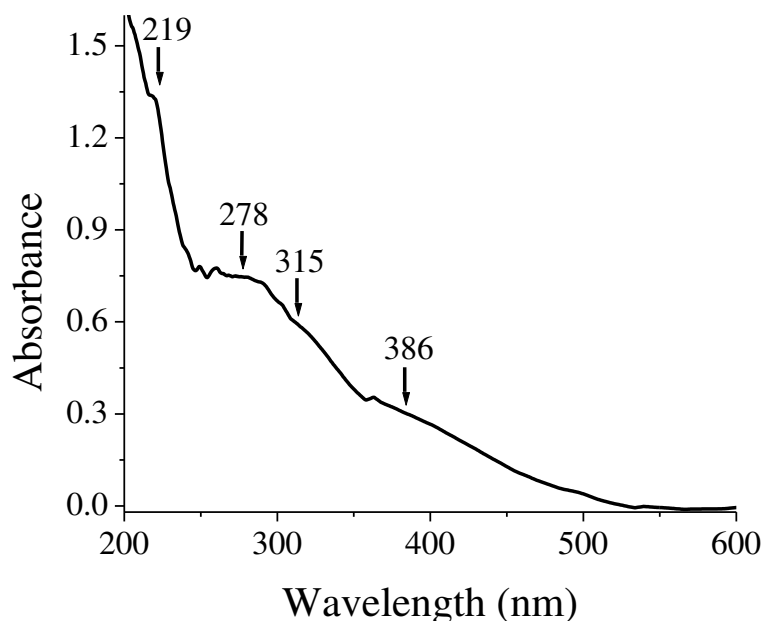
#### 4.3.6. UV-visible spectral study

Fig. 4.4 and Fig. 4.5 reproduces spectra of ligand, neat and polymer-grafted complexes and Table 4.5 includes UV-visible spectral data. Ligand  $\text{H}_2\text{sal-iah}$  (**I**) exhibits three spectral bands at 220, 279 and 321 nm in the UV region corresponding to  $\sigma \rightarrow \sigma^*$ ,  $\pi \rightarrow \pi^*$  and  $n \rightarrow \pi^*$  transitions, respectively. The additional band at 289 nm having intensity similar to  $\pi \rightarrow \pi^*$  transition is possibly due to its splitting. All these bands also appear in the spectra of complexes **4.1** and **4.2** with slight variations. In addition, they also exhibit a low intense band at 380 (in **4.1**) and ca. 400 nm (in **4.2**) originating due to the transfer of charge from phenolate oxygen atom to an empty d-orbital of the molybdenum atom (LMCT). Spectrum of **4.3** recorded in Nujol has very similar but

broad electronic spectral patterns [Fig. 4.5]. The expected LMCT transition in **4.3** could only be observed around 386 nm as a weak shoulder in Nujol possibly due to poor loading of complex in polymer matrix while bands in the UV region are similar to that observed in **4.1** and **4.2**.



**Figure 4.4.** Electronic spectra of (a)  $\text{H}_2\text{sal-iah}$  (**I**), (b)  $[\text{Mo}^{\text{VI}}\text{O}_2(\text{sal-iah})(\text{MeOH})]$  (**4.1**) and (c)  $[\text{Mo}^{\text{VI}}\text{O}(\text{O}_2)(\text{sal-iah})(\text{MeOH})]$  (**4.2**) recorded in methanol.



**Figure 4.5.** Electronic spectrum of PS-[Mo<sup>VI</sup>O<sub>2</sub>(sal-iah)(MeOH)] (4.3) recorded after dispersing it in Nujol.

**Table 4.5.** Electronic spectral data of ligand and complexes.

Compound	Solvent	$\lambda_{\max}/\text{nm}$ ( $\epsilon/\text{M}^{-1}\text{cm}^{-1}$ )
H <sub>2</sub> sal-iah	MeOH	220 ( $5.98 \times 10^4$ ), 279 ( $3.42 \times 10^4$ ), 289 ( $3.04 \times 10^4$ ), 321 ( $1.48 \times 10^4$ )
[Mo <sup>VI</sup> O <sub>2</sub> (sal-iah)(MeOH)]	MeOH	220 ( $4.56 \times 10^4$ ), 279 ( $2.30 \times 10^4$ ), 289 ( $2.06 \times 10^4$ ), 320 ( $0.96 \times 10^4$ ), 380 ( $2.06 \times 10^3$ )
[Mo <sup>VI</sup> O(O <sub>2</sub> )(sal-iah)(MeOH)]	MeOH	218 ( $3.91 \times 10^4$ ), 279 ( $2.33 \times 10^4$ ), 289 ( $2.16 \times 10^4$ ), 322 ( $1.37 \times 10^4$ ), 400 ( $2.55 \times 10^3$ )
PS-[Mo <sup>VI</sup> O <sub>2</sub> (sal-iah)(MeOH)]	Nujol	219, 278, 315, 386

#### 4.3.7. $^1\text{H}$ and $^{13}\text{C}$ NMR studies

The  $^1\text{H}$  NMR spectra of  $\text{H}_2\text{sal-iah}$  (**I**) and  $[\text{Mo}^{\text{VI}}\text{O}_2(\text{sal-iah})(\text{MeOH})]$  (**4.1**) are shown in Fig. 4.6 and their typical chemical shifts are presented in Table 4.6. The  $^1\text{H}$  NMR spectrum of ligand exhibits single singlet for phenolic  $-\text{OH}$  proton while two sets of singlet with about 1:2 ratio each for azomethine ( $-\text{CH}=\text{N}-$ ), methylene ( $-\text{CH}_2-$ ), NH (of  $-\text{C}(\text{O})-\text{NH}-$  group) and NH (of indole) protons, indicating its existence in two isomeric forms. The absence of signal due to NH of  $-\text{C}(\text{O})-\text{NH}-$  group in the complexes supports the enolisation of the ketonic group and consequent replacement of H by the metal ion. Similarly, absence of phenolic proton signal in complexes indicates the coordination of the phenolic oxygen after proton replacement. The two azomethine signals appearing at 8.38 and 8.41 ppm merge into one and resonate at down field due to the coordination of the azomethine nitrogen. Protons associated with aromatic, methyl and NH (of indole) groups appear at nearly same positions in ligand as well as in complexes. Thus,  $^1\text{H}$  NMR data supplement the inference obtained by IR spectral study.

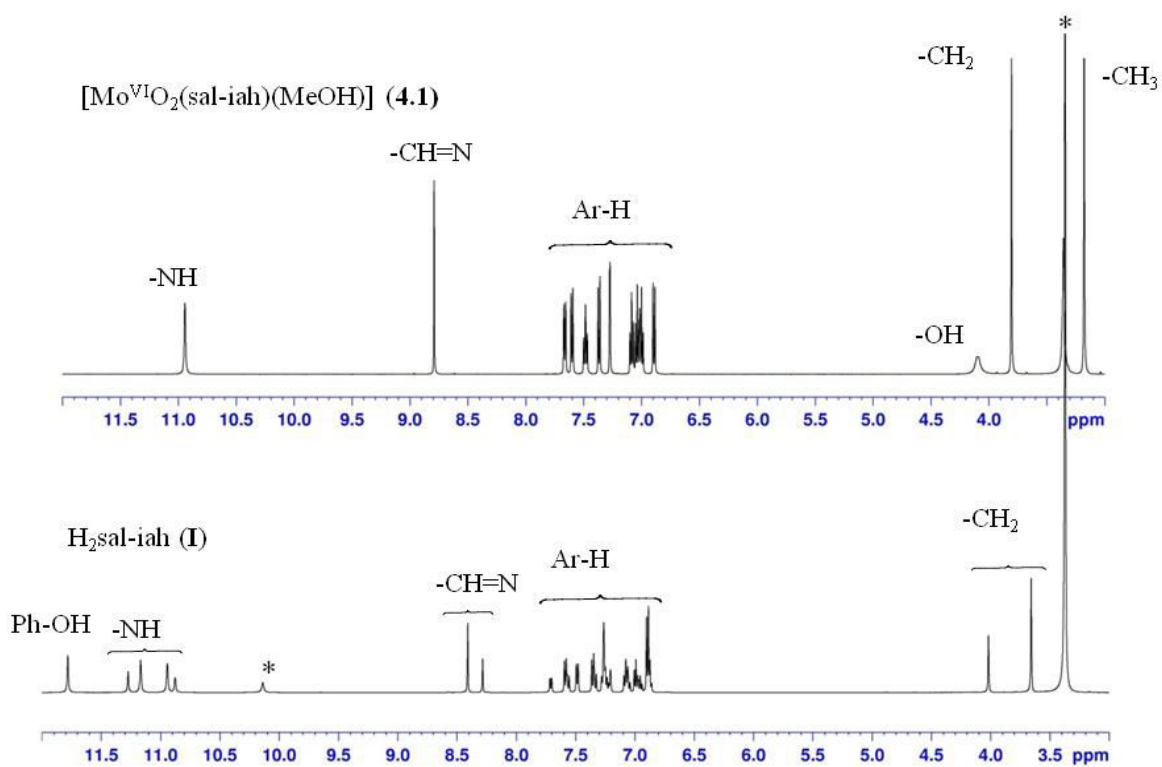


**Figure 4.6.** <sup>1</sup>H NMR spectra of H<sub>2</sub>sal-iah (I) and  $[\text{Mo}^{\text{VI}}\text{O}_2(\text{sal-iah})(\text{MeOH})]$  (4.1).

**Table 4.6.**  $^1\text{H}$  NMR chemical shifts [ $\delta$  in ppm] of ligand and complexes recorded in DMSO- $d_6$ .

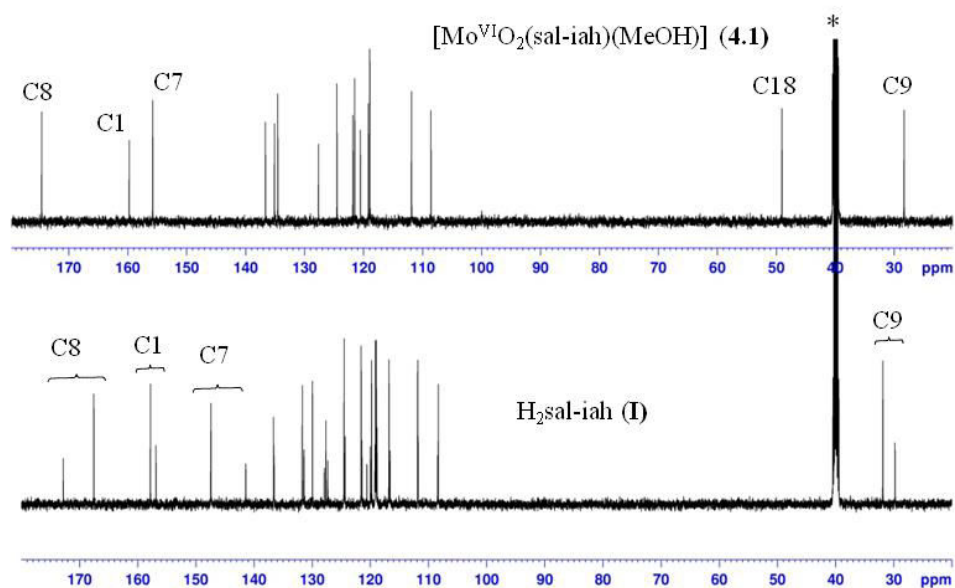
Compound <sup>a</sup>	–OH (phenolic)	–NH– (hydrazide)	–NH– (indole)	–CH=N–
<b>I</b>	11.80 (br, 1H)	11.17, 11.27 (s, 1H)	10.88, 10.94 (s, 1H)	8.38, 8.41 (s, 1H)
<b>4.1</b>	-	-	10.94 (s, 1H)	8.79 (s, 1H)
<b>4.2</b>			10.90 (s, 1H)	8.90 (s, 1H)
Compound <sup>a</sup>	–CH <sub>2</sub> –	–CH <sub>3</sub>	Aromatic	–OH (alcoholic)
<b>I</b>	3.66, 4.02 (s, 2H)		6.86-7.72 (m, 9H)	-
<b>4.1</b>	3.80 (s, 2H)	3.17 (s, 3H)	6.88-7.67 (m, 9H)	4.09 (br, 1H)
<b>4.2</b>	3.82 (s, 2H)	3.12 (s, 3H)	6.88-7.80 (m, 9H)	4.05 (br, 1H)

<sup>a</sup> Letters given in parentheses indicate the signal structure: s = singlet, m = multiplet, br = broad (unresolved).

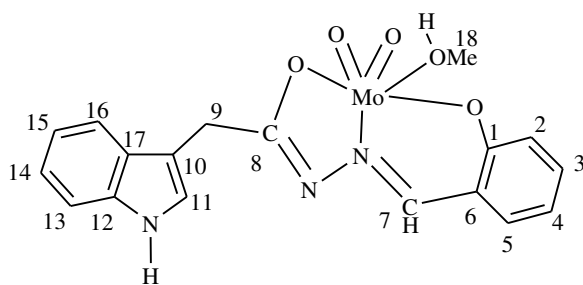
The  $^{13}\text{C}$  NMR spectra of  $\text{H}_2\text{sal-iah}$  (**I**) and  $[\text{Mo}^{\text{VI}}\text{O}_2(\text{sal-iah})](\mathbf{4.1})$  have been recorded which also supplement  $^1\text{H}$  NMR spectral information for the elucidation of the structure of the complex. Table 4.7 provides  $^{13}\text{C}$  NMR spectral data and Fig. 4.7 reproduces their spectra. Assignments of the peaks are based on the intensity patterns of the chemical shift and on the coordination-induced shifts ( $\Delta\delta$ ) ( $\Delta\delta = \delta_{\text{complex}} - \delta_{\text{ligand}}$ ) of the signals for carbon atoms in the vicinity of the coordinating atoms [150]. Similar to the  $^1\text{H}$  NMR spectrum,  $\text{H}_2\text{sal-iah}$  (**I**) exhibits two sets of signal for most carbons while complex resonates single set of signal for each carbon except to those carbons where center of symmetry exist. For carbons where center of symmetry exist e.g. aromatic



carbons, they exhibit less number of signals. A large coordination-induced shift for C1 (carbon bearing phenolic oxygen), C7 (carbon bearing azomethine nitrogen) and C8 (carbon bearing enolic oxygen) atoms demonstrate the coordination of these functionalities to the molybdenum. A considerable up field shift of methylene (C9) carbon has also been noticed in complex. A new signal at 49 ppm suggests the coordination of methanol to the molybdenum.



**Figure 4.7.**  $^{13}\text{C}$  NMR spectra of  $\text{H}_2\text{sal-iah}$  (I) and  $[\text{Mo}^{\text{VI}}\text{O}_2(\text{sal-iah})(\text{MeOH})]$  (4.1).

**Table 4.7.**  $^{13}\text{C}$  NMR spectral data of ligand and complexes

Compound	C <sub>1</sub>	C <sub>2</sub> -C <sub>5</sub>	C <sub>6</sub>	C <sub>7</sub>	C <sub>8</sub>	C <sub>9</sub>
<b>I</b>	156.8, 157.8	116.6, 116.8, 131.3, 131.6, 119.9, 120.5, 127.8, 129.9	118.8, 118.9	141.4, 147.4	167.5, 172.7	29.7, 31.8
<b>4.1</b>	159.7	118.9, 135.1, 121.5, 134.5	118.9	155.7	174.5	28.3

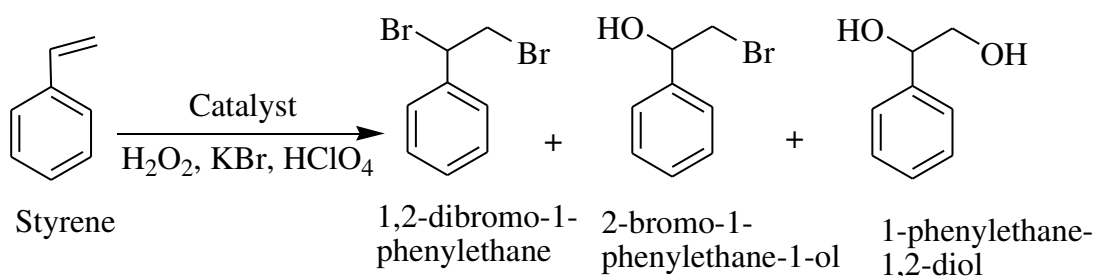
Compound	C <sub>10</sub> , C <sub>11</sub> , C <sub>12</sub>	C <sub>13</sub> - C <sub>17</sub>	C <sub>18</sub>
<b>I</b>	108.3, 108.4, 124.3, 124.4, 136.5, 136.6	111.80, 111.89, 119.07, 119.09, 119.1, 119.7, 121.4, 121.5, 127.3, 127.6	-
<b>4.1</b>	108.5, 124.5, 136.6	111.8, 120.5, 121.8, 119.2, 127.6	49.0

### 4.3.8. Catalytic activity studies

#### 4.3.8.1. Oxidative bromination of styrene

Vanadium (neat as well as polymer supported) and neat molybdenum complexes have been used as catalyst to study oxidative bromination of styrene [62,63,89,105,139,142,144]. We have considered polymer supported complex PS-[Mo<sup>VI</sup>O<sub>2</sub>(sal-iah)(MeOH)] (**4.3**) to carry out the oxidative bromination of styrene using 30 % aqueous H<sub>2</sub>O<sub>2</sub> as an oxidant and three products namely 1,2-dibromo-1-

phenylethane, 2-bromo-1-phenylethane-1-ol and 1-phenylethane-1,2-diol were obtained along with small amount of un-identified product; Scheme 4.2. The main products were identified and confirmed by  $^1\text{H}$  NMR spectroscopy as well as by GC-MS after their separation, and are the same as reported earlier [62,63,89,105,139,142,144].



**Scheme 4.2.** Oxidative bromination products of styrene.

With the objective to conclude suitable reaction conditions for the maximum conversion of styrene different parameters, namely, the amounts of catalyst, oxidant (mol of  $\text{H}_2\text{O}_2$  per mol of styrene),  $\text{HClO}_4$  and KBr were tested. Acid was found to be essential to carry out the catalytic bromination.

In order to optimize the catalyst amount, three different amounts of catalyst i.e. 0.010, 0.015 and 0.020 g were taken for the fixed amount of styrene (1.04 g, 10 mmol),  $\text{H}_2\text{O}_2$  (2.27 g, 20 mmol), KBr (2.38 g, 20 mmol) and  $\text{HClO}_4$  (1.43 g, 10 mmol, added in four equal portions at  $t = 0, 15, 30$  and  $45$  min of the reaction time) in  $\text{CH}_2\text{Cl}_2\text{-H}_2\text{O}$  (40 mL, v/v) solvent system and the reaction was carried out at  $40^\circ\text{C}$  for 2 h. As shown in Fig. 4.8, a maximum of 67 % conversion was achieved with 0.010 g of catalyst. Upon increasing catalyst amount to 0.015 g the conversion of styrene improved to 75 % but no appreciable improvement was noted with 0.020 g of catalyst. Therefore, 0.015 g of catalyst was considered optimum for the maximum conversion of styrene.

The amount of  $\text{HClO}_4$  was optimized by taking substrate to  $\text{HClO}_4$  ratios of 1:1, 1:2 and 1:3 under above reaction conditions; Fig. 4.9. The addition of  $\text{HClO}_4$  to the

catalytic reaction mixture in four equal portion at  $t = 0, 15, 30$  and  $45$  min for each set of reaction was the minimum condition to avoid decomposition of the catalyst. At a substrate to  $\text{HClO}_4$  ratio of 1:1, only 75% conversion was obtained in 2 h of reaction time but this conversion reached 96% at molar ratio of 1:2. On increasing this ratio further to 1:3 reduced the conversion time but the overall conversion of styrene remained nearly constant. Therefore, styrene to  $\text{HClO}_4$  molar ratio of 1:2 was taken for further optimization of other parameters. Other acid like  $\text{H}_2\text{SO}_4$  could also be used successfully with nearly same result.

To understand the effect of oxidant, three different styrene : aqueous 30 %  $\text{H}_2\text{O}_2$  molar ratios viz. 1:1, 1:2, and 1:3 were considered for a fixed amount of styrene (1.04 g, 10 mmol) and catalyst (0.015 g). As illustrated in Fig. 4.10, increasing the styrene to oxidant ratio from 1:1 to 1:2 increases the conversion from 67 to 96%. However, further increasing this ratio to 1:3 shows no predominant conversion. Thus substrate to  $\text{H}_2\text{O}_2$  ratio of 1:2 was considered the best one for the maximum oxidative bromination of styrene.

Similarly, for styrene (1.04 g, 10 mmol), catalyst (0.010 g),  $\text{CH}_2\text{Cl}_2\text{-H}_2\text{O}_2$  (40 mL, v/v),  $\text{H}_2\text{O}_2$  (2.27 g, 20 mmol) and aqueous  $\text{HClO}_4$  (2.86 g, 20 mmol, added as mentioned above), three different amounts of KBr i.e. 10, 20 and 30 mmol were taken and the reaction was carried out at  $40^\circ\text{C}$ . The obtained conversion was only 44 % with 10 mmol KBr but increasing the amount to 20 mmol improved this conversion to 96% which further improved to 99% at 30 mmol KBr as shown in Fig. 4.11. Therefore, 20 mmol KBr was considered the best one for the maximum conversion of styrene.

Table 4.8 provides conversion of styrene under different reaction conditions and selectivity of different reaction products under particular condition after 2 h of reaction time. From the data presented in Table 4.8, it is clear that the best suited reaction conditions for the maximum oxidative bromination of 10 mmol of styrene are (entry no. 4): PS- $[\text{Mo}^{\text{VI}}\text{O}_2(\text{sal-iah})(\text{MeOH})]$  (0.015 g),  $\text{HClO}_4$  (2.86 g, 20 mmol), aqueous 30%  $\text{H}_2\text{O}_2$  (2.27 g, 20 mmol) and KBr (2.38 g, 20 mmol).

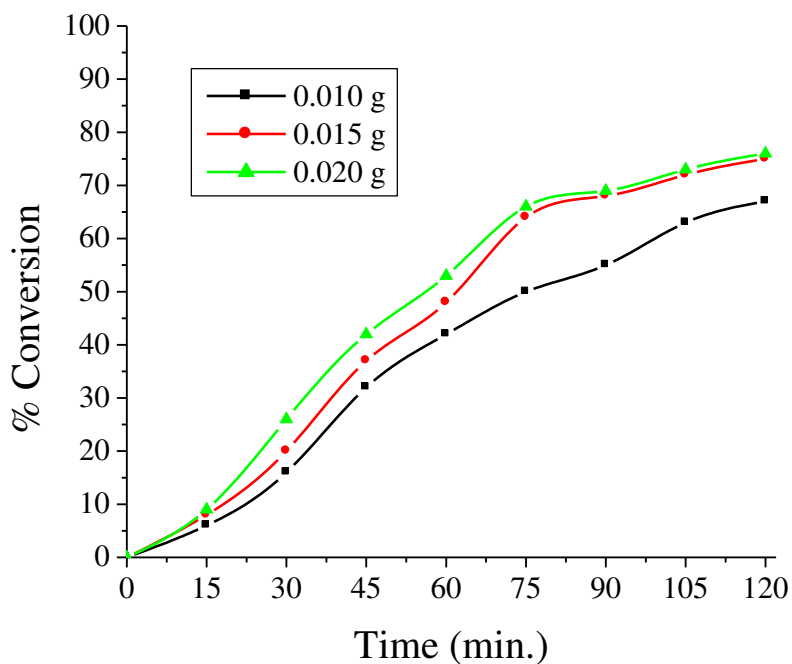


**Figure 4.8** Effect of amount of catalyst on the oxidative bromination of styrene. For reaction conditions refer to Table 4.8.

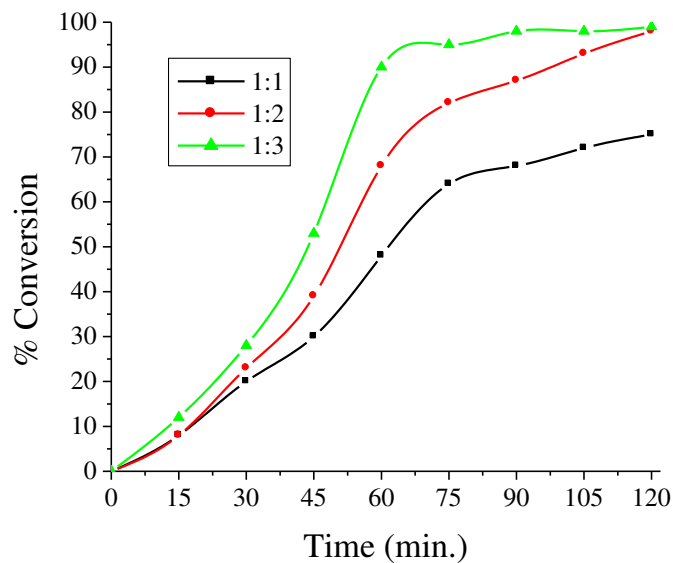


**Figure 4.9.** Effect of amount of  $\text{HClO}_4$  on the oxidative bromination of styrene. For reaction conditions refer to Table 4.8.

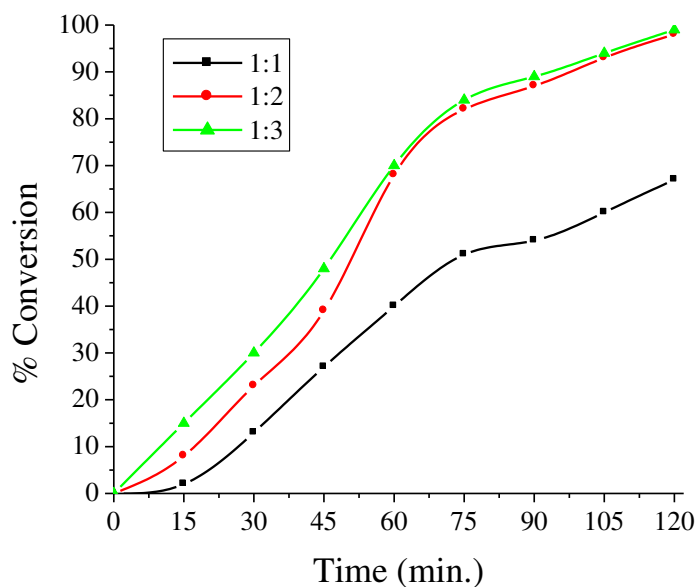


**Figure 4.10.** Effect of amount of  $\text{H}_2\text{O}_2$  ( $\text{H}_2\text{O}_2$ / styrene molar ratio) on the oxidative bromination of styrene. For reaction conditions refer to Table 4.8.

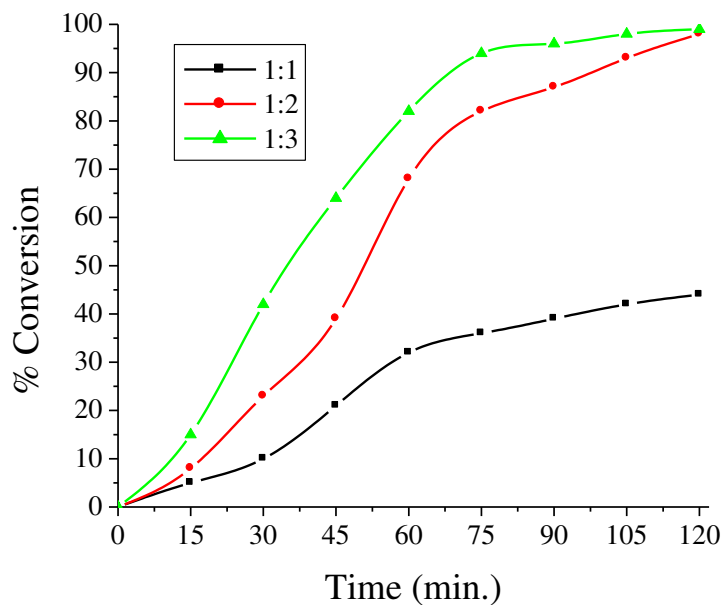


**Figure 4.11.** Effect of amount of KBr on the oxidative bromination of styrene. For reaction conditions refer to Table 4.8.

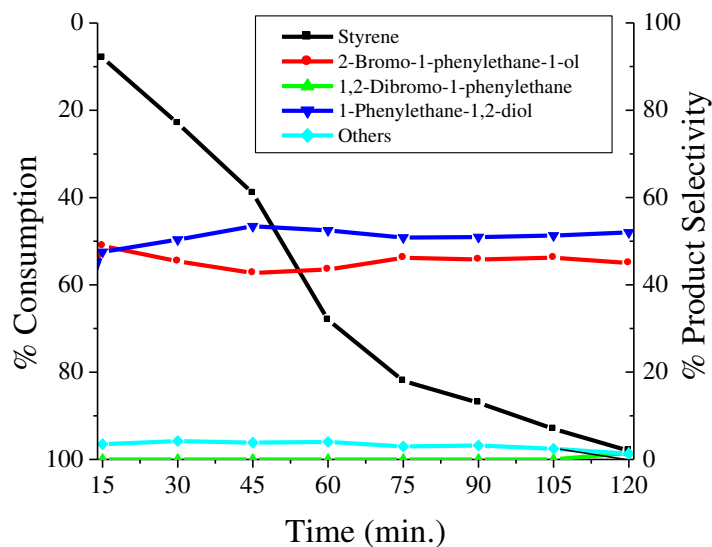


**Figure 4.12.** Consumption of styrene and variation in the selectivity of different reaction products as a function of time.

**Table 4.8.** Results of oxidative bromination of styrene (1.04 g, 10 mmol) using catalyst PS-[Mo<sup>VI</sup>O<sub>2</sub>(sal-iah)(MeOH)] (**4.3**) after 2 h of reaction time.

Entry No.	KBr (g, mmol, eq.) <sup>a</sup>	H <sub>2</sub> O <sub>2</sub> (g, mmol, eq.)	HClO <sub>4</sub> (g, mmol, eq.)	Catalyst (g)	CH <sub>2</sub> Cl <sub>2</sub> /H <sub>2</sub> O (v/v, mL)
1	2.38, 20, 2	2.27, 20, 2	1.43, 10, 1	0.010	20/20
2	2.38, 20, 2	2.27, 20, 2	1.43, 10, 1	0.015	20/20
3	2.38, 20, 2	2.27, 20, 2	1.43, 10, 1	0.020	20/20
4	2.38, 20, 2	2.27, 20, 2	2.86, 20, 2	0.015	20/20
5	2.38, 20, 2	2.27, 20, 2	4.29, 30, 3	0.015	20/20
6	2.38, 20, 2	1.13, 10, 1	2.86, 20, 2	0.015	20/20
7	2.38, 20, 2	3.39, 30, 3	2.86, 20, 2	0.015	20/20

8	1.19, 10, 1	2.27, 20, 2	2.86, 20, 2	0.015	20/20
9	3.57, 30, 3	2.27, 20, 2	2.86, 20, 2	0.015	20/20
Entry No.	% conv., TOF (h <sup>-1</sup> )	% selectivity			
		% mono- bromo	% di- bromo	% di-ol	% others
1	67, 1506	35.4	1.9	59.9	2.7
2	75, 1124	37.2	2.7	59.1	1.1
3	76, 854	39.2	1.4	56.8	2.6
4	96, 1439	45.0	2.0	51.2	1.7
5	99, 1484	13.5	2.8	81.4	2.3
6	67, 1004	38.3	2.9	57.6	1.2
7	99, 1484	29.2	2.2	66.2	2.5
8	44, 659	55.0	2.3	41.9	0.8
9	99, 1484	24.7	1.9	71	2.4

<sup>a</sup> eq. = equivalent amount.

For 96% conversion of styrene after 2 h of reaction time under these conditions, the selectivity of the reaction products follows the order: 1-phenylethane-1,2-diol (51.2%) > 2-bromo-1-phenylethane-1-ol (45.0%) > 1,2-dibromo-1-phenylethane (2.0%). The consumption of styrene and the selectivity of different products under the optimized reaction conditions have also been analyzed as a function of time and are presented in Fig. 4.12. The selectivity of the formation of 1-phenylethane-1, 2-diol and 2-Bromo-1-phenylethane-1-ol starts with ca. 46 and 48%, respectively. With time these conversions slowly change and end up at 51.2 and 45.0%, respectively. The selectivity of the formation of 1,2-dibromo-1-phenylethane and other un-identified products always remains below 2% during these periods. Catalytic potential of **4.3** compares well with the activities shown by other molybdenum and vanadium complexes [62,63,89,105,139,142,144].



The catalytic activity of the recovered catalyst from two fresh runs, after washing with acetonitrile and drying, was also carried out and result shows about 95% conversion, indicating the recyclability of the catalyst. Under the above reaction conditions the catalytic activity of neat complex  $[\text{Mo}^{\text{VI}}\text{O}_2(\text{sal-iah})(\text{MeOH})]$  (**4.1**) gave 92% conversion where selectivity of the reaction products is similar to the one obtained by supported complex. Thus, catalytic potential of supported as well as neat complexes both are good but the recyclability of the supported catalyst makes it better over the non-supported one. In the absence of catalyst, the reaction mixture gave ca. 45% conversion of styrene under above optimized reaction conditions.

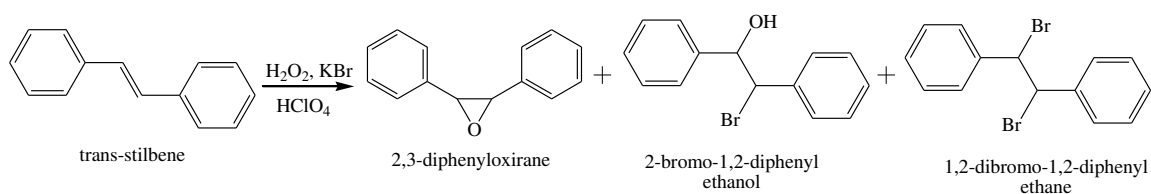
#### 4.3.8.2. Oxidative bromination of *trans*-stilbene

A biphasic chloroform-water system was found to be suitable to carry out oxidative bromination of *trans*-stilbene. Oxidative bromination of *trans*-stilbene gave mainly three products (i) 2,3-diphenyloxirane (*trans*-stilbene oxide), (ii) 2-bromo-1,2-diphenylethanol and (iii) 1,2-dibromo-1,2-diphenylethane; Scheme 4.3. About 2 h was required to acquire equilibrium with maximum conversion. The reaction conditions for the maximum oxidative bromination of *trans*-stilbene were also optimized considering all these parameters stated above such as amounts of catalyst, aqueous 30%  $\text{H}_2\text{O}_2$ , KBr and 70%  $\text{HClO}_4$ . Details of the reaction conditions, the corresponding oxidative brominated and other products, and % selectivity of different products under various conditions are summarized in Table 4.9. It is clear from the table that the optimized reaction conditions (entry no. 5) for this reaction are: *trans*-stilbene (0.90 g, 5 mmol), KBr (2.36 g, 20 mmol) aqueous 30%  $\text{H}_2\text{O}_2$  (2.27 g, 20 mmol) catalyst precursor (0.015 g), aqueous 70%  $\text{HClO}_4$  (2.86 g, 20 mmol) and  $\text{CHCl}_3/\text{H}_2\text{O}$  (40 mL, 50%, v/v). Under these conditions, a maximum of 96 % conversion of *trans*-stilbene was obtained where selectivity of the reaction products follows the order: 2-bromo-1,2-diphenylethanol (49.0%) > 1,2-

dibromo-1,2-diphenylethane (47.5%) > 2,3-diphenyloxirane (*trans*-stilbene oxide) (1.9%)

The catalytic activity obtained here compares well with the literature.  $\text{NH}_4\text{VO}_3$  catalyzed oxidative bromination of *trans*-stilbene with moderate conversion in aqueous medium in the presence of  $\text{H}_2\text{O}_2$ , KBr and HBr has been reported by Hirao et al. [151]. A maximum of 91% conversion of *trans*-stilbene with the selectivity order of 2,3-diphenyloxirane (*trans*-stilbene oxide) (66%) > 1,2-dibromo-1,2-diphenylethane (24%) > 2-bromo-1,2-diphenylethanol (8%) was obtained by PS-im[ $\text{V}^{\text{V}}\text{O}_2(\text{pan})$ ] (Hpan = 1-(2-pyridylazo)-2-naphthol) [63].

The catalytic activity of the recovered catalyst shows almost similar (93 %) conversion and neat complex  $[\text{Mo}^{\text{VI}}\text{O}_2(\text{sal-iah})(\text{MeOH})]$  gave 90% conversion with essentially similar selectivity of reaction products. Control experiment without catalyst under above reaction conditions gave only 51 % conversion of *trans*-stilbene while only 2 % conversion of was obtained in the absence of KBr. In the absence of oxidant and KBr, no formation of *trans*-stilbene oxide confirms that dioxido group of catalyst does not transfer its oxygen to the substrate directly. Thus, neat as well as supported catalyst both enhances the reaction while the recyclability of the supported catalyst makes it better over the non-supported one.



**Scheme 4.3.** Oxidative bromination products of *trans*-stilbene.

### 4.3.9. Reactivity of [Mo<sup>VI</sup>O<sub>2</sub>(sal-iah)(MeOH)] (4.1) with H<sub>2</sub>O<sub>2</sub> and possible reaction pathway

The formation of [MoO(O<sub>2</sub>)]<sup>2+</sup> intermediate using [MoO<sub>2</sub>]<sup>2+</sup> complexes has been established in the literature. We have been able to isolate peroxido complex [Mo<sup>VI</sup>O(O<sub>2</sub>)(sal-iah)(MeOH)] (4.2) by the reaction of H<sub>2</sub>O<sub>2</sub> and characterize it. Its in situ formation has also been established here by electronic absorption spectroscopy. Thus, the titration of a methanolic solution of 4.1 ( $3.64 \times 10^{-4}$  M) with 30 % H<sub>2</sub>O<sub>2</sub> (one drop) dissolved in 10 mL of MeOH results in the shift of 380 nm band to 400 nm along with increase in intensity (inset of Fig. 4.13). The intensities of other bands i.e. bands at 320, 289, 279 and 220 nm in diluted methanolic solution ( $7.2 \times 10^{-5}$  M) increases regularly without shifting (Fig. 4.13). The shape of final spectrum is similar to the spectrum of peroxide complex 4.2, thus verifying the formation of similar oxidoperoxido species in solution as well.

**Table 4.9.** Results of oxidative bromination of *trans*-stilbene (0.90 g, 5 mmol) using catalyst PS-[Mo<sup>VI</sup>O<sub>2</sub>(sal-iah)(MeOH)] (4.3) after 2 h of reaction time.

Entry No.	KBr (g, mmol, eq.) <sup>a</sup>	H <sub>2</sub> O <sub>2</sub> (g, mmol, eq.)	HClO <sub>4</sub> (g, mmol, eq.)	Catalyst (g)	CHCl <sub>3</sub> /H <sub>2</sub> O (v/v, mL)
1	2.38, 20, 4	2.27, 20, 4	4.29, 30, 6	0.015	20/20
2	2.38, 20, 4	2.27, 20, 4	4.29, 30, 6	0.020	20/20
3	2.38, 20, 4	2.27, 20, 4	4.29, 30, 6	0.025	20/20
4	2.38, 20, 4	2.27, 20, 4	1.43, 10, 2	0.015	20/20
5	2.38, 20, 4	2.27, 20, 4	2.86, 20, 4	0.015	20/20

6	2.38, 20, 4	1.13, 10, 2	2.86, 20, 4	0.015	20/20
7	2.38, 20, 4	1.70, 15, 3	2.86, 20, 4	0.015	20/20
8	1.19, 10, 2	2.27, 20, 4	2.86, 20, 4	0.015	20/20
9	1.79, 15, 3	2.27, 20, 4	2.86, 20, 4	0.015	20/20
Entry No.	% conv., TOF (h <sup>-1</sup> )	% selectivity			
		% mono- bromo	% di-bromo	% T.S.O. <sup>b</sup>	% others
1	97, 727	35.5	56.4	4.3	3.8
2	97, 545	39.4	56.3	3.2	1.0
3	98, 441	40.8	55.6	2.2	1.5
4	57, 427	46.4	50.6	2.6	0.4
5	96, 720	49.0	47.5	1.9	1.6
6	80, 600	43.7	48.3	4.4	3.6
7	81, 607	46.2	36.9	10.6	6.0
8	40, 300	55.9	33.1	6.9	4.2
9	78, 585	56.5	36.8	3.4	3.3

<sup>a</sup> eq. = equivalent amount. <sup>b</sup> T.S.O. = trans-stilbene oxide.

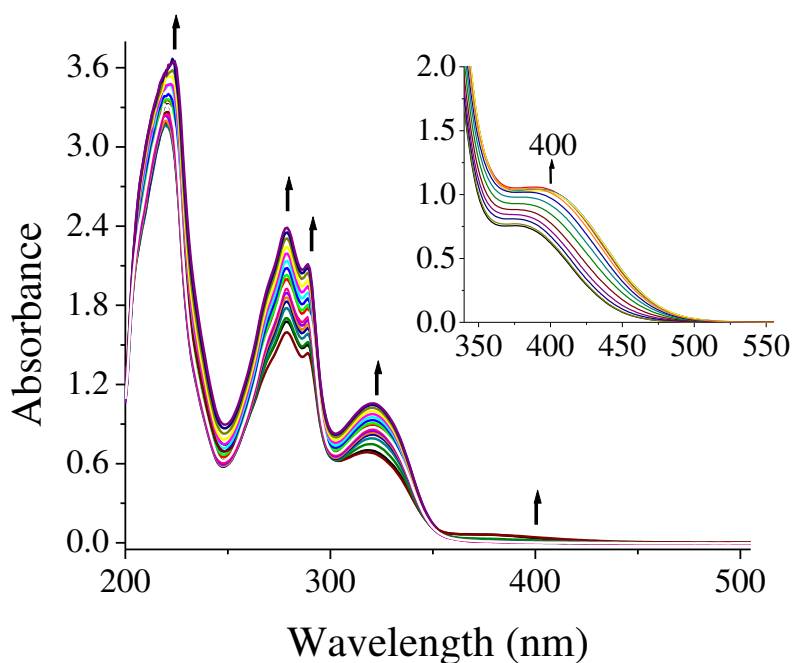
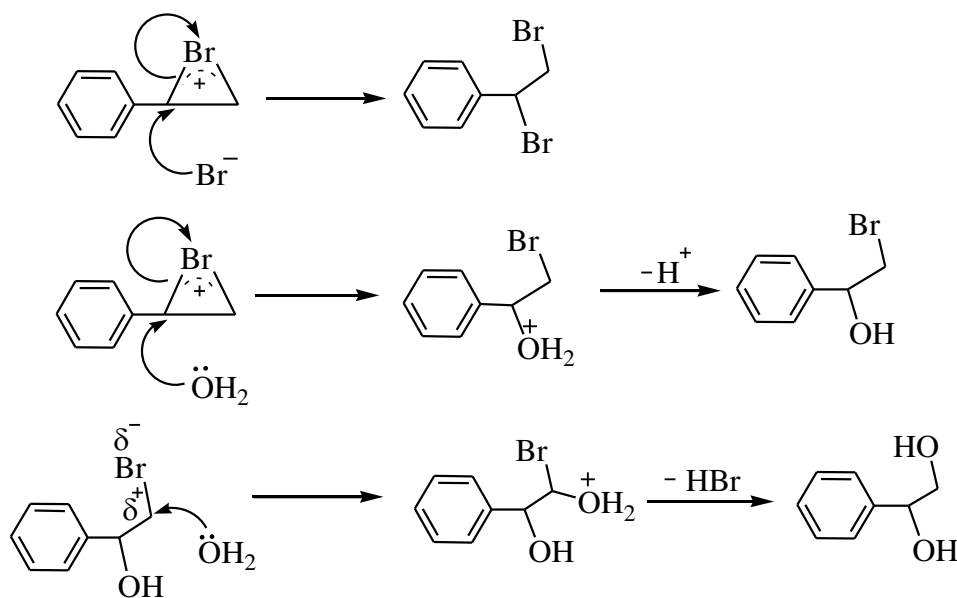


**Figure 4.13.** UV-vis spectral changes observed during titration of  $[\text{Mo}^{\text{VI}}\text{O}_2(\text{sal-iah})(\text{MeOH})]$  (**4.1**) with  $\text{H}_2\text{O}_2$ . The spectra recorded after successive addition of one drop portions of dilute  $\text{H}_2\text{O}_2$  (1 drop of 30%  $\text{H}_2\text{O}_2$  in 10 ml MeOH) to 22 mL of  $7.2 \times 10^{-5}$  M methanolic solution of **4.1**. Inset shows similar spectral changes with  $3.64 \times 10^{-4}$  M solution of **4.1** in methanol.

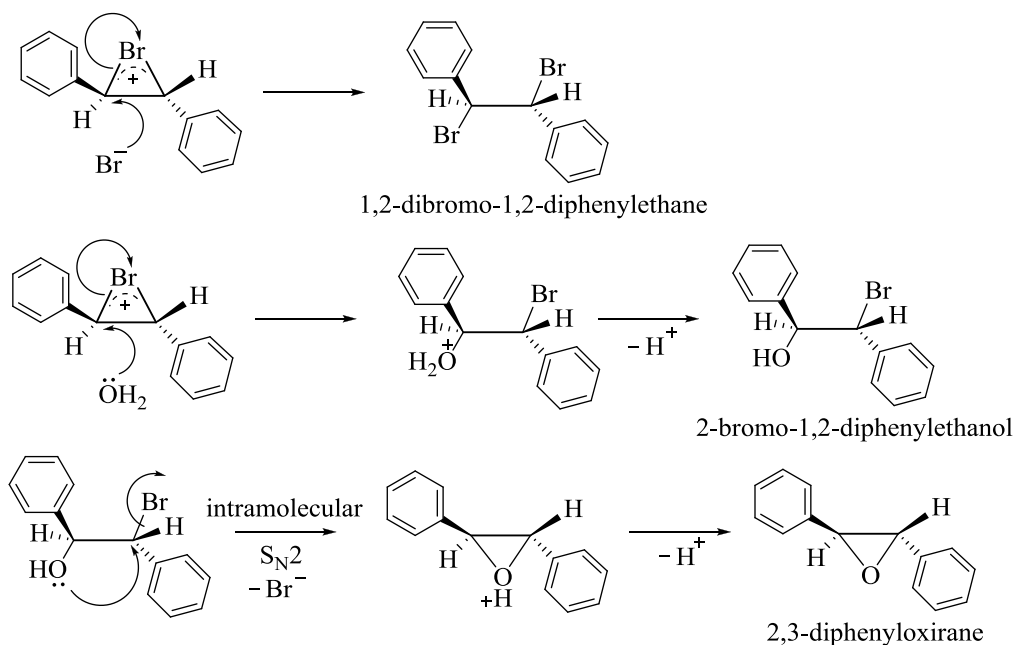
It is normally accepted that V-dependent bromoperoxidase enzymes (V-BrPOs) [26,63,88,105,139] in the presence of hydrogen peroxide [152], forms a peroxido intermediate derivative which oxidizes the bromide ion to bromine equivalent intermediate. This intermediate then either brominates an organic substrate or reacts with another molecule of  $\text{Br}^-$  to form bromine. The peroxide  $[\text{MoO}(\text{O}_2)]^{2+}$  intermediate species form here may similarly oxidize the bromide (to  $\text{Br}_2$ ,  $\text{Br}_3^-$  and/or  $\text{HOBr}$ ), which may react with styrene to give bromonium ion as intermediate. The attack of nucleophile  $\text{Br}^-$  on the  $\alpha$ -carbon of the intermediate gives 1,2-dibromo-1-phenylethane while attack of  $\text{H}_2\text{O}$  gives 2-bromo-1-phenylethane-1-ol. The nucleophile  $\text{H}_2\text{O}$  may further attack on

the  $\alpha$ -carbon of 2-bromo-1-phenylethane-1-ol to give 1-phenylethane-1,2-diol (Scheme 4.4) [63]. The poor selectivity of dibromo product is possibly due to its fast sequential conversion into the mono-bromo derivative, which in turn converts into diol. We have also tested the conversion of monobromo derivative alone under the optimized reaction conditions and observed the formation of 1-phenylethane-1,2-diol. Thus the formation of good amount of 1-phenylethane-1,2-diol is justified under any experimental conditions mentioned in Table 4.8. The presence of acid in the aqueous phase is possibly promoting the protonation of the peroxido moiety and the presence of KBr is essential to get reasonable amount of brominated product(s).

Following similar mechanisms (Scheme 4.5) may also be proposed for the formation of different products upon oxidative bromination of *trans*-stilbene [63].



**Scheme 4.4.** Proposed mechanisms for the formation of three main products, after the bromonium ion is formed by action of catalytically generated HOBr on styrene.



**Scheme 4.5.** Proposed mechanisms for the formation of products, after the bromonium ion is formed by action of catalytically generated HOBr on *trans*-stilbene.

#### 4.4. Conclusions

Complex  $[\text{Mo}^{\text{VI}}\text{O}_2(\text{sal-iah})(\text{MeOH})]$  (**4.1**) with dibasic tridentate ONO donor ligand  $\text{H}_2\text{sal-iah}$  (**I**) derived from salicylaldehyde and indole-3-acetic hydrazide has been prepared which can also be converted, by treatment with  $\text{H}_2\text{O}_2$ , to the corresponding peroxido-complex  $[\text{Mo}^{\text{VI}}\text{O}(\text{O}_2)(\text{sal-iah})(\text{MeOH})]$  (**4.2**). Complex **4.1** has also been grafted successfully through covalent bonding of the nitrogen of the indole group to chloromethylated polystyrene cross-linked with 5% divinylbenzene {now abbreviated as PS- $[[\text{Mo}^{\text{VI}}\text{O}_2(\text{sal-iah})(\text{MeOH})]$  (**4.3**)}.

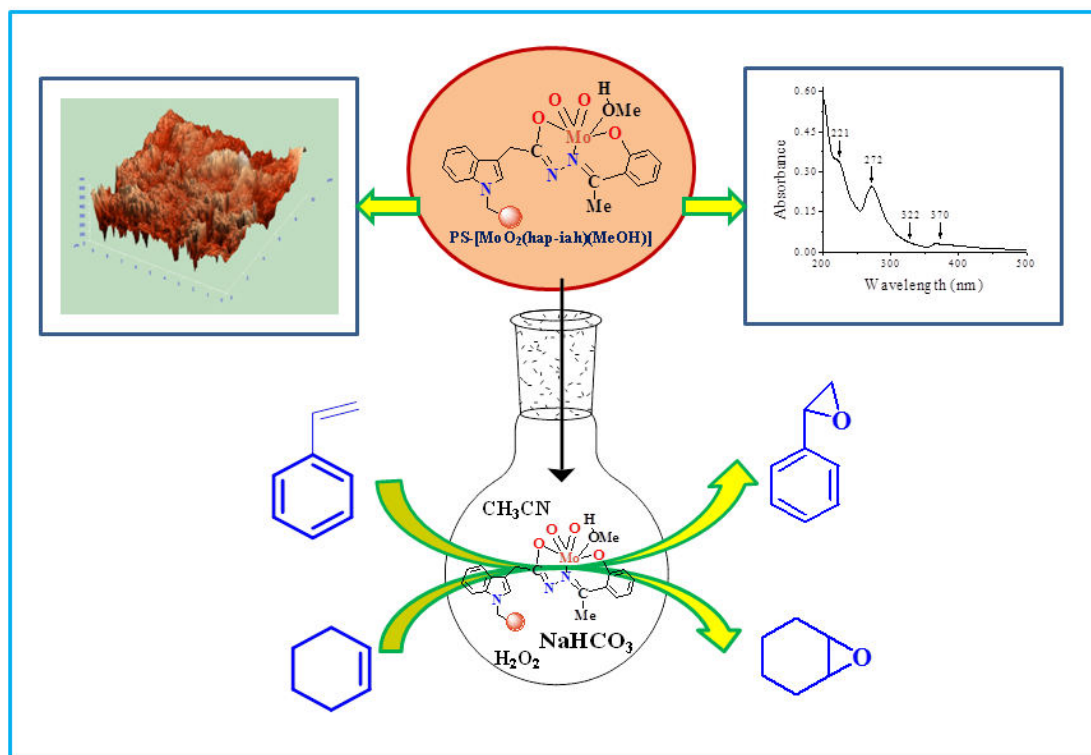
Oxidative bromination of styrene and *trans*-stilbene has been successfully carried out using **4.1** and **4.3** as catalyst precursor. The presence of some of the metal centers on the surface of the polymer in **4.3** due to insertion of spacer between polymer support and catalyst possibly allowed its better interaction with substrates and oxidant during catalytic reaction, also observed earlier [107], resulting in better performance of the catalyst. Further, the recyclability of **4.3** over non-polymer analog makes it useful functional

model analog of haloperoxidases. A moderate conversions of the substrates in the absence of the catalyst has also been obtained but the selectivity profiles of the reaction products differ significantly. The peroxido species, similar to  $[\text{Mo}^{\text{VI}}\text{O}(\text{O}_2)(\text{sal-iah})(\text{MeOH})]$  (**4.2**) isolated in the solid state, has also been demonstrated to form in solution which oxidizes bromide, in the presence of acid, which in turn reacts with styrene and *trans*-stilbene to give corresponding bromonium ion as intermediate. This intermediate is responsible for different reaction products of substrates.



# CHAPTER 5

Sodium bicarbonate assisted oxidation, by  $\text{H}_2\text{O}_2$ , of styrene and cyclohexene using polymer grafted dioxidomolybdenum(VI) complex as a catalyst



## 5.1. Introduction

Development of polymer-grafted metal complexes based catalysts, having potentials for technological applications for environmentally benign synthetic routes to fine chemicals, have attracted attention of researchers [23-26,56,61,80-83]. Our effort using chloromethylated polystyrene cross-linked with divinylbenzene (PS-CH<sub>2</sub>Cl) as a solid support to graft vanadium complexes and use them as catalyst precursors have contributed much in this direction because of their thermal stability, recyclability and high turnover rates [25,26].

Homogeneous molybdenum complexes have potential catalytic applications in the oxidation and oxidative bromination of organic substrates including oxidation of sulfides [6,74,117-119,121-126,128-135]. However, immobilizations of these homogeneous catalysts on solid support and exploit them as potential industrial catalysts find limited entry in the literature [24,56,61,74]. In our recent effort we reported polymer grafted dioxidomolybdenum(VI) complex and demonstrated its catalytic potential for the oxidative bromination of organic substrates. Spacer (extra CH<sub>2</sub> with indole group) presents between polymer support and catalyst improved the performance of the catalyst by allowing the effective interaction of catalytic center with substrates and oxidant during catalytic reaction [108].

The objective of the present work is the grafting of dioxidomolybdenum(VI) complex of the indole-derived ONO donor ligand H<sub>2</sub>hap-iah (**II**) into chloromethylated polystyrene, its characterization and study catalytic potential towards the oxidation of styrene and cyclohexene in the presence of NaHCO<sub>3</sub>. It has been found that NaHCO<sub>3</sub> improves catalytic efficiency for the oxidation of organic compounds in presence of H<sub>2</sub>O<sub>2</sub> as terminal oxidant [153-156]. The corresponding non polymer-grafted molybdenum complex has also been prepared which helped in proposing suitable reaction mechanism and comparing its catalytic performance.

## 5.2. Experimental

### 5.2.1. Materials

All chemicals and solvents of analytical reagent grades were used as such and details of other materials are presented in previous Chapters.

### 5.2.2. Physical methods and analysis

The atomic force microscopic imaging was performed on a scanning probe microscope from NTEGRA (NT-MDT) in a semi-contact mode. Other instrumentation details are presented in Chapter 2.

### 5.2.3. Synthesis

#### 5.2.3.1. [Mo<sup>VI</sup>O<sub>2</sub>(hap-iah)(MeOH)] (5.1)

A stirred solution of H<sub>2</sub>hap-iah (**II**) (0.307 g, 1 mmol) in methanol (15 mL) was treated with [Mo<sup>VI</sup>O<sub>2</sub>(acac)<sub>2</sub>] (0.329 g, 1 mmol) dissolved in methanol (15 mL) and the obtained reaction mixture was refluxed for ca. 6 h on a water bath. After reducing the solvent volume to ca. 10 mL and standing the solution at room temperature in air for 24 h, the yellow crystalline compound precipitated which was filtered off, washed with methanol and dried *in vacuo*. Yield 0.39 g (84%) *Anal. Cal.* for C<sub>19</sub>H<sub>19</sub>N<sub>3</sub>O<sub>5</sub>Mo (465): C, 49.09; H, 4.12; N, 9.03. Found: C, 48.8; H, 4.1; N, 9.1%.

#### 5.2.3.2. PS-[Mo<sup>VI</sup>O<sub>2</sub>(hap-iah)(MeOH)] (5.2)

Chloromethylated polystyrene (2.0 g) was suspended in DMF (15 mL) to swell for 2 h. A solution of [Mo<sup>VI</sup>O<sub>2</sub>(hap-iah)(MeOH)] (2.0 g, 4.28 mmol) in DMF (15 mL) was added to the above suspension followed by triethylamine (2.66 g) in ethylacetate (15 mL), and the obtained reaction mixture was heated at 90 °C for 36 h with continuous but slow stirring. After cooling to room temperature, the polymer-grafted complex was

separated by filtration, washed with hot DMF, followed by hot methanol and dried in an oven in air at 110 °C.

#### **5.2.4. Catalytic activity**

Polymer-grafted catalyst was initially kept in CH<sub>3</sub>CN for 1h before use. The catalytic oxidation of styrene and cyclohexene was carried out in a 50 mL flask fitted with a water circulated condenser.

##### **5.2.4.1. Oxidation of styrene**

In a typical reaction, styrene (0.52 g, 5 mmol), catalyst (0.030 g), aqueous 30% H<sub>2</sub>O<sub>2</sub> (1.70 g, 15 mmol) and NaHCO<sub>3</sub> (0.168 g, 2 mmol) were placed in acetonitrile (5 mL) with stirring and the temperature of the reaction mixture was set to 60 °C for 4 h. At every 1 h small aliquot of the reaction mixture was withdrawn, extracted by n-hexane and analyzed quantitatively by gas chromatograph. Only one product was formed whose identity was confirmed by GC-MS. The effects of various parameters, such as amount of oxidant, amount of sodium bicarbonate, catalyst, temperature and solvent volume were studied to see their effect on the conversion and selectivity of the reaction product.

##### **5.2.4.2. Oxidation of cyclohexene**

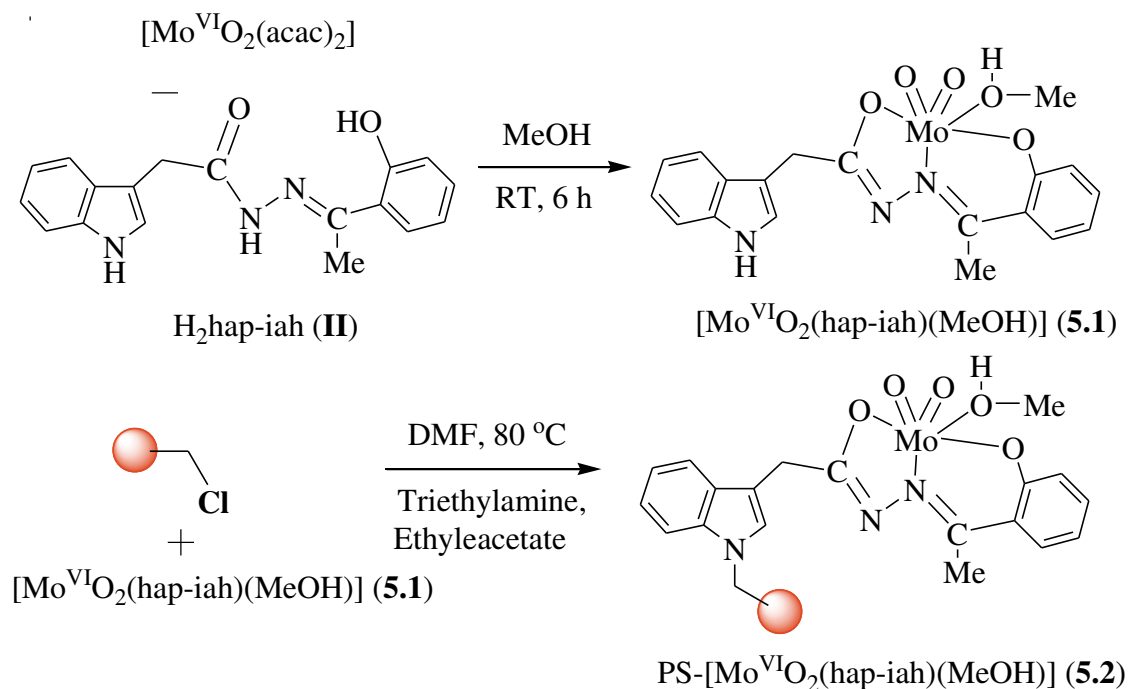
Catalyst (0.030 g), cyclohexene (0.410 g, 5 mmol), NaHCO<sub>3</sub> (0.126 g, 1.5 mmol), aqueous 30 % H<sub>2</sub>O<sub>2</sub> (1.135 g, 10 mmol) were stirred at 50 °C in 3 mL CH<sub>3</sub>CN for 3 h. At every 30 min small aliquot of the reaction mixture was withdrawn, extracted by n-hexane and analyzed quantitatively by gas chromatograph. Only one product was formed which was confirmed by GC-MS.

### 5.3. Results and discussion

#### 5.3.1. Synthesis and characterization

Equimolar amounts of indole-3-acetic hydrazide and *o*-hydroxy acetophenone react in refluxing methanol to give ligand H<sub>2</sub>hap-iah (**II**). Its reaction with [Mo<sup>VI</sup>O<sub>2</sub>(acac)<sub>2</sub>] in 1:1 ratio in refluxing MeOH gave [Mo<sup>VI</sup>O<sub>2</sub>(hap-iah)(MeOH)] (**5.1**). The whole synthetic procedure is presented in Scheme 5.1. The complex is fairly soluble in methanol, DMF and DMSO. Its structure was confirmed by elemental analyses, spectroscopic characterization (IR, electronic, <sup>1</sup>H and <sup>13</sup>C NMR) and thermogravimetric pattern. The ligand coordinates through its dianionic (ONO) functionalities.

The reaction of chloromethylated polystyrene (cross linked with 5% divinylbenzene) with dioxidomolybdenum(VI) complex **5.1** in DMF at 80 °C in the presence of triethylamine leads to the formation of polymer-grafted complex PS-[Mo<sup>VI</sup>O<sub>2</sub>(hap-iah)(MeOH)] (**5.2**). The labile proton of NH group of the indole reacts with CH<sub>2</sub>Cl group of polymer during this process (Scheme 5.1). The ICP-MS analysis of molybdenum in the polymer-grafted complex suggests molybdenum loading of 0.31 mmol g<sup>-1</sup> of polymer in **5.2**.



**Scheme 5.1.** Synthetic routes to prepare **5.1** and **5.2**. PS represents the backbone of the chloromethylated polystyrene.

### 5.3.2. Field emission-scanning electron micrograph (FE-SEM) and energy dispersive X-ray analysis (EDAX) studies

A comparative study using FE-SEM along with EDAX was carried out taking single bead of pure chloromethylated polystyrene and polymer-grafted complex **5.2**. The pure chloromethylated polystyrene bead has smooth and flat surface and shows mainly carbon and chlorine content on the surface, as evaluated by energy dispersive X-ray analysis, while beads of grafted complex show slight darkening of the top layer suggesting the inclusion of metal complex into polymer matrices. Due to insertion of spacer between polymer support and complex, the presence of some of the metal centers on the surface of the polymer was spotted by EDAX study where as high as 7% molybdenum content was noted along with C, N, O and Cl, confirming the grafting of metal complex in polystyrene beads. These observations suggest that part of the

covalently bonded complex is present on the surface while remaining is at various sites. The EDAX profile (see Fig. 5.1) and the images of field emission-scanning electron micrographs (Fe-SEM) of single beads of pure chloromethylated polystyrene and polymer-grafted complex PS-[Mo<sup>VI</sup>O<sub>2</sub>(hap-iah)(MeOH)] (**5.2**) are presented in Fig. 5.2.

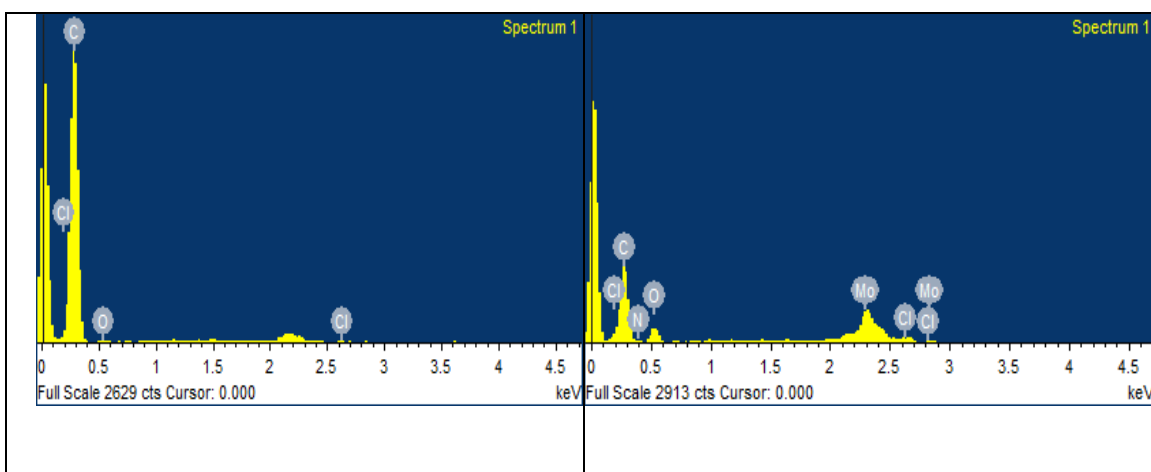


**Figure 5.1.** EDAX profiles of chloromethylated polystyrene (left) and PS-[Mo<sup>VI</sup>O<sub>2</sub>(hap-iah)(MeOH)] (**5.2**) (right).

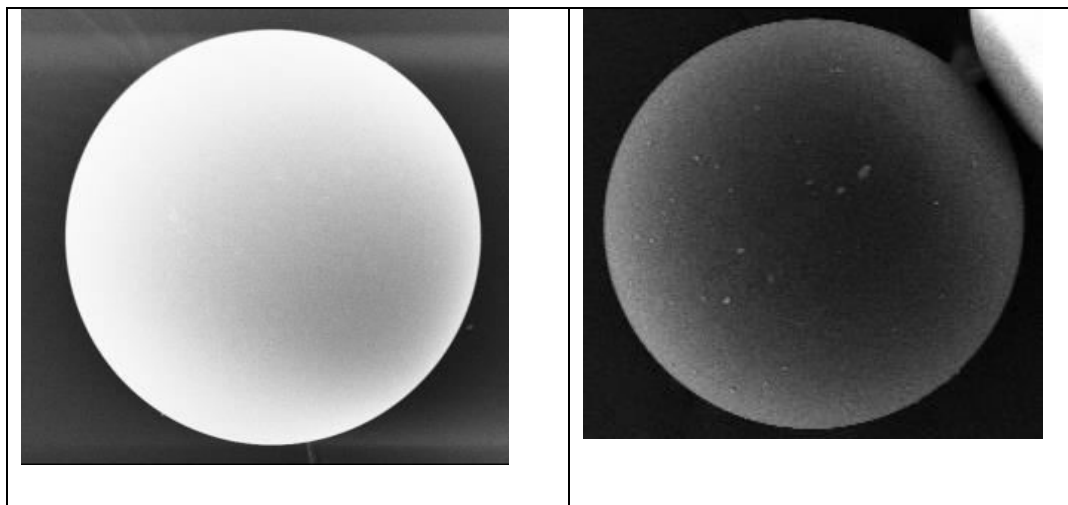


**Figure 5.2.** Scanning electron micrographs (SEM) of chloromethylated polystyrene (left) and PS-[Mo<sup>VI</sup>O<sub>2</sub>(hap-iah)(MeOH)] (**5.2**) (right).

### 5.3.3. Atomic force microscopic (AFM) study

We have obtained AFM images (Fig. 5.3, left) and respective 3d views (Fig 5.3, right) of PS-CH<sub>2</sub>Cl and PS-[Mo<sup>VI</sup>O<sub>2</sub>(hap-iah)(MeOH)] (**5.2**) to see morphological changes before and after complex grafting. The surface roughness and mean height as measured by AFM are 76.5 nm and 484.7 nm, respectively for PS-CH<sub>2</sub>Cl whereas these values are 52.2 nm, 310.0 nm, respectively for PS-[Mo<sup>VI</sup>O<sub>2</sub>(hap-iah)(MeOH)] (**5.2**). The net reduction in these values confirms the grafting of complex in the pores of PS-CH<sub>2</sub>Cl beads [64,157-159]. This observation supplements the conclusion drawn from ICP-MS, TGA and EDAX.



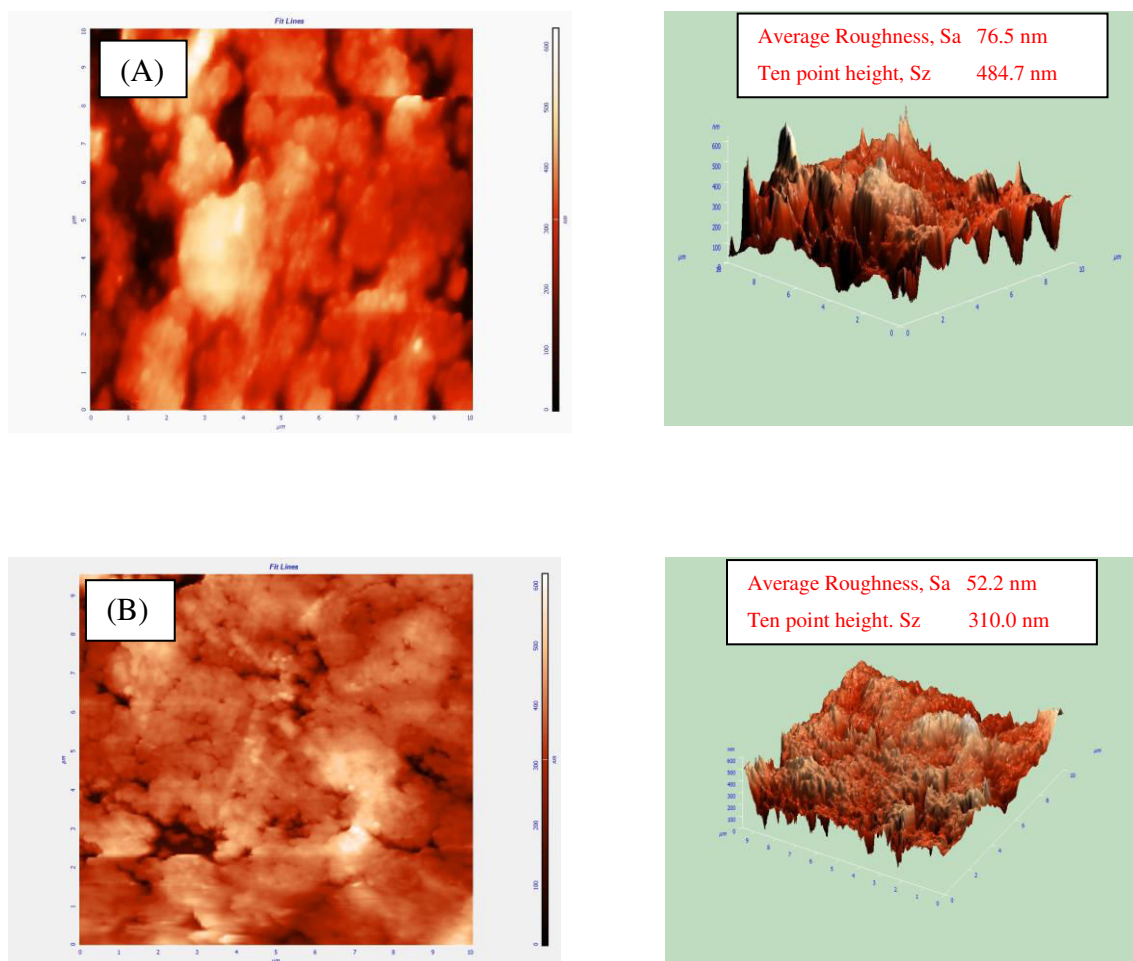


**Figure 5.3.** AFM images (left) and respective 3d-views (right) of PS-CH<sub>2</sub>Cl (A) and PS-[Mo<sup>VI</sup>O<sub>2</sub>(hap-iah)(MeOH)] (B).

#### 5.3.4. Thermogravimetric study

Thermogravimetric analysis profile of [Mo<sup>VI</sup>O<sub>2</sub>(hap-iah)(MeOH)] (5.1) under an oxygen atmosphere shows its stability up to ca. 120 °C. There after it loses weight exothermically between 120 and 180 °C equivalent to one coordinated methanol (Obs. 6.6 %; Anal. Cal. 6.8%). The solvent free complex decomposes in two major fragments with exothermic weight loss on further increasing the temperature. This decomposition

completes at ca. 540 °C with the formation of 29.9% MoO<sub>3</sub> (theoretical value of 30.9%). The weight loss of polymer-grafted complex PS-[Mo<sup>VI</sup>O<sub>2</sub>(hap-iah)(MeOH)] (**5.2**) starts at ca. 100 °C and completes at ca. 300 °C with a total loss of ca. 15% suggesting the presence of coordinated as well as trapped solvent. On further increasing the temperature it decomposes with exothermic weight loss in three overlapping fragments. The final residue of 5.0 % (equivalent to 0.34 mmol g<sup>-1</sup> of Mo in **5.2**) at ca. 470 °C suggests the formation of MoO<sub>3</sub> and grafting of complex **5.2** into polymer.

### 5.3.5. IR spectral studies

The IR spectral data of Schiff base ligand (**II**) and molybdenum complexes (**5.1** and **5.2**) are given in Table 5.1. The IR spectrum of ligand exhibits two distinct bands at 3190 and 1672 cm<sup>-1</sup> due to  $\nu(\text{NH})$  and  $\nu(\text{C}=\text{O})$  modes, respectively, indicative of its ketonic nature in the solid state. The absence of these bands in the spectra of both complexes suggests the enolisation of the amide functionality and subsequent coordination of enolic oxygen to the metal ion after proton replacement. A new band appearing at ca. 1281 cm<sup>-1</sup> is assigned to the  $\nu(\text{C}-\text{O})$  (enolic) stretching of the coordinated hydrazone fragment. The sharp band appearing at 1624 cm<sup>-1</sup> due to azomethine group moves towards lower wave number by 21 cm<sup>-1</sup> (in **5.1**), 28 cm<sup>-1</sup> (in **5.2**) is consistent with the coordination of azomethine nitrogen to the molybdenum. The band at 3350 cm<sup>-1</sup> corresponding to the free -OH group of ligand is also present in complexes **5.1** and **5.2** possibly suggesting the presence of coordinated methanol. The presence of multiple bands of medium intensity observed in the region 2800–2900 cm<sup>-1</sup> in all complexes suggests the existence of -CH<sub>2</sub> group. In addition, the neat complex **5.1** displays two sharp bands at 910 and 932 cm<sup>-1</sup> due to the  $\nu_{\text{sym}}(\text{O}=\text{Mo}=\text{O})$  and  $\nu_{\text{asym}}(\text{O}=\text{Mo}=\text{O})$  modes, respectively. These bands are indicative of the presence of a cis-[Mo<sup>VI</sup>O<sub>2</sub>] structure. In the corresponding polymer-bound molybdenum complex these bands do not resolve clearly due to poor loading of metal complex and only one band was observed at 904 cm<sup>-1</sup>.

The chloromethylated polystyrene displays strong peaks at 1264 and 673  $\text{cm}^{-1}$  due to C–H wagging ( $-\text{CH}_2\text{Cl}$ ) and C–Cl stretch, respectively [90]. The absence of these peaks in PS-[Mo<sup>VI</sup>O<sub>2</sub>((hap-iah)(MeOH))] (**5.2**) suggests the covalent bonding of chloromethylated polystyrene with [Mo<sup>VI</sup>O<sub>2</sub>((hap-iah)(MeOH))] (*cf.* Scheme 5.1) through nitrogen of the indole ring. The absence of  $\nu(\text{NH})$  band appearing at 3120  $\text{cm}^{-1}$  in **5.1** further supplements this statement.

**Table 5.1.** IR spectral data ( $\text{cm}^{-1}$ ) of compounds

Compound	$\nu(\text{OH})$	$\nu(\text{NH})$	$\nu(\text{C}=\text{O})$	$\nu(\text{C}=\text{N})$	$\nu(\text{O}=\text{Mo}=\text{O})$
H <sub>2</sub> hap-iah	3350	3190	1672	1624	
[Mo <sup>VI</sup> O <sub>2</sub> (hap-iah)(MeOH)]	3350	3120	-	1603	910(s), 932(s)
PS-[Mo <sup>VI</sup> O <sub>2</sub> (hap-ah)(MeOH)]	3400	-	-	1596	904(s)

### 5.3.6. UV-visible spectral studies

The UV-visible spectra of the ligand (**II**) and neat complex (**5.1**) measured in methanol are shown in Fig. 5.4 while Table 5.2 includes spectral data. Three ligand absorption bands are observed at 220, 274 and 319 nm which are assigned to  $\sigma \rightarrow \sigma^*$ ,  $\pi \rightarrow \pi^*$  and  $n \rightarrow \pi^*$  transitions, respectively. Similar kind of absorption bands with slight shift are also observed in complex **5.1**. Complex **5.1** also exhibits a charge transfer band at 373 nm originating due to transfer of partial electron density from phenolate oxygen atom to an empty d-orbital of the molybdenum atom. Spectrum of **5.2** recorded in Nujol has very similar but weak electronic spectral patterns [Fig. 5.5]. Bands in the UV region are similar to that observed in **5.1** but the expected LMCT transition in **5.2** could only be observed around 370 nm as a weak shoulder in Nujol possibly due to poor loading of complex in the polymer matrix.

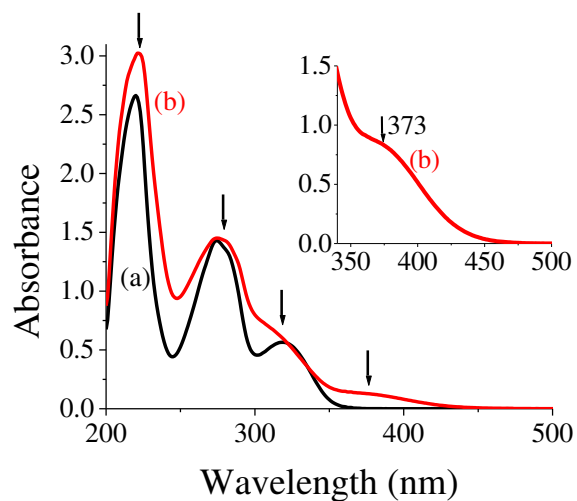


**Figure 5.4.** Electronic spectra of (a)  $H_2hap-iah$  (**II**) and (b)  $[Mo^{VI}O_2(hap-iah)(MeOH)]$  (**5.1**) recorded in methanol.

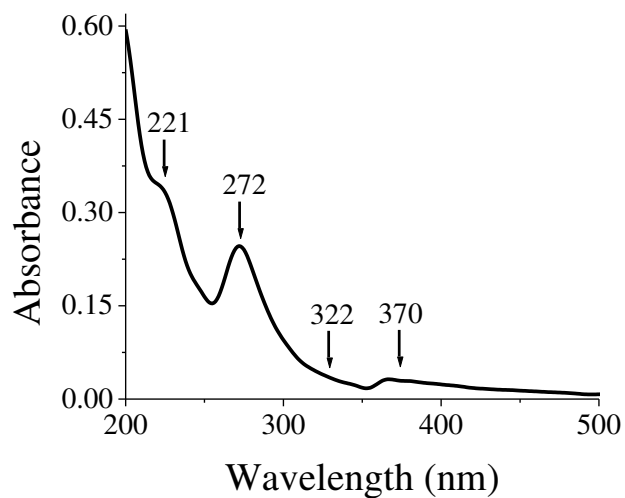


**Figure 5.5.** Electronic spectrum of  $PS-[Mo^{VI}O_2(hap-iah)(MeOH)]$  (**5.2**) recorded after dispersing it in Nujol.

**Table 5.2.** UV-visible spectral data of ligand and complexes.

Compound	Solvent	$\lambda_{\max}/\text{nm}$ ( $\epsilon/\text{M}^{-1}\text{cm}^{-1}$ )
H <sub>2</sub> hap-iah	MeOH	220 ( $3.82 \times 10^4$ ), 274 ( $2.05 \times 10^4$ ), 319 ( $0.81 \times 10^4$ )
[Mo <sup>VI</sup> O <sub>2</sub> (hap-iah)(MeOH)]	MeOH	222 ( $5.68 \times 10^4$ ), 275 ( $2.72 \times 10^4$ ), 318 ( $1.14 \times 10^4$ ), 373 ( $2.53 \times 10^3$ )
PS-[Mo <sup>VI</sup> O <sub>2</sub> (hap-iah)(MeOH)]	Nujol	221, 272, 322, 370

### 5.3.7. <sup>1</sup>H and <sup>13</sup>C NMR studies

The <sup>1</sup>H NMR spectra of H<sub>2</sub>hap-iah (**II**) and [Mo<sup>VI</sup>O<sub>2</sub>(hap-iah)(MeOH)] (**5.1**) are shown in Fig. 5.6 and their typical chemical shifts are presented in Table 5.3. The <sup>1</sup>H NMR spectrum of ligand exhibits three signals at  $\delta = 13.21$  (s, 1H), 11.14 (s, 1H) and 10.92 (s, 1H) ppm for phenolic –OH, –NH (of –C(O)–NH– group) and –NH (of indole) protons, respectively. The absence of signal due to NH of –C(O)–NH– group in **5.1** supports the enolisation of the ketonic group and consequent replacement of H by the metal ion. Similarly, absence of phenolic proton signal in **5.1** indicates the coordination of the phenolic oxygen after proton replacement. Protons associated with aromatic, methyl (of *o*-hydroxyacetophenone) and NH (of indole group) groups appear at nearly same positions in ligand as well as in complex. In addition, methyl and -OH protons of methanol were observed at  $\delta = 3.17$  (s, 3H) and 4.1 (b, 1H) ppm.

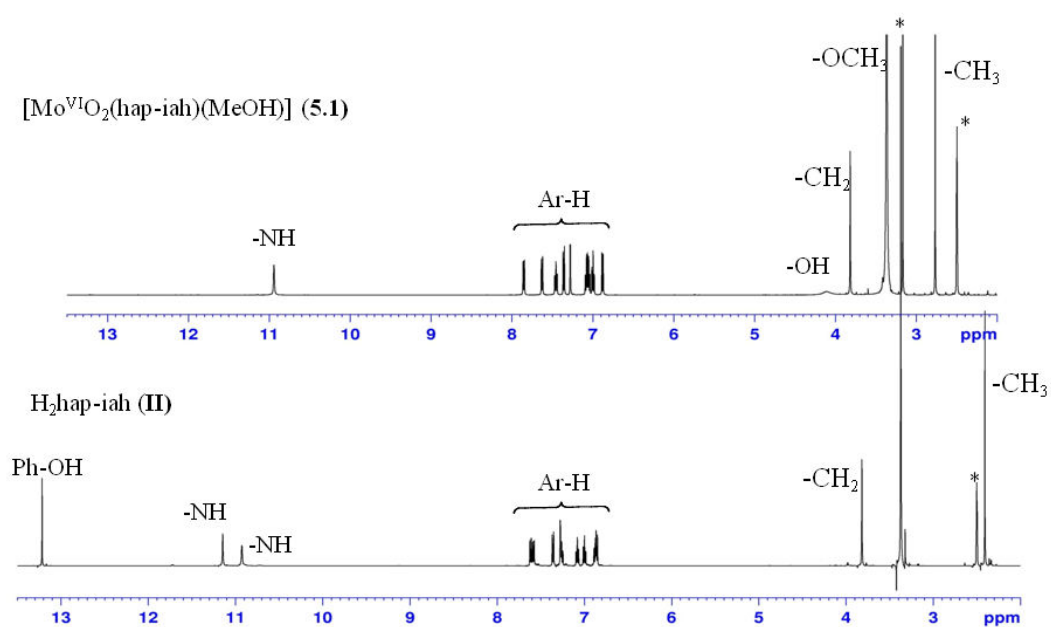


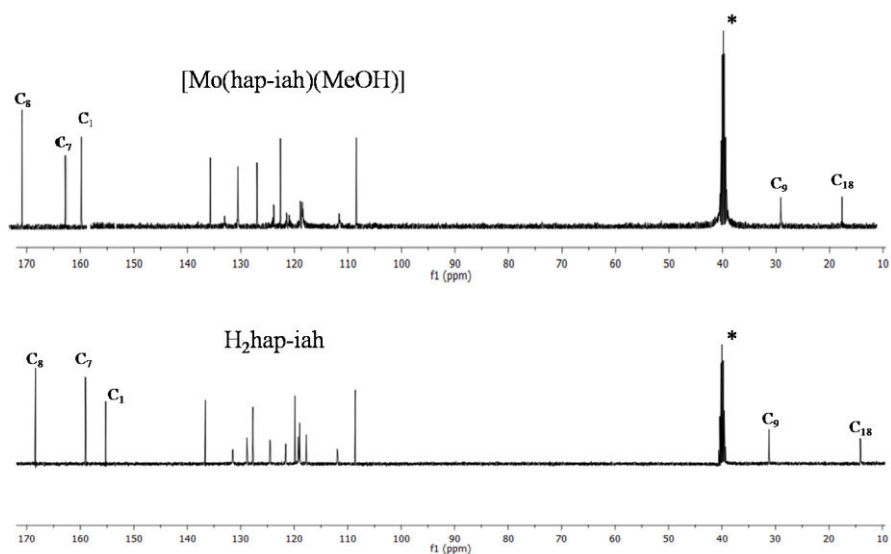
**Figure 5.6.** <sup>1</sup>H NMR spectra of H<sub>2</sub>hap-iah (II) and  $[\text{Mo}^{\text{VI}}\text{O}_2(\text{hap-iah})(\text{MeOH})]$  (5.1).

**Table 5.3.**  $^1\text{H}$  NMR chemical shifts [ $\delta$  in ppm] of ligand and complex recorded in  $\text{DMSO-d}_6$ .

Compound <sup>a</sup>	–OH (phenolic)	–NH– (hydrazide)	–NH– (indole)	–C(CH <sub>3</sub> )=N– (azomethine)
<b>II</b>	13.21 (s, 1H)	11.14 (s, 1H)	10.92 (s, 1H)	2.40 (s, 3H)
<b>5.1</b>	-	-	10.94 (s, 1H)	2.76 (s, 3H)
Compound <sup>a</sup>	–CH <sub>2</sub> –	CH <sub>3</sub>	Aromatic	–OH (alcoholic)
<b>II</b>	3.81 (s, 2H)	-	6.84-7.62 (m, 9H)	-
<b>5.1</b>	3.82 (s, 2H)	3.17 (s, 3H)	6.87-7.86 (m, 9H)	4.1 (br, 1H)

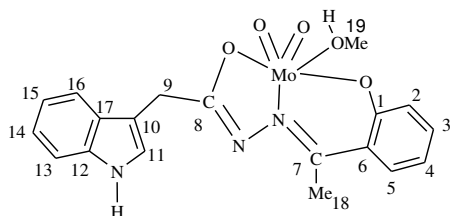
<sup>a</sup> Letters given in parentheses indicate the signal structure: s = singlet, m = multiplet, br = broad (unresolved).

Table 5.4 provides  $^{13}\text{C}$  NMR spectral data of  $\text{H}_2\text{hap-iah}$  (**II**) and  $[\text{Mo}^{\text{VI}}\text{O}_2(\text{hap-iah})(\text{MeOH})]$  (**5.1**) and Fig. 5.7 reproduces their spectra. For aromatic carbons less number of signals were observed due to the presence of center of symmetry. A large coordination-induced shift for  $\text{C}_1$  (carbon bearing phenolic oxygen),  $\text{C}_7$  (carbon bearing azomethine nitrogen) and  $\text{C}_8$  (carbon bearing enolic oxygen) atoms demonstrate the coordination of these functionalities to the molybdenum. A considerable up field shift of  $\text{C}_9$  (methylene) carbon and down field shift of  $\text{C}_{18}$  (methyl) carbon was also noticed in complex. The signal of co-ordinated MeOH in  $^{13}\text{C}$  NMR could not be located possibly due to the replacement of MeOH by DMSO in solution. However, this could be located at  $\delta = 51.0$  ppm in  $\text{CDCl}_3$ .



**Figure 5.7.**  $^{13}\text{C}$  NMR spectra of  $\text{H}_2\text{hap-iah}$  (**II**) and  $[\text{Mo}^{\text{VI}}\text{O}_2(\text{hap-iah})(\text{MeOH})]$  (**5.1**) recorded in  $\text{DMSO-d}_6$ .

**Table 5.4**  $^{13}\text{C}$  NMR spectral data of ligand and complexes



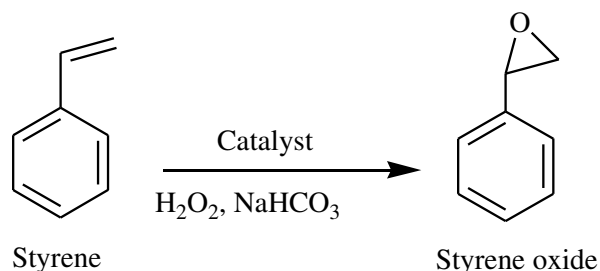
Compound	$\text{C}_1$	$\text{C}_2\text{-C}_5$	$\text{C}_6$	$\text{C}_7$	$\text{C}_8$	$\text{C}_9$
<b>II</b>	155.2	117.7, 131.5, 121.6, 128.8	118.9	159.0	168.4	31.2
<b>5.1</b>	160.4 (5.2)	119.0, 133.9, 121.9, 131.4	119.0	163.7 (4.7)	172.8 (4.4)	28.9
Compound	$\text{C}_{10}, \text{C}_{11}, \text{C}_{12}$		$\text{C}_{13}\text{-C}_{17}$		$\text{C}_{18}$	
<b>II</b>	108.5, 127.7, 136.6		111.9, 124.5, 119.8, 118.9, 127.7		14.1	
<b>5.1</b>	108.7, 124.6, 136.7		111.9, 121.6, 121.9, 119.1, 127.7		17.3 (3.2)	



### 5.3.8. Catalytic activity studies

#### 5.3.8.1. Oxidation of styrene with $\text{H}_2\text{O}_2$ in presence of $\text{NaHCO}_3$ catalyzed by PS- $[\text{Mo}^{\text{VI}}\text{O}_2(\text{hap-iah})(\text{MeOH})]$ (5.2)

At least five oxidation products have been obtained using polymer-anchored catalysts PS- $[\text{V}^{\text{IV}}\text{O}(\text{sal-ohyba})\cdot\text{DMF}]$  [56] and PS- $\text{K}[\text{V}^{\text{V}}\text{O}(\text{O}_2)(\text{L})]$  [L = 2-(2-pyridyl)benzimidazole and 2-(3-pyridyl)benzimidazole ] [42]. Oxidation of styrene, catalyzed by polymer supported complex PS- $[\text{Mo}^{\text{VI}}\text{O}_2(\text{hap-iah})(\text{MeOH})]$  (5.2), using aqueous 30%  $\text{H}_2\text{O}_2$  as oxidant did not proceed. Addition of  $\text{NaHCO}_3$  to the reaction mixture activated the catalytic oxidation process efficiently and gave mainly styrene oxide along with small amount of un-identified product; Scheme 5.2. Such  $\text{NaHCO}_3$  assisted oxidation of styrene has been reported in the literature [153-156].



**Scheme 5.2.**  $\text{NaHCO}_3$  activated oxidation products of styrene using  $\text{H}_2\text{O}_2$  as the oxidant.

The reaction conditions were optimized for the maximum oxidation of styrene, considering different parameters like amounts of catalyst,  $\text{H}_2\text{O}_2$ ,  $\text{NaHCO}_3$ , volume of  $\text{CH}_3\text{CN}$  and effect of temperature. In order to optimize the catalyst amount, three different amounts of catalyst i.e. 0.010, 0.020 and 0.030 g were taken for the fixed amount of styrene (0.52 g, 5 mmol),  $\text{H}_2\text{O}_2$  (1.70 g, 15 mmol) and  $\text{NaHCO}_3$  (0.168 g, 2 mmol) in 5 mL  $\text{CH}_3\text{CN}$  solvent and the reaction was carried out at 60 °C for 4 h. As shown in Fig. 5.8, a maximum of 31 % conversion was achieved with 0.010 g of catalyst in 4 h of reaction time. This conversion improved to 59% upon increasing the catalyst

amount to 0.020 g. Further increasing the amount to 0.030 g, the conversion of styrene improved to 68%. Therefore, 0.030 g of catalyst was taken for the maximum conversion of styrene.

The amount of  $\text{NaHCO}_3$  was optimized by taking 0.5, 1 and 2 mmol of  $\text{NaHCO}_3$  under above reaction conditions; Fig. 5.9. A maximum of 30% conversion was obtained with 0.5 mmol (0.042 g)  $\text{NaHCO}_3$  in 4 h of reaction time. Increasing this amount to 1 mmol (0.084 g) the conversion improved to 38 % and 68% conversion of styrene was obtained with 2 mmol (0.168 g) of  $\text{NaHCO}_3$ .

To understand the effect of oxidant, three different styrene : aqueous 30 %  $\text{H}_2\text{O}_2$  molar ratios viz. 1:1, 1:2, and 1:3 were considered for a fixed amount of styrene (0.52 g, 5 mmol),  $\text{NaHCO}_3$  (0.168 g, 2 mmol) and catalyst (0.030 g) in 5 mL of  $\text{CH}_3\text{CN}$ . As illustrated in Fig. 5.10, increasing the styrene to oxidant ratio from 1:1 to 1:2 increases the conversion from 25% to 52% and further increasing this ratio to 1:3 shows 68% conversion. Thus substrate to  $\text{H}_2\text{O}_2$  ratio of 1:3 was considered the best one for the maximum oxidation of styrene. The volume of acetonitrile was optimized by using three different volume of acetonitrile (5, 10 and 15 mL); Fig. 5.11. In 5 mL acetonitrile the conversion was 68% while increasing the volume of solvent did not improve any conversion. Under above optimized reaction conditions, temperature of the reaction mixture was also optimized and found that 60 °C is the most suitable one to obtained highest conversion as shown in Fig. 5.12.

Table 5.5 summarizes all conditions and conversion obtained under particular condition. From the data presented in Table 5.5, it is clear that the best suited reaction conditions for the maximum oxidation of 5 mmol of styrene at 60 °C are (entry no. 3):  $\text{PS-}[\text{Mo}^{\text{VI}}\text{O}_2(\text{hap-iah})(\text{MeOH})]$  (0.030 g),  $\text{NaHCO}_3$  (0.168 g, 2 mmol ), aqueous 30%  $\text{H}_2\text{O}_2$  (1.70 g, 15 mmol) and acetonitrile (5 mL).

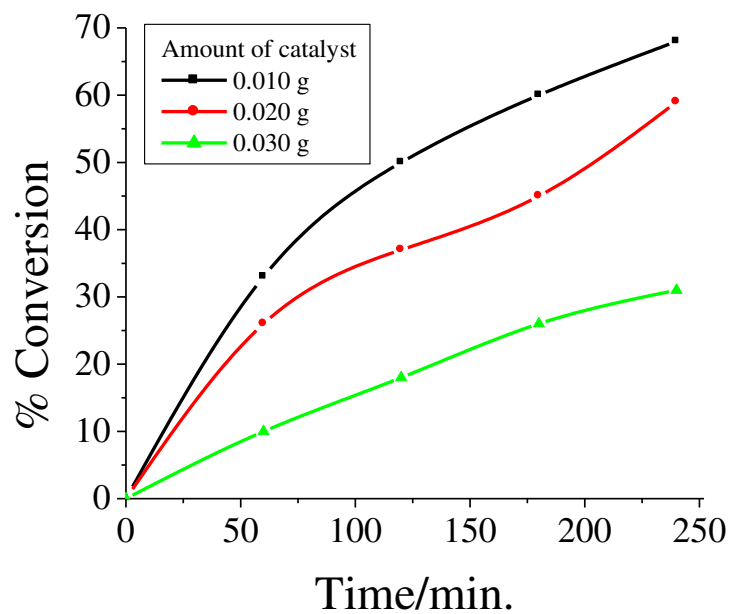


**Figure 5.8.** Effect of amount of catalyst on the oxidation of styrene. For reaction conditions refer to Table 5.5.

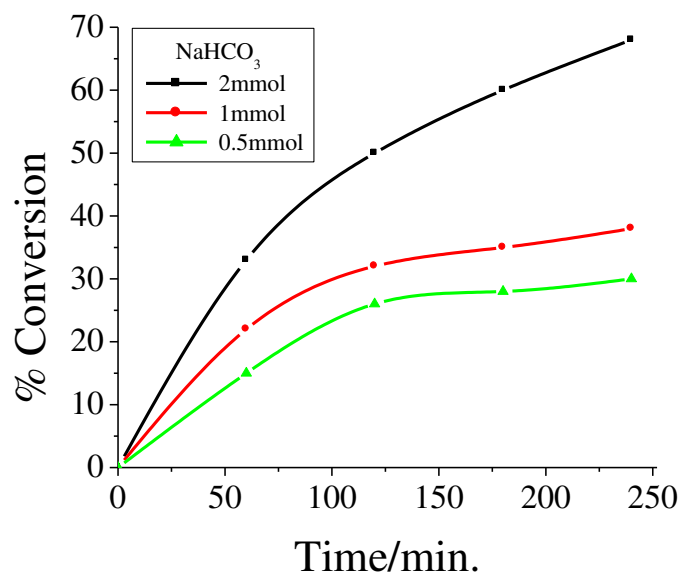


**Figure 5.9.** Effect of amount of  $\text{NaHCO}_3$  on the oxidation of styrene. For reaction conditions refer to Table 5.5.

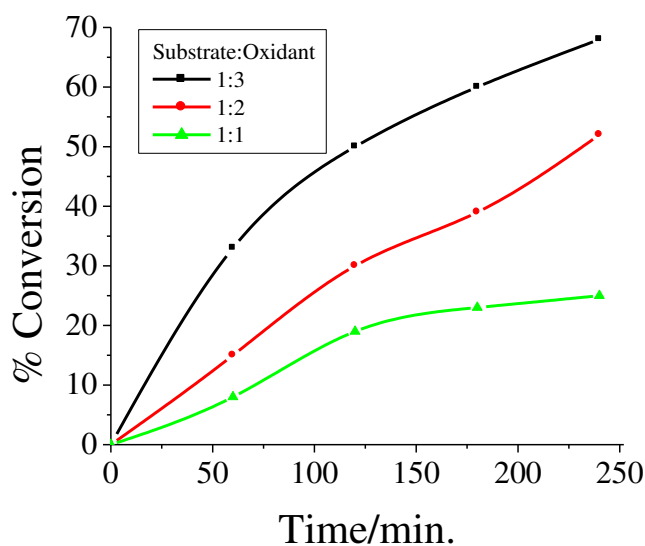


**Figure 5.10.** Effect of amount of  $\text{H}_2\text{O}_2$  ( $\text{H}_2\text{O}_2$ / styrene molar ratio) on the oxidation of styrene. For reaction conditions refer to Table 5.5.

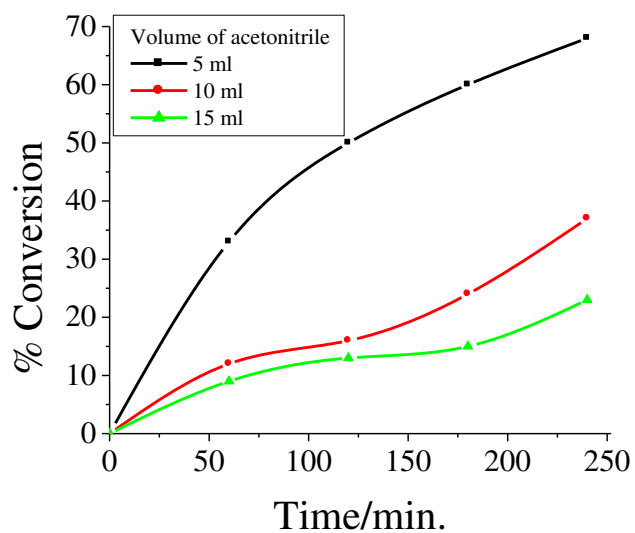


**Figure 5.11.** Effect of volume of CH<sub>3</sub>CN on the oxidation of styrene. For reaction conditions refer to Table 5.5.

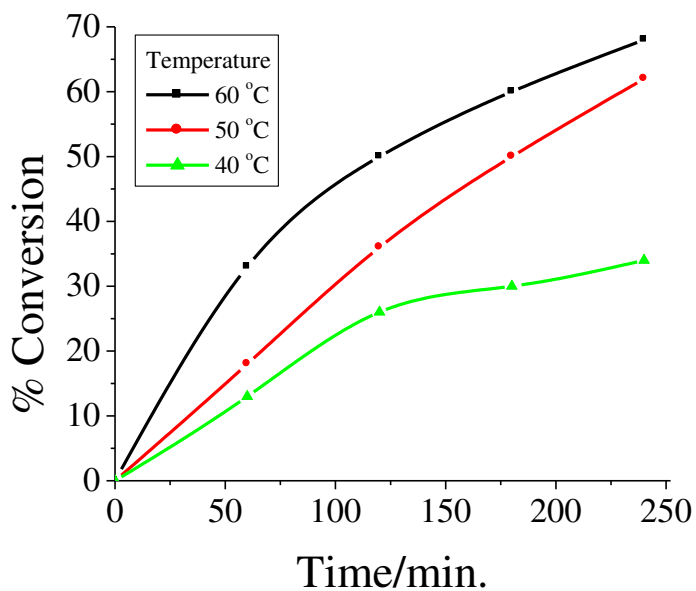


**Figure 5.12.** Effect of temperature on the oxidation of styrene. For reaction conditions refer to Table 5.5.

**Table 5.5.** Results of oxidation of styrene (0.52 g, 5 mmol) using catalyst PS-[Mo<sup>VI</sup>O<sub>2</sub>(hap-iah)(MeOH)] (**5.2**) after 4 h of reaction time.

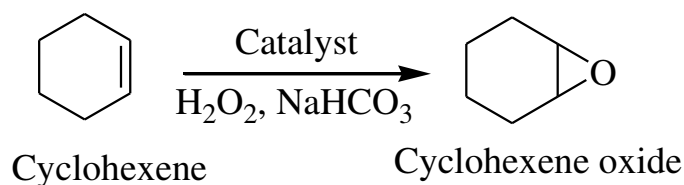
Entry No.	Catalyst (g)	NaHCO <sub>3</sub> (g, mmol)	H <sub>2</sub> O <sub>2</sub> (g, mmol)	CH <sub>3</sub> CN (mL)	Temp. (°C)	conv. (%)	TOF (h <sup>-1</sup> )
1	0.010	0.168, 2	1.70 , 15	5	60	31	210
2	0.020	0.168, 2	1.70 , 15	5	60	59	200
3	0.030	0.168, 2	1.70 , 15	5	60	68	154
4	0.030	0.042, 0.5	1.70 , 15	5	60	30	68
5	0.030	0.084, 1	1.70 , 15	5	60	38	86
6	0.030	0.168, 2	0.567 , 5	5	60	25	56
7	0.030	0.168, 2	1.135, 10	5	60	52	117
8	0.030	0.168, 2	1.70 , 15	10	60	37	84
9	0.030	0.168, 2	1.70 , 15	15	60	23	12
10	0.030	0.168, 2	1.70 , 15	5	40	34	77
11	0.030	0.168, 2	1.70 , 15	5	50	62	140

The reaction was also carried out at room temperature under the same conditions in the presence of NaHCO<sub>3</sub> only and it gave 16% conversion of styrene. A blank reaction (i.e. in the absence of catalyst while using H<sub>2</sub>O<sub>2</sub> and NaHCO<sub>3</sub>) under the above reaction conditions gave 19% conversion while in the absence of NaHCO<sub>3</sub> no reaction takes place. All these suggest the important role of NaHCO<sub>3</sub> in assisting the catalytic ability of complex. Under the above optimised reaction conditions the neat complex [Mo<sup>VI</sup>O<sub>2</sub>(hap-iah)(MeOH)] (**5.1**) and recovered polymer anchored catalyst gave 66% and 65% conversion, respectively. Thus, catalytic potential of supported as well as neat complexes both are good but the recyclability of the supported catalyst makes it better over the non-supported one.

**5.3.8.2. Oxidation of cyclohexene with H<sub>2</sub>O<sub>2</sub> in presence of NaHCO<sub>3</sub> catalyzed by PS-[Mo<sup>VI</sup>O<sub>2</sub>(hap-iah)(MeOH)] (5.2)**

We have also tested the NaHCO<sub>3</sub> assisted catalytic activity of **5.2** for the oxidation of cyclohexene using 30% H<sub>2</sub>O<sub>2</sub> in acetonitrile and cyclohexene oxide was obtained as the major product (Scheme 5.3) along with some minor products but their overall percentage is extremely low. About 3 h was required to acquire equilibrium with maximum conversion. The obtained main product was confirmed by GC–MS after its extraction by n-hexane from the reaction mixture.

The reaction conditions for the maximum oxidation of cyclohexene were also optimized considering all these parameters stated above such as amounts of catalyst, aqueous 30% H<sub>2</sub>O<sub>2</sub>, NaHCO<sub>3</sub>, volume of acetonitrile and temperature of the reaction mixture. Thus, for 5 mmol (0.41 g) of cyclohexene, four different amounts of catalyst (0.010, 0.020, 0.030 and 0.040 g), 30 % aqueous H<sub>2</sub>O<sub>2</sub> (5, 7.5, 10 and 15 mmol), NaHCO<sub>3</sub> (1, 1.5, 2 and 3 mmol) were taken in acetonitrile (3, 5, 7 and 10 mL) and the reaction was carried out at different temperatures (30, 40, 50 and 60 °C). Figs. 5.13 to 5.17 presents whole profiles under different reactions conditions and Table 5.6 summarizes all the conditions and conversions obtained under a particular set of conditions. The best suited reaction conditions concluded (entry no. 16 of Table 5.6) with 93% conversion of cyclohexene are: catalyst (0.030 g), 30 % aqueous H<sub>2</sub>O<sub>2</sub> (1.135 g, 10 mmol) and NaHCO<sub>3</sub> (0.126 g, 1.5 mmol) in acetonitrile (3 mL) at 50 °C.



**Scheme 5.3.** NaHCO<sub>3</sub> activated oxidation product of cyclohexene using H<sub>2</sub>O<sub>2</sub> as the oxidant.

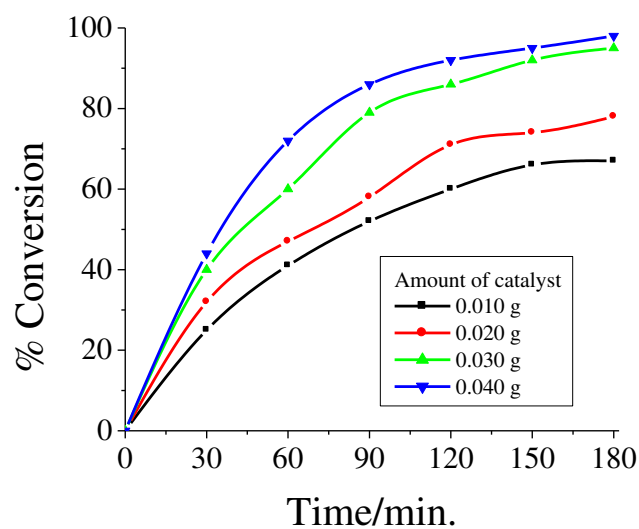


**Figure 5.13.** Effect of amount of catalyst on the oxidation of cyclohexene. For reaction conditions refer to Table 5.6.

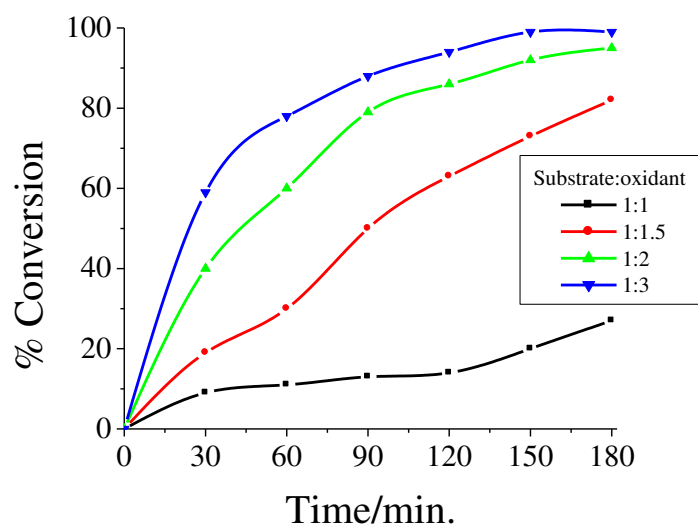


**Figure 5.14.** Effect of amount of  $H_2O_2$  ( $H_2O_2$ /styrene molar ratio) on the oxidation of cyclohexene. For reaction conditions refer to Table 5.6.



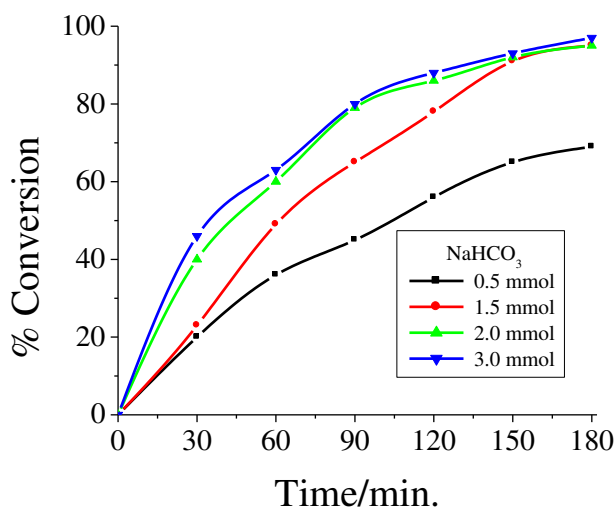


**Figure 5.15.** Effect of amount of  $\text{NaHCO}_3$  on the oxidation of cyclohexene. For reaction conditions refer to Table 5.6.

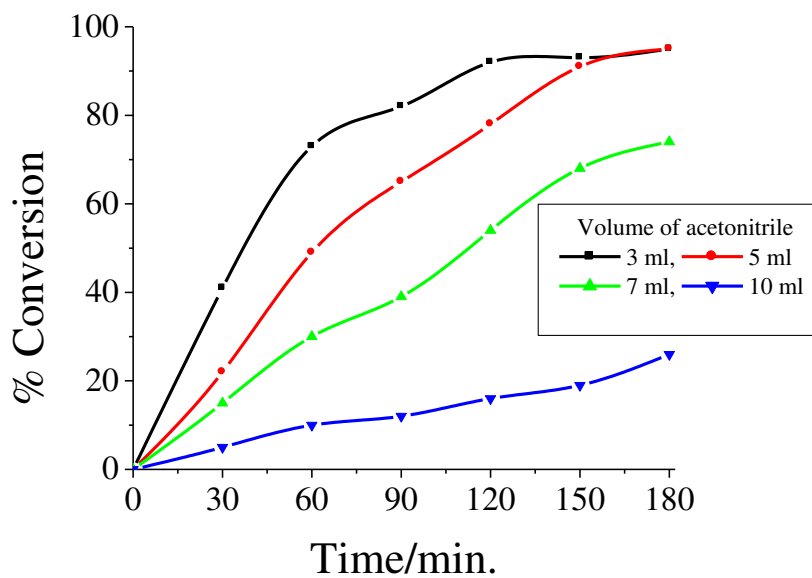


**Figure 5.16.** Effect of volume of  $\text{CH}_3\text{CN}$  on the oxidation of cyclohexene. For reaction conditions refer to Table 5.6.

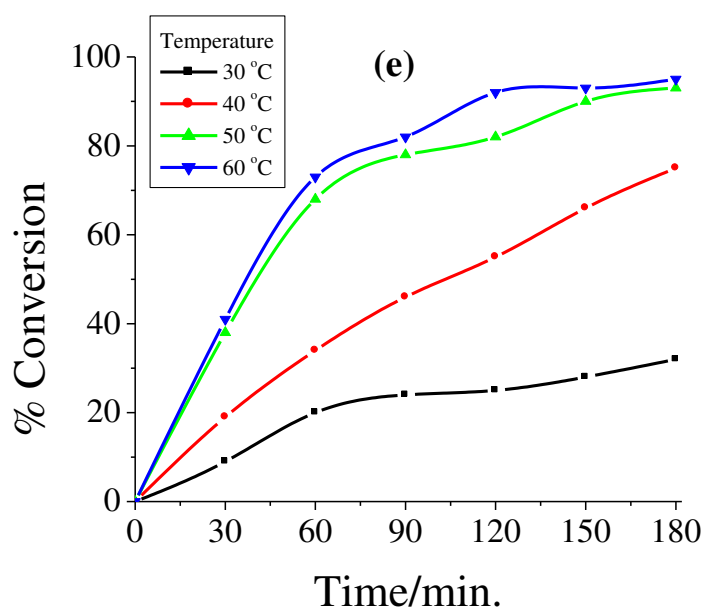


**Figure 5.17.** Effect of temperature on the oxidation of cyclohexene. For reaction conditions refer to Table 5.6.

A maximum of 40 % conversion of cyclohexene was obtained without catalyst (i.e. in the presence of  $\text{H}_2\text{O}_2$  and  $\text{NaHCO}_3$ ) under above reaction conditions while no conversion was obtained in the absence of  $\text{NaHCO}_3$ . Oxidation reaction of cyclohexene under same conditions at room temperature gave 32% conversion (Table 5.6). The catalyst remains insoluble in the above reaction conditions and hence can be easily separated by simple filtration followed by washing. The oxidation of cyclohexene was also carried out with the recycled catalyst under the optimized reaction conditions. Only a small decrease in conversion (1%) shows that the catalyst is stable and reusable. A 91% conversion was obtained with  $[\text{Mo}^{\text{VI}}\text{O}_2(\text{hap-iah})(\text{MeOH})]$  (**5.1**). Thus, neat as well as supported catalyst both enhances the reaction while the recyclability of the supported catalyst makes it better over the non-supported one.

**Table 5.6.** Results of oxidation of cyclohexene (0.41 g, 5 mmol) using catalyst PS- $[\text{Mo}^{\text{VI}}\text{O}_2(\text{hap-iah})(\text{MeOH})]$  (**5.2**) after 3 h of reaction time.

Entry No.	Catalyst (g)	NaHCO <sub>3</sub> (g, mmol)	H <sub>2</sub> O <sub>2</sub> (g, mmol)	CH <sub>3</sub> CN (mL)	Temp. (°C)	Conv. (%)	TOF (h <sup>-1</sup> )
1	0.010	0.168, 2	1.135, 10	5	60	67	605
2	0.020	0.168, 2	1.135, 10	5	60	78	352
3	0.030	0.168, 2	1.135, 10	5	60	95	286
4	0.040	0.168, 2	1.135, 10	5	60	98	664
5	0.030	0.168, 2	0.567, 5	5	60	27	081
6	0.030	0.168, 2	0.851, 7.5	5	60	82	247
7	0.030	0.168, 2	1.70, 15	5	60	99	298
8	0.030	0.084, 1	1.135, 10	5	60	69	208
9	0.030	0.126, 1.5	1.135, 10	5	60	95	286
10	0.030	0.252, 3	1.135, 10	5	60	97	292
11	0.030	0.126, 1.5	1.135, 10	3	60	95	286
12	0.030	0.126, 1.5	1.135, 10	7	60	74	223
13	0.030	0.126, 1.5	1.135, 10	10	60	26	078
14	0.030	0.126, 1.5	1.135, 10	3	30	32	096
15	0.030	0.126, 1.5	1.135, 10	3	40	75	226
16	0.030	0.126, 1.5	1.135, 10	3	50	93	280

### 5.3.9. Reactivity of [Mo<sup>VI</sup>O<sub>2</sub>(hap-iah)(MeOH)] (**5.1**) with H<sub>2</sub>O<sub>2</sub> and NaHCO<sub>3</sub> and possible reaction pathway

It is well known fact that *cis*-dioxidomolybdenum(VI) complexes give the corresponding [Mo<sup>VI</sup>O(O<sub>2</sub>)]<sup>2+</sup> complexes on treatment with H<sub>2</sub>O<sub>2</sub> [56,108]. Starting from **5.1** such peroxidomolybdenum(VI) complex could not be isolated possibly due to its poor stability. However, its formation in methanol could be established by electronic absorption spectroscopy by reacting it with H<sub>2</sub>O<sub>2</sub>. Thus, drop wise addition of a dilute H<sub>2</sub>O<sub>2</sub> solution (one drop 30 % H<sub>2</sub>O<sub>2</sub> dissolved in 10 mL of MeOH) to 20 mL of 3.33 × 10<sup>-4</sup> M solution of **5.1** results in the spectroscopic changes presented in Fig. 5.18. The band at 373 nm shifts to 390 nm with isosbestic point at 418 nm along with decrease in

intensity (inset 'A' of Fig. 5.18). Further addition of up to 10 drops of above  $\text{H}_2\text{O}_2$  solution results in only gain in intensity of this band (inset 'B' of Fig. 5.18). In diluted methanolic solution ( $5.32 \times 10^{-5}$  M) of **5.1**, the intensity of bands at 318, 275 nm increases and the intensity of band at 222 nm decrease regularly without much shifting (Fig. 5.18). These changes should indicate the interaction of  $[\text{Mo}^{\text{VI}}\text{O}_2(\text{hap-iah})(\text{MeOH})]$  (**5.1**) with  $\text{H}_2\text{O}_2$  and the plausible formation of  $[\text{Mo}^{\text{VI}}\text{O}(\text{O}_2)(\text{hap-iah})(\text{MeOH})]$  in methanol; Eq. 5.1.

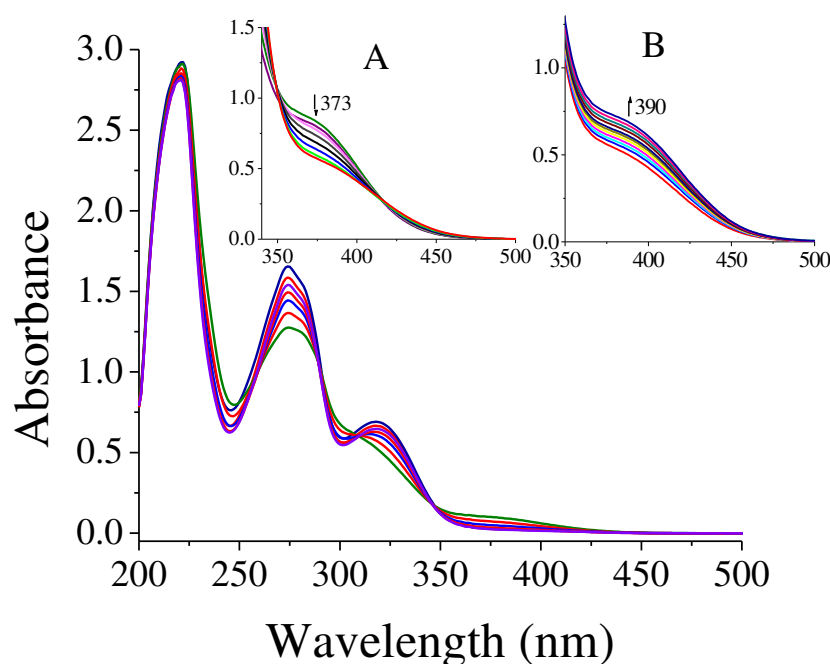
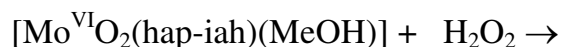


**Figure 5.18.** UV-vis spectral changes observed during titration of  $[\text{Mo}^{\text{VI}}\text{O}_2(\text{hap-iah})(\text{MeOH})]$  (**5.1**) with  $\text{H}_2\text{O}_2$ . The spectra recorded after successive addition of one drop portions of dilute  $\text{H}_2\text{O}_2$  (1 drop of 30%  $\text{H}_2\text{O}_2$  in 10 ml MeOH) to 25 mL of  $5.32 \times 10^{-5}$  M methanolic solution of **5.1**. Inset shows similar spectral changes with  $3.33 \times 10^{-4}$  M solution of **5.1** in methanol.





We have also carried out similar titration of  $[\text{Mo}^{\text{VI}}\text{O}_2(\text{hap-iah})(\text{MeOH})]$  (5.1) with  $\text{H}_2\text{O}_2$  in the presence of  $\text{NaHCO}_3$  to understand their combined effect during catalytic action. Thus, after adding only few drops of a mixture of  $\text{NaHCO}_3$  and  $\text{H}_2\text{O}_2$  exactly similar spectral changes, as observed by adding reasonable amount of  $\text{H}_2\text{O}_2$  alone to 5.1, was obtained hinting the quick formation of oxidoperoxido species (Figs. 5.19 to 5.21). Literature reports the formation of  $\text{HCO}_4^-$  (peroxymonocarbonate) instantly [153-156] on reaction of  $\text{NaHCO}_3$  with  $\text{H}_2\text{O}_2$ . This species reacts with  $[\text{Mo}^{\text{VI}}\text{O}_2]^{2+}$  complex to generate  $[\text{Mo}^{\text{VI}}\text{O}(\text{O}_2)]^{2+}$  intermediate more rapidly compared to  $\text{H}_2\text{O}_2$  alone following another intermediate species as shown in Scheme 5.4 [155,156]. Thus efficient formation of intermediate  $[\text{Mo}^{\text{VI}}\text{O}(\text{O}_2)]^{2+}$  species enhances the transfer of oxygen to the substrate during catalytic oxidation to give final product.

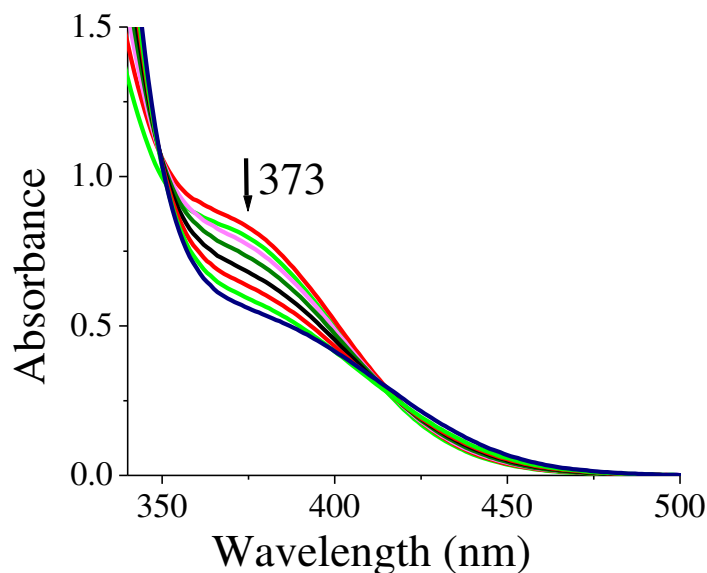


**Figure 5.19.** The spectra recorded after successive addition of one drop portions of dilute mixture [1 drop of 30%  $\text{H}_2\text{O}_2$  and 0.03g (0.357 mmol) in 10 ml MeOH] to 20 mL of  $3.22 \times 10^{-4}$  M methanolic solution of  $[\text{MoO}_2(\text{hap-iah})(\text{MeOH})]$ .

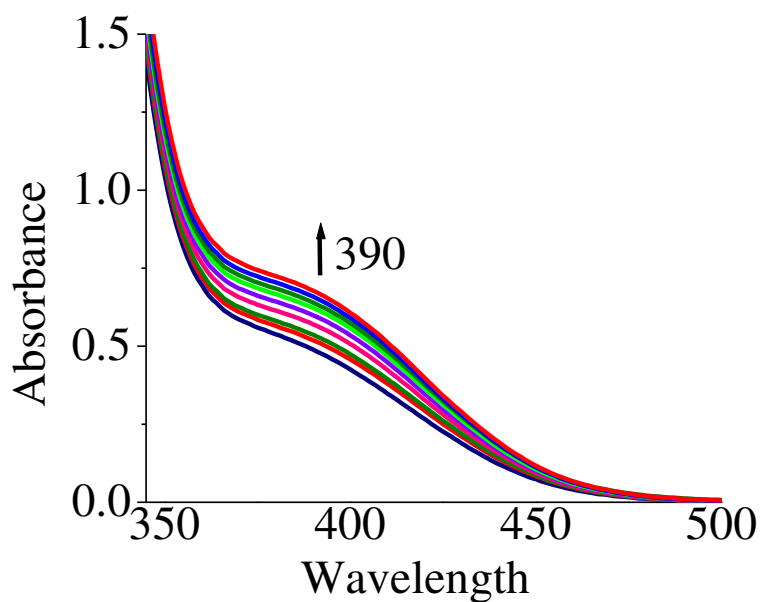


**Figure 5.20.** Spectral changes in the expanded region of 350 nm to 500 nm.

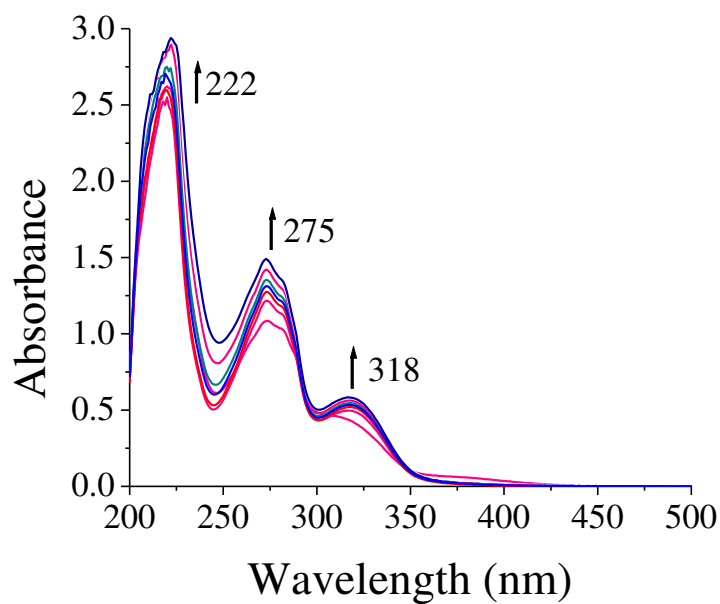
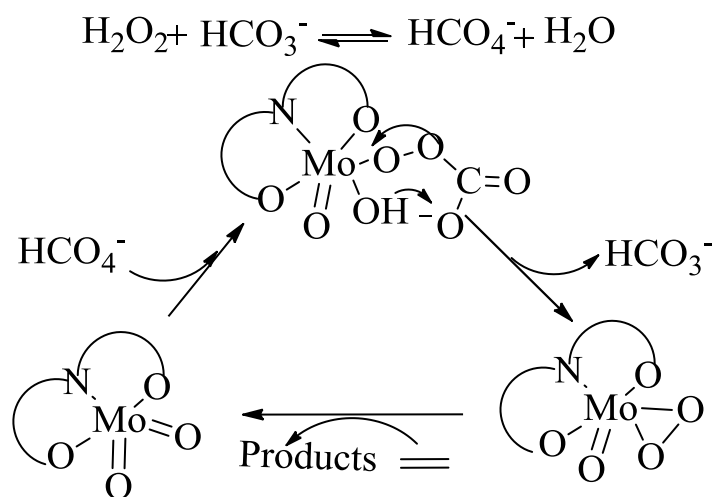


**Figure 5.21.** The spectra recorded after successive addition of one drop portions of dilute mixture [1 drop of 30% H<sub>2</sub>O<sub>2</sub> and 0.03g (0.357 mmol) in 10 ml MeOH] to 22 mL of  $3.22 \times 10^{-4}$  M methanolic solution of [MoO<sub>2</sub>(hap-iah)(MeOH)].



**Scheme 5.4.** Proposed catalytic mechanism for the oxidation of alkenes.

#### 5.4. Conclusions

Complex  $[\text{Mo}^{\text{VI}}\text{O}_2(\text{hap-iah})(\text{MeOH})]$  (**5.1**) with  $\text{H}_2\text{hap-iah}$  (**II**), a dibasic tridentate ONO donor ligand derived from *o*-hydroxyacetophenone and indole-3-acetic hydrazide, has been prepared. Complex **5.1** has also been grafted successfully in chloromethylated polystyrene cross-linked with 5% divinylbenzene (PS) through covalent bonding of the nitrogen of the indole group.  $\text{NaHCO}_3$  assisted oxidation of styrene and cyclohexene has been carried out by grafted complex  $\{\text{PS}-[\text{Mo}^{\text{VI}}\text{O}_2(\text{hap-iah})(\text{MeOH})]\}$  (**5.2**) using aqueous  $\text{H}_2\text{O}_2$  as oxidant. Styrene under optimized reaction conditions gave mainly styrene oxide as oxidized product while oxidation of cyclohexene gave cyclohexene oxide selectively. The intermediate peroxido species, expected to be involved during catalytic action, has also generated from solution of **5.1** and studied by UV-Vis. The presence of some of the catalytic centers on the surface of the polymer, as detected by EDAX study possibly allowed their better interaction with substrates and oxidant during catalytic reaction resulting in better performance of the catalyst. The polymer-grafted

complex shows better conversions than its neat counterpart. The polymer-grafted complex also provides additional advantage over its homogeneous counterpart in terms of recyclable catalytic system, increased catalyst lifetime and easier separation from the reaction mixture.



# REFERENCES

1. J.H. Clark and D.J. Macquarrie, "Heterogeneous catalysis in liquid phase transformations of importance in the industrial preparation of fine chemicals", *Org. Process Res. Dev.*, 1 (1997) 149–162.
2. M. Trilla, R. Pleixats, M. W. C. Man, C. Bied, and J. J. E. Moreau, "Hybrid Organic-Inorganic Materials from di-(2-pyridyl)amine-palladium dichloride complex as recoverable catalysts for Suzuki, Heck and Sonogashira reactions", *Adv. Synth. Catal.*, 350 (2008) 577–590.
3. R. Wang, B. Gao and W. Jiao, "A novel method for immobilization of Co tetraphenylporphyrins on P(4VP-co-St)/SiO<sub>2</sub>: Efficient catalysts for aerobic oxidation of ethylbenzenes", *Appl. Surface Sci.*, 255 (2009) 4109–4113.
4. K. Soai, M. Watanabe and A. Yamamoto, "Enantioselective addition of dialkylzinc to aldehyde using heterogeneous chiral catalysts immobilized on alumina and silica gel", *J. Org. Chem.*, 55 (1990) 4832–4835.
5. P. Barbaro, C. Bianchini, V. D. Santoro, A. Meli, S. Moneti, R. Psaro, A. Scaffidi, L. Sordelli and F. Vizza, "Hydrogenation of arenes over silica-supported catalysts that combine a grafted rhodium complex and palladium nanoparticles: Evidence for substrate activation on Rh<sub>single-site</sub>-Pd<sub>metal</sub> moieties", *J. Am. Chem. Soc.*, 128 (2006) 7065–7076.
6. M. Masteri-Farahani, F. Farzaneh and M. Ghandi, "Synthesis of tetradentate N<sub>4</sub>Schiff base dioxomolybdenum (VI) complex within MCM-41 as selective catalyst for epoxidation of olefins", *Catal. Commun.*, 8 (2007) 6–10.
7. A. Indra, S. Basu, D.G. Kulkarni, C.S. Gopinath, S. Bhaduri and G.K. Lahiri, "MCM-41-supported ruthenium carbonyl cluster-derived catalysts for asymmetric hydrogenation reactions", *Appl. Catal. A: Gen.*, 344 (2008) 124–130.
8. S. L. Jain, B. S. Rana, B. Singh, A. K. Sinha, A. Bhaumik, M. Nandi and B. Sain, "An improved high yielding immobilization of vanadium Schiff base complexes on mesoporous silica via azide-alkyne cycloaddition for the oxidation of sulfides", *Green Chem.*, 12 (2010) 374–377.
9. T. Joseph, S. S. Deshpande, S. B. Halligudi, A. Vinu, S. Ernst and M. Hartmann, "Hydrogenation of olefins over hydridochlorocarbonyltris(triphenylphosphine) ruthenium(II) complex immobilized on MCM-41 and SBA-15", *J. Mol. Catal. A: Chem.*, 206 (2003) 13–21.
10. T. Joseph and S. B. Halligudi, "Oxyfunctionalization of limonene using vanadium complex anchored on functionalized SBA-15", *J. Mol. Catal. A: Chem.*, 229 (2005) 241–247.

11. P. Oliveira, A. Machado, A. M. Ramos, I. M. Fonseca, F. M. Braz Fernandes, A. M. Botelho do Rego and J. Vital, "A new and easy method for anchoring manganese salen on MCM-41", *Catal. Lett.*, 114 (2007) 192–197.
12. S. Sahoo, P. Kumar, F. Lefebvre and S.B. Halligudi, "Enantioselective hydrogenation of olefins by chiral iridium phosphorothioite complex covalently anchored on mesoporous silica", *J. Catal.*, 254 (2008) 91–100.
13. S. Sahoo, P. Kumar, F. Lefebvre and S.B. Halligudi, "Synthesis of chiral sulfoxides by enantioselective sulfide oxidation and subsequent oxidative kinetic resolution using immobilized Ti–binol complex", *J. Catal.*, 262 (2009) 111–118.
14. T. Sasaki, M. Tada, C. Zhong, T. Kume and Y. Iwasawa, "Immobilized metal ion-containing ionic liquids: Preparation, structure and catalytic performances in Kharasch addition reaction and Suzuki cross coupling reactions", *J. Mol. Catal. A: Chem.*, 279 (2008) 200–209.
15. K. Wang, G. J. Kennedy and R. A. Cook, "Hydroxyapatite-supported  $\text{Rh}(\text{CO})_2(\text{acac})$  (acac = acetylacetonate): Structure characterization and catalysis for 1-hexene hydroformylation", *J. Mol. Catal. A: Chem.*, 298 (2009) 88–93.
16. N. Madhavan, T. Takatani, C. D. Sherrill and M. Weck, "Macrocyclic cyclooctene-supported  $\text{AlCl}_3$ –Salen catalysts for conjugated addition reactions: Effect of linker and support structure on catalysis", *Chem. Eur. J.*, 15 (2009) 1186–1194.
17. M. Moghadam, S. Tangestaninejad, V. Mirkhani, I. M. Baltork and N. S. Mirbagheri, "Molybdenum hexacarbonyl supported on functionalized multi-wall carbon nanotubes: Efficient and highly reusable catalysts for epoxidation of alkenes with tert-butyl hydroperoxide", *J. Org. Chem.*, 695 (2010) 2014–2021.
18. F. Esnaashari, M. Moghadam, V. Mirkhani, S. Tangestaninejad, I. M. Baltork, A. R. Khosropour and M. Zakeri, "Multi-wall carbon nanotubes supported molybdenyl acetylacetonate: Efficient and highly reusable catalysts for epoxidation of alkenes with tert-butyl hydroperoxide", *Mat. Chem. & Phys.*, 137 (2012) 69–75.
19. A.J. Pardey, N. Manosalva, M. Bartolini, J. Molina, M. C. Ortega, L.D'Ornelas, C. Chinea, C. Scott, P. Betancourt, C. Urbina, D. Moronta, and R.P. Feazell, "Synthesis, characterization and catalytic properties of coordination complexes based on  $[\text{Mo}(\text{CO})_3(\text{CH}_3\text{CN})_3]$  and poly(4-vinylpyridine)", *Catal. Lett.*, 122 (2008) 274–280.
20. R. Arshady, G. W. Kenner and A. Ledwith, "The introduction of chloromethyl groups into styrene-based polymers, 1. Synthesis of 4-chloromethylstyrene and 4-methoxymethylstyrene and their co-polymerizations with styrene", *Makromol.*

- Chem.*, 177 (1976) 2911–2918.
21. R. B. Merrifield, “Solid phase peptide synthesis: The synthesis of a tetrapeptide”, *J. Am. Chem. Soc.*, 85 (1963) 2149–2154.
  22. S. Mohanraj and W. T. Ford, “Phase-transfer-catalyzed chlorination of poly(p-methylstyrene)”, *Macromolecules*, 19 (1986) 2470–2472.
  23. K. C. Gupta, A. K. Sutar and C.-C. Lin, “Polymer-supported Schiff base complexes in oxidation reactions”, *Coord. Chem. Rev.*, 253 (2009) 1926–1946.
  24. M. R. Maurya, “Catalytic applications of polymer-supported molybdenum complexes in organic transformations”, *Curr. Org. Chem.*, 16 (2012) 73–88.
  25. M. R. Maurya and J. Costa Pessoa, “Polymer-bound metal complexes as catalysts: Synthesis, characterization, reactivity and catalytic activity in E-H bond activation”, *J. Organometal. Chem.*, 696 (2011) 244–254.
  26. M. R. Maurya, A. Kumar and J. Costa Pessoa, “Vanadium complexes immobilized on solid supports and their use as catalysts for oxidation and functionalization of alkanes and alkenes”, *Coord. Chem. Rev.*, 255 (2011) 2315–2344.
  27. A. Syamal and M. M. Singh, “Novel polystyrene-anchored copper(II), nickel(II), cobalt(II), iron(III), zinc(II), cadmium(II), zirconium(IV), molybdenum(V), molybdenum(VI) and uranium(VI) complexes of the chelating resin containing the Schiff base derived from salicylaldehyde and 1-amino-2-naphthol-4-sulfonic acid”, *React. Polym.*, 21 (1993) 149–158.
  28. Y. Wang, Y. Chang, R. Wang and F. Zha, “Preparation and catalytic oxidation by polymer supported 4-(2-pyridylazo) resorcinol-metal complexes”, *J. Mol. Catal. A: Chem.*, 159 (2000), 31–35.
  29. M. R. Maurya, “Structural models of vanadate-dependent haloperoxidases, their reactivity, immobilization on polymer support and catalytic activities”, *J. Chem. Sci.*, 123 (2011) 215–228.
  30. M. R. Maurya, M. Kumar and S. Sikarwar, “Polymer-anchored oxoperoxo complexes of vanadium(V), molybdenum(VI) and tungsten(VI) as catalyst for the oxidation of phenol and styrene using hydrogen peroxide as oxidant”, *React. Funct. Polym.*, 66 (2006) 808–818.
  31. M. R. Maurya and S. Sikarwar, “Oxidation of phenol and hydroquinone catalysed by copper(II) and oxovanadium(IV) complexes of N,N'-bis(salicylaldene)diethylenetriamine (H<sub>2</sub>saldien) covalently bonded to chloromethylated polystyrene”, *J. Mol. Catal. A: Chem.*, 263 (2006) 175–185.

32. W. Trakarnpruk and W. Kanjina, "Preparation, characterization, and oxidation catalysis of polymer supported ruthenium and cobalt complexes", *Ind. Eng. Chem. Res.*, 47 (2008) 964–968.
33. M. R. Maurya and S. Sikarwar, "Oxovanadium(IV) complex of  $\beta$ -alanine derived ligand immobilized on polystyrene for the oxidation of various organic substrates", *Catal. Commun.*, 8 (2007) 2017–2024.
34. M. R. Maurya, M. Kumar, A. Kumar and J Costa Pessoa, "Oxidation of *p*-chlorotoluene and cyclohexene catalysed by polymer-anchored oxovanadium(IV) and copper(II) complexes of amino acid derived tridentate ligands", *Dalton Trans.*, (2008) 4220–4232.
35. L. Canali, D. C. Sherrington and H. Deleuze, "Synthesis of resins with pendently-bound chiral manganese-salen complexes and use as heterogeneous asymmetric alkene epoxidation catalysts", *React. Funct. Polym.*, 40 (1999) 155–168.
36. R. Ando, T. Yagyu and M. Maeda, "Characterization of oxovanadium(IV)-Schiff-base complexes and those bound on resin, and their use in sulfide oxidation", *Inorg. Chim. Acta*, 357 (2004) 2237–2244.
37. X.-Q. Yu, J.-S. Huang, W.-Y. Yu and C.-M. Che, "Polymer-supported ruthenium porphyrins: Versatile and robust epoxidation catalysts with unusual selectivity", *J. Am. Chem. Soc.*, 122 (2000) 5337–5342.
38. S. L. Jain, J. K. Joseph, F. E. Kühn and O. Reiser, "An efficient synthesis of poly(ethylene glycol)-supported iron(II) porphyrin using a click reaction and its application for the catalytic olefination of aldehydes", *Adv. Synth. Catal.*, 351 (2009) 230–234.
39. F. Minutolo, D. Pini and P. Salvadori, "Polymer-bound chiral (salen) Mn (III) complex as heterogeneous catalyst in rapid and clean enantioselective epoxidation of unfunctionalised olefins", *Tetrahedron Lett.*, 37 (1996) 3375–3378.
40. G. Grivani, S. Tangestaninejad, M. H. Habibi and V. Mirkhani, "Epoxidation of alkenes by a highly reusable and efficient polymer-supported molybdenum carbonyl catalyst", *Catal. Commun.*, 6 (2005) 375–378.
41. M. R. Maurya, A. Arya, A. Kumar and J. Costa Pessoa, "Polystyrene bound oxidovanadium(IV) and dioxidovanadium(V) complexes of histamine derived ligand for the oxidation of methyl phenyl sulfide, diphenyl sulfide and benzoin", *Dalton trans.*, (2009) 2185–2195.

42. M. R. Maurya, M. Kumar and U. Kumar, "Polymer-anchored vanadium, molybdenum and copper complexes of bidantate ligand as catalyst for the liquid phase oxidation of organic substance", *J. Mol. Catal. A: Chem.*, 273 (2007) 133–143.
43. M. R. Maurya, M. Kumar and A. Arya, "Model dioxovanadium(V) complexes through direct immobilization on polymer support, their characterization and catalytic activities", *Catal. Commun.*, 10 (2008) 187–191.
44. A. Barbarini, R. Maggi, M. Muratori, G. Sartori and R. Sartorio, "Enantioselective sulfoxidation catalyzed by polymer-supported chiral Schiff base-VO(acac)<sub>2</sub> complexes", *Tetrahedron: Asym.*, 15 (2004) 2467–2473.
45. R. S. Walmsley, N. Torto, S. Chigome and Z.R. Tshentu, "Towards the development of fiber-based oxidovanadium(IV) catalysts for the oxidation of thioanisole", *Catal. Lett.*, 142 (2012) 243–250.
46. M. R. Maurya, A. Arya, A. Kumar, M. L. Kuznetsov, F. Avecilla and J. Costa Pessoa, "Polymer-bound oxidovanadium(IV) and dioxidovanadium(V) complexes as catalysts for the oxidative desulfurization of model fuel diesel", *Inorg. Chem.*, 49 (2010) 6586–6600.
47. G. Zampella, P. Fantucci, V. L. Pecoraro and L. De Gioia, "Reactivity of peroxo forms of the vanadium haloperoxidases cofactor. A DFT investigation", *J. Am. Chem. Soc.*, 127 (2005) 953–960.
48. T. S. Smith II and V. L. Pecoraro, "Oxidation of organic sulfides by vanadium haloperoxidase model complexes", *Inorg. Chem.*, 41 (2002) 6754–6760.
49. A. E. Anderson, M. P. Weberski, Jr., and C. C. McLauchlan, "Phosph(on/in)ate-bridged vanadium(IV) dimers: synthesis and characterization", *Inorg. Chem.*, 51 (2012) 8719–8728.
50. M. P. Weberski, Jr. and C. C. McLauchlan, "Synthesis, reactivity, and x-ray structural characterization of a vanadium(III) oxidation pre-catalyst, (CpP<sup>OEt</sup>Co)VC12(DMF)", *Inorg. Chem. Commun.*, 10 (2007) 906–909.
51. C. C. McLauchlan and K.J. McDonald, "Cocrystallization of dichloro-(N,N-dimethylformamide)[hydrotris(pyrazol-1-yl)borato]vanadium(III) with its partially oxidized analog chloro(N,N-dimethylformamide)[hydrotris(pyrazol-1-yl)borato]oxovanadium(IV)", *Acta Crystallogr., Sect. E: Struct. Rep. Online* 2006, 62, m588–m590.
52. M. R. Maurya, S. Sikarwar and P. Manikandan, "Oxovanadium(IV) complex of 2-( $\alpha$ -hydroxyethyl)benzimidazole covalently bonded to chloromethylated polystyrene for oxidation of benzoin", *Appl. Catal. A: Gen.*, 315 (2006) 74–82.

53. M.R. Maurya, U. Kumar and P. Manikandan, Synthesis and Characterisation of Polymer-Anchored Oxidovanadium(IV) Complexes and Their Use for the Oxidation of Styrene and Cumene, *Eur. J. Inorg. Chem.*, (2007) 2303–2314.
54. M. R. Maurya, M. Kumar and S. Sikarwar, “Polymer-anchored oxoperoxo complexes of vanadium(V), molybdenum(VI) and tungsten(VI) as catalyst for the oxidation of phenol and styrene using hydrogen peroxide as oxidant”, *React. Funct. Polym.*, 66 (2006) 808–818.
55. V. Hulea and E. Dumitriu, “Styrene oxidation with H<sub>2</sub>O<sub>2</sub> over Ti-containing molecular sieves with MFI, BEA and MCM-41 topologies”, *Appl. Catal. A: Gen.*, 277 (2004) 99–106.
56. M. R. Maurya, U. Kumar and P. Manikandan, “Polymer supported vanadium and molybdenum complexes as potential catalysts for the oxidation and oxidative bromination of organic substrates”, *Dalton. Trans*, (2006) 3561–3575.
57. S. Suresh, S. Skaria and S. Ponrathnam, “Polymer-supported vanadium salt as a catalyst for the oxidation of phenols”, *Synth. Commun.*, 26 (1996) 2113–2117.
58. R. Pathak and G. N. Rao, “Oxidation of 2,6-di-*tert*-butylphenol with polymer-anchored molybdenyl and vanadyl complexes”, *J. Mol. Catal. A: Chem.*, 130 (1998) 215–220.
59. M. R. Maurya, A. Arya, U. Kumar, A. Kumar, F. Avecilla and J. Costa Pessoa, “Polymer-bound oxidovanadium(IV) and dioxidovanadium(V) complexes: synthesis, characterization and catalytic application for the hydroamination of styrene and vinyl pyridine”, *Dalton Trans.*, (2009) 9555–9566.
60. M. R. Maurya, U. Kumar, I. Correia, P. Adão and J. Costa Pessoa, “Polymer bound oxidovanadium(IV) complex of L-cysteine derived ligand for the oxidative amination of styrene”, *Eur. J. Inorg. Chem.*, (2008) 577–587.
61. M. R. Maurya, A. Arya, P. Adão and J. Costa Pessoa, “Immobilization of oxovanadium(IV), dioxomolybdenum(VI) and copper(II) complexes on polymer for the liquid phase oxidation of styrene, cyclohexene and ethylbenzene”, *Appl. Catal. A: Gen.*, 351 (2008) 239–252.
62. M.R. Maurya, N. Chaudhary and F. Avecilla, “Polymer-grafted and neat vanadium(V) complexes as functional mimics of haloperoxidases”, *Polyhedron*, 67 (2014) 436–448.
63. Mannar R. Maurya, Nikita Chaudhary, Amit Kumar, Fernando Avecilla and J. Costa Pessoa, “Polystyrene bound dioxidovanadium(V) complexes of 2-

- acetylpyridine derived ligands for catalytic oxidations”, *Inorg. Chim. Acta*, 420 (2014) 24–38.
64. Mannar R. Maurya, Nikita Chaudhary, Fernando Avecilla, Pedro Adão and J. Costa Pessoa, “Oxidovanadium(IV) and dioxidovanadium(V) complexes of hydrazones of 2-benzoylpyridine and their catalytic applications”, *Dalton Trans.*, 44 (2015) 1211–1232.
65. M.R. Maurya, N. Chaudhary, F. Avecilla, and I. Correia, “Mimicking peroxidase activity by a polymer-supported oxidovanadium(IV) Schiff base complex derived from salicylaldehyde and 1,3-diamino-2-hydroxypropane”, *J. Inorg. Biochem.*, (2015), <http://dx.doi.org/10.1016/j.jinorgbio.2015.01.012>
66. S. D. Leinonen, C. Sherrington, A. Sneddon, D. McLoughlin, J. Corker, C. Canevali, F. Morazzoni, J. Reedijk and S. B. D. Spratt, “Molecular structural and morphological characterization of polymer-supported Mo(VI) alkene epoxidation catalysts”, *J. Catal.*, 183 (1999) 251–266.
67. R. Mbeleck, K. Ambroziak, B. Saha and D. C. Sherrington, “Stability and recycling of polymer-supported Mo(VI) alkene epoxidation catalysts”, *React. Funct. Polym.*, 67 (2007) 1448–1457.
68. K. Ambroziak, R. Mbeleck, Y. He, B. Saha and D.C. Sherrington, “Investigation of batch alkene epoxidations catalyzed by polymer-supported Mo(VI) complexes”, *Ind. Eng. Chem. Res.*, 48 (2009) 3293–3302.
69. S. Gil, R. Gonzalez, R. Mestres, V. Sanz and A. Zapater, “Alkene epoxidations catalysed by Mo(VI) supported on Merrifield’s polymer”, *React. Funct. Polym.*, 42 (1999) 65–72.
70. S. Tangestaninejad, M. H. Habibi, V. Mirkhani, M. Moghadam and G. Grivani, “Readily prepared polymer-supported molybdenum carbonyls as novel reusable and highly active epoxidation catalysts”, *Inorg. Chem. Comm.*, 9 (2006) 575–578.
71. S. Tangestaninejad, V. Mirkhani, M. Moghadam and G. Grivani, “Readily prepared heterogeneous molybdenum-based catalysts as highly recoverable, reusable and active catalysts for alkene epoxidation”, *Catal. Commun.*, 8 (2007) 839–844.
72. G. Grivani, S. Tangestaninejad, M.H. Habibi V. Mirkhani and M. Moghadam, “Epoxidation of alkenes by a readily prepared and highly active and reusable heterogeneous molybdenum-based catalyst”, *Appl. Catal. A: Gen.*, 299 (2006) 131–136.



73. G. Grivani, S. Tangestaninejad and A. Halili, "A readily prepared, highly reusable and active polymer-supported molybdenum carbonyl Schiff base complex as epoxidation catalyst", *Inorg. Chem. Commun.*, 10 (2007) 914–917.
74. G. Grivani and A. Akherati, "Polymer-supported bis (2-hydroxyanyl) acetylacetonato molybdenyl Schiff base catalyst as effective, selective and highly reusable catalyst in epoxidation of alkenes", *Inorg. Chem. Commun.*, 28 (2013) 90–93.
75. J. J. Boruah, S. P. Das, S. R. Ankireddy, S. R. Gogoi and N. S. Islam, "Merrifield resin supported peroxomolybdenum(VI) compounds: recoverable heterogeneous catalysts for the efficient, selective and mild oxidation of organic sulfides with H<sub>2</sub>O<sub>2</sub>", *Green Chem.*, 15 (2013) 2944–2959.
76. I. Cazaux, and C. Caže, "Asymmetric epoxidation catalyzed by polymer-anchored amino alcohol-molybdenum complexes", *React. Polym.*, 20 (1993) 87–97.
77. R. K. Bhatia and G.N. Rao, "Oxidation of benzoin with anchored vanadyl and molybdenyl Catalysts", *J. Mol. Catal. A: Chem.*, 121 (1997) 171–178.
78. J. J. Boruah, S. P. Das, R. Borah, S. R. Gogoi and N. S. Islam, "Polymer-anchored peroxo compounds of molybdenum and tungsten as efficient and versatile catalysts for mild oxidative bromination", *Polyhedron*, 52 (2013) 246–254.
79. J. J. Boruah, D. Kalita, S. P. Das, S. Paul and N. S. Islam, "Polymer-anchored peroxo compounds of vanadium(V) and molybdenum(VI): synthesis, stability, and their activities with alkaline phosphatase and catalase", *Inorg. Chem.*, 50 (2011) 8046–8062.
80. D. C. Sherrington in: *Supported Reagents and Catalyst in Chemistry* (Ed.: B. K. Hodnett, A. P. Keybett, J. H. Clark, K. Smith), Royal Society of Chemistry, Cambridge (1998) p. 220.
81. L. Canali and D. C. Sherrington, "Utilisation of homogeneous and supported chiral metal(salen) complexes in asymmetric catalysis", *Chem. Soc. Rev.*, 28 (1999) 85–93.
82. D.C. Sherrington, "Polymer-supported metal complex alkene epoxidation catalysts", *Catal. Today*, 57 (2000) 87–104.
83. N. E. Leadbeater and M. Marco, "Preparation of polymer-supported ligands and metal complexes for use in catalysis", *Chem. Rev.*, 102 (2002) 3217–3273.
84. T. Punniyamurthy and L. Rout, "Recent advances in copper-catalyzed oxidation of organic compounds", *Coord. Chem. Rev.*, 252 (2008) 134–154.

85. R. A. Rowe and M. M. Jones, "Vanadium (IV) oxy(acetylacetonate)", *Inorg. Synth.*, 5 (1957) 113–116.
86. A. Rockenbauer and L. Korecz, "Automatic computer simulations of ESR spectra", *Appl. Mag. Res.*, 10 (1996) 29–43.
87. M. R. Maurya, S. Khurana, C. Schulzke and D. Rehder, "Dioxo- and oxovanadium(V) complexes of biomimetic hydrazone ONO donor ligands: Synthesis, characterisation, and reactivity", *Eur. J. Inorg. Chem.*, (2001) 779–788.
88. M.R. Maurya, S. Agarwal, C. Bader, M. Ebel and D. Rehder, "Synthesis, characterisation and catalytic potential of hydrazonovanadium(V) model complexes with  $[\text{VO}]^{3+}$  and  $[\text{VO}_2]^+$  cores", *Dalton Trans.*, (2005) 537–544.
89. M.R. Maurya, C. Haldar, A. Kumar M.L. Kuznetsov, F. Avecilla and J. Costa Pessoa, "Vanadium complexes having  $[\text{VO}]^{2+}$ ,  $[\text{VO}]^{3+}$  and  $[\text{VO}_2]^+$  cores with hydrazones of 2,6-diformyl-4-methylphenol: Synthesis, characterization, reactivity, and catalytic potential", *Dalton Trans.*, 42 (2013) 11941–11962.
90. P. Arroyo, S. Gil, A. Munoz, P. Palanca, J. Sanchos and V. Sanz, "Polymer-supported molybdenyl thioglycolate as oxygen atom transfer reagent", *J. Mol. Catal. A: Chem.*, 160 (2000) 403–408.
91. I. Cavaco, J. Costa Pessoa, M. T. Duarte, R. T. Henriques, P. M. Matias and R. D. Gillard, "Crystal and molecular structure of  $[\text{V}_2\text{O}_3(\text{sal-L-val})_2(\text{H}_2\text{O})]$  (sal-L-val = N-salicylidene-L-valinate) and spectroscopic properties of related complexes", *J. Chem. Soc., Dalton Trans.*, (1996) 1989–1996.
92. J. Costa Pessoa, M. J. Calhorda, I. Cavaco, I. Correia, M. T. Duarte, V. Felix, R. T. Henriques, M. F. M. Piedade and I. Tomaz, "Molecular modelling studies of N-salicylideneamino acidato complexes of oxovanadium(IV), molecular and crystal structure of a new dinuclear  $\text{LOV}^{\text{IV}}\text{-O-V}^{\text{V}}\text{OL}$  mixed valence complex", *J. Chem. Soc., Dalton Trans.*, (2002) 4407–4415.
93. L. F. Vilas Boas and J. Costa Pessoa in: *Comprehensive coordination chemistry* (Ed.: G. Wilkinson, R. D. Gillard, J. A. McCleverty), Pergamon, Oxford, 1987, pp. 453–583.
94. K. Wüthrich, "E.S.R. (electron spin resonance) investigation of  $\text{VO}^{2+}$  complex compounds in aqueous solution. II", *Helv. Chim. Acta*, 48 (1965) 1012–1017.
95. N. D. Chasteen in "Biological Magnetic Resonance", (Ed.: J. Reuben), Plenum, New York, (1981), p. 53.

96. D. Rehder, C. Weidemann, A. Duch and W. Pribsch, "Vanadium-51 shielding in vanadium(V) complexes: a reference scale for vanadium binding sites in biomolecules", *Inorg. Chem.*, 27 (1988) 584–587.
97. S.B. Kumar, S.P. Mirajkar, G.C.G. Pais, P. Kumar and R. Kumar, "Epoxidation of styrene over a titanium silicate molecular sieve TS-1 using dilute H<sub>2</sub>O<sub>2</sub> as oxidizing agent", *J. Catal.*, 156 (1995) 163–166.
98. T. Joseph, D. Srinivas, C.S. Gopinath and S.B. Halligudi, "Spectroscopic and catalytic activity studies of VO(Saloph) complexes encapsulated in zeolite-Y and Al-MCM-41 molecular sieves", *Catal. Lett.*, 83 (2002) 209–214.
99. M.R. Maurya, A.K. Chandrakar and S. Chand, "Oxidation of phenol, styrene and methyl phenyl sulfide with H<sub>2</sub>O<sub>2</sub> catalyzed by dioxovanadium(V) and copper(II) complexes of 2-aminomethylbenzimidazole-based ligand encapsulated in zeolite-Y", *J. Mol. Catal. A: Chem.*, 263 (2007) 227–237.
100. M. R. Maurya, S. Sikarwar, T. Joseph, P. Manikandan and S. B. Halligudi, "Synthesis, characterisation and catalytic potentials of polymer anchored copper(II), oxovanadium(IV) and dioxomolybdenum(VI) complexes 2-(2-hydroxymethyl)benzimidazole", *React. Funct. Polymer*, 63 (2005) 71–83.
101. C.-G. Jia, F.-Y. Jin, M.-Y. Huang and Y.-Y. Jiang, "Poly(maleic acid-co-styrene)-triruthenium cluster-catalyzed oxidation of styrene with molecular-oxygen", *React. Polymer*, 23 (1994) 33–38.
102. J. D. Koola and J. K. Kochi, "Cobalt-catalyzed epoxidation of olefins. Dual pathways for oxygen-atom transfer", *J. Org. Chem.*, 52 (1987) 4545–4553.
103. W. Nam, R. Ho and J. S. Valentine, "Iron-cyclam complexes as catalysts for the epoxidation of olefins by 30% aqueous hydrogen peroxide in acetonitrile and methanol", *J. Am. Chem. Soc.*, 113 (1991) 7052–7054.
104. A.G.J. Ligtenbarg, R. Hage and B.L. Feringa, "Catalytic oxidations by vanadium complexes", *Coord. Chem. Rev.*, 237 (2003) 89–101.
105. V. Conte, A. Coletti, B. Floris, G. Licini and C. Zonta, "Mechanistic aspects of vanadium catalysed oxidations with peroxides", *Coord. Chem. Rev.*, 255 (2011) 2165–2177.
106. J.A.L. da Silva, J.J.R. Fraústo da Silva and A.J.L. Pombeiro, "Oxovanadium complexes in catalytic oxidations", *Coord. Chem. Rev.*, 255 (2011) 2232–2248.
107. M.R. Maurya and N. Kumar, "Chloromethylated polystyrene cross-linked with divinylbenzene and grafted with vanadium(IV) and vanadium(V) complexes

- having ONO donor ligand for the catalytic activity”, *J. Mol. Catal. A: Chem.*, 383–384 (2014)172–181.
108. M.R. Maurya, N. Kumar and F. Avecilla, “Polymer and non-polymer-grafted dioxidomolybdenum(VI) complexes having ONO donor ligand and their catalytic activities for the oxidative bromination of organic substrates”, *J. Mol. Catal. A: Chem.*, 392 (2014) 50–60.
109. H.B. ten Brink, H.L. Dekker, H.E. Schoemaker and R. Wever, “Oxidation reactions catalyzed by vanadium chloroperoxidase from *Curvularia inaequalis*”, *J. Inorg. Biochem.*, 80 (2000) 91–98.
110. G.D. Christian and W.C. Purdy, “The residual current in orthophosphate medium”, *J. Electroanal. Chem.*, 3 (1959), 363–367.
111. P.C. Pandey and A.K. Pandey, “Electrochemical sensing of dopamine and pyrogallol on mixed analogue of prussian blue nanoparticles modified electrodes—role of transition metal on the electrocatalysis and peroxidase mimetic activity”, *Elect. Acta*, 109 (2013) 536–545.
112. A.T.T. Hsieh, R.M. Sheahan and B.O. West, “Dioxouranium(VI) complexes with N-salicylsalicylaldehydes and their Lewis base adducts”, *Aust. J. Chem.*, 28 (1975) 885–891.
113. N.R. Sangeetha, V. Kavita, S. Wocadlo, A.K. Powell and S. Pal, “Vanadium(V) complexes of O,N,O-donor tridentate ligands containing the  $\{V^VO(OMe)\}^{2+}$  unit: syntheses, structures and properties”, *J. Coord. Chem.*, 51 (2000) 55–66.
114. D. Feng, Z.-Y. Gu, J.-R. Li, H.-L. Jiang, Z. Wei and H.-C. Zhou, “Zirconium-metalloporphyrin PCN-222: mesoporous metal-organic frameworks with ultrahigh stability as biomimetic catalysts”, *Angew. Chem.*, 51(2012) 10307–10310.
115. N. Puvvada, P.K. Panigrahi, D. Mandal and A. Pathak, “Shape dependent peroxidase mimetic activity towards oxidation of pyrogallol by  $H_2O_2$ ”, *RSC. Advances*, 2(2012) 3270–3273.
116. H. Tauber, “Oxidation of pyrogallol to purpurogallin by crystalline catalase”, *J. Biol. Chem.*, 205(1953) 395–400.
117. M.M. Farahani, F. Farzaneh and M. Ghandi, “Synthesis and characterization of molybdenum complexes with bidentate schiff base ligands within nanoreactors of MCM-41 as epoxidation catalysts”, *J. Mol. Catal. A: Chem.*, 248 (2006) 53–60.

118. K. Ambroziak, R. Pelech, E. Milchert, T. Dziembowska and Z. Rozwadowski, "New dioxomolybdenum(VI) complexes of tetradentate schiff base as catalysts for epoxidation of olefins", *J. Mol. Catal. A: Chem.*, 211 (2004) 9–16.
119. Y. Sui, X. Zeng, X. Fang, X. Fu, Y. Xiao, L. Chen, M. Li and S. Cheng, "Syntheses, structure, redox and catalytic epoxidation properties of dioxomolybdenum(VI) complexes with schiff base ligands derived from tris(hydroxymethyl)amino methane", *J. Mol. Catal. A: Chem.*, 270 (2007) 61–67.
120. J. Zhao, X. Zhou, A.M. Santos, E. Herdtweck, C. C. Romao and F.E. Kühn, "Molybdenum(VI) cis-dioxo complexes bearing sugar derived chiral schiff-base ligands: synthesis, characterization, and catalytic applications", *Dalton Trans.*, (2003) 3736–3742.
121. X. Zhou, J. Zhao, A.M. Santos and F.E. Kühn, "Molybdenum(VI) cis -dioxo complexes with chiral schiff base ligands: synthesis, characterization, and catalytic applications", *Z.Naturforsch.*, 59b (2004) 1223–1228.
122. J. M. Sobczak and J. J. Ziolkowski, "Molybdenum complex-catalysed epoxidation of unsaturated fatty acids by organic hydroperoxides", *Appl. Catal. A*, 248 (2003) 261–268.
123. M. Bagherzadeh, R. Latifi, L. Tahsini, V. Amani, A. Ellern and L. K. Woo, "Synthesis, characterization and crystal structure of a dioxomolybdenum(VI) complex with a N,O type bidentate schiff base ligand as a catalyst for homogeneous oxidation of olefins", *Polyhedron*, 28 (2009) 2517–2521.
124. A. Rezaeifard, I. Sheikshoae, N. Monadi and M. Alipour, "Synthesis, characterization and pronounced epoxidation activity of cis-dioxomolybdenum(VI) tridentate schiff base complexes using tert-butyl hydroperoxide", *Polyhedron*, 29 (2010) 2703–2709.
125. J. Pisk, D. Agustin, V. Vrdoljak and R. Poli, "Epoxidation processes by pyridoxal dioxomolybdenum(VI) (pre) catalysts without organic solvent", *Adv. Synth. Catal.*, 353 (2011) 2910–2914.
126. J. Pisk, B. Prugovečki, D. Matković-Čalogović, R. Poli, D. Agustin and V. Vrdoljak, "Charged dioxomolybdenum(VI) complexes with pyridoxal thiosemicarbazone ligands as molybdenum(V) precursors in oxygen atom transfer process and epoxidation (pre)catalysts", *Polyhedron*, 33 (2012) 441–449.
127. K.C. Gupta and A.K. Sutar, "Catalytic activities of Schiff base transition metal complexes", *Coord. Chem. Rev.*, 252 (2008) 1420–1450.

128. M. E. Judmaier, C. Holzer, M. Volpe and N. C. Mösch-Zanetti, "Molybdenum(VI) dioxocomplexes employing schiff base ligands with an intramolecular donor for highly selective olefin epoxidation", *Inorg. Chem.*, 51 (2012) 9956–9966.
129. X. Lei and N. Chelamalla, "Dioxomolybdenum(VI) complexes with linear and tripodal tetradenate ligands: Synthesis, structures and their use as olefin epoxidation catalysts", *Polyhedron*, 49 (2013) 244–251.
130. J.M. Mitchell and N.S. Finney, "New molybdenum catalysts for alkyl olefin epoxidation. Their Implications for the mechanism of oxygen atom transfer", *J. Am. Chem. Soc.*, 123 (2001) 862–269.
131. K. Jeyakumar and D.K. Chand, "Application of molybdenum(VI) dichloride dioxide ( $\text{MoO}_2\text{Cl}_2$ ) in organic transformations", *J. Chem. Sci.*, 121 (2009) 111–123.
132. Z. Hu, X. Fu and Y. Li, "Olefin epoxidation catalyzed by Schiff base molybdenum (VI) complexes immobilized onto zirconium poly (styrene-phenylvinylphosphonate)-phosphate", *Inorg. Chem. Commun.*, 14 (2011) 497–501.
133. M. Bagherzadeh, M. M. Haghdoost, M. Amini and P.G. Derakhshandeh, "Molybdenum oxo–peroxo complex: A very fast catalyst for oxidation and reduction of sulfur-based compounds", *Catal. Commun.*, 23 (2012) 14–19.
134. R. D. Chakravarthy, K. Suresh, V. Ramkumar and D. K. Chand, "New chiral molybdenum complex catalyzed sulfide oxidation with hydrogen peroxide", *Inorg. Chim. Acta*, 376 (2011) 57–63.
135. I. Sheikshoaie, A. Rezaeifard, N. Monadi and S. Kaafi, "A novel tridentate Schiff base dioxo-molybdenum(VI) complex: Synthesis, crystal structure and catalytic performance in green oxidation of sulfides by urea hydrogen peroxide", *Polyhedron*, 28 (2009) 733–738.
136. A. Butler, M. J. Clague and G. E. Meister, "Vanadium Peroxide Complexes", *Chem. Rev.*, 94 (1994) 625–638.
137. C. J. Schneider, J. E. Penner-Hahn and V. L. Pecoraro, "Elucidating the Protonation Site of Vanadium Peroxide Complexes and the Implications for Biomimetic Catalysis", *J. Am. Chem. Soc.*, 130 (2008) 2712–2713.
138. P. Adao, J. Costa Pessoa, R. T. Henriques, M. L. Kuznetsov, F. Avecilla, M. R. Maurya, U. Kumar and I. Correia, "Synthesis, characterization and application of vanadium-salan complexes in oxygen transfer reactions", *Inorg. Chem.*, 48 (2009) 3542–3561.

139. V. Conte and B. Floris, "Vanadium catalyzed oxidation with hydrogen peroxide", *Inorg. Chim. Acta*, 363 (2010) 1935–1946.
140. M. R. Maurya, A. A. Khan, A. Azam, S. Ranjan, N. Mondal, A. Kumar, F. Avecilla and J. Costa Pessoa, "Vanadium complexes having  $[V^{IV}O]^{2+}$  and  $[V^VO_2]^+$  cores with binucleating dibasic tetradentate ligands: Synthesis, characterization, catalytic and antiamebic activities", *Dalton Trans.*, 39 (2010) 1345–1360.
141. M. R. Maurya, A. A. Khan, A. Azam, S. Ranjan, N. Mondal, A. Kumar and J. Costa Pessoa, "Dinuclear oxidovanadium(IV) and dioxidovanadium(V) complexes of 5,5-methylenebis(dibasic tridentate) ligands: Synthesis, spectral characterisation, reactivity, and catalytic and antiamebic activities", *Eur. J. Inorg. Chem.*, (2009) 5377–5390.
142. M. R. Maurya, C. Halder, A. A. Khan, A. Azam, A. Salahuddin, A. Kumar and J. Costa Pessoa, "Synthesis, Characterization, Catalytic and Antiamebic Activity of Vanadium Complexes of Binucleating Bis(dibasic tridentate ONS donor) Ligand Systems", *Eur. J. Inorg. Chem.*, 15 (2012) 2560–2577.
143. S. Pasayat, S.P. Dash, S. Roy, R. Dinda, S. Dhaka, M.R. Maurya, W. Kaminsky, Y.P. Patil and M. Nethaji, "Synthesis, structural studies and catalytic activity of dioxidomolybdenum(VI) complexes with aroylhydrazones of naphthol-derivative", *Polyhedron*, 67 (2014) 1–10.
144. M.R. Maurya, S. Dhaka and F. Avecilla, "Synthesis, characterization and catalytic activity of dioxidomolybdenum(VI) complexes of tribasic pentadentate ligands", *Polyhedron*, 67 (2014) 145–159.
145. G. J.J. Chen, J. W. McDonald and W. E. Newton, "Synthesis of Mo(IV) and Mo(V) Complexes Using Oxo Abstraction by Phosphines. Mechanistic Implications", *Inorg. Chem.*, 15 (1976) 2612–2615.
146. G.M. Sheldrick, *SHELXS-97: An Integrated System for Solving Crystal Structures from Diffraction Data*, Revision 5.1, University of Göttingen, Germany, 1997.
147. A. Rezaeifard, I. Sheikhshoae, N. Monadi, and H. S. Evans, "Synthesis, crystal structure, and catalytic properties of novel dioxidomolybdenum(VI) complexes with tridentate schiff base ligands in the biomimetic and highly selective oxygenation of alkenes and sulfides", *Eur. J. Inorg. Chem.*, (2010) 799–806.
148. A. Syamal and M.R. Maurya, "Coordination chemistry of schiff base complexes of molybdenum", *Coord. Chem., Rev.*, 95 (1989) 183–238.

149. A. D. Westland, F. Haque and J-M. Bouchard, "Peroxo complexes of molybdenum and tungsten stabilized by oxides of amines, phosphines, and arsines. Stability studies", *Inorg. Chem.*, 19 (1980) 2255–2259.
150. A. D. Keramidas, A. B. Papaioannou, A. Vlahos, T. A. Kabanos, G. Bonas, A. Makriyannis, C. P. Raptopoulou and A. Terzis, "Model Investigations for Vanadium–Protein Interactions. Synthetic, Structural, and Physical Studies of Vanadium(III) and Oxovanadium(IV/V) Complexes with Amidate Ligands", *Inorg. Chem.*, 35 (1996) 357–367.
151. T. Moriuchi, M. Yamaguchi, K. Kikushima and T. Hirao, "An efficient vanadium-catalyzed bromination reaction", *Tetrahedron Lett.*, 48 (2007) 2667–2670.
152. V. Conte, O. Bortolini, M. Carraro and S. Moro, "Models for the active site of vanadium–dependent haloperoxidases: Insight into the solution structure of peroxo vanadium compounds", *J. Inorg. Biochem.*, 80 (2000) 41–49.
153. D. E. Richardson, H. Yao, K. M. Frank and D. A. Bennett, "Equilibria, Kinetics, and Mechanism in the Bicarbonate Activation of Hydrogen Peroxide: Oxidation of Sulfides by Peroxymonocarbonate", *J. Am. Chem. Soc.*, 122( 2000) 1729–1739.
154. B. S. Lane, M. Vogt, V. J. DeRose and K. Burgess, "Manganese-catalyzed epoxidations of alkenes in bicarbonate solutions", *J. Am. Chem. Soc.*, 124 (2002)11946–11954.
155. S.K. Maiti, S. Dinda, S. Banerjee, A.K. Mukherjee and R. Bharracharyya, "Oxidoperoxidotungsten(VI) Complexes with Secondary Hydroxamic Acids: Synthesis, Structure and Catalytic Uses in Highly Efficient, Selective and Ecologically Benign Oxidation of Olefins, Alcohols, Sulfides and Amines with H<sub>2</sub>O<sub>2</sub> as a Terminal Oxidant", *Eur. J. Inorg. Chem.*, (2008) 2038–2051.
156. M. Bagherzadeh, M. Aminia, H. Parastar, M. Jalali-Heravi, A. Ellern and L.K. Woo, "Synthesis, X-ray structure and oxidation catalysis of a oxido-peroxido molybdenum(VI) complex with tridentate shiff base ligand", *Inorg. Chem. Commun.*, 20 (2012) 86–89.
157. A. S. Ogunlaja, W. Chidawanyika, E. Antunes, M. A. Fernandes, T. Nyokong, N. Torto and Z. R. Tshentu, "Oxovanadium(IV)-catalysed oxidation of dibenzothiophene and 4,6-dimethyldibenzothiophene", *Dalton Trans.*, 41 (2012) 13908–13918.
158. R. S. Walmsley, A. S. Ogunlaja, M. J. Coombes, W. Chidawanyika, C. Litwinski, N. Torto, T. Nyokong and Z. R. Tshentu, "Imidazole-functionalized polymer microspheres and fibers – useful materials for



## References.....

---

- immobilization of oxovanadium(IV) catalysts” *J. Mater. Chem.*, 22(2012) 5792–5800.
159. Z. R. Tshentu, C. Togo and R. S. Walmsley, “Polymer-anchored oxovanadium(IV) complex for the oxidation of thioanisole, styrene and ethylbenzene”, *J. Mol. Catal. A: Chem.*, 318 (2010) 30–35.

SUMMARY  
&  
CONCLUSIONS

Synthesis of new polymer-supported vanadium and molybdenum complexes, their characterization and catalytic potentials for various organic transformations have been reported in the present thesis. To achieve the goal two new Schiff bases H<sub>2</sub>sal-iah [H<sub>2</sub>sal-iah (**I**) = Schiff base derived from salicylaldehyde and indole-3-acetic hydrazide] and H<sub>2</sub>hap-iah [H<sub>2</sub>hap-iah (**II**) = Schiff base derived from *o*-hydroxy acetophenone and indole-3-acetic hydrazide] have been used. The polymer-supported vanadium complex, PS-[V<sup>IV</sup>O(sal-iah)(H<sub>2</sub>O)] (**2**) has been isolated by direct reaction of chloromethylated polystyrene cross-linked with 5% divinylbenzene with the corresponding neat complex [V<sup>IV</sup>O(sal-iah)(H<sub>2</sub>O)] (**1**). Complex PS-[V<sup>IV</sup>O(sal-iah)(H<sub>2</sub>O)] has been converted into PS-[V<sup>V</sup>O(OMe)(sal-iah)] (**3**) by passing air in the methanolic suspension of **2** in the presence of KOH. The dioxidovanadium(V) complex K[V<sup>V</sup>O<sub>2</sub>(sal-iah)]·H<sub>2</sub>O (**4**) has also been synthesized by the aerial oxidation of [V<sup>IV</sup>O(sal-iah)(H<sub>2</sub>O)] in methanol in the presence of KOH. All these complexes have been characterized by various spectroscopic techniques (IR, electronic, NMR (<sup>1</sup>H and <sup>51</sup>V), electron paramagnetic resonance (EPR)), thermal, field-emission scanning electron micrographs (FE–SEM) as well as energy dispersive X-ray (EDAX) studies.

The polymer-grafted complex PS-[V<sup>V</sup>O(OMe)(sal-iah)] has been used for the oxidation of styrene and cyclohexene using H<sub>2</sub>O<sub>2</sub> as an oxidant. Under the optimized reaction conditions, styrene gave a maximum of 95 % conversion after 6 h of reaction with the main products having a selectivity order of: benzaldehyde (66.9%) > benzoic acid (16.6%) > phenyl acetaldehyde (5.2%) > 1-phenylethane-1,2-diol (4.5%) > styrene oxide (3.3%). Oxidation of cyclohexene gave four products with the selectivity order: cyclohexene epoxide (39.3%) > 2-cyclohexene-1-ol (23.9%) > cyclohexane-1,2-diol (22.9%) > 2-cyclohexene-1-one (7.9%). Non-polymer supported complex K[V<sup>V</sup>O<sub>2</sub>(sal-iah)]·H<sub>2</sub>O has shown equally good catalytic potential towards styrene and cyclohexene but the recyclability and heterogeneity tests of polymer-grafted complex make it better over neat analog.

Oxidomethoxido vanadium(V) complex [V<sup>V</sup>O(OMe)(hap-iah)] (**5**) has been prepared and structurally characterized. Its polymer-grafted complex PS-

[V<sup>V</sup>O(OMe)(hap-iah)] (**6**) has been prepared by interacting oxidomethoxido vanadium(V) complex, [V<sup>V</sup>O(OMe)(hap-iah)], with chloromethylated polystyrene cross-linked with 5% divinylbenzene in DMF. The polymer-grafted complex is able to perform the oxidation of pyrogallol in pH 7 phosphate buffer solution. The catalytic activity of homogeneous catalyst [V<sup>V</sup>O(OMe)(hap-iah)] (**5**) is equally good. However, easy separation of polymer-grafted complex from the reaction medium of pH 7 buffer and the reusability without considerable decrease in activity, suggest that it can be employed to perform environment friendly peroxidase mimetic activity like oxidation of pyrogallol.

Polymer-grafted complex, PS-[Mo<sup>VI</sup>O<sub>2</sub>(sal-iah)(MeOH)] (**7**) as well as corresponding neat complex, [Mo<sup>VI</sup>O<sub>2</sub>(sal-iah)(MeOH)] (**8**) has been synthesized and characterized by various spectroscopic techniques (IR, electronic, NMR (<sup>1</sup>H and <sup>13</sup>C)), thermal, field-emission scanning electron micrographs (FE-SEM) as well as energy dispersive X-ray (EDAX) studies. Complex [Mo<sup>VI</sup>O<sub>2</sub>(sal-iah)(MeOH)] (**8**) has also been characterized by single crystal X-ray diffraction analysis. Oxidative bromination of styrene and *trans*-stilbene has been successfully carried out using PS-[Mo<sup>VI</sup>O<sub>2</sub>(sal-iah)(MeOH)] (**7**) as heterogeneous catalyst, demonstrating the functional similarity to haloperoxidases. Recyclable ability and better catalytic ability over non-grafted analog make it useful functional model of haloperoxidases. The peroxido complex [Mo<sup>VI</sup>O(O<sub>2</sub>)(sal-iah)(MeOH)] (**9**) has also been isolated and characterized. It has also been demonstrated to form in solution which oxidizes bromide, in the presence of acid to give corresponding bromonium ion as intermediate, which in turn reacts with styrene and *trans*-stilbene. This bromonium ion intermediate is responsible for different reaction products of substrates.

Complex [Mo<sup>VI</sup>O<sub>2</sub>(hap-iah)(MeOH)] (**10**) has also been synthesized and then grafted successfully in chloromethylated polystyrene cross-linked with 5% divinylbenzene (PS) through covalent bonding of the nitrogen of the indole group and characterized by various spectroscopic techniques (IR, electronic, NMR (<sup>1</sup>H and <sup>13</sup>C)), thermal, atomic force microscopy (AFM), field-emission scanning electron micrographs (FE-SEM) as well as energy dispersive X-ray (EDAX) studies. The isolated complex PS-

[Mo<sup>VI</sup>O<sub>2</sub>(hap-iah)(MeOH)] (**11**) is good catalyst precursors for the oxidation of styrene and cyclohexene. In the presence of sodium bicarbonate and 30 % *aq.* H<sub>2</sub>O<sub>2</sub> as oxidant, styrene gave mainly styrene oxide as a major product. Oxidation of cyclohexene gave cyclohexene oxide selectively. No conversion of substrates in the absence of NaHCO<sub>3</sub> was obtained and thus demonstrates the importance of NaHCO<sub>3</sub> for such catalysts. Both of these complexes upon treatment with NaHCO<sub>3</sub> and H<sub>2</sub>O<sub>2</sub> in methanol instantly generate oxidoperoxido species which is considered to be the intermediate species responsible for the transfer of oxygen to the substrates during catalytic oxidation. The polymer-grafted complex also provides additional advantage over its homogeneous counterpart in terms of recyclable catalytic system, increased catalyst lifetime and easier separation from the reaction mixture.

It has been observed that inserting spacer (an extra CH<sub>2</sub> group) between polymer support and catalyst enhanced the catalytic performance of grafted catalysts possibly due to the presence of more catalytic centers on the surface of polymer support which allow the better interaction of catalytic center with substrate and oxidant during catalytic reaction. The achievements presented in this study contribute significantly to our knowledge and may have future industrial applications.